

Development of extensional growth basins:

A field based study, Svalbard, Norway

Aleksandra Anna Smyrak-Sikora

Thesis for the degree of Philosophiae Doctor (PhD)
University of Bergen, Norway
2020

UNIVERSITY OF BERGEN



Development of extensional growth basins:

A field based study, Svalbard, Norway

Aleksandra Anna Smyrak-Sikora



Thesis for the degree of Philosophiae Doctor (PhD)
at the University of Bergen

Date of defense: 27.02.2020

© Copyright Aleksandra Anna Smyrak-Sikora

The material in this publication is covered by the provisions of the Copyright Act.

Year: 2020

Title: Development of extensional growth basins:

Name: Aleksandra Anna Smyrak-Sikora

Print: Skipnes Kommunikasjon / University of Bergen

PREFACE

Scientific environment

This PhD thesis was submitted to the Department of Earth Science at the University of Bergen, Norway (UiB) in accordance with the requirements for the degree of Philosophiae Doctor (PhD). The work presented in this PhD thesis has been conducted at the Department of Arctic Geology at The University Centre in Svalbard (UNIS) where I was employed as a PhD candidate.

Main supervisor:

Professor Snorre Olaussen (The University Centre in Svalbard, UNIS)

Co-supervisors:

Professor Alvar Braathen (University of Oslo and UNIS)

Professor William Helland-Hansen (University of Bergen and UNIS)

Professor Jan Inge Faleide (University of Oslo)



Structure of the thesis

This is an article-based dissertation divided into two main parts and two appendices:

PART I

Part I of the thesis introduces the scientific objectives and motivation behind the study and presents an overview of the scientific background. The following chapters outline the geological setting of the studied areas and list methods performed during this research. In Part I the main results from the 4 scientific articles are synthesised and discussed in respect to the regional geology and concepts of the evolution of growth basins. This part finishes with an outline of possible further work.

PART II

Part II of the thesis presents the four scientific articles that form the main body of this PhD dissertation.

Appendices

Supplementary material includes abstracts of articles and submitted manuscripts partly linked to the thesis in Appendices A-D. Appendices E-H present a list all publications, conference abstracts, workshops presentations and teaching conducted for the period from 2012 to 2019.

List of Publications

ARTICLE 1

Smyrak-Sikora, A., Johannessen E. P., Olausen S., Sandal, G. & Braathen, A. (2018): "Sedimentary architecture during Carboniferous rift initiation - the arid Billefjorden Trough, Svalbard", *Journal of the Geological Society*, 176(2), 225-252. <https://doi.org/10.1144/jgs2018-100>

ARTICLE 2

Smyrak-Sikora, A., Nicolaisen J. B., Braathen A., Johannessen E. P., Olausen S. & Stemmerik, L. (prepared for submission to *Basin Research*): "Impact of dip slope growth faults on mixed carbonate-evaporite dominated deposits – Carboniferous Billefjorden Trough in Svalbard, Norway"

ARTICLE 3

Smyrak-Sikora, A., Osmundsen, P. T., Braathen, A., Ogata, K., Anell, I., Mulrooney, M. & Zuchuat, V. (2019): "Architecture of growth basins in a tidally-influenced, prodelta to delta-front setting: the Triassic succession of Kvalpynten, East Svalbard", *Basin Research*.
<https://doi.org/10.1111/bre.12410>

ARTICLE 4

Ogata, K., Mulrooney, M. J., Braathen, A., Maher, H., Osmundsen, P. T., Anell, I., **Smyrak-Sikora, A.** & Balsamo, F. (2018): "Architecture, deformation style and petrophysical properties of growth fault systems: the Late Triassic deltaic succession of southern Edgeøya (East Svalbard)", *Basin Research*, 30(5), 1042-1073.
<https://doi.org/10.1111/bre.12296>

Appendix A:

Haile, B. G., Czarniecka, U., Xi, K., **Smyrak-Sikora, A.**, Jahren, J., Braathen, A., Hellevang, H. (2019): "Hydrothermally induced diagenesis: Evidence from shallow marine-deltaic sediments, Wilhelmøya, Svalbard", *Geoscience Frontiers*, 10. 2. <https://doi.org/10.1016/j.gsf.2018.02.015>

Appendix B:

Senger, K., Brugmans, P., Grundvåg, S.-A., Jochmann, M., Nøttvedt, A., Olausen, S., Skotte, A. & **Smyrak-Sikora, A.** (2019): "Petroleum, coal and research drilling onshore Svalbard: a historical perspective", *Norwegian Journal of Geology*, 99.3. <https://hdl.handle.net/10037/16619>

Appendix C:

Maher, H., Senger, K., Braathen, A., Mulrooney, M.J., **Smyrak-Sikora, A.**, Osmundsen, P.T & Ogata, K. (Submitted to *Tectonics*) "Mesozoic-Cenozoic regional stress field evolution in Svalbard"

Appendix D:

Anell, I., Zuchuat, V., Röhnert, A. D., **Smyrak-Sikora, A.**, Buckley, S., Lord, G., Ogata, K., Osmundsen, P. T., Olausen, S., Maher, H., Midtkandal, I. & Braathen, A. (Submitted to *Basin Research*) "Increased tide influence on the sedimentary architecture and sand distribution of a prograding Triassic coastline across a structural high, SW Edgeøya, Svalbard".

"Reprints were made with permission from The Geological Society of London (Article 1) and International Association of Sedimentologists and European Association of Geoscientists and Engineers and John Wiley & Sons Ltd (Articles 3 and 4).

Authorship and workload of thesis

Aleksandra Smyrak-Sikora is a sole author of the Part I of the PhD thesis and principal author of three of four manuscripts included in Part II. The table below presents the approximate contribution of Aleksandra Smyrak-Sikora and co-authors to each of the manuscripts.

Article 1: Sedimentary architecture during Carboniferous rift initiation - the arid Billefjorden Trough, Svalbard	
Principal author	Aleksandra Smyrak-Sikora
Co-authors	Erik Johannessen, Snorre Olaussen, Geir Sandal, Alvar Braathen
Text	Smyrak-Sikora
Figures	Smyrak-Sikora
Table with Facies associations	Johannessen, Olaussen, Smyrak-Sikora
Fieldwork	Smyrak-Sikora, Sandal, Johannessen, Olaussen,
Data processing	Smyrak-Sikora, Johannessen, Olaussen,
Discussion and revision of earlier manuscript versions	Johannessen, Olaussen, Braathen
Approximate total contribution	Smyrak-Sikora (70%)
	Other authors (30 %)
Status of manuscript	Published in Journal of the Geological Society

Article 2: Impact of dip slope growth faults on mixed carbonate-evaporite dominated deposits – Carboniferous Billefjorden Trough in Svalbard, Norway	
Principal author	Aleksandra Smyrak-Sikora
Co-authors	Jakob B. Nicolaisen, Alvar Braathen, Erik Johannesen, Snorre Olaussen, Lars Stemmerik
Text	Smyrak-Sikora, Stemmerik, Braathen, Olaussen
Figures	Smyrak-Sikora, Nicolaisen (contribution to Figs 8 and 11)
Table with Facies associations	Nicolaisen, Johannessen, Olaussen, Stemmerik, Smyrak-Sikora
Fieldwork	Smyrak-Sikora, Nicolaisen, Johannessen, Olaussen, Stemmerik
Data processing	Smyrak-Sikora, Braathen, Nicolaisen, Stemmerik
Discussion and revision of earlier manuscript versions	Stemmerik, Braathen, Nicolaisen, Olaussen, Johannessen,
Approximate total contribution	Smyrak-Sikora (60%)
	Other authors (40%)
Status of manuscript	Prepared for submission to Basin Research

Article 3: Architecture of growth-basins in a tidally influenced, prodelta to delta front setting: the Triassic succession of Kvalpynten, East Svalbard

Principal author	Aleksandra Smyrak-Sikora
Co-authors	Per Terje Osmundsen, Alvar Braathen, Kei Ogata, Ingrid Anell, Mark J. Mulrooney, Valentin Zuchuat
Text	Smyrak-Sikora
Figures	Smyrak-Sikora
Table with Facies	Smyrak-Sikora, Zuchuat, Anell
Fieldwork	Smyrak-Sikora, Osmundsen, Braathen, Ogata, Anell, Mulrooney,
Data processing	Smyrak-Sikora
Discussion and revision of earlier manuscript versions	Osmundsen, Braathen, Mulrooney, Zuchuat, Anell, Ogata
Approximate total contribution	Smyrak-Sikora (80 %)
	Other authors (20 %)
Status of manuscript	Published in Basin Research

Article 4: Architecture, deformation style and petrophysical properties of growth fault systems: the Late Triassic deltaic succession of southern Edgeøya (East Svalbard)

Principal author	Kei Ogata
Co-authors	Mark J. Mulrooney, Alvar Braathen, Harmon Maher, Per Terje Osmundsen, Ingrid Anell, Aleksandra Smyrak-Sikora, Fabrizio Balsamo
Text	Ogata, Mulrooney
Figures	Ogata
Fieldwork	Ogata, Mulrooney, Braathen, Maher, Osmundsen, Anell, Smyrak-Sikora
Data processing	Ogata, Mulrooney
Discussion and revision of earlier manuscript versions	Ogata, Mulrooney, Braathen, Maher, Osmundsen, Smyrak-Sikora (contribution to sedimentary deposition within growth faults hanging walls and to the concept model)
Approximate total contribution	Ogata (60%)
	Other authors (40 %)
Status of manuscript	Published in Basin Research

Funding, software and data access

The PhD position was internally financed by the University Centre in Svalbard (UNIS), funded by the Norwegian Ministry of Education and Research.

Two manuscripts of the thesis (Article 3 and Article 4) were written as a part of “Trias North - Reconstructing the Triassic northern Barents shelf” project led by the University of Oslo, co-funded by industry industry and research Council of Norway (RCN) grant number 234152 and industry partners; Edison Norway, Lundin Norway, RWE Dea Norway, Equinor Statoil, Tullow Oil and the Research Council of Norway (RCN grant number 234152). Several fieldwork campaigns in Billefjorden (forming the foundation for Article 1 and Article 2) were financed with internal funding from UNIS. Additional field and operational support came from Arctic Field Grants (awarded in years 2014 and 2016) by the Svalbard Science Forum (SSF), and from the joint industry and RCN-sponsored Research Centre for Arctic Petroleum Exploration (ARCEX; grant number 228107).

Academic software licenses were kindly provided by Schlumberger (Petrel), Virtual Outcrop Geology Group, NORCE Norwegian Research Centre, Bergen, Norway (Lime) and Midland Valley (MOVE).

The thesis contains a collection of originally collected field-based data supported by digital elevation data and aerial images from the Norwegian Polar Institute.

Acknowledgements

When, in March 2011, I entered the building of the University Centre in Svalbard (UNIS) my first thought was: "I want to work here". This dream came true only a year later when I started my long but very rewarding journey through the PhD project. Firstly, I would like to thank my supervisor Snorre Olausen for offered chance to develop this exciting project in Arctic rift basin geology, his patience and trust. Transition from research conducted in structural geology of metamorphic rocks to basin analysis was not easy and Snorre always served with the guidance, help and tutoring. Huge acknowledgments go to Alvar Braathen, who has introduced me to the outcrops of Billefjorden and Edgeøya, and always offered great support and advice. William Helland Hansen and Jan Inge Faleide are acknowledged for their supervision on the project. I strongly appreciate the scientific freedom and multiple possibilities for development and collaboration I had during the research.

I would like to thank my field companions and dear colleagues Erik Johannessen, Lars Stemmerik, Per Terje Osmundsen, Kim Senger, Mark Mulrooney, Ingrid Anell, Kei Ogata, Geir Sandal, Jakob Nicolaisen, Tore Aadland, Tyler Steward, Tone Sorento, Harmond Maher, Berit Husteli and Luka Blažić for amazing outdoor experiences and good discussions about the rocks. Marija Jensen, Hanna Rósa Hjálmarsdóttir, Aga Nowak, Tom Birchall, Malte Jochmann, Hanne Christiansen and Andy Hodson are strongly acknowledged for their supporting words and actions in house at UNIS. I want to thank to the Logistics Department at UNIS for teching me to prioritise the safety and their help in facilitating the field works. Winfried Dalmmann is thanked for shearing the maps allowing to easy improvements.

I would like to dedicate this thesis to my daughters Malwina and Ismena, who teach me every single day that imagination has no limits. I appreciate the support from my parents Wanda and Wiesiek, Grandma Zosia, Aneta, Pela, and Dominika who helped with home-work logistics near the end of the project. Finally, I would not make it without my beloved husband Sebastian, who I thank for his consistent support, the ongoing believe in my potential, for his 'life practicality' and good humor.

Abstract

The growth style and evolution of syn-sedimentary faults influence the architecture of the basin and thus control both the geometries and distribution of sedimentary facies belts. The architecture of sedimentary basin fill reflects a combination of tectonic and climatic controls that are relatively unique for each geological setting. This statement was tested in Svalbard, Norway, where recent post-glacial topography and a lack of vegetation reveal unique outcrops that allow detailed investigation of spatio-temporal basin fill development. Field studies were conducted in two locations: in the Upper Carboniferous Billefjorden Trough outcropping in central Spitsbergen, and in Kvalpynten, Edgeøya, where an array of Upper Triassic growth faults is exposed. This body of work consists of four scientific articles. Field-based results from detailed sedimentological logging, structural measurements and geological mapping were combined with analysis of three-dimensional outcrop models (derived from LIDAR scans and photogrammetry). Published data such as lithostratigraphy from the boreholes and sedimentary logs were also integrated to form an extensive and coherent database.

A ca. 25 km wide basin fill of the Billefjorden Trough records the transition from a continental to a paralic sedimentary facies that formed in response to the opening of a connection to the sea. Early syn-rift deposition occurred in a basin segmented into the hanging wall blocks of meso-scale (tens to hundred meters of displacement) growth faults, in partly isolated sub-basins. In this phase the Billefjorden Trough was a symmetrical basin. Later on, half-graben geometry developed during the rift climax, highlighted by deposition of up to 400 meters of alluvial fan deposits confined to the master fault zone. Meso-scale faults have segmented the dip slope into proximal and distal parts. The tectonic impact on the basin fill was the greatest near the master fault zone and in the proximal dip slope. The imprint of eustatic sea level prevails over the

tectonic influence in the distal dip slope. Rift reorganization and narrowing phase redefine the basin configuration, which is less asymmetric than in the rift climax and subsides more slowly. Growth fault displacement maxima define zones on the footwall blocks, with evaporite dissolution and formation of stratiform breccias. A narrow, centrally located depocenter on the hanging wall block formed between two antithetic faults, was protected against dissolution and contains thick beds of evaporites.

The world-class growth faults in Kvalpynten bound twelve ca. 250-800 m wide basins filled with prodelta to lower delta front mudstones and shales. The basin fills consist of tens of meters thick, coarsening upward units, where the sandy parts represent tidal dunes and bars detached from the delta front deposits. Faults have developed due to differential compaction of the water-saturated, underlying organic-rich mudstones and the prodelta mudstones. The sediments were deposited on the structural slope dipping against the direction of prograding delta system. The structural control is reflected in syn-kinematic, late syn-kinematic and post-kinematic accommodation that in combination with relative sea level controlled the type and stacking patterns of the architectural elements filling the basins.

Combined results from the tectonically-driven development of the Billefjorden rift and differential compaction-driven Kvalpynten growth faults allow discussion of the similarities and differences that result from, among other things, the driving mechanisms of faulting, the size and the type of basin fill (i.e. siliciclastic vs. mixed but -carbonate-evaporite dominated deposits). Despite the diverse scale, the extensional systems developed in both locations display similar evolution of a half-graben geometry that is pre-dated by symmetrical graben.

Contents

PREFACE	3
Scientific environment	3
Structure of the thesis	4
List of Publications	5
Authorship and workload of thesis	7
Funding, software and data access	9
Acknowledgements	10
Abstract	12
Contents	14
PART I	17
Introduction	18
Motivation and objectives	21
Scientific background	23
How do normal faults grow?	26
Folds associated with normal faults	28
Rift basin evolution	29
Geological settings	32
Geology of Svalbard	32
Upper Paleozoic	33
Mesozoic	37
Cenozoic	40

The Billefjorden Trough	40
Billefjorden Fault Zone	41
Deposition within the Billefjorden Trough	46
Pre-rift stratigraphy	46
Syn-rift stratigraphy	47
<i>Hultberget Formation</i>	47
<i>The Minkinfjellet Formation</i>	49
<i>Wordiekammen Formation</i>	50
Upper Triassic deltaic system in the eastern part of Svalbard	51
Data and methods	56
Limitations of expansion index	58
Summary of the scientific articles	61
Article 1	62
Article 2	63
Article 3	65
Article 4	67
Discussion and conclusions	69
System 1: Billefjorden Trough	69
Rift initiation	69
Billefjorden Trough evolution	71
Early syn-rift (Phase 1)	74
Rift climax (Phase 2)	74
Rift reorganisation and narrowing (Phase 3)	75
Models of fault growth in Billefjorden Trough	77
System 2	78
Half-graben evolution: similarities and differences in Carboniferous and Triassic basins (System 1 and 2)	81
Differences between System 1 and System 2	81
Similarities between System 1 and System 2	82
Further work	85
References	87

PART II	115
ARTICLE 1	117
ARTICLE 2	147
ARTICLE 3	209
ARTICLE 4	241
APPENDICES	275
Appendix A	277
Appendix B	280
Appendix C	282
Appendix D	284
Appendix E	287
Appendix F	288
Appendix G	290
Appendix H	293

PART I

Introduction

Svalbard is a Norwegian Arctic archipelago comprising all islands located between 74°-81° north and 10°-35° east. Spitsbergen is the biggest island of Svalbard while Edgeøya is the third biggest island located in its eastern part (Fig.1). Although 60% of Svalbard is covered by glaciers the remaining parts offer good, occasionally excellent, access to outcropping sedimentary rock successions from Neoproterozoic to present, only by missing Upper Cretaceous and large part of Neogene strata (Fig. 2).

Svalbard occupies the uplifted north-western corner of the Barents Shelf, an intracratonic basin that belongs to the Eurasian continental plate. To the west Svalbard is bounded by the sheared margin of the De Geer Transform Zone formed in response to Cenozoic seafloor spreading in the Norwegian Greenland Sea. To the north Svalbard is bounded by the passive margin of the Eurasian basin (Fig. 1; Faleide et al., 2008). The Caledonian Orogeny was followed by orogenic collapse and the Svalbardian compressional event in the Devonian (c.f. Harland et al., 1974; Piepjohn et al., 2000; Bergh et al., 2011). Following these events, the geological history of Svalbard can be simplified to four main events: i) Late Palaeozoic extension ii) Mesozoic sag and epicontinental basins; iii) Paleogene contractional tectonics and foreland basin development followed by rifting in the Greenland Sea; iv) Neogene passive margin, uplift, erosion and glaciation.

This thesis contributes to conceptual investigations of two growth fault-bounded basin fill systems, i.e., growth basins. The study also fills a gap in regional tectono-stratigraphic investigations of the mentioned stratigraphic intervals exposed in Svalbard. Articles 1 and 2 discuss the three syn-rift phases of Serpukhovian-Moscovian succession. The first phase is dominated by siliciclastics while the second and third phases consist mostly of mixed

carbonate-evaporite deposits (Fig. 2 and 3). Articles 3 and 4 deal with Upper Triassic growth faults developed in a prodelta to distal delta front and tidal depositional settings (Fig. 2 and 3).

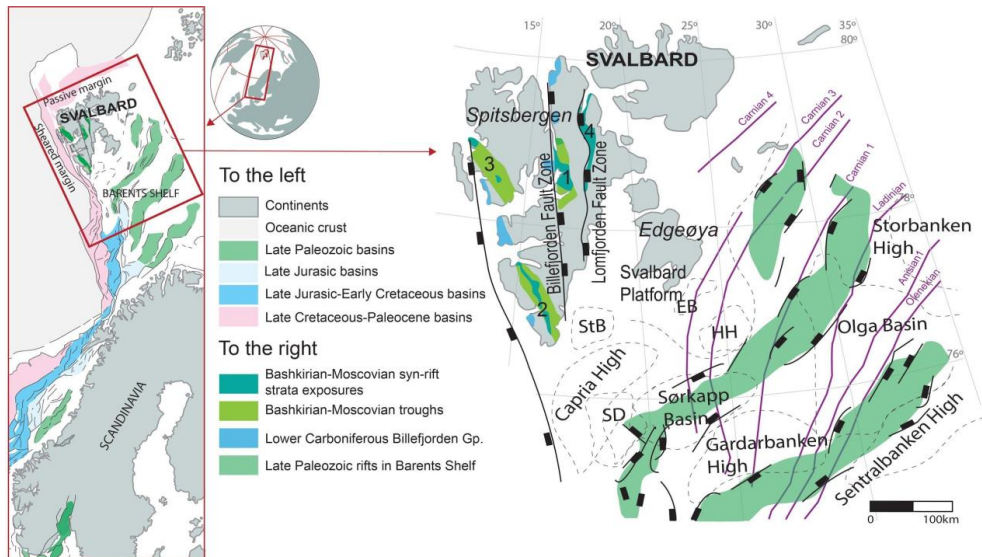
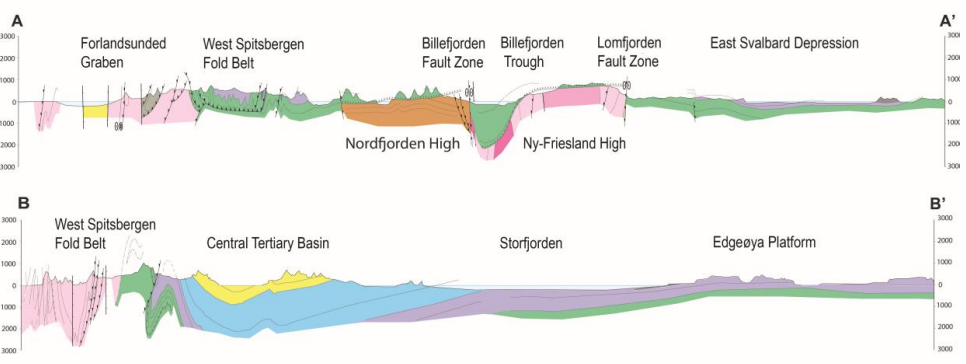
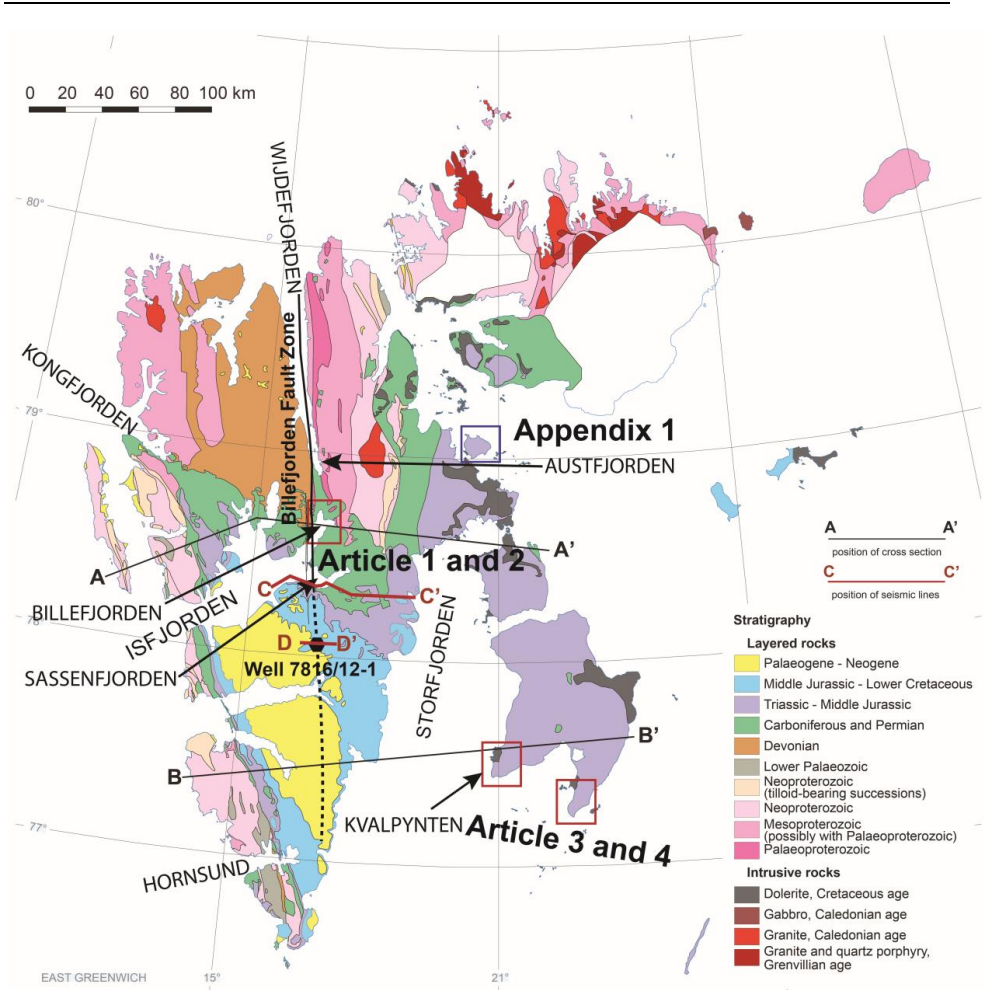


Fig. 1. Palaeozoic structures of Svalbard and the SW Barents Shelf.

Palaeozoic rift basins are shaded with green, Upper Carboniferous basins in Svalbard are marked with: 1: The Billefjorden Trough, 2: The Inner Hornsund Trough, 3: St. Jonsfjorden Trough, 4 the Lomfjorden Trough. Purple lines mark the position of clinoforms (deltaic platform edge in Anell et al., 2014) that prograded in the Triassic across the Barents Shelf. Modified from Dallmann et al., (2004); Faleide et al., (2008) and Anell et al., (2014, 2016). StB: Størfjorden Basin, EB: Edgeøya Basin, SD: Sørkap depression, HH: Hopen High.

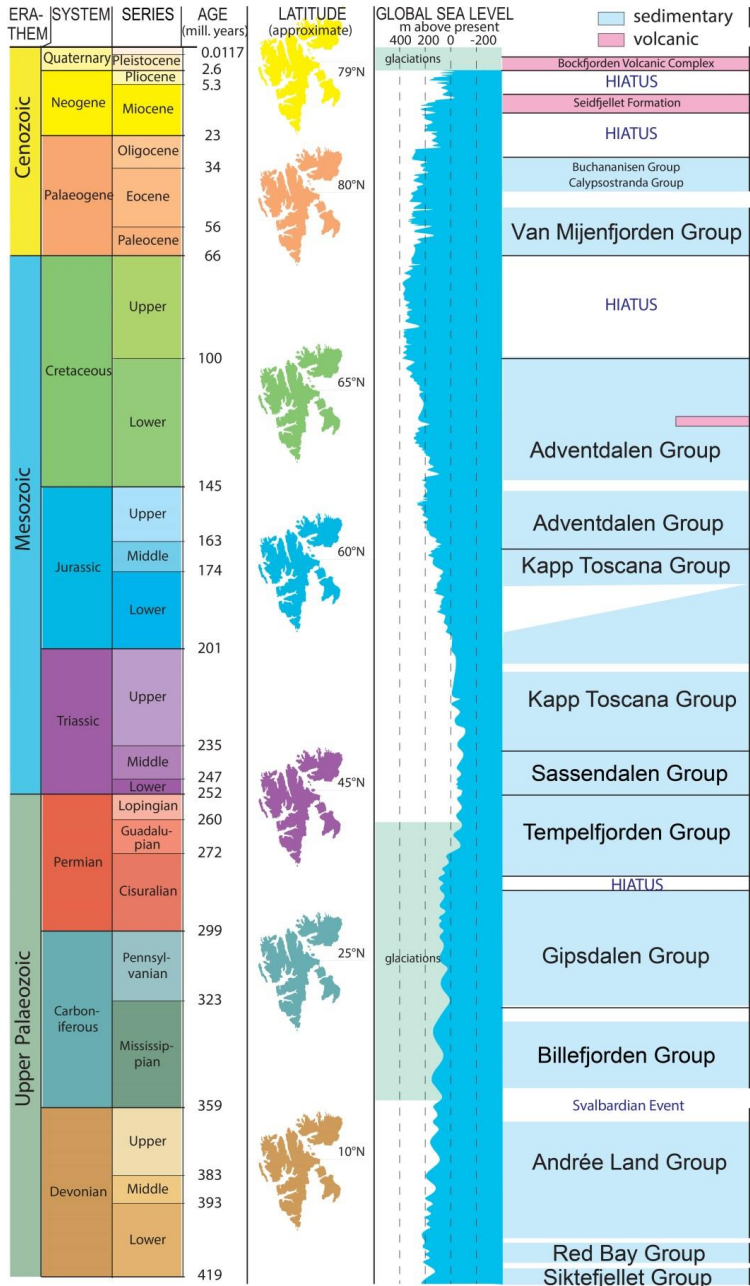
Next page: Fig. 2. Geological map of Svalbard (without Bjornøya) and simplified W-E profiles across Scalbard from Dallmann (2015).



Motivation and objectives

The world-class outcrops in Svalbard can compete with places such as the Corinth Rift or the Suez Rift in the accessibility and quality of exposures and have been understudied with respect to tectono-stratigraphic interactions. The aim of this study is to examine the relationship between evolution of extensional growth-faults in relation to the development of accommodation and facies belts. This is achieved by investigating growth-faulted basins in Upper Paleozoic and Lower Mesozoic sedimentary succession in Svalbard.

- The first objective was to investigate sedimentary response to early syn-rift faulting that occurred in an arid, subtropical climate. This is achieved by detailed tectono-stratigraphic investigations of siliciclastic-dominated early syn-rift fill of the Carboniferous Billefjorden Trough (Article 1).
- The second objective was to investigate a half-graben dip slope evolution during deposition of carbonate-evaporite strata significantly affected by growth faults and associated folds. Lidar scan analysis of the Billefjorden Trough dip slope outcrops combined with field mapping and sedimentary logging address this objective in Article 2.
- The third objective was to establish a detailed tectono-stratigraphic evolution of the Billefjorden Trough. New tectono-stratigraphic model and division into: early syn-rift, rift climax and rift reorganization and narrowing phases outline the configuration of the trough and architecture of associated basin fill presented in Articles 1 and 2.
- The fourth objective was to determine the sedimentary architecture of a growth-faulted Late Triassic succession of Kvalpynten, Edgeøya. Articles 3 and 4 discuss the evolution of faulting and depositional settings within a fault-bounded array of growth-basins developed within prograding deltaic succession.



Article 3 and 4

Article 1 and 2

Fig. 3. Stratigraphic column and main depositional units in Svalbard modified from Dallmann et al., (2015).

Scientific background

Tectono-stratigraphy is a discipline in geology that rapidly expanded in the last three decades. The cradle of onshore studies were the rifts of Suez (e.g. Gawthorpe et al., 1990,1997; Gawthorpe & Hardy, 2002; Sharp et al., 2000a,b; Jackson et al., 2002, 2005; Young et al., 2003) and the rifts of central Greece (Gawthorpe & Hurst, 1993; Gawthorpe et al., 1994, Gawthorpe & Leeder 2000, Ford et al., 2013; Gawthorpe et al., 2018). More recent tectono-stratigraphic reconstructions and models of extensional fault growth and linkage cover onshore and offshore examples around the globe (e.g. Corfield & Sharp et al., 2000; Dawers & Underhill, 2000; Back et al., 2008; Henstra et al., 2017; Mulrooney et al., 2018; Serck & Braathen, 2019).

A growth-fault basin is a sedimentary depocentre that thickens towards growth fault(s) (e.g. Harms & Price, 1992). Growth basin evolution is strongly controlled by the fault-induced subsidence that, among other agents, influences basin architecture and the distribution of sedimentary facies (e.g. Schlische 1991; Gawthorpe & Leeder, 2000; Dawers & Underhill, 2000; Jackson et al., 2002; Serck & Braathen, 2019). Typically, a fault is described as 'a planar fracture or discontinuity in a volume of rock, across which there has been significant displacement as a result of rock-mass movement'. The dip-slip normal faults are recognised when the hanging wall (rocks above the fault) is displaced downwards in relation to the footwall (e.g. Dennis, 1967; Peacock et al., 2000), i.e. when σ_3 is located horizontally.

This study focuses on normal 'growth faults' that are defined by an increase in displacement down the dip of the fault (Ocamb, 1961). A syn-depositional nature of growth faults is expressed as a thickening of sedimentary strata in the hanging wall near the fault in respect to the footwall or in the hanging wall away from the fault (Ocamb, 1961).

Normal faults form due to extensional tectonic forces in the crust, or they can be gravity-driven. In rift systems, growth faults are developed in response to tensile stresses that act during lithospheric stretching and thinning (e.g. McKenzie, 1978; Barr, 1987; Duncan & Turcotte, 1994). This process builds up a brittle strain in the continental crust and causes a thick-skinned faulting and associated thin-skinned deformation.

Gravity-driven normal faults are thin-skinned faults that have developed due to gravitational collapse when sediments become critically unstable as they build out over a slope. The faults' displacements are, therefore, in the downslope direction. They form often in the prograding deltaic deposits (e.g. Edwards, 1976; Gibbs 1984; Bhattachayra & Davies 2001; Osmundsen et al., 2014; Fielding, 2015), where typically listric (scoop-shaped) faults are facilitated by a weak detachment layer such as evaporites or over-pressured mud. Growth faults within deltaic systems are not restricted to basins formed within extensional lithospheric stress (Martinsen, 1989; Burhannudinnur & Morley, 1997; Morley et al., 2003; Wignall & Best, 2004; van der Zee & Urai, 2005; Back et al., 2008;) but can develop in tectonically stable epicontinental seas (Edwards, 1976; Nemeč et al., 1988; Prestholm & Walderhaug, 2000; Osmundsen et al., 2014), or in foreland basins (Bhattacharya & Davies, 2001; Bouroullec et al., 2004; Shultz & Hubbard, 2005; Fielding et al., 2015; Braathen et al., 2018a).

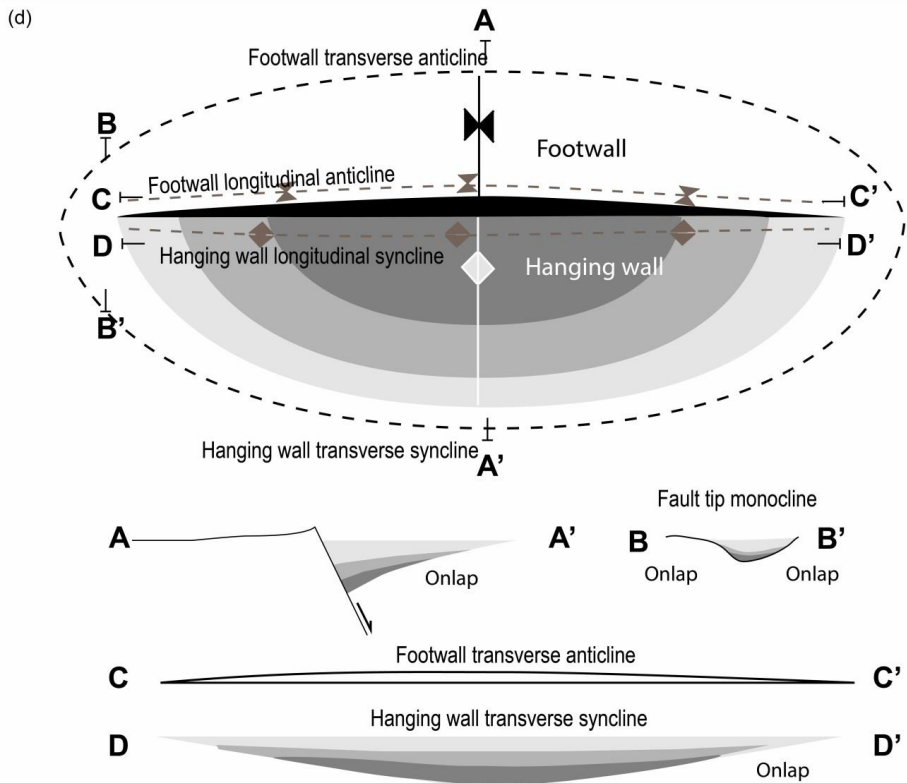
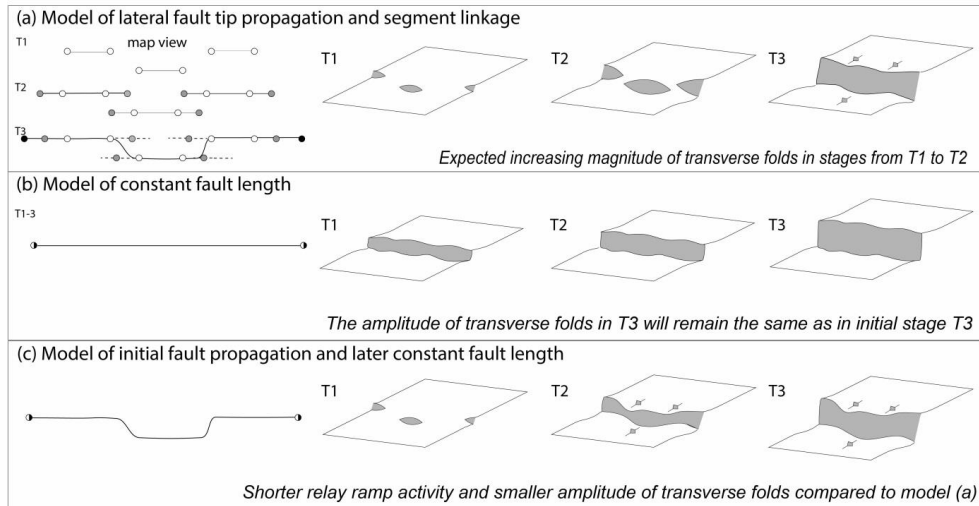


Fig. 4. (a-c) synthesis of fault growth models, modified from Cartwright et al., (1996), Walsh et al., (2002) and Rotevatn et al., (2019); (d) Fault-related folds, modified from Schlische (1991, 1995) and Gawthorpe et al., (1997).

How do normal faults grow?

In map view, fault zones consist of multiple fault segments occurring at different-scales which can vary in orientation. During extensional deformation individual fault arrays go through several more or less distinct stages that are reflected in the sedimentary basin fill (Fig. 4; Prosser, 1993; Gupta et al., 1998; Gawthorpe & Leeder, 2000; McLeod et al., 2002; Leppard & Gawthorpe, 2006; Gabrielsen, 2015). With ongoing extension, the structures record strain localization from many small faults in the fault initiation stage, through fault intersection and linkage stage, to fewer, larger faults in the through-going fault stage (Cowie et al., 2000; Gawthorpe & Leeder, 2000).

Currently, there are two competing conceptual models describing the growth of normal faults (Fig. 4 a-b; e.g., Morley and Wonganan, 2000; Kim and Sanderson, 2005; Jackson & Rotevatn, 2013; Jackson et al., 2017; Liu et al., 2017; Rotevatn et al., 2019). Firstly, the well-known model of fault propagation suggests that normal faults grow by synchronous increase in displacement and length ('isolated fault model'; e.g., Cartwright et al., 1996). As the faults lengthen by tip propagation they overlap and link with other fault segments by the formation and subsequent breaching of the relay ramp (Fig. 4a; Walsh & Watterson, 1988; Dawers et al., 1993; Cartwright et al., 1996; Dawers & Anders, 1995; Walsh et al., 2003; Jackson & Rotevatn, 2013; Fossen & Rotevatn, 2016; Childs et al., 2017; Liu et al., 2017; Rotevatn et al., 2019). An individual earthquake ruptures and displaces the rock mass. The cumulative displacement from following earthquakes accrues systematically on faults (Walsh & Watterson, 1988; Cowie & Scholz, 1992; Dawers et al., 1993; Cartwright et al., 1996; Dawers & Anders, 1995; Nicol et al., 2010). According

to the fault propagation model the maximum displacement on an individual fault segment (D) increases relatively to the fault trace length (L), following the equation:

$$D = cLn$$

where c is a constant and n is a parameter that varies in a range from 1.0 – 1.5 (e.g., Walsh and Watterson, 1988; Cartwright et al., 1995; Dawers and Anders, 1995; Schlische et al., 1996; McLeod et al., 2000).

On the contrary, the less-known model of a fault constant-length suggests rapid establishment of fault length early in their slip history and subsequent accrual of displacement without major length increases (Fig. 4b; e.g. Walsh et al., 2002, 2003; Nicol et al., 2005, 2010; Giba et al., 2012; Jackson and Rotevatn, 2013; Jackson et al., 2017; Rotevatn et al., 2018; Rotevatn et al., 2019). The constant length model implies changes in D-L scaling over time as a fault grows (Rotevatn & Fossen, 2012), with L-dominated growth followed by D-dominated growth. This model typically is linked with reactivation of the pre-existing faults (Meyer et al., 2002; Walsh et al., 2002; Paton, 2006; Giba et al., 2012; Jackson & Rotevatn, 2013; Rotevatn & Jackson, 2014; Rotevatn et al., 2018) that propagate upwards and result in relatively quick establishment of fault length.

Recently, Rotevatn et al., (2019) indicated that faults following solely one growth model do exist in nature (Fig. 4c). Rotevatn et al., (2019), however, also documented that more often both propagating and constant-length fault behaviours occur in nature, but they dominate in different stages of the fault's life. The growth of most faults is characterized by two stages: an initial stage of length establishment (20–30% of fault lifespan) that also involves accumulation of 10–60% of the final fault displacement. This stage is characterized by rapid tip propagation, relay formation, relay breaching and

segment linkage. In the second stage (70–80% of fault lifespan), best described by the constant-length model, displacement accrual dominates without significant further fault lengthening.

Folds associated with normal faults

There are several types of folds associated with extensional faults over a wide range of scales. Schlische (1995) classified such folds as:

- Longitudinal folds that have hinges parallel to the fault. This group includes:
 - i) drag folds and fault-tip monoclines above propagating fault tips (narrow hanging wall synclines and footwall anticlines that form as a result of fault propagation);
 - ii) reverse drag folds that form in response to displacement decrease with distance from the fault surface;
 - ii) rollover anticlines (fault-bend folds) are formed along the listric faults to accommodate the fault shape;
- Transverse folds are at a high angle to the fault trace and form due to differential displacement along the fault length from the maxima in the fault centre to the fault tips. This group includes:
 - i) Hanging wall synclines in the fault centre (displacement maximum)
 - ii) Hanging wall anticlines near the fault tips, in the fault segment overlap zone
 - iii) Footwall anticlines in the fault segment centre
 - iv) Footwall synclines near the fault tips

Extensional fault-related folds exert a strong influence on syn-kinematic basins morphology, modifying accommodation, drainage patterns and sedimentary stacking and add complexity to the fault-bounded models of basin evolution (e.g. Schlische, 1995; Gawthorpe *et al.*, 1997; Gawthorpe & Leeder, 2000; Corfield & Sharp 2000; Sharp *et al.*, 2000; Jackson *et al.*, 2002; Serck & Braathen, 2019).

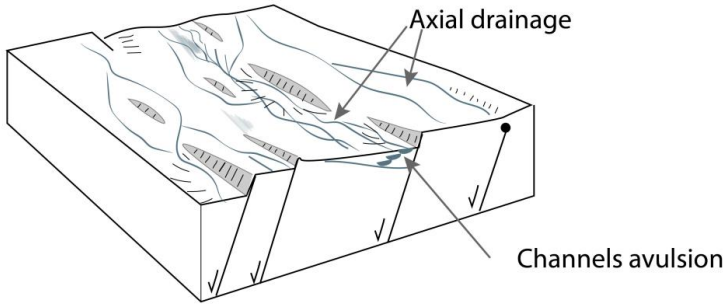
Rift basin evolution

The spatio-temporal evolution of fault-bounded sedimentary systems is considered to be significantly influenced by tectonics, in addition to climate, eustatic sea level variation and bedrock lithology. The impact of tectonic is especially seen as erosion on the footwalls and increased rate of sediment flux, and allocation of accommodation on the hanging walls (Posser 1993, Gawthorpe & Leeder, 2000).

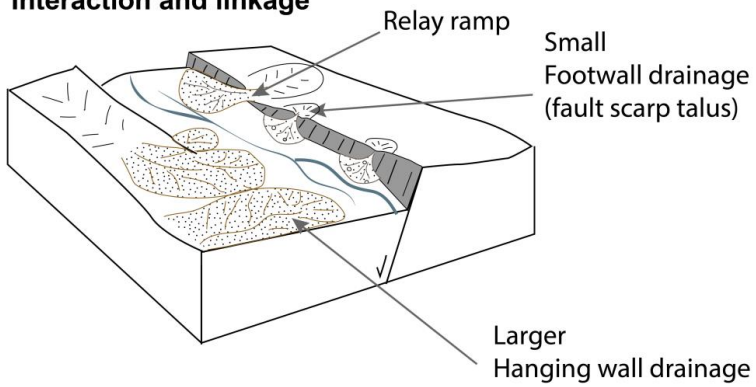
Large-scale configuration of rift basins is often characterized by a major basin bounding fault(s) with subsidiary synthetic and antithetic faults. Similar to the individual fault array growth (Fig. 4a), early stages of rift development are characterized by numerous small, isolated, fault-bounded basins, with displacement transverse to a dominant major basin-bounding fault during the rift climax (Fig. 5; Crossley, 1984; Watson *et al.*, 1987; Schlische & Olsen 1990). Distinct stages of rift evolution can be recognized in a geological record, each with characteristic linked depositional systems (e.g. Gawthorpe & Leeder, 2000).

Next page: Fig. 5. *Conceptual model of rift basin development, including drainage types, modified from Leeder & Gawthorpe (1987), Posser (1993), Gawthorpe & Leader (2000) and Articles 1 and 2.*

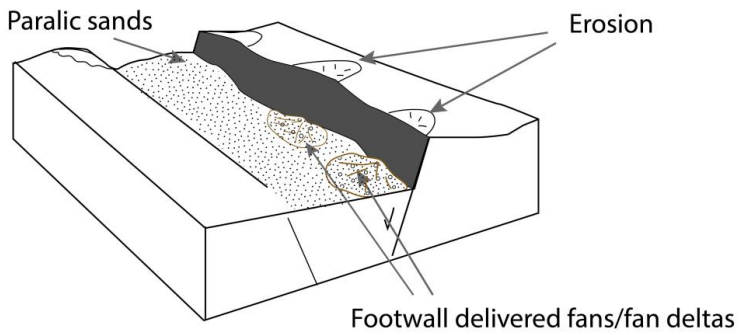
Initiation



Interaction and linkage



Through-going fault zones



In the rift initiation stage, subsidence develops in small isolated sub-basins (Fig. 5; Gupta et al., 1998; Gawthorpe & Leeder, 2000), and is balanced by sedimentation (Posser, 1993). The basin-scale drainage is dominated by axial input from antecedent mature drainage basins (Posser et al., 1993, Gawthorpe & Leeder, 2000). In this stage pre-rift topography and bathymetry might control the development of effective drainage networks (e.g. Jackson et al., 2005).

As faults laterally grow and interact, the relay zones (Fossen & Rotevatn, 2016) become an entry way for detritus from the hinterland (Gawthorpe & Leeder, 2000). In half-grabens, the asymmetry of rift basin margins controls the development of transverse drainage catchments; smaller on the footwall and larger on the hanging wall rift shoulders (Leeder & Jackson, 1993; Eliet & Gawthorpe 1995; Ravnås & Steel, 1998; Gawthorpe & Leader, 2000). Strain localized to fewer faults during the rift climax results in a pronounced increase in subsidence rates (Prosser, 1993; Gupta et al., 1998; McLeod et al., 2002; Leppard & Gawthorpe, 2006). This may lead to sediment starvation due to sediment source offset and small drainage basins. In this stage, minor eustatic sea level changes typically are not recorded (Posser et al., 1993).

Tectonic subsidence decreases in the post-rift stage and the basin fill records an increase in grain size due to expansion of footwall drainage basins and an increase in progradation. Post-rift stage deposition is likely to record minor eustatic changes (Posser et al., 1993).

Geological settings

The research results outlined in this thesis represents two locations in Svalbard (Figs 1 and 2). Articles 1 and 2 describe the study area within inner Billefjorden that focus on Serpukhovian-Moscovian age deposits. Articles 3 and 4 address growth faults developed in the Upper Triassic strata in Edgeøya. The geological overview presented after a brief introduction to the geology of Svalbard focus on these two geological periods.

Geology of Svalbard

The bedrock of Svalbard and the western Barents Shelf consolidated during the Caledonian orogeny, which has formed in response to the collision of Laurentia and Baltica and a closure of the Iapetus Ocean (i.e. Barentsian Caledonides in Gee et al., 2006; Harland et al., 1974; Gee & Tebenkov, 2004; Gee et al., 2008, 2013). Deformation, metamorphism, crustal magmatism and accretion of older basement provinces along shear zones in Svalbard occurred ca. 450–410 Ma ago (Late Ordovician- Early Devonian; Gee & Tebenkov, 2004; Gee, 2006). Recent studies date the metamorphism along the shear zones of Billefjorden and SW Spitsbergen to 420-410 Ma (Faehnrich et al., *in review*; Majka pers. comm.).

Since the early Palaeozoic, Svalbard gradually drifted from south of the equator to its present position at 76-80°N (Fig. 3; Scotese et al., 1979; Torsvik et al., 2002). Sedimentary post-Caledonian successions recorded a change in climate zone controlled in a large degree by the paleo-latitude of Svalbard. The climate conditions impacted both the facies associations and the mineralogy of the sediments (e.g. Steel & Worsley, 1984).

Upper Paleozoic

The post-Caledonian sedimentary basin located in the central part of the northern Spitsbergen has accumulated up to several km thick Old Red Sandstone strata of Late Silurian to Latest Devonian (Figs 2-3; Piepjohn et al., 2000, Blomeier et al., 2003; Braathen et al., 2018). Subsequently, a significant shortening of the Old Red Basin with the compressional west-directed folding and thrusting, i.e. Svalbardian phase (Harland & Gayer, 1972), is suggested to have taken place after Late Famennian and before Late Tournaisian time, (Fig. 3; Piepjohn et al., 2000; Bergh et al., 2011).

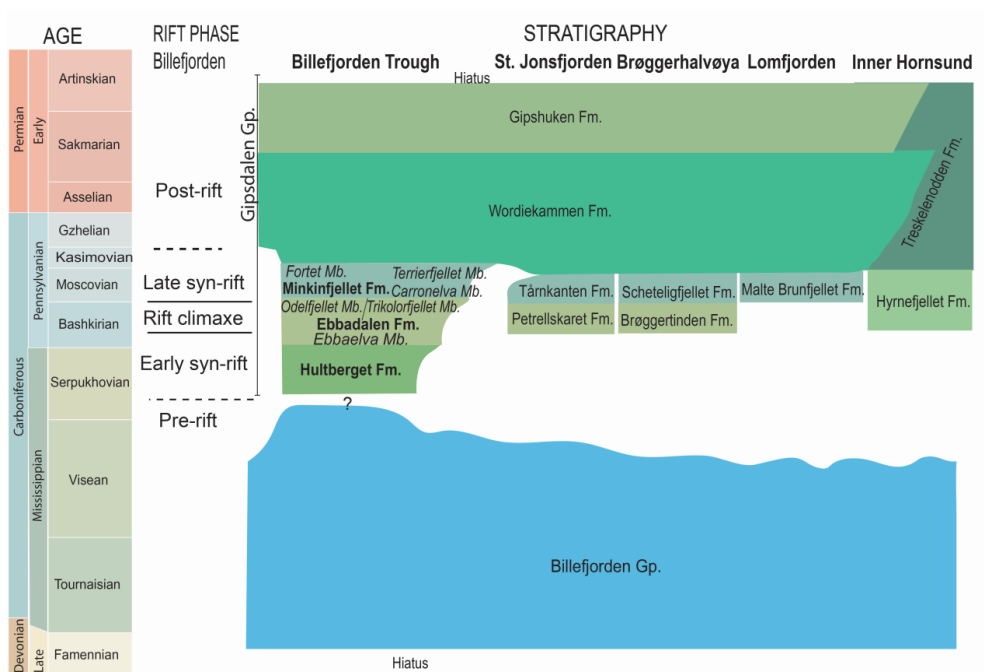


Fig. 6 Stratigraphy of the pre-, syn-, and post-rift Upper Carboniferous deposits modified from Dallmann (1999), Braathen et al., (2011) and Article 1.

Late Devonian to Lower Carboniferous deposits (Figs 2 and 6) are widespread across Spitsbergen and unconformably overlie the deformed Devonian and Lower Paleozoic succession and pre-Caledonian basement. The Fammenian to Visean Billefjorden Group represents a continental succession that recorded a humid and warm climate indicated by the presence of coal seams (Figs 3 and 6; Gjelberg & Steel, 1981). The basin fill was deposited in broad sag basin(s) that were subsiding, accompanied by periods of localised fault activity (Cutbill & Challinor, 1965; Gjelberg & Steel, 1981).

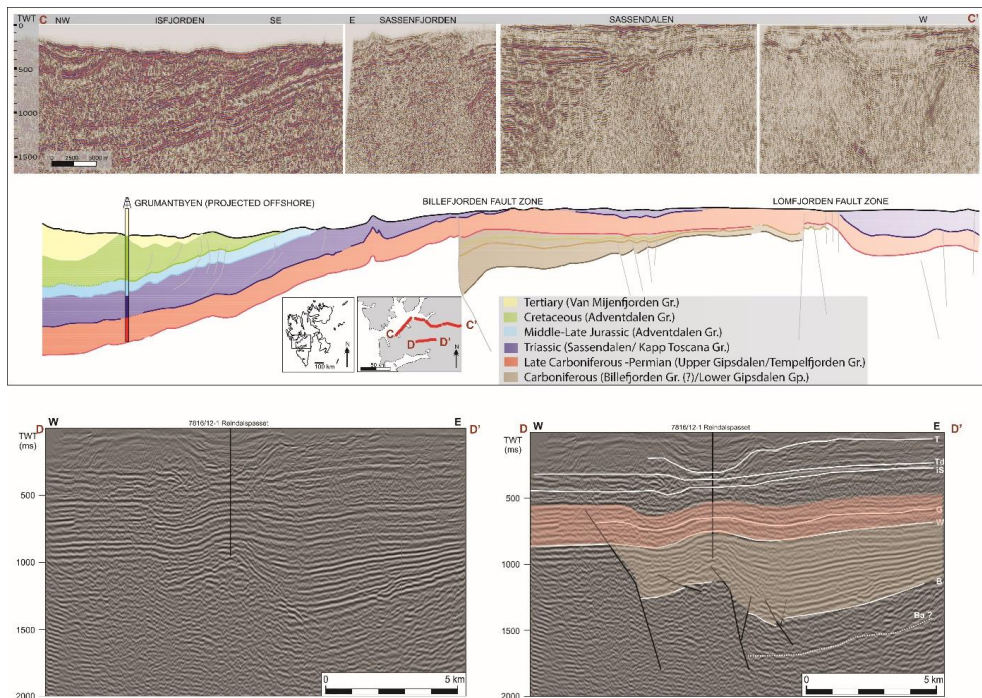


Fig. 7. Seismic profiles and interpretations that indicate subsurface deposits of Billefjorden Trough under the younger sedimentary strata; modified from Bælum & Braathen, (2012) and Anell et al., (2014).

The Upper Carboniferous (Pensylvanian) and Permian were periods of glaciations and deglaciations of Gondwana (Fig. 3; Gastaldo et al., 1996).

Rapid shifts in global-scale icehouse to greenhouse conditions caused frequent eustatic sea level fluctuations (of 60 m+/-15m in Carboniferous; c.f. Crowley & Baum, 1991). Variations in eustatic sea level, i.e. base level changes, affected the depositional environment not only in glaciated areas but also in near-equatorial regions.

In the Carboniferous, Svalbard was located at a paleo-latitude of 20–25° north (Fig. 3; Steel & Worsley, 1984; Dallmann et al., 2015). During the transition from Mississippian to Pennsylvanian, the paleo-climate shifted from humid tropical to warm, arid to semi-arid climate recorded by the deposits of the Gipsdalen Group (Figs 3 and 6; Holliday & Cutbill, 1972; Gjelberg & Steel, 1981; Johannessen & Steel, 1992). Near the onset of the climate change, north-south trending rift basins developed in response to regional-scale tectonic extension that covered also the western Barents Shelf (Gudlaugsson et al., 1998; Faleide et al., 2008; Anell et al., 2016). In Svalbard the rift basins were filled with alluvial and paralic to mixed carbonate-evaporite deposits (Cutbill & Challinor, 1965; Holliday & Cutbill 1972; Gjelberg & Steel, 1981; Steel & Worsley, 1984; Johannessen & Steel, 1992; Braathen et al., 2011; Articles 1 and 2). Remnants of these rift systems outcrop in Spitsbergen and are imaged on the subsurface seismic data (Fig. 7).

In the central part of Spitsbergen, the rift system that developed along the eastern flank of the north-south striking Billefjorden Fault Zone (Basin 1 on Fig. 1) is seen in subsurface and is confirmed by petroleum exploration drilling by Norsk Hydro in 1991 (Reindalspasset well 7816/12-1 on Figs 2 and 7; Bælum & Braathen, 2012; Nøttvedt et al., 1993; Senger et al., 2019). Further north, the presence of a rift fill is shown on the seismic in Sassenfjorden and Billefjorden (Fig. 7; Bælum & Braathen, 2012; Anell et al., 2014) before it crops out in the Billefjorden Trough (Figs 1-2; e.g. Cutbill & Challinor, 1965; Holliday and Cutbill, 1972; Gjelberg & Steel, 1981; Steel & Worsley, 1984 Johannessen

& Steel, 1992, Braathen et al., 2011; Articles 1 and 2). Although this basin fill is eroded in northern Spitsbergen, some extensional faults can be correlated along Wijdefjorden (Fig. 2).

The remains of westward located, north-south trending rift system are found along western Spitsbergen (Fig. 1, Basins 2 and 3). This system is less well defined both in ages and basin configuration because of the scattered outcrop pattern of isolated basin fill blocks and deeper previous burial due to younger transpressional deformation (Fig. 2; Bergh et al., 2000; Maher & Welbon, 1992). The outcropping basin fills are classified as the Inner Hornsund Trough (Fig. 1, basin 2 and Figs 2 and 6) and St. Jonsfjorden Trough (Fig. 1, basin 3; Gjelberg & Steel, 1981; Steel & Worsley, 1984; Dallmann et al., 1999, 2015). Up to 55 m thick basin fill outcropping in isolated locations can be found along Lomfjorden Fault Zone in north-eastern Spitsbergen (Lomfjorden Trough *sensu* Schreibner et al., (2015); Fig. 1, Basin 4; Fig.6). In addition, seismic-based studies in eastern Svalbard recognise late Palaeozoic active basin-horst topography of uplifted Edgeøya Platform, the NE-SW elongated Edgeøya basin (EB on Fig.1) and the Hopen High to the SE (Fig. 1; Anell et al., 2016). A small and deep Edgeøya Basin was filled with up to 3 km of Carboniferous deposits (Harland, 1997). However the exact age of these basins remains unknown.

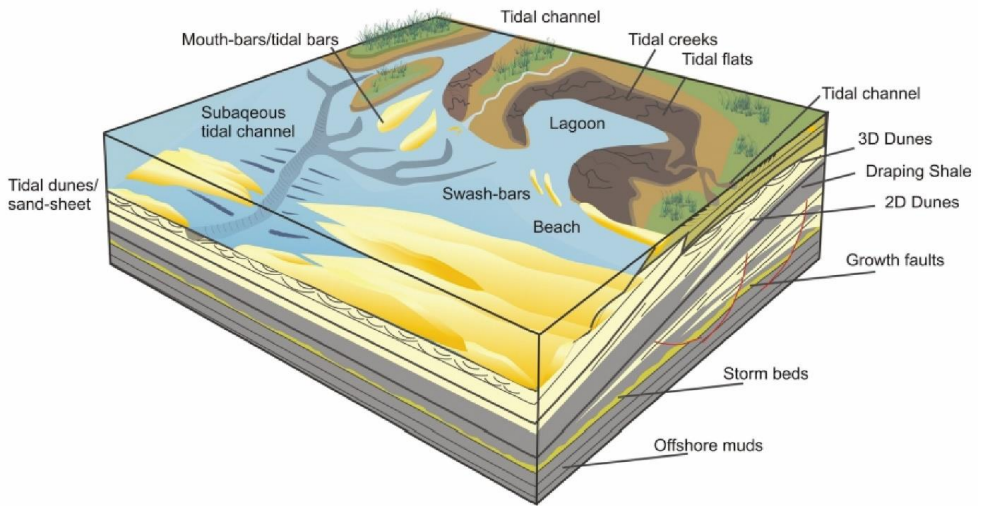
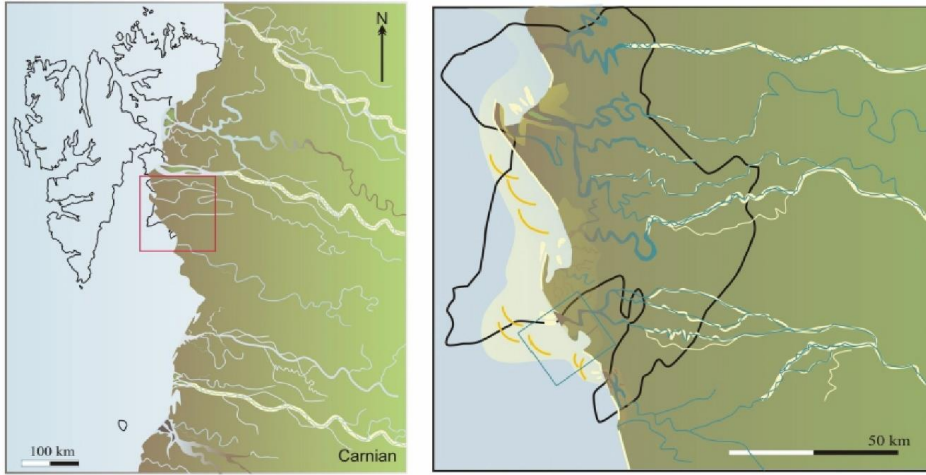
In summary, “Mid”- Carboniferous extension facilitated localised subsidence in narrow rift Basins 1-4 and Edgeøya Basin (Fig.1) separated by highlands that express a regional-scale horst and graben system configuration. Less extensive extensional tectonic activity along Billefjorden Fault Zone in central Spitsbergen occurred also in the Permian (Ahlborn & Stemmerik, 2015; Sorento et al., 2019). In southwestern Spitsbergen some potential movements are recorded into Middle Triassic (Krajewski & Weitschat, 2015).

From the upper Pennsylvanian, Svalbard and the Barents Shelf become a platform dominated by deposition of mixed carbonate-evaporite deposits of the Upper Gipsdalen Group (Fig. 3; Stemmerik & Worsley, 1989; Worsley, 2008). In the Kungurian, the depositional system gradually changed from warm water carbonate deposits of the Gipsdalen Group to temperate water carbonate and silica deposits of the Tempelfjorden Group (Fig. 3; Blomeier et al., 2009; Blomeier et al., 2011, Matysik et al., 2018). The carbonate factory was ended in the latest Permian (Changsigian) by income of fine grained siliciclastics from the denudation of the Uralian mountain chain in east of Barents Shelf (Blomeier et al. 2013).

Mesozoic

The Svalbard Platform (Fig. 1) established by the Mesozoic was considered as a sag or epicontinental basin. Potentially, reactivation of older lineaments facilitated the thin-skinned mild growth faulting on Edgeøya (Articles 3 and 4; Anell et al., 2013; 2016; Osmundsen et al., 2014). Differences in thickness of Permian and Triassic deposits reported between wells of Edgeøya and Hopen (Harland, 1997) indicate higher subsidence in the southeast of the Svalbard Platform that potentially reflects a regional slope and deeper waters towards the shelf located southeast.

Fig. 8 A depositional model for the formation of the De Geerdalen deposits on Edgeøya around the Carnian time period featuring a large prograding delta-plain advancing NW and increasingly W across the Barents Shelf (from Anell et al., submitted). Triassic stratigraphy of Svalbard and Barents Shelf, grey boxes mark a hiatus; modified after Riis et al., (2008); Formations ages are from Vigran et al., (2014), Paterson & Mangerud (2015), Smelror et al., (2018); Rismyhr et al., (2019);



		West Spitsbergen	East Svalbard	Edgeøya	Barents Shelf	
Triassic	Upper	Rhaetian	Hiatus	Neogene erosion	Tubåen Fm.	
		Norian	Flatsalen Fm.		Flatsalen Fm.	Hiatus
		Carnian	De Geerdalen Fm.	De Geerdalen Fm.	De Geerdalen Fm.	Fruholmen Fm.
	Middle	Ladinian	Tschermakfjellet Fm.	Tschermakfjellet Fm.	Tschermakfjellet Fm.	Snadd Fm.
		Anisian	Bravaisberget Fm.	Botheheia Fm.	Botheheia Fm.	Kobbe Fm.
		Olenekian	Tvillingodden Fm. Vardebukta Fm.	Vikinghøgda Fm.	Vikinghøgda Fm.	Klappmyss Fm. Havert Fm.
	Lower	Induan				

In the early to middle Triassic the Svalbard Platform was covered by a shallow shelf that was filled with sediments sourced from the east and west (the Sassendalen Group; Figs 3 and 8; Mørk et al., 1982, 1999). By Late Ladinian the western source was not active and deltaic systems advancing towards north-west across the Barents Shelf reached and probably crossed over Svalbard (Kapp Toscana Group; Figs 1, 3 and 8; Riis et al., 2008; Høy & Lundschieen, 2011; Anell et al 2013; Klausen et al., 2019). The main source areas for the deltaic system were the Uralide Mountains and the Fennoscandian Shield (Riis et al., 2008; Glørstad-Clark et al., 2010; Høy & Lundschieen, 2011; Anell et al 2013; Klausen et al., 2017).

Towards the latest Triassic and Early Jurassic the subsidence of the basins in the central part of the Barents Sea and Svalbard Platform gradually decreased (Ryseth, 2014). This process is linked to the movement of the Novaya Zemlya Fold -and-Thrust Belt and development of a forebulge with associated hiatuses, subaerial unconformities and condensed units. In Spitsbergen it is recorded with a 20 m thick sandstone-shale unit of the Rathanian to Pliensbachian (Drachev, 2016; Faleide et al., 2018; Olausen et al., 2018; Müller et al., 2019; Rismyhr et al., 2019).

Late Jurassic sedimentation organic-rich marine strata (Adventdalen Group; Figs 2 and 3) occurred in renewed regional subsidence (Olausen et al., 2018; Koevoets et al., 2016, 2018). Subsequently, in Early Cretaceous the entire northernmost Barents Sea and northern Svalbard were uplifted and eroded as a consequence of the opening of the Amerasin Basin accompanied with magmatism of the High Arctic Large Igneous Province (HALIP; Maher, 2001; Buchan, et al., 2006; Polteau et al., 2016; Minakov et al., 2012; Corfu et al., 2013; Senger et al., 2014; Petrov et al., 2016). The southward tilt resulted in the progradation of sand-rich deposits towards the south, south east and south west (Steel & Worsley, 1984; Gjelberg & Steel, 1995; Worsley, 2008;

Midtkandal & Nystuen, 2009; Marin et al., 2016; Grundvåg & Olausson, 2017; Grundvåg et al., 2017; 2019).

Cenozoic

Transpressional tectonics in the Paleogene has formed the West Spitsbergen Fold-and-Thrust Belt (WSFTB; Fig. 2) that is linked to the Eurekan deformation and plate reorganization in the north Atlantic (Dallmann et al., 1993; Braathen et al., 1995, 1999; Maher & Braathen, 1995; Bergh et al., 1997, Faleide et al., 2008; Blinova et al., 2013, Piepjohn et al., 2015). A north-south striking foreland basin (the Central Tertiary Basin, CTB) that stretches from Kongsfjorden in north to the southern tip of Spitsbergen was filled with up to 2 km thick Paleogene deposits (Figs 2-3; Steel et al., 1981, 1985; Helland-Hansen, 1990; Müller & Spielhagen, 1990; Brun & Steel, 2003; Jochmann et al., in press). The compressional stress of Eurekan deformation was transferred further east and reactivated older lineaments, including the Billefjorden Fault Zone (Fig. 2; Haremo & Andersen, 1992; McCann & Dallmann, 1996; Bælum & Braathen, 2012). Subsequently, the Oligocene transtension led to the formation of a passive margin west of Spitsbergen (Faleide et al, 2008; Lasabuda et al., 2018).

The present elevated position of Svalbard in respect to the Barents Shelf was formed by the Late Cretaceous uplift combined with Eurekan deformation, coupled with isostatic rebound in the Holocene (Dimakis et al., 1998; Worsley, 2008; Henriksen et al., 2011). This resulted in present day exhumation of the metamorphic succession and the sedimentary cover (Fig. 2).

The Billefjorden Trough

Article 1 and Article 2 present a tectono-sedimentary evolution of the Serpukhovian-Moscovian Billefjorden Trough (Figs 3 and 6). The Billefjorden

Trough is ca. 25 km wide continental rift basin developed on the hanging wall of the east dipping Billefjorden Fault Zone (BFZ; Figs 9 and 10) Cutbill & Challinor, 1965; Holliday & Cutbill, 1972; Harland et al., 1974; Johannessen, 1980). The syn-rift basin fill initiated in Serpukhovian and continued at least to the Moscovian, potentially extending to the Gzhelian/Kasimovian (Fig. 6; Dallmann, 1993). Minor, post-rift fault activity along the BFZ persisted into the Permian (Stemmerik & Worsley, 2005; Maher & Braathen, 2011; Ahlborn & Stemmerik, 2015; Sorento et al., 2019). The westward thickening basin fill consists of up to 2000 m of mixed siliciclastics, evaporites and carbonates deposited in an arid subtropical climate (Fig. 9-10 Cutbill & Challinor, 1965; Holliday & Cutbill, 1972; Johannessen, 1980; Johannessen & Steel, 1992; Articles 1 and 2).

Billefjorden Fault Zone

Significant N-S striking fault zones in Svalbard, including the Billefjorden Fault Zone (BFZ; Figs 1 and 2), are inherited from the Caledonian orogeny (Harland et al., 1974). The BFZ stretches out from the Wijdefjorden in the north through central Spitsbergen (Fig. 2; Harland et al., 1974; Lamar et al., 1986; Haremo & Andersen, 1992; Manby et al., 1994; McCann et al., 1996; Bælum & Braathen 2012). On seismic profiles, the BFZ can be traced southwards under Mesozoic cover into Storfjorden (Fig. 7; Haremo et al., 1990; McCann & Dallmann, 1996; Bælum & Braathen, 2012). The extent of the BFZ is also indicated by aeromagnetic data (Johannessen & Steel, 1992). The BFZ consists of an array of steep faults that generally dip to the east and show varying displacements and geometries along the strike (Haremo et al., 1990; Bælum & Braathen, 2012). Some of the faults have been reactivated repeatedly in different stress regimes (e.g. Haremo & Andersen, 1992; McCann & Dallmann, 1996; Bælum & Braathen, 2012).

The Billefjorden lineament juxtaposes the Ny Friesland pre-Caledonian basement on the hanging wall (Hecla Hoek succession in Harland (1969)) against the deformed Devonian basin fill of the Nordfjorden High block (Figs 2, 9 and 10; Harland et al., 1974; Johannessen, 1980). In central Spitsbergen this contact is exposed along the Balliolbreen Fault (BF) that dips to the east and shows a reverse offset of ca. 10 km (Fig. 10; Bælum & Braathen, 2012). The basement of the Ny Friesland High is formed by green schist to amphibolite metamorphic facies of Atomfjella Complex, deformed and metamorphosed during the Caledonian orogeny (Harland 1969, 1997; Bazarnik et al., 2019). The metamorphic basement underlying the Billefjorden Trough exposes a few km wide shear zone of Caledonian age that predates the brittle deformation along BFZ (Harland 1974) and forms an important boundary of basement provinces (e.g. Harland, 1974; Michalski et al 2011; Bazarnik et al., 2019). The sinistral deformation associated with lower amphibolite - uppermost greenschist facies was dated recently to ca. 420 Ma (Majka pers. comm.) In Billefjorden, the Nordfjorden High comprises Devonian red to brown continental to marine siliciclastics deposited in a wide basin (e.g. Blomeier et al., 2003). The Devonian basin fill was deformed during a compressional west-directed folding and thrusting, correlated with the large magnitude transtension of the Svalbardian event that took place after Late Famennian (Piepjohn et al., 2000; Bergh et al., 2011).

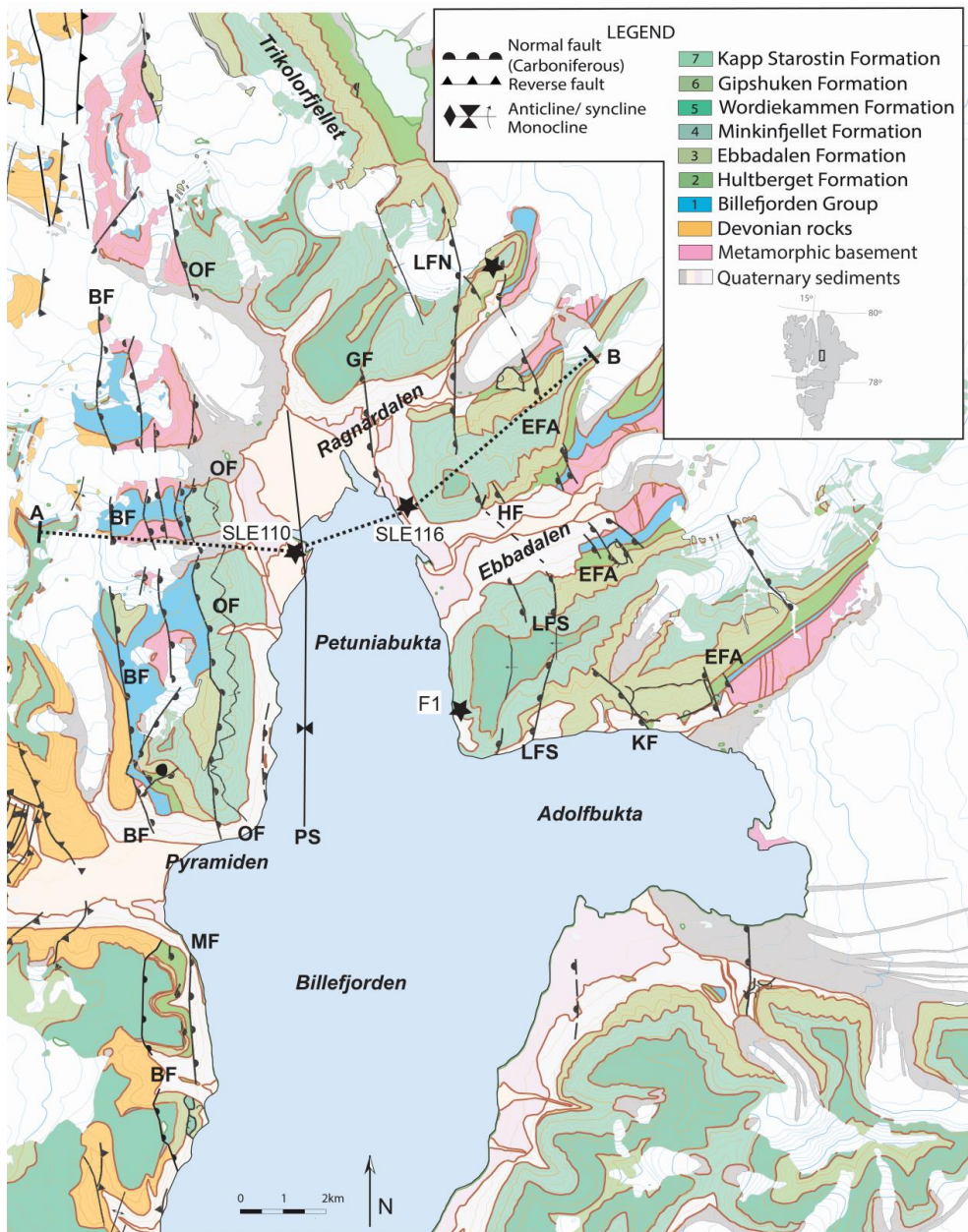


Fig. 9. Geological map of inner Billefjorden, modified from Dallmann et al., (2004). BF- Balliolbreen fault, OF- Odellfjelet fault, MF- Mimmerbukta fault, GF- Gizehfjellet fault, LFN- Lovehøvdn fault north, LFS- Lovehøvdn fault south,

LFZ- Lovehøvdén fault zone, HF- Hultberget fault, KF- Kampesteindalen fault, EFA- Ebbabreen fault array, PS- Petuniabukta syncline; SLE110 and SLE116- position of Russian wells from Verba (2013).

In the Carboniferous, the main offset of the BFZ was accommodated along the extensional Odellfjellet fault that dip to the east (OF; Figs 9 and 10; Braathen et al., 2011). The dip-slip movement along the OF offsets the metamorphic basement by approximately 2 km. The extensional displacement along OF led to the development of the hanging wall Petuniabukta syncline (PS), with a steep western limb gentle passing eastward towards the dipslope basin. Near Pyramiden, the extensional displacement was transferred along a relay zone to the BF (Figs 9 and 10; Braathen et al., 2011) and the recently mapped Mimerbukta fault (MF; Fig. 9).

The dipslope located east from BFZ was segmented by an array of antithetic, i.e. west dipping, syn-depositional faults (Figs 9 and 10; Maher & Braathen 2011; Braathen et al., 2011; Articles 1 and 2). The dipslope faults include, from the east: Ebbabreen Fault Array, EFA (Ebbabreen Fault in Harland et al., (1974) and basement Fault in Braathen et al., (2011); Kampesteindalen Fault, KF, Løvehovden Fault Zone, LFZ (Løvehovden Fault in Maher & Braathen (2011) and Braathen et al., (2011)), Hultberget Fault, HF and Gizehfjellet Fault, GF. Some of the faults were reactivated with reverse offsets of 50-200 m in the Paleogene during the Eurekan tectonic event (Haremo & Andersen, 1988; Haremo et al., 1990; Manby et al., 1994; McCann & Dallmann, 1996; Braathen et al., 1999; Bergh et al., 2000, Bælum & Braathen 2012).

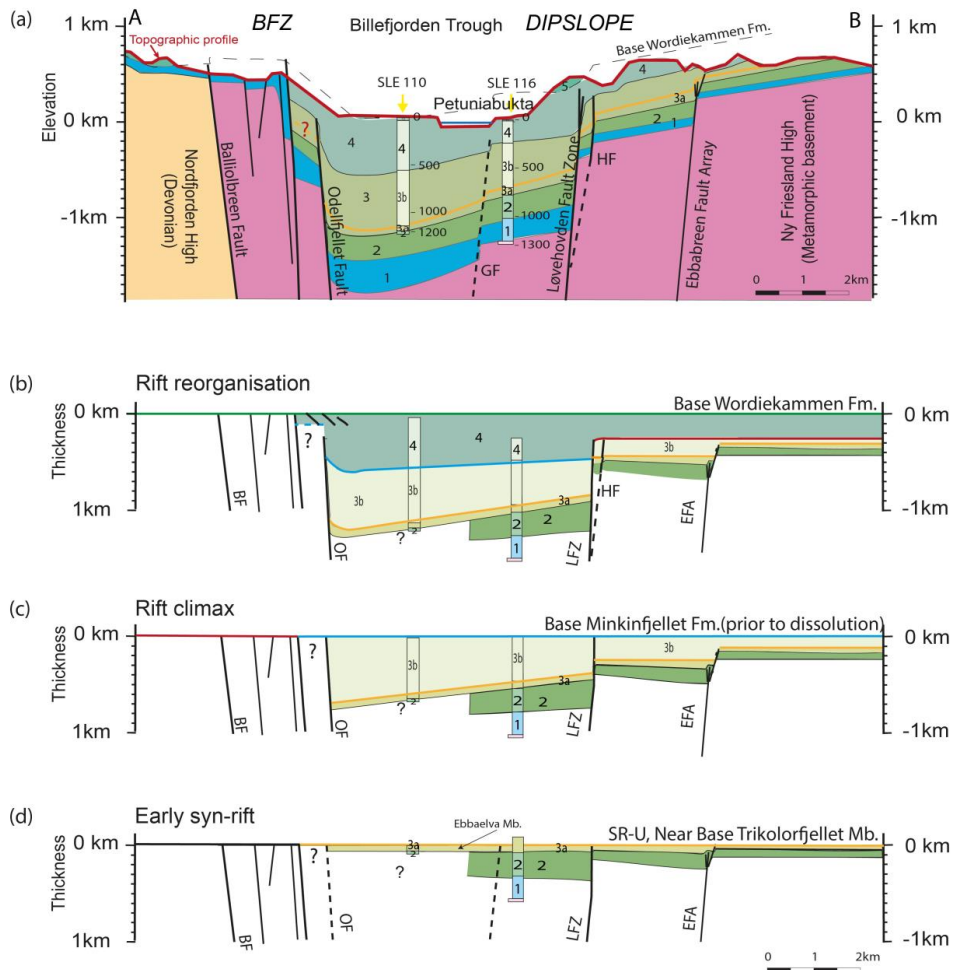


Fig. 9 (a) Geological cross-section AB, modified from Braathen et al., (2011)
 See Fig. 8 for location of the cross-section and for a legend of the involved formations; **(b-d)** conceptual reconstruction of the deposition along profile AB, from Article 2. Litostratigraphic columns are from boreholes from Verba (2013).
 BF- Balliolbreen fault, OF- Odellfjellet fault, GF- Gizehfjellet fault, LFZ- Loveshøvdan fault zone, HF- Hultberget fault, EFA- Ebbabreen fault array; SR-U- Shoreface ravinement unconformity (from Article 1).

Deposition within the Billefjorden Trough

Exposures of the Billefjorden Trough deposits stretch along the 60 km- long section in central Spitsbergen (Figs 1 and 9). The basin fill to the north has been eroded while further south was covered by Mesozoic platform deposits. Westwards thickening and coarsening syn-kinematic succession towards the BFZ that bounds the basin to the west define the half-graben fill geometry (Fig. 10; Gjelberg & Steel, 1981; Johannessen & Steel, 1994; Braathen et al., 2011). To the east the basin fill onlaps Lower Carboniferous strata and metamorphic basement of Ny Friesland block (Holliday & Cutbill, 1972).

Pre-rift stratigraphy

In central Spitsbergen, the Lower Carboniferous Billefjorden Group deposits overly the folded and thrust-faulted Devonian strata and metamorphic basement (Fig. 6). In the Billefjorden area, the Billefjorden Group is composed of up to 250 m thick yellow, mature sandstones interfingering with coal seams, dark shales and conglomerates (Holliday & Cutbill, 1972; Cutbill et al., 1976; Gjelberg & Steel, 1981). Those deposits represent a humid climate of the Late Tournaisian to Visean age (Gjelberg & Steel, 1981; Piepjohn et al., 2000). This succession is preserved in faulted blocks formed during younger deformation, hampering the reconstructions of basin configuration (Cutbill & Challinor, 1965; Gjelberg & Steel, 1981, Braathen et al., 2011; Koehl & Muñoz-Barrera, 2018). In the Billefjorden area, however, the deposits of the Billefjorden Group are exposed within and outside of the Billefjorden Trough while thicknesses and facies changes cannot be clearly correlated with any of the known Pennsylvanian-age faults. Therefore, the deposition of the Billefjorden Group pre-dates the syn-rift succession (Braathen et al., 2011; Article 1).

Syn-rift stratigraphy

The syn-rift fill of the Billefjorden Trough consists of the Late Serpukhovian Hultberget Formation, the Bashkirian Ebbadalen Formation and the Moscovian Minkinjellet Formation (Fig. 6; Cutbill & Challinor, 1965; Holliday & Cutbill, 1972; Johannessen, 1980; Johannessen & Steel, 1992; Dallmann, 1993). The late syn-rift fill to post-rift fill also includes the lower Wordiekammen Formation (Maher & Braathen, 2011; Ahlborn & Stemmerik, 2015). The syn-rift deposits are characterized by rapid facies and thickness variations along and across structural elements. The first phase consists of a mixture of continental and shallow marine siliciclastic deposits, with few evaporite and carbonate beds. In the second and third phase of basin evolution, widespread mixed carbonate and evaporite facies prevail, interbedded with alluvial fan deposits and a few siliciclastics in shallow marine and fluvial belts, accompanied by many local unconformities (Cutbill & Challinor, 1965; Johannessen & Steel, 1992; Article 1 and 2).

Hultberget Formation

The syn-rift phase begins in the (late ?) Serpukhovian with minor fault movement (Article 1) during the deposition of red coloured shales and sandstones of Hultberget Formation (Johannessen, 1980; Johannessen & Steel, 1992). The Hultberget Formation has a typically unconformable lower boundary towards the Billefjorden Group. The formation is composed of up to 150 m of red beds (Gjelberg, 1984) of varying thickness across the basin. The red-coloured mudstone and siltstone dominated formation is intersected by calcrete paleosols and flat laminated or cross stratified fine and medium-grained red-coloured sandstones and scattered conglomerates. Holliday & Cutbill (1972), Gjelberg (1984) and Johannessen & Steel (1992) interpreted the formation to represent an extensive alluvial flood basin deposited within an

arid to semi-arid climate. The sandstone and the few conglomerates represent ephemeral stream deposits. In older studies the Hultberget Formation was classified as the Hultberget Member that was included in the Billefjorden Group (Cutbill & Challinor, 1965; Holliday & Cutbill, 1972; Cutbill et al., 1976).

Ebbadalen Formation

The Bashkirian Ebbadalen Formation (Cutbill & Challinor, 1965) consists of the lower siliciclastic-dominated Ebbaelva Member and the upper evaporites and carbonate-rich Trikolorfjellet Member, which passes laterally into alluvial fans of the Odelfjellet Member (Johannessen & Steel, 1992). The formation has been often referred to as transition beds in a transgressive system from continental red beds of the Hultberget Formation to the overlying marine-dominated Minkinfjellet Formation (Cutbill & Challinor, 1965; Holliday & Cutbill, 1972). The lower boundary, previously described as an unconformity (Cutbill & Challinor, 1965; Holliday & Cutbill, 1972), is marked by a subaerial exposure surface (Article 1).

The lower **Ebbaelva Member** (Holliday & Cutbill, 1972) is a siliciclastic-dominated succession of up to 165 m thick alluvial and nearshore marine sandstones and shales with thin carbonates and evaporates intercalations. The Ebbaelva Member represents braided stream, playa lake, salinas, lagoonal, shabka and barrier shoreline deposits (Holliday & Cutbill, 1972; Johannessen, 1980, Article 1). The mixed continental nearshore marine strata were deposited in several hundred meters to kilometres scale sub-basins developed in the hanging wall blocks of growth faults (Article 1). Two basin-scale back-stepping facies association belts are suggested to form due to marine transgression associated with the opening of a connection to the sea in the north (Article 1).

The **Odellfjelet Member** is developed along the BFZ and consists of up to 400 m of red, grey and yellowish coloured conglomerates and sandstones, and yellow dolomites, interpreted as alluvial fans, fan-deltas, with subordinate shoreline and aeolian deposits of an arid to semiarid climate (Johannessen, 1980; Johannessen & Steel, 1992). The source for a coarse material was the Devonian strata eroded from the uplifted footwall block of the BFZ. The alluvial fans were confined to the relays and proximal hanging wall of the BFZ. These alluvial fans document a transverse drainage pattern along relay ramps (Braathen et al., 2011).

The **Trikolorfjellet Member** is dominated by up to 240 m thick white gypsum/anhydrite layers interbedded with black carbonates, black and red shales that represent alluvial, tidal to open marine conditions (Holliday & Cutbill, 1972; Johannessen, 1980; Johannessen & Steel, 1992). Each of the ca. 30 carbonate- gypsum couples represent cyclic salinas to open marine conditions controlled mostly by eustatic sea level changes (Article 2). A thick package of red shale in the lower part as well as red-shale and sandstone interval in the uppermost part are correlated with the two cycles of prograding alluvial fans of the Odellfjellet Member (Article 2).

The Minkinfjellet Formation

The mixed carbonate-evaporite dominated Minkinfjellet Formation (Minkinfjellet Member in Cutbill & Challinor, 1965) is subdivided into Carronelva, Fortet and Terrierfjellet members. The formation has been deposited in shallow, tidally influenced marine basin onlapping the Ny Friesland block to the east (Dallmann, 1993; Lønøy, 1995; Eliassen & Talbot, 2003). The lower, **Carronelva Member** consists of mixed carbonates, evaporites with minor clastic beds delivered from subaerially exposed structural highs

(Eliassen & Talbot, 2003). The upper **Terrierfjellet Member** is depleted in siliciclastics due to the basin transgression (Eliassen & Talbot, 2003).

The **Fortet Member** is developed locally and consists of carbonate breccia formed by karstification of the carbonate-evaporite succession of the Minkinfjellet Formation and Trikorfjellet Member due to the dissolution of gypsum beds (Lønøy, 1995; Eliassen & Talbot, 2003). The vertical breccia bodies (pipes) of the Fortet Member are located along the faults (i.e. Løvehovden Fault Zone) and are interpreted to form in Lower Permian, in a post-rift phase of the Billefjorden Trough (Eliassen & Talbot, 2003, 2005).

Horizontal stratiform breccias (Eliassen & Talbot, 2003, 2005) are located along the flanks of the Billefjorden Trough. Article 2 links their development with uplifted footwall blocks of syn-sedimentary faults. A corresponding succession located in the central part of the Billefjorden Trough, along down-faulted block of Løvehovden Fault Zone, is rich in gypsum that was protected from dissolution (Article 2).

Wordiekammen Formation

The late syn-rift phase involves the lower member of the Wordiekammen Formation (the Cadelfjellet Member) which covers both flanks of the Billefjorden Trough but it thickens within the basin (Maher & Braathen, 2011; Pickard et al., 1996; Ahlborn & Stemmerik, 2015). The formation starts with an unconformity at the base of the 'Black Crag beds' (Cutbill & Challinor, 1965; Dallmann, 1993). This boundary coincides with a transition from a dolomite-dominated sequence of Minkinfjellet Formation to an overlying limestone-dominated section.

Upper Triassic deltaic system in the eastern part of Svalbard

Articles 3 and 4 focus on the outcrops of growth faults located in Kvalpynten, Edgeøya that developed in prodelta and distal delta front deposits (Fig. 2).

In Triassic, the Late Palaeozoic basin subsidence slowed down and several internal basin highs were established in the Barents Sea and also the Svalbard platform formed as a high (Fig. 1; Faleide et al., 1984, 2015; Anell et al., 2014, 2016, 2019). This structural high caused a pronounced paleo-slope along its eastern flank, dipping against the deltaic sediments prograding from the south-east. Significant decrease in the accommodation impacted a lack of aggradation and differential advancement rates of the clinofolds (Anell et al., 2013, 2016)

In the latest Permian and Triassic, the Barents Shelf and Svalbard were a boreal, epicontinental basin with water depths in the range 200–400 m (Anell et al., 2014; 2016; Høy & Lundschieen, 2011). From latest Permian in the east the basin was progressively filled by a mud and fine grained immature sand-dominated deltaic system that sourced debris mainly from the Uralides to the southeast, and partly from the Baltic shield to the south (Riis et al., 2008; Worsley 2008; Glørstad-Clark et al., 2011; Høy & Lundschieen 2011; Klausen et al., 2015, 2017, 2019; Eide et al., 2017, Rossi et al., 2019). This depositional system is expressed as sets of northeast-prograding clinofolds in seismic data (Fig. 1; Riis et al., 2008; Worsley 2008; Glørstad-Clark et al., 2010, 2011; Høy & Lundschieen 2011; Lundschieen et al. 2014; Klausen et al., 2015, 2017; Anell et al., 2014, 2016). This gigantic Triassic deltaic system reached the Svalbard Platform in the Carnian to Early Norian (Høy & Lundschieen 2011, Anell et al., 2014) and is represented by the De Geerdalen Formation (Fig. 11; Høy & Lundschieen 2011; Klausen et al., 2014, 2015, 2018, 2019). Later in the Early Norian, the Barents Sea and Svalbard, along with a large part of the

Arctic, were flooded (Johannessen & Embry, 1989; Ryseth, 2014; Klausen et al., 2015; Lord et al., 2019; Rismyhr et al., 2019).

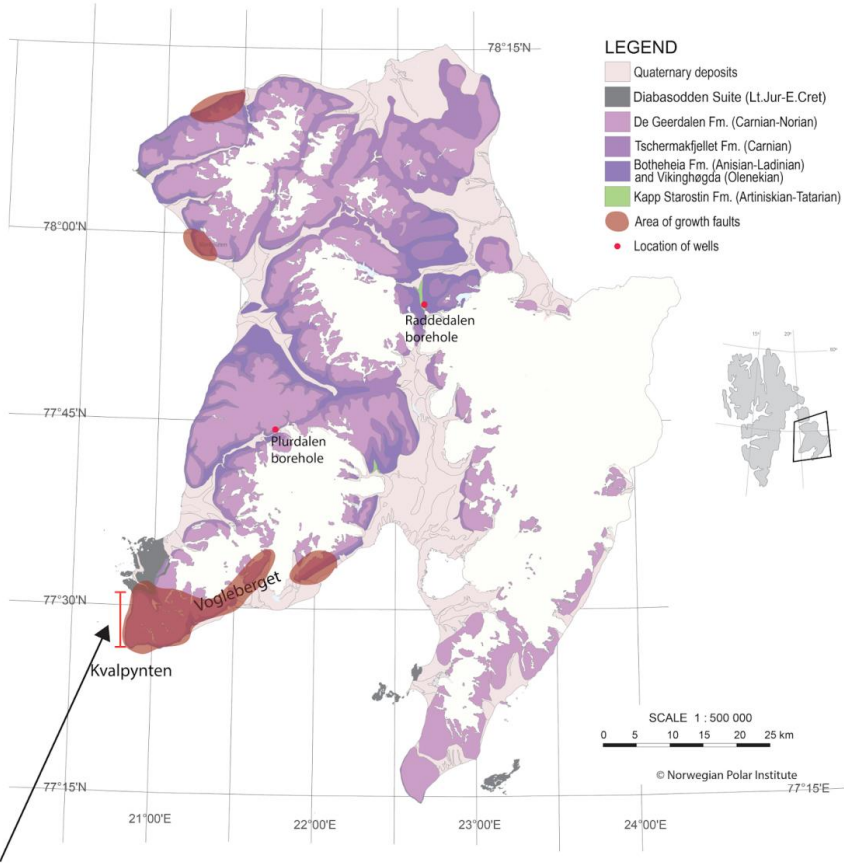
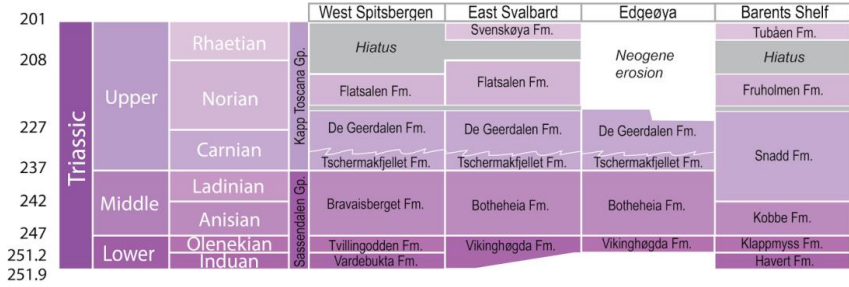
Fig. 11 (next page). Geological map of Edgeøya. The position of study area in Kvalpynten is outlined. Location of reported growth faults is marked in red.

Below: photography and photogrammetric model of Kvalpynten.

Photogrammetric models can be found: Kvalpynten west:

<https://www.svalbox.no/portfolio/kvalpyntenwest/> and Kvalpynten south:

<https://www.svalbox.no/portfolio/kvalpyntensouth/>



Kvalpynten



The outcrops of Edgeøya record a deltaic system, where the offshore marine black organic-rich mudstones of the Anisian-Ladinian Botneheia Formation are overlain by prodelta mudstones and siltstones of the Tschermakfjellet Formation, and delta front to delta top sandstones and mudstones with thin coal seams of the De Geerdalen Formation (Figs 8 and 11; Mørk et al., 1982, Høy & Lundschein 2011). The Botneheia Formation exposes as bluish-weathering organic-rich black shales deposited under anoxic to dysoxic sea floor conditions (Mørk et al., 1982; Mørk, 1999; Mørk et al., 1999; Krajewski, 2008). The offshore analogue to the Botneheia Formation is a prolific source rock in the southwestern Barents Sea (Worsley, 2008, Henriksen et al., 2011). The Tschermakfjellet Formation (Mørk et al., 1982) is composed of dark grey, silty shale and siltstones with thin sandstone beds. The De Geerdalen Formation represents forward and backstepping delta and paralic deposits that include the deposits of: inner shelf, delta front, shoreline, tidal flats, delta- and coastal plain with paleosols and thin coal seams and alluvial environment (Flood et al., 1971; Mørk et al., 1982; Mørk et al., 1999; Klausen & Mørk 2014; Rød et al., 2014; Lord et al., 2014). Tidal influence is common in all nearshore marine facies (Röhner, 2016; Haile et al., 2018; Anell et al., submitted).

Growth faults with tens to hundreds of meters of offsets are developed on Edgeøya (at Klinkhamaren, Øhmanfjellet, Tjuvfjordskarvet and Kvalpynten) as well as on Wilhelmøya, in prodelta to delta front shales and sandstones of the Tschermakfjellet and De Geerdalen formations (Figs 8 and 11; Edwards 1976; Riis et al., 2008; Anell et al., 2014; Rød et al., 2014; Osmundsen et al., 2014; Article 4). The faults strike WNW-ESE and show normal, dip-slip movement, with local strike slip components (Anell et al., 2013; Osmundsen et al., 2014; Article 4). In Kvalpynten, the succession is segmented by listric and planar growth faults into 12 isolated, 200-800 m wide grabens and half-grabens situated in prodelta to delta slope (Article 3 and 4). The growth faults' hanging wall basins contain shales and sandstones arranged in coarsening-upward

units (Edwards, 1976; Osmundsen et al., 2014; Article 3). The growth fault activity abruptly ceased as indicated by continuous draping shale deposited during a flooding event (Osmundsen et al., 2014; Article 3). Syn-kinematic succession was followed by the undisturbed deposition of the De Geerdalen Formation.

Data and methods

Research presented in this thesis explores onshore outcrops using diverse techniques that include: sedimentological logging, structural measurements and traditional geological field mapping with Field Move App integrated with mapping on aerial images (ArcGIS) and detailed 3D model interpretations (in LIME). Article 2 is to a large extent based on mapping helicopter-based LIDAR scans acquired in the inner part of Billefjorden in 2007, and draped with ca. 1800 high resolution pictures (e.g. Rittersbacher et al., 2013). In article 3 an analysis of 9-km long section of the photogrammetric outcrop model around southern Edgeøya has been performed. The photogrammetric model was created with GPS-oriented images from a Canon EOS 6D, collected from boats in 2014 at a fixed distance from the cliffs. The Structure from Motion (SfM) method (e.g. Chandler & Buckley, 2016) was applied to create a high-resolution digital elevation model that was draped with the detailed outcrop photographs, which allowed examination of basin-fill geometries on scales of metres to hundreds of metres. Both lidar and photogrammetric model were interpreted by the author in LIME software (Buckley et al., 2019). LIME allows for the measurement of distance between points, and the three-point determination of the strike and dip of surfaces.

Location 1: Billefjorden, North-central Spitsbergen.

Articles 1 and 2 describe a ca. 160 km² area dominated by Carboniferous strata. The main focus was on outcrops located east of Petuniabukta (From Wordiekammen to Sfinksen) and near Pyramiden (Figs 2 and 9). Updates on the geological map by Dallmann et al., (2004) include also ca. 10 km² at Odellfjellet and 14 km² at Trikolorfjellet.

Carboniferous syn-rift strata have been studied during 10 field- trips in spring and summer seasons from 2012 to 2016, amounting in total duration to ca. 15

weeks. Article 1 presents 27 sedimentary logs with cumulative length of 1778 m. Article 2 includes analysis of 1150 m of newly logged succession, combined with 2500 m of stratigraphy covered by Russian wells 110 and 116 (Verba, 2013) and 400 m of logs published by Eliassen & Tabot (2003).

Location	Article	3D model type	Aquisition year	Nb. of pictures	3D model resol.	Sediment. logs in 1:50
Billefjorden	1					1778 m
Billefjorden	2	LIDAR	2008	1800	around 50 cm/pix	1150 m
Kvalpynten	3	Photogrammetry	2014	>4000	21.6 cm/pix	1511 m
Kvalpynten	4	Photogrammetry	2014	>4000	21.6 cm/pix	

Table 1. New dataset that contributes to scientific articles 1-4.

Location 2: Edgeøya, Kvalpynten

Article 3 and part of Article 4 focus on ca. 12 km² of Upper Triassic deposits in Kvalpynten, SE Edgeøya. The 9 km long cliff section has been reproduced on the photogrammetric model. Edgeøya was visited by the author twice. In 2012, 8 field days were mainly located in Kvalpynten. In 2014, 2 weeks long fieldwork included locations on Edgeøya, i.e. Kvalpynten (Articles 3 and 4) and Svartpynten (Article 4), and Wilhelmøya (Appendix A). 1511 m of logs in 1:50 scale was collected on Edgeøya by Trias North project participants; digitized by the author in 1:50 and 1:400 scale and followed by sedimentary facies analysis. The 680 m of logs contributed to the analysis presented in Article 3.

Limitations of expansion index

The expansion index (E; Thorsen, 1963; Groshong, 2006) is widely used to constrain the growth history of a syn-depositional fault and is expressed as:

$$E = T_{HW}/T_{FW}$$

where T_{HW} is the hanging wall thickness, measured at a profile perpendicular to fault strike and as close to the fault as possible to obtain the maximum thickness. T_{FW} is the footwall thickness. To make the equation valid, T_{FW} must exceed zero, therefore E cannot be used in cases with erosion or non-deposition on the footwall (i.e. the thickness of a layer in a footwall cannot be zero).

In the pre-kinematic interval $E = 1$. Values $E > 1$ indicate an increase of syn-kinematic deposition on the hanging wall during the fault growth. If $E < 1$, it means that the syn-kinematic deposition dominates on the footwall (fault shows reverse kinematics).

In Article 2, the evolution of fault arrays/zones in rift basins is discussed by using '*stratigraphic throw*' and '*incremental fault throw*'. These parameters are more suitable than the expansion index in rift basin studies where footwall strata are missing due to erosion or a non-deposition (e.g. Liu et al., 2017). Fault displacement (i.e. the difference between the final and initial positions of a point measured along the fault plane; green arrow on the Fig. 12) is the cumulative result of multi-episodic fault activity and a parameter typically used to describe deformation along the fault. In Billefjorden, due to the scree-cover of parts of the faults and the monoclinical character of the strata located above the brittle faults, displacement cannot be calculated and, therefore, *Stratigraphic throw* (ST; blue arrow on the Fig. 12) has been used. ST is expressed as the elevation difference (Z) between the base of the marker bed

on the footwall (Z_n FW) and hanging wall (Z_n HW) blocks compensated for a regional tilt (Z_D in Fig. 12).

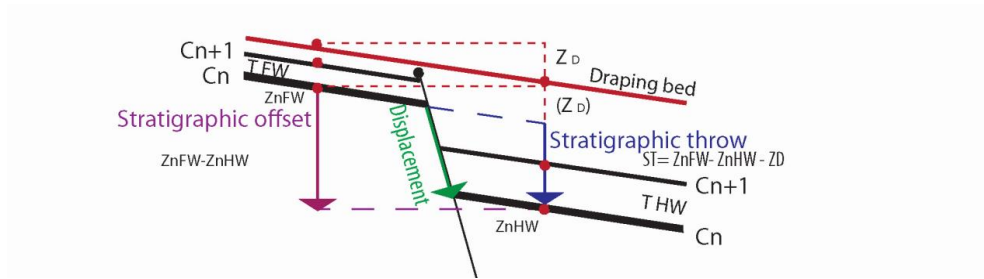


Fig. 12. Explanation of measured elements: n - number of bed. C -carbonate marker bed; T - thickness;

The elevations of the following layers (red dots, C_n , C_{n1} , C_{n2} ...) have been measured in the lidar model along semi-vertical profiles, on the footwall (Z_{nFW}) and the hanging wall (Z_{nHW}) with the same distance from the fault. The regional dip of the bedding has been calculated using elevation differences along a surface that drapes the fault (Z_D) and extracted from the calculated throw ($ST = Z_{nFW} - Z_{nHW} - Z_D$). ST values have been plotted against the elevation of the bed on the footwall (Z_{nFW}/ST plots in Article 2).

The 'incremental fault throw' (IFT) of a growth fault is the thickness difference of corresponding beds between the hanging wall and footwall fault block. It has been preferred over the commonly used *expansion index* (Jackson & Rotevatn, 2013; Reeve et al., 2015) to compensate for potential hiatuses or erosion in the footwall (e.g. Liu et al., 2017). The thickness of intervals (T), i.e. the elevation differences between the two following marker beds, $T = C_{n2} - C_{n1}$ (n - number of a following bed) were calculated in the footwall (T_{FW}) and hanging wall (T_{HW}) blocks. In the next step, the footwall thickness has been subtracted from the hanging wall thickness $IFT = T_{HW} - T_{FW}$ as a measure of *incremental fault throw*. In Article 2 the *incremental fault throw* has been

plotted against an average elevation of the interval on the footwall. The calculations do not include decompaction.

Summary of the scientific articles

Article 1

Article 1: "Sedimentary architecture during Carboniferous rift initiation - the arid Billefjorden Trough, Svalbard" is the first of two articles that address the sedimentary architecture of the Carboniferous (Serpukhovian to Moscovian) Billefjorden Trough. The Billefjorden Trough is a north-south striking rift basin filled with mixed, siliciclastic evaporite and carbonate facies deposited in a warm and arid climate. This study focuses on the early syn-rift fill that is dominated by siliciclastics of Late Serpukhovian- Early Bashkirian age (i.e. Hultberget Formation and Ebbaelva Member of the Ebbadalen Formation; Phase 1).

The basin fill begins with aggrading deposits (Stage 1) that consist of red shale and fluvial sandstones developed in continental settings. The transition from Stage 1 to Stage 2 marks an opening of connection with the sea and basin transgression. Following Stages 2 and 3 are represented by two backstepping paralic units of fluvial, deltaic and shallow marine sandstones and shales with minor evaporite and carbonate beds. In this study we define a number of widespread syn-sedimentary, meso-scale faults that have affected the distribution of sedimentary facies and internal drainage pattern in the basin. Through the analysis of the architecture of syn-kinematic deposits we discuss how the fault grows in length. In periods of increased tectonic activity, the fault's hanging wall blocks hosted standing water bodies, such as lagoons or playa lake, while non-deposition or condense succession developed in the footwall position. Syn-sedimentary faults impacted also the principal axial drainage in the basin.

The analysis of early syn-rift deposits (Phase 1) along the westward-eastward oriented profile allows recognition that the basin fill was segmented within a number of faulted blocks 1.5- 3 km wide. Overall, however, the accommodation was fairly symmetrical and the basin resembles a graben structure.

Article 2

Manuscript 2 entitled: “Impact of dip-slope growth faults on mixed carbonate-evaporite dominated deposits – Carboniferous Billefjorden Trough in Svalbard, Norway” is a second article also focusing on the evolution of the north-south striking mid- Carboniferous Billefjorden Trough. The basin fill consists of mixed, siliciclastic evaporite and carbonate facies deposited in a warm and arid climate. In this study the focus was on successions that belong to Upper Ebbadalen and Minkinfjellet Formations (Phases 2 and 3 of basin development). This succession is dominated by evaporites and carbonates interfingering with conglomerates and sandstones near the boundary towards the Billefjorden Fault Zone to the west. This article takes advantage of the integration of numerous data sets, including sedimentary logs, field mapping, two published lithostratigraphic columns from boreholes and a lidar scan 3D model that covers an extensive part of the study area.

This research demonstrates impacts of faults on evaporite- carbonate deposits. Detailed analysis of the lidar model allowed the identification of two interacting and linking fault segments. The zones of highest footwall uplift are marked by subaerial dissolution of evaporites and development of breccias formed by residue carbonate clasts.

This article also introduces the division of the Billefjorden Trough fill into 3 phases:

- Phase 1, early syn-rift: symmetrical graben development (addressed in Article1)
- Phase 2, rift climax: associated with asymmetric subsidence (half-graben) with formation of alluvial fans sourcing from the master fault zone (Billefjorden Fault Zone) located to the west. On the dip-slope the meso-scale faults that were initiated during Phase 1 reach their maxima

of displacement in early rift climax and gradually lose their displacement towards the Phase 3.

- Phase 3, basin reorganization and narrowing: the fault zone on the dipslope that is antithetic to the Billefjorden Fault Zone acts to balance the displacement. This structural style resulted in reorganization of the half-graben geometry of Phase 2 into a narrow, fairly symmetrical depocentre located near the fault zone where sediments were protected from dissolution and the uplifted shelf on the distal dipslope that periodically experienced subaerial exposure.

Article 3

The article: "Architecture of growth basins in a tidally-influenced, prodelta to delta-front setting: the Triassic succession of Kvalpynten, East Svalbard" addresses the sedimentary architecture of small-scale basins (hundreds of meters in width) developed in the hanging walls of growth faults in Kvalpynten, Edgeøya. The succession corresponds to the deposits of a distal deltaic system that prograded in the Triassic across the Barents Shelf, sourced mainly from the Uralides mountain chain in the southeast. The set of growth faults is displayed along the lower part of a 9 km long and 350-400 m high cliff. The sedimentary succession is segmented into 12 half-grabens and grabens that range in width between 250 and 800 m. The basin fills are organized into three to five, 25-60 m thick mudstones and sandstones coarsening-upwards units (CU) within the Upper Triassic Tschermakfjellet and Lower De Geerdalen formations. The mudstone and muddy sandstone-dominated lower part of the CU units typically shows normal graded, slumped beds and soft sedimentary structures that represent a prodelta to lower delta deltafront. This part passed upward into tidally affected heterolithic and sandstones interpreted as tidal bars and dunes detached from the delta top.

Four types of accommodation within growth basins have been recognized: fully compartmentalized basins represented by (i) half-grabens and (ii) grabens, (iii) partly disconnected, late syn-kinematic accommodation and (iv) post-kinematic accommodation not deformed by growth faults. This study also recognized eight types of architectural elements. The stacking patterns of architectural elements depend on: the relative sea level/sediment supply settings, type of accommodation (i-iv), and the relation to single faulting events that govern the erosion and local redistribution of sediments.

The growth successions are represented by both mudstones and shales and disregard the potential faulting mechanism due to a gravitational delta front collapse, rather supporting the recently proposed model of differential compaction of prodelta deposits coupled to the tectonic reactivation of deeper Palaeozoic structures. Noticeable is that development of all observed half-grabens is preceded by an initial phase of symmetric accommodation that is later transferred into asymmetric accommodation as the listric fault that dips to the south begins to dominate.

Article 4

The article entitled: “Architecture, deformation style and petrophysical properties of growth fault systems: the Late Triassic deltaic succession of southern Edgeøya (East Svalbard) “ is complementary to Article 3 and focuses mostly on the structural analysis of the growth faults developed in the Triassic succession of southern Edgeøya, with less emphasis being given to the sedimentary facies and architecture of the basin fills. The study area is broader than in Article 3 and includes two locations east of Kvalpynten. Emphasis is nonetheless given to the Kvalpynten section where the best exposures are found along a N-S oriented, ca. 350 m high cliff section.

In the study area two trends of basin-bounding faults are recognised, with a dominant E-W to NW-SE trend, and a subordinate NE-SW trend, with displacements in the order of meters to tens of meters. These faults bound the basin fills that consist of coarsening and thickening upward units of shales and sandstones up to tens of meters thick, reflecting different stages of fault growth. These are grouped into three categories based on the shape of the fault plane (planar vs. listric), and the stratigraphic level of the detachment horizon (i.e. basal shale interval). Brittle, steep and planar, deeply-rooted faults display no evidence of rotation (1st order of faults). Listric faults show evidence for ductile deformation and are flattening and sole out in the top of Botneheia Formation (2nd order of faults). The population of smaller scale, listric faults (3rd order faults) is developed in the hanging wall blocks of 2nd order faults. The 3rd order faults detach at the base of one of the shaly coarsening upward units that fill up the half-grabens.

The meso-scale observations are confirmed by micro-scale analysis informing about hydroplastic deformation predating the brittle deformation. The growth faults are interpreted to form due to differential compaction of water-saturated

mudstones facilitated by the slope dipping towards the prograding deltaic sequence and loading of the coarse delta front and top deposits. In addition, the thin-skinned failing in unstable deposits could be triggered by the reactivation of Paleozoic basement-rooted fault zones during the Uralide foreland deformation.

Discussion and conclusions

Two fault systems have been investigated in outcrops that differ in their geological context (Fig. 14). System 1, represented by the Billefjorden Trough, has formed in response to regional extension and is one of the onshore examples of rift basins that developed during the Carboniferous across the Barents Shelf (Faleide et al., 2008). System 1 is known to continue for over 60 km along strike. The basin width is estimated to be ca. 25 km, while the complementary faulted blocks were about 1.5- 3 km wide (Articles 1 and 2). System 2, studied in Kvalpynten, is exposed along a 9 km long outcrop, but similar faults are known from other locations on Edgeøya (Fig. 11), and also from Barentsøya (Mørk, pers. comm.). Individual basin widths in System 2 are 250-800 m (Article 3). The faults formed due to the differential compaction of the shale underlying the coarse deltaic sediments, accompanied by mild tectonic movements on reactivated deep-rooted faults (Anell et al., 2013; Article 4).

System 1: Billefjorden Trough

Rift initiation

The exact momentum of rift initiation is difficult to recognise in the sedimentary record (e.g. Jackson et al., 2005). In Billefjorden Trough the entire Hultberget Formation is assigned to the syn-rift unit due to its thickness decrease on the uplifted fault blocks (Johannessen, 1980; Johannessen & Steel 1992; Braathen et al., 2011). Similar arid climate, early syn-rift deposits are recorded in the Suez rift by Jackson et al., (2005) and the boundary is exposed as a subaerial erosive surface that marks the base of incised valley fill of the early syn-rift Abu Zenima Formation. Jackson et al., (2005) show that the orientation of paleo-valleys is not related to any rift-related structural trend, indicating a pre-rift topography. As in the Billefjorden case (article 1), the growth of the

early syn-rift faults in the Abu Zenima Formation can be documented higher up in the succession. Jackson et al., (2005) discuss the rate of growth along the early syn-rift faults that may be too small to overprint the pre-rift topography; therefore, the precise moment of rift initiation cannot be recognised.

In Billefjorden, the Hultberget Formation is a shale-rich unit typically covered by glacial deposits and scree which limits the interpretation of the lower part of the formation. A hiatus between the Billefjorden Group and Hultberget Formation is suggested due to some or all of the Visean and lower Serpukhovian successions missing (Dallmann et al. 1999). The recent studies suggest, however, the occurrence of the mid to late Visean deposits that belong to the upper part of Billefjorden Group and narrow the time gap between the two units (Lopez et al., 2019). It is difficult to distinguish if the erosive character of the base Hultberget Formation boundaries on the rift shoulders is due to the uplift-related erosion, or the non-deposition/condensed-deposition and passive fill of topography predating the active rifting, similar to the Suez rift case. Article 1 documents a growth section/wedge in the upper Hultberget Formation and interprets this growth fault activity as a moment of Billefjorden rift initiation. This is in agreement with Cutbill et al., (1976) who interpreted that the uplift along the East Dickson Land Axis (i.e. the footwall of the BFZ) took place near the top of Hultberget Formation (former Hultberget Member in Cutbill et al., (1976)).

An outcrop of 40 m thick succession was recently exposed due to the glacier retreat in Austfjorden, north of Billefjorden (Fig. 2) and represents the strata located below the central part of the Billefjorden Trough. This succession of meandering channel fills and overbank mudstones exposes a gradual transition from the Billefjorden Group to Hultberget Formation. This transition is expressed by a change from rooted, grey coloured overbank, with seathearth and coal beds of the Billefjorden Group, to the red-coloured overbank deposits

with rhizoliths and calcretes of the Hultberget Formation (Olaussen et. al., 2019). The exposure located on the hanging wall of the BFZ suggests a lack of major depositional breaks, erosion or a large hiatus. The transition can be largely explained by a change in the climate from humid to arid conditions. Contrary to the work by Koehl & Muñoz-Barrera (2018), no syn-depositional fault activity or any change in basin configuration between the pre-rift Billefjorden Group and the overlying lower Hultberget Formation can be documented. The syn-kinematic deposition can be seen higher up in the succession belonging to the upper Hultberget Formation (in preparation).

Rift phase/ name	Sta- ge	Member	Format- ion	Type of deposition	Active faults	Basin configurati on
1 Early syn- rift	1		Hult- berget	Continental red shales and sandstones	BF, OF?, LFZ, KF, EFA	Small sub-basins, symmetric. basin
	2	Ebbaelva	Ebba- dalen	Mixed continental and paralic	BF, OF, LFZ, KF, EFA	
	3	Ebbaelva		Mixed paralic and marine	BF, OF, PF?, LFZ, KF, EFA	
2 Rift climax		Trikolor- fjellet / Odellfjelet		Red conglomerates, sandstones and shales, evaporites and carbonates	BF, OF, PF?, MF, LFZ, HF, KF, EFA	Half-graben
3 Rift reorganization and narrowing		Carronelva and Terjefjellet	Minkin- fjellet	Evaporites, carbonates and yellow sandstones	BF, OF, LFZ, GF?	More symmetric.

Table 2. Summary of evolution of the Billefjorden Trough

Billefjorden Trough evolution

All well-known models of half-graben evolution assume the asymmetrical development of subsidence from the rift initiation phase, and the half-graben geometry is later enhanced during the rift climax phase (*sensu* Posser, 1993;

Leeder & Gawthorpe 1987; Schlische, 1991; Posser et al., 1993; Schlische et al., 1996; Ravnås & Steel, 1997, 1998; Gawthorpe & Leeder, 2000). Typically, faults with the greatest subsidence during the rift initiation phase grow and link into larger faults or fault zones during the rift-climax phase, whereas smaller faults become inactive (Walsh & Watterson 1988; Cartwright et al., 1995; Dawers & Anders 1995; Cowie & Shipton 1998; Gupta et al., 1998; Meyer et al., 2002). Reconstructions of the Billefjorden Trough evolution introduced in Articles 1 and 2 inform us about the distinct basin-configuration model. This study divides the Billefjorden Trough deposits into: (1) symmetrical early syn-rift fill, (2) rift climax (half-graben) fill and (3) rift reorganisation and narrowing fill (Fig. 13 and Tab. 2). This development contradicts the traditional model of half-graben evolution and has profound implications for facies development and their geometries, as well as for paleo-drainage patterns.

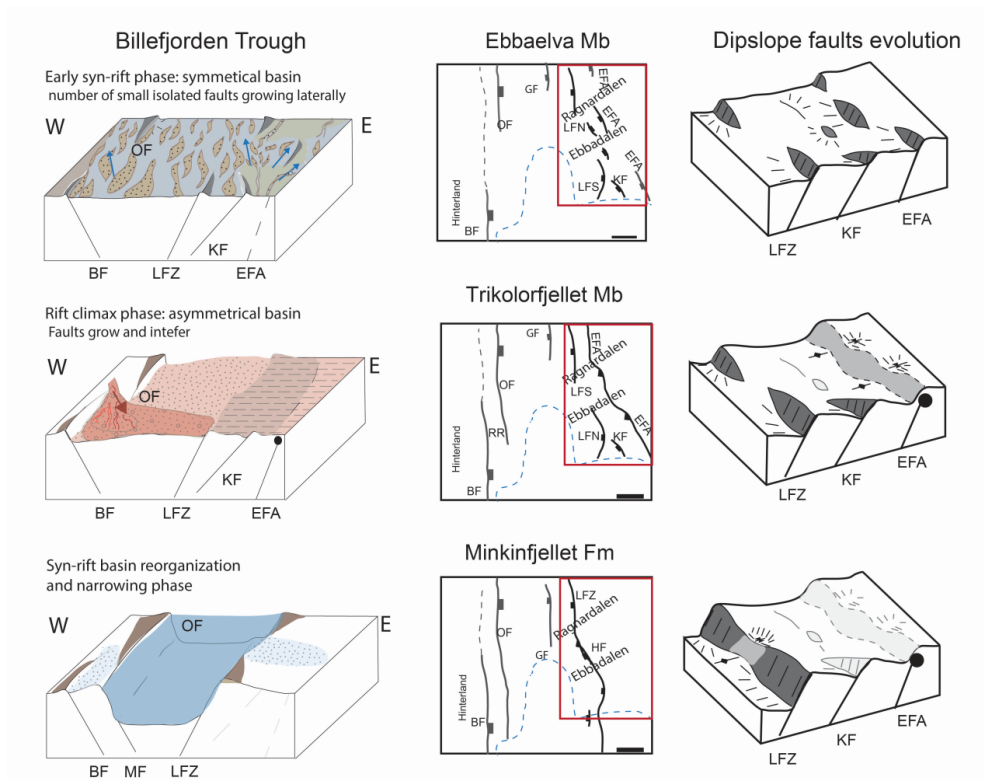


Fig. 13. Reconstructions of tectono-stratigraphic evolution of the Billefjorden Trough (from Article 2) shown as a basin-scale block diagram (left column), map of active fault segments (middle column) and block-diagram of the dip slope faults. The reconstructions are made for the main phases 1-3 of basin evolution. LFN- Løvehovden Fault North, LFS- Løvehovden Fault South, EFA- Ebbabreen fault array, KF- Kampesteindalen fault, GF- Gzselfjellet fault, MF- Mimerbukta fault.

Early syn-rift (Phase 1)

During the rift initiation stage, the subsidence is balanced by sediment supply (Posser, 1993; Jackson et al., 2006; Young et al., 2003). In Billefjorden, this stage is represented by deposition dominated by siliciclastics within small, isolated basins bounded by meso-scale faults (tens to 200 m offsets) assigned to the early syn-rift phase (Article 1). Phase 1 includes aggrading continental Hultberget Formation overlain by paralic backstepping facies belts of the Ebbaelva Member of the Lower Ebbadalen Formation. The recorded paleo-drainage is axial to the faults, locally adjusting to the morphology of growing faults, and the transverse, footwall-delivered drainage pattern is not observed (e.g. Leeder & Jackson 1993; Eliet & Gawthorpe 1995; Ravnås & Steel, 1998). The segments of BFZ that later formed a master fault zone were only mildly active, with offsets corresponding to the deformation along an array of antithetic faults, i.e. EFA, KF and LFZ (Fig. 13). The subsidence along segmented fault blocks was fairly symmetrical across the basin, defining the early-syn-rift graben geometry (Fig. 10).

Rift climax (Phase 2)

In the Billefjorden Trough, the rift climax phase (Article 2) includes mixed evaporite-carbonate-siliciclastic deposition of Triolorfjellet and Odellfjellet Members belonging to the upper Ebbadalen Formation. The rift climax is interpreted due the highest tectonic subsidence during that phase, estimated at ca. 15 m/100 kyr (Article 2). The rift-climax succession thickens towards the BFZ and indicates significant change in both basin configuration and depositional environments compared to Phase 1 (Fig. 9). Increased tectonic activity along BFZ was highlighted by the development of a relay zone near Pyramiden, between the laterally growing OF and BF (Braathen et al., 2011). The relay zone was likely initiated at the transition from Phase 1 to Phase 2, after the deposition of basin-wide braided river system (Unit 3 in Article 1).

This braided river system suggests a northerly paleo-transport direction, and therefore must pre-date the southwards tilted relay ramp. The BFZ became a master fault zone that controlled the development of a half-graben with an hanging wall dipslope located to the east (Fig. 13). This westward tilted dipslope was segmented by the EFA, KF and LFZ. Pulses of tectonic activity indicated by prograding lower fan correlate with maximum growth of the EFA (Article 2).

During a rift climax a pronounced increase in subsidence commonly leads to the development of sediment-starved hanging wall basins (Prosser, 1993; Gupta et al., 1998; McLeod et al., 2002; Leppard & Gawthorpe, 2006). Prosser (1993) ascribes the deposition of the coarser material to an immediate post-rift stage. In contrast, rift climax deposits in the Billefjorden Trough are dominated by alluvial siliciclastics that represent the largest grain size from all the deposits of the trough. Sedimentary facies such as continental alluvial conglomerates, sandstones and shales demonstrate that sedimentation kept up with the subsidence, periodically filling up the basin. Aggrading/prograding footwall-delivered alluvial fans (Article 2) indicate basin transverse footwall drainage. Hanging wall drainage is not recorded, most likely due the absence of a sufficient detritus source located to the east. All these observations imply that the Billefjorden Trough is a minor rift basin that might belong to a larger system which continues to the east.

Rift reorganisation and narrowing (Phase 3)

This study identifies the rift reorganisation and narrowing phase, a late syn-rift stage that records a decrease in tectonic subsidence to an estimated 2 - 7 m/100 kyr (Article 2). By Phase 3, the easternmost dipslope faults (i.e. KF and EFA) are no longer active. The displacement along the dipslope was transferred and localised along the LFZ at the onset of Moscovian. This was most likely associated with lateral linkage of two fault segments, LFS and LFN,

along with the uplift of footwall blocks (Fig. 13). Elevated footwall transverse anticlines (Fig. 4) became exposed to meteoritic water, allowing localised gypsum dissolution. As a result, the stratiform dissolution breccias highlight the position of the biggest footwall rebound of linking fault segments.

Two main types of karst features are recognised within the Billefjorden Trough fill. The Fortet Member of Minkinjfellet Formation consist of vertical breccia bodies (pipes) interpreted as sinkholes, and clustered, rounded bodies representing a paleo-cave fill (Eliassen & Tabot 2005). These paleo-karst features are located along the LFZ and GF and suggest that the dissolution pattern could have been controlled by the fracture network around the faults. A second type of dissolution feature is represented by extensive (> 100s of meters) bedding-parallel, stratiform breccias. These are developed mainly along the upper boundary of the Trikolorfjellet Member on the footwall of the LFZ and as two- three levels within Minkinjfellet Formation (Article 2). The stratiform breccias along the Trikolorfjellet Member boundary are interpreted to form syn-kinematically on the surface of uplifted fault blocks (Article 2). Structural control over the location of this stratiform breccia interval is discussed in Article 2. Field observations also show that the round breccia bodies truncate the syn-sedimentary faults, and have therefore likely formed post-kinematically. This implies that there were several dissolution events in different time periods.

Near the master fault zone, the linkage of LFS and LFN coincides with the shut down of the Pyramiden relay ramp due to southward lateral progradation of OF and possible interaction with both BF and the southwards located Mimerbukta Fault (MF, Fig.8).

The main depocentre was allocated in the middle part of the Billefjorden Trough, between OF to the west and LFZ to the east (Fig. 13) while relatively less-subsiding platforms were located along the western and eastern flanks of

the basin. The platforms experienced periods of condensed deposition, subaerial exposure and dissolution of evaporites (Article 2). The gypsum-rich succession in the central part of the Billefjorden Trough was protected against dissolution in the hanging wall blocks of LFZ, OF and MF.

Models of fault growth in Billefjorden Trough

Three models of fault growth were summarised in the Scientific Background (Fig. 4): (i) fault tip propagation and linkage, (ii) constant fault length and (iii) a combined model, recently presented by Rotevatn et al. (2019). Each of these models would be differently displayed in the syn-kinematic basin fill, especially by an impact on the amplitude of fault transverse folds and duration of relay ramp structures (Fig. 5). The constant length model (ii) should be characterised by the smallest (if any) amplitude of fault-related folds. This model, due to rapid length establishment, should not display any relay features. In the constant length model, therefore, both fault-related transverse folds and the relay ramp, if present, would be active for a short time only, without any significant impact on the preserved basin fill. The combined model (iii) would be characterized by transverse faults, but their expected amplitude and width would be smaller than in the model of fault linkage. Also, the time span of relay ramp activity would be shorter when combined with the first model.

These 3 models can be discussed in respect to the development of EFA, LFZ and BFZ. In early syn-rift, the basin fill along EFA formed in response to lateral fault growth. The potential interaction with another southward located fault segment is discussed in Article 1. For this fault array, a model of constant fault growth is not supported. Although there is a lack of high resolution stratigraphic control on the basin fill, it can be roughly estimated that the lateral growth from northern to southern Ebbadalen (Units 1-4 in Article 1) lasted for ca. 30% of the EFA time span. After the length was established, the increase

of displacement could take about 20-30% (from unit 4, i.e. the middle Ebbaelva Member to the lower red shale interval in the lower Trikolorfjellet Member, see Fig. 5 in Article 2 for details), while the gradual dying phase takes ca. 30-40% of the time span. This very approximate estimation of EFA evolution could support (iii) combined model of fault growth (Rotevatn et al., 2019) but it is not conclusive.

LFZ was active for a longer period than EFA and most likely evolved from two individual segments that initiated in (late?) Serpukhovian to Late Bashkirian. Near the onset of Moscovian, the LFS and LFN interacted and were soft-linked. The linking location of the fault segments is expressed as a kink in the fault trace and development of a monocline (Fig. 13; Maher & Braathen, 2011). Both fault segments most likely did not hard-link, but rather acted synchronously in Moscovian, bounding a centrally located depocentre of the Billefjorden Trough. Segment growth, interaction and (soft) linkage would take, approximately, over 50-60% of a lifespan of LFZ. This reconstruction of LFZ thus supports the model (i) of fault lateral growth and linkage.

The BFZ development begins with isolated fault segments active during early syn-rift phase (Article 1). In rift climax (Upper Bashkirian) a long-lasting relay ramp was formed due to lateral fault tip propagation and interaction between OF and BF, highlighted by the presence of Odelfjellet fault tip monocline (Braathen et al., 2011). The evolution of the described part of the BFZ combined with the termination of the Pyramiden relay ramp in Moscovian supports rather the (i) model of lateral fault growth. The approximate interaction of OF with BF took over 50% of the life span of these faults.

System 2

Initiation and growth of faults in Kvalpynten.

System 2 was studied in outcrops and on the photogrammetric model of the Kvalpynten cliffs and is limited to a long, single profile. The studies of System 2 are therefore lacking the good 3D control that analysis of System 1 benefitted from.

The initiation of growth faults in Kvalpynten took place during the deposition of the prodelta to lower delta front Tschermakfjellet Formation (Article 3 and 4). The studies of the oldest basin fills are challenged by the juxtaposition of mudstone in the footwall against the mudstone in the hanging wall blocks and, therefore, a lack of reference structures. Some minor compressional thrust faults might be seen in the shale-rich horst (eg. Horst H6 in the Fig. 14). Similar structures that indicate shortening are seen in the lower delta front/prodelta deposits and are interpreted as gravity-induced deep water fold-and-thrust belts (e.g. Braathen et al., 2018; Ings & Beaumont, 2010). At Kvalpynten, the shortening was followed by extensional faulting and mudstone dominated basin fills.

The oldest recognised coarsening upward unit is located within Basins B1 in the northern part of the studied cliff and in Basins B6-B7 located more central (System 2 in Fig. 14). From these two positions, younger faults and basin fills are overstepping in a southward direction. This configuration might indicate southward (in the N-S profile) tilt of the basin floor that controls emplacement of the younger faults and associated basin fills.

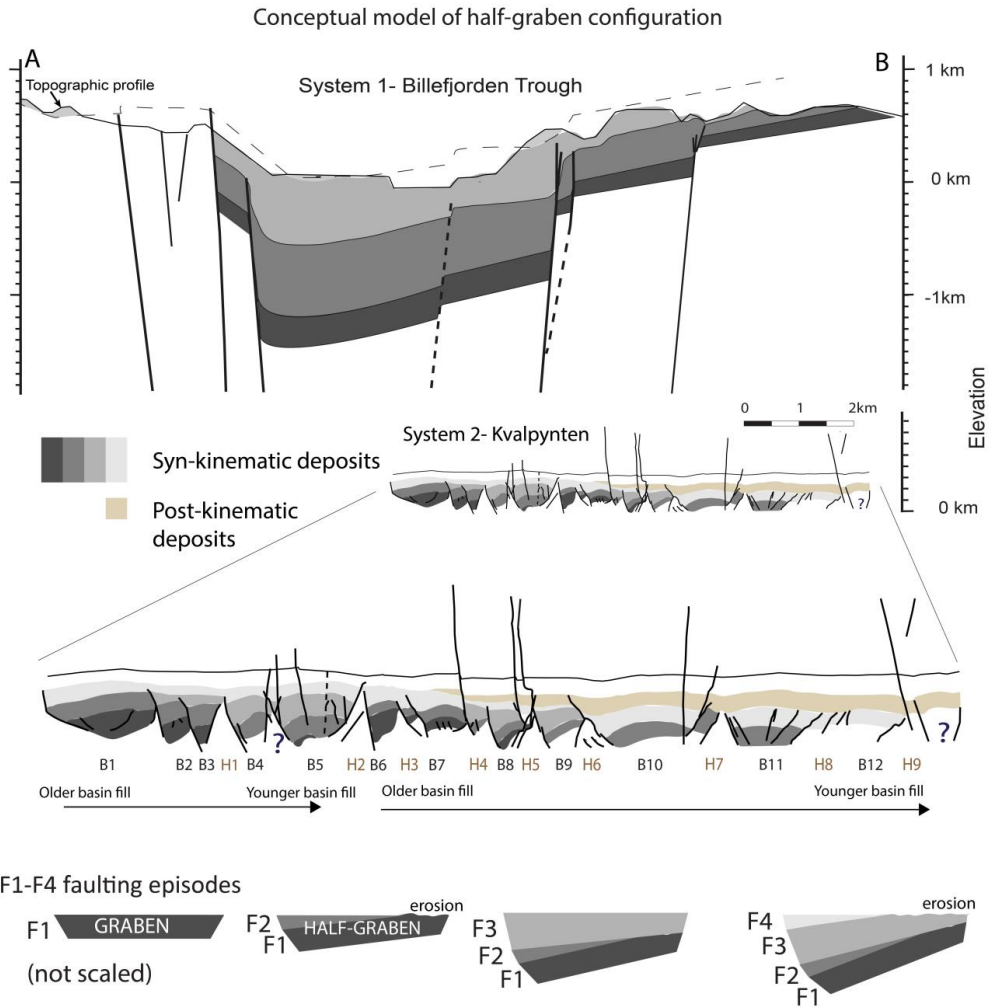


Fig. 14. Conceptual, scale-independent model 'from graben to half-graben' evolution; B- basin, H- Horst.

Half-graben evolution: similarities and differences in Carboniferous and Triassic basins (System 1 and 2)

Differences between System 1 and System 2

- Lithology

An obvious difference between Systems 1 and 2 is the lithology, which was controlled to a large degree by a warm and arid climate in the Carboniferous vs. a temperate climate in the Triassic. The detritus for a System 1 was sourced locally from the uplifted footwall blocks and structural highs and, therefore, was rather limited. The catchment's size and position were governed by the basin configuration (Article 1 and 2). System 2 was supplied with the detritus from the orogenic belt of Uralides that supported the gigantic-scale deltaic system of the Barents Shelf (Riis et al., 2008; Worsley 2008; Glørstad-Clark et al., 2011; Høy & Lundschein 2011; Klausen et al., 2015, 2017, 2019; Eide et al., 2017, Rossi et al., 2019).

- Deformation style

The lithology has an influence on the deformation style. System 1 consists of tectonically induced deep-rooted faults that clearly show their growth through lateral tip propagation developed in ductile-deformed evaporites, and progressive interaction and linkage with neighbouring faults. This interaction is seen through evolution of relay ramps and fault tip monoclines. The presence of evaporites that tend to deform in a more ductile style has determined the development of fault tip and fault-propagation monoclines in System 1 (Maher & Braathen 2011; Braathen et al., 2011; Article 2).

System 2 is dominated by thin-skinned faulting that detaches on the shale. The faults bounding the half-grabens are listric and hanging wall blocks form rollover anticlines. Fault tip or fault propagation monoclines are not often seen

in this system, likely due to the thin-skinned character of the faults facilitated by a shallow detachment horizon.

- Lateral vs vertical expansion of the system

System 1 occupies the same location from the initial stage. With ongoing deformation, the subsidence becomes more focused in the central part of the basin (i.e. during the rift reorganization and narrowing phase). System 2 rather shows lateral translation of the faults in the southern direction, which can be seen as two zones with the oldest basin fills located in the northern parts, and the younger depocentres gradually down-stepping to the south (Fig. 14). This direction coincides with a S to SW dipping paleo-slope on the flank of the Svalbard Platform (Articles 3 and 4). Therefore, System 2 can be considered as largely controlled by the configuration of the basin floor.

- Rapid vs gradual termination of deformation

In System 1, the transition from the syn-rift to the post-rift phase is gradual and challenging to interpret. Renewed tectonic activity or differential compaction of up to 2 km of basin fill could influence the accommodation in post-rift strata. In contrast, the cessation of faulting is rapid in System 2, as expressed by the fairly uniform post-kinematic draping units (Fig. 14).

Similarities between System 1 and System 2

Despite their fundamental differences, Systems 1 and 2 also display some similarities:

- Drainage patterns recorded in siliciclastic facies

The drainage pattern recorded in System 2 (Article 3) resembles similarities to the early syn-rift drainage reconstructed in System 1 (Phase 1; Article 1). In both cases meso-scale hanging wall blocks were hosting depocentres that

were exploited by axial drainage, i.e. parallel to the bounding growth faults. Relatively small fault-related topography/bathymetry prevented the development of transverse drainage but rather controlled local scale deviation in axial drainage towards the hanging wall subsidence maxima and away from the uplifting footwall blocks. In System 1, the early syn-rift relay ramps were sediment transit points between sub-isolated early syn-rift sub-basins (Article 1). This was not, however, observed in System 2, which was limited by the observations along the 2D profile.

In System 1 during rift climax (i.e. half-graben geometry), relay ramps were the entry points for the sediments that came from the hinterland and were deposited in the hanging wall depocentre (Article 2). Subaqueous slides and potentially structureless sandstone wedges are the only record of fault-transverse sediment supply from the footwall blocks in System 2.

In both systems the transverse drainage from/along the hanging wall was not recorded during the development of half-graben geometry (Articles 2 and 3). In System 1 this was due to the lack of an eastern source, which suggests the drowning of the easternmost flank of the rift due to potential interaction with another depocentre located to the east (see discussion above). In System 2, the regional paleo-slope was towards S-SW, i.e. in the direction of all half-graben hanging walls, which could restrict the development of hanging wall transverse drainage.

- Intrabasinal erosion

Both systems show intra-basinal erosion of the relatively uplifted strata along the distal dipslope. In System 1 this is associated mainly with non-deposition/condensed deposition in the early synrift (Article 1), while later in the rift reorganization phase the entire distal dipslope formed a platform developed on the footwall block of the meso-scale fault zone (i.e. LFZ, Article

2). System 2 exposes erosional events on the uplifted flanks of the rotated fault blocks that likely were sediment sources for the subaqueous slides and structure-less sandstone wedges.

- Evolution of a half-graben from an initial symmetrical basin (Fig. 14)

System 1 reveals the tectonically-driven evolution of the basin configuration from a symmetrical graben to a half-graben (Articles 1 and 2 and the discussion above). The early syn-rift phase System 1 appears to begin with a number of sub-basins that resemble meso-scale configuration similar to the domino model (Fig. 9d). Later, the rift system up-scaled to a larger (regional)-scale domino model, where the Billefjorden Trough is likely one element (one domino) within a wider rift system.

Similar evolution from symmetrical to asymmetrical basin has been documented in System 2, where symmetrical basin fill deposited within a depocentre and bounded by a pair of antithetic faults is overlain by wedge-shaped deposits formed while the south dipping faults prevailed (Article 3). This transformation from grabens to half-graben might have been induced by the S-SW tilted paleo-slope (Articles 3 and 4), where the half-graben blocks might have been gravity-driven 'slides' along the detachment zone (Article 4).

Further work

The spectacular outcrops of the Billefjorden Trough deposits provide an opportunity to study interaction of faulting and sedimentary processes in great detail. This field lab is used extensively during the geological courses at UNIS. Ongoing acquisition of cheap and effective photogrammetry, using Structure-from-Motion, will soon provide even more detailed, geo-referenced models of the outcropping strata. The studies of Billefjorden Trough are, however, suffering from a lack of good quality seismic data, both onshore and offshore. Tools that create synthetic seismic records might partly fill this gap, and will also contribute to enhancement of onshore-offshore correlations in this region. Further work, is, however, required in order to address a number of scientific questions that address:

- The basin configuration of the broader pre-rift Billefjorden Group and its link to the Billefjorden Trough.
- Reconstruction of the basin inversion with emphasis on selective reactivation of fault segments. What is a controlling agent of the reactivation? Is it fault orientation, dip angle, shape of fault plane or the tectonic history of a fault segment?

Tectono-stratigraphic reconstructions of the Billefjorden Trough should be also upscaled across the entire NW Barents Shelf. This could be done by integration of 3D geometric outcrop-based models with seismic, magnetic, gravity and magnetotelluric data, and with information from the onshore and offshore boreholes.

References

- Ahlborn, M. & Stemmerik, L. (2015): Depositional evolution of the Upper Carboniferous – Lower Permian Wordiekammen carbonate platform, Nordfjorden High, central Spitsbergen, Arctic Norway. *Norwegian Journal of Geology*, 95.1: 91-126.
- Anell, I., Braathen, A., Olaussen, S., & Osmundsen, P. T. (2013): Evidence of faulting contradicts a quiescent northern Barents Shelf during the Triassic. *First Break*, 31(6): 67-76.
- Anell, I. M., Braathen, A., & Olaussen, S. (2014): The Triassic–Early Jurassic of the northern Barents Shelf: a regional understanding of the Longyearbyen CO₂ reservoir. *Norwegian Journal of Geology*, 94, 83-98.
- Anell, I. M., Faleide, J. I., & Braathen, A. (2016). Regional tectono-sedimentary development of the highs and basins of the northwestern Barents Shelf. *Norwegian Journal of Geology*, 96(1), 27-41.
- Anell, I., Indrevær, K., & Serck, C. S. (2019): Influence of structural highs on Triassic deposition on the western Barents Shelf. In: Chiarella, D., Archer, S. G., Howell, J. A., Jackson, C. A.-L., Kombrink, H. & Patruno, S. (eds) *Cross-Border Themes in Petroleum Geology II: Atlantic Margin and Barents Sea*. Geological Society, London, Special Publications, 495: 1-13.
- Back, S., Strozyk, F., Kukla, P. A., & Lambiase, J. J. (2008): Three-dimensional restoration of original sedimentary geometries in deformed basin fill, onshore Brunei Darussalam, NW Borneo. *Basin Research*, 20(1): 99– 117.
- Barr, D. (1987): Structural/stratigraphic models for extensional basins of half-graben type. *Journal of Structural Geology*, 9(4): 491-500.

-
- Bazarnik, J., Majka, J., McClelland, W. C., Strauss, J. V., Kościńska, K., Piepjohn, K., Elvevold S., Czupyt, Z., & Mikuš, T. (2019): U-Pb zircon dating of metaigneous rocks from the Nordbreen Nappe of Svalbard's Ny-Friesland suggests their affinity to Northeast Greenland. *Terra Nova*, 1-9.
- Bergh, S. G., Braathen, A., & Andresen, A. (1997): Interaction of basement-involved and thin-skinned tectonism in the Tertiary fold-thrust belt of central Spitsbergen, Svalbard. *AAPG bulletin*, 81(4): 637-661.
- Bergh, S. G., Maher, H. D., & Braathen, A. (2000): Tertiary divergent thrust directions from partitioned transpression, Brggerhalvya, Spitsbergen. *Norsk Geologisk Tidsskrift*, 80(2): 63-81.
- Bergh, S., Maher, H., and Braathen, A. (2011): Late Devonian transpressional tectonics in Spitsbergen, Svalbard, and implications for basement uplift of the Sørkapp–Hornsund High: *Journal of the Geological Society*, 168(2): 441-456.
- Bhattacharya, J. P., & Davies, R. K. (2001): Growth faults at the prodelta to delta-front transition, Cretaceous Ferron sandstone, Utah. *Marine and Petroleum Geology*, 18(5): 525– 534.
- Blinova, M., Faleide, J. I., Gabrielsen, R. H., & Mjelde, R. (2013): Analysis of structural trends of sub-sea-floor strata in the Isfjorden area of the West Spitsbergen Fold-and-Thrust Belt based on multichannel seismic data. *Journal of the Geological Society*, 170(4): 657-668.
- Blomeier, D., Wisshak, M., Joachimski, M., Freiwald, A., & Volohonsky, E. (2003): Calcareous, alluvial and lacustrine deposits in the Old Red Sandstone of central north Spitsbergen (Wood Bay Formation, Early Devonian). *Norwegian Journal of Geology* 83(4): 281-289.

-
- Blomeier, D., Scheibner, C., & Forke, H. (2009): Facies arrangement and cyclostratigraphic architecture of a shallow-marine, warm-water carbonate platform: the Late Carboniferous Ny Friesland Platform in eastern Spitsbergen (Pyefjellet Beds, Wordiekammen Formation, Gipsdalen Group). *Facies*, 55(2): 291-324.
- Blomeier, D., Dustira, A., Forke, H., & Scheibner, C. (2011): Environmental change in the Early Permian of NE Svalbard: from a warm-water carbonate platform (Gipshuken Formation) to a temperate, mixed siliciclastic-carbonate ramp (Kapp Starostin Formation). *Facies*, 57(3): 493-52.
- Blomeier, D., Dustira, A. M., Forke, H., & Scheibner, C. (2013): Facies analysis and depositional environments of a storm-dominated, temperate to cold, mixed siliceous-carbonate ramp: the Permian Kapp Starostin Formation in NE Svalbard. *Norwegian Journal of Geology*, 93(2): 75-93.
- Bouroullec, R., Cartwright, J. A., Johnson, H. D., Lansigu, C., Quémener, J. M., & Savanier, D. (2004): Syndepositional faulting in the Grès d'Annot Formation, SE France: High-resolution kinematic analysis and stratigraphic response to growth faulting. P. Joseph, S.A. Lomas (Eds.), In *Deep-water Sedimentation in the Alpine Basin of SE France: New Perspectives on the Gres D'Annot and Related Systems*, 221, *Geology Society Special Publication*, 241-265.
- Braathen, A., & Bergh, S. G. (1995): Kinematics of Tertiary deformation in the basement-involved fold-thrust complex, western Nordenskiöld Land, Svalbard: tectonic implications based on fault-slip data analysis. *Tectonophysics*, 249(1-2): 1-29.
- Braathen, A., Bergh, S. G., & Maher, H. D. Jr (1999): Application of a critical wedge taper model to the Tertiary transpressional fold-thrust belt on Spitsbergen. *Geological Society of America Bulletin*, 111: 1468– 1485.
- Braathen, A., Bælum, K., Maher, H. Jr, & Buckley, S. J. (2011): Growth of extensional faults and folds during deposition of an evaporite-dominated half-graben

-
- basin; the Carboniferous Billefjorden Trough, Svalbard. *Norwegian Journal of Geology* 91(3): 131– 161.
- Braathen, A., Midtkandal, I., Mulrooney, M. J., Appleyard, T. R., Haile, B. G., & van Yperen, A. E. (2018): Growth-faults from delta collapse—structural and sedimentological investigation of the Last Chance delta, Ferron Sandstone, Utah. *Basin Research*, 30(4), 688– 707.
- Braathen, A., Osmundsen, P. T., Maher, H., & Ganerød, M. (2018): The Keisarhjelmen detachment records Silurian-Devonian extensional collapse in Northern Svalbard. *Terra Nova*, 30(1): 34– 39.
- Buchan, K. L., Ernst, R. E., Hanski, E., Mertanen, S., Rämö, T., & Vuollo, J. (2006). Giant dyke swarms and the reconstruction of the Canadian Arctic islands, Greenland, Svalbard and Franz Josef Land. *Dyke swarms: time markers of crustal evolution*, 27-48.
- Buckley, S. J., Ringdal, K., Naumann, N., Dolva, B., Kurz, T. H., Howell, J. A., & Dewez, T. J. (2019): LIME: Software for 3-D visualization, interpretation, and communication of virtual geoscience models. *Geosphere*, 15(1): 222-235.
- Burhannudinnur, M., & Morley, C. K. (1997): Anatomy of growth fault zones in poorly lithified sandstones and shales: Implications for reservoir studies and seismic interpretation: Part 1, outcrop study. *Petroleum Geoscience*, 3(3): 211– 224.
- Bælum, K., and Braathen, A., (2012): Along-strike changes in fault array and rift basin geometry of the Carboniferous Billefjorden Trough, Svalbard, Norway: *Tectonophysics*, 546–547: 38-55.
- Bäckström, S. A., & Nagy, J. (1985). Depositional history and fauna of a Jurassic phosphorite conglomerate (the Brentskardhaugen Bed) in Spitsbergen. *Norsk Polarinstitut Skrifter* 183, 1–61.
- Cartwright, J. A., Mansfield, C., & Trudgill, B. (1996): The growth of normal faults by segment linkage. In: Buchanan, P.G., Nieuwland, D.A. (Eds.), *Modern*

Developments in Structural Interpretation, Validation and Modelling. *Geology Society London Special Publication*, 99(1): 163-177.

- Chandler, J. H., & Buckley, S. (2016). Structure from motion (SFM) photogrammetry vs terrestrial laser scanning. In M. B. Carpenter & C. M. Keane (Eds.), *Geoscience Handbook 2016, AGI Data Sheets (5th edn.)*. Section 20.1. Alexandria, USA: American Geosciences Institute.
- Childs, C., Holdsworth, R. E., Jackson, C. A. L., Manzocchi, T., Walsh, J. J., & Yielding, G. (2017): Introduction to the geometry and growth of normal faults. In: *The Geometry and Growth of Normal Faults*, Childs C, et al., (eds), Geological Society, London, Special Publications, 439(1), 1-9.
- Corfield, S., & Sharp, I. R. (2000): Structural style and stratigraphic architecture of fault propagation folding in extensional settings: a seismic example from the Smørbukk area, Halten Terrace, Mid-Norway. *Basin Research*, 12(3-4): 329-341.
- Corfu, F., Polteau, S., Planke, S., Faleide, J. I., Svensen, H., Zayoncheck, A., & Stolbov, N. (2013): U–Pb geochronology of Cretaceous magmatism on Svalbard and Franz Josef Land, Barents Sea large igneous province. *Geological Magazine*, 150(6): 1127-1135.
- Cowie, P. A., & Scholz, C. H. (1992): Displacement-length scaling relationship for faults: data synthesis and discussion. *Journal of Structural Geology*, 14(10): 1149-1156.
- Crowley, T. J., & Baum, S. K., (1991): Estimating Carboniferous sea-level fluctuations from Gondwanan ice extent: *Geology*, 19(10): 975-977.
- Cutbill, J., & Challinor, A., (1965): Revision of the stratigraphical scheme for the Carboniferous and Permian rocks of Spitsbergen and Bjørnøya: *Geological Magazine*, 102(05): 418-439.

-
- Cutbill, J. L., Henderson W.G., & Wright N. Jr., (1976). The Billefjorden Group (Early Carboniferous) of Central Spitsbergen. Norsk Polarinstitutt Skrifter 164, 57–87.
- Dallmann, W. K., (1993): Notes on the stratigraphy, extent and tectonic implications of the Minkinfjellet Basin, Middle Carboniferous of central Spitsbergen: Polar Research, 12(2): 153-160.
- Dallmann, W. K., Andresen, A., Bergh, S. G., Maher jr, H. D., & Ohta, Y. (1993): Tertiary fold-and-thrust belt of Spitsbergen, Svalbard. Norsk Polarinstitut Meddelelser, 128: 1-41.
- Dallmann, W. K., Piepjohn, K., & Blomeier, D. (2004): Geological map of Billefjorden, Central Spitsbergen, Svalbard: with geological excursion guide. Norsk Polarinstitut. 1
- Dallmann, W. K., Elvevold, S., Majka, J., & Piepjohn, K. (2015): Tectonics and tectonothermal events. In: Geoscience Atlas of Svalbard (Ed. by Dallmann, W.K.). Norsk Polarinstitut Rapportserie, 148: 175–223.
- Dallmann, W. K. (Ed.). (1999). Lithostratigraphic lexicon of Svalbard: review and recommendations for nomenclature use: Upper Palaeozoic to Quaternary bedrock. Norsk Polarinstitut.
- Dawers, N. H., Anders, M. H., & Scholz, C. H. (1993): Growth of normal faults: Displacement-length scaling. *Geology*, 21(12): 1107-1110.
- Dawers, N. H., & Anders, M. H. (1995): Displacement-length scaling and fault linkage. *Journal of Structural Geology*, 17(5): 607-614.
- Dawers, N. H., & Underhill, J. R. (2000): The role of fault interaction and linkage in controlling synrift stratigraphic sequences: Late Jurassic, Statfjord East area, northern North Sea. *AAPG bulletin*, 84(1): 45-64.
- Dennis, J. G. (Ed.). (1967): International tectonic dictionary: English terminology. American Association of Petroleum Geologists, 1-196.

-
- Dimakis, P., Braathen, B. I., Faleide, J. I., Elverhøi, A., & Gudlaugsson, S. T. (1998): Cenozoic erosion and the preglacial uplift of the Svalbard–Barents Sea region. *Tectonophysics*, 300(1-4): 311-327.
- Drachev, S. S. (2016): Fold belts and sedimentary basins of the Eurasian Arctic. *Arktos*, 2(1): 21.
- Duncan, C. C., & Turcotte, D. L. (1994): On the breakup and coalescence of continents. *Geology*, 22(2): 103-106.
- Eide, C. H., Klausen, T. G., Katkov, D., Suslova, A. A., & Helland-Hansen, W. (2017): Linking an Early Triassic delta to antecedent topography: Source-to-sink study of the southwestern Barents Sea margin. *AAPG Bulletin*, 130(1-2): 263-283.
- Eliassen, A., & Talbot, M. R., (2003): Sedimentary facies and depositional history of the mid-Carboniferous Minkinfjellet Formation, Central Spitsbergen, Svalbard: *Norwegian Journal of Geology* 83(4); 229-318.
- Eliassen, A., & Talbot, M. R., (2005): Solution-collapse breccias of the Minkinfjellet and Wordiekammen Formations, Central Spitsbergen, Svalbard: a large gypsum palaeokarst system: *Sedimentology*, 52(4): 775-794.
- Eliet, P. P., & Gawthorpe, R. L. (1995): Drainage development and sediment supply within rifts, examples from the Sperchios basin, central Greece. *Journal of the Geological Society*, 152(5): 883-893.
- Edwards, M. B. (1976): Growth faults in Upper Triassic deltaic sediments. Svalbard. *AAPG Bulletin*, 60(3), 341– 355.
- Faehnrich K., Majka J., Schneider D., Mazur S., Manecki M., Ziemniak G., Wala V.T., Strauss J.V. (2019): Geochronological constraints on Caledonian strike–slip displacement in Svalbard, Norway, with implications for the evolution of the Arctic. *Terra Nova*, *in review*

-
- Faleide, J. I., Gudlaugsson, S. T., & Jacquart, G. (1984): Evolution of the western Barents Sea. *Marine and Petroleum Geology*, 1(2): 123-150.
- Faleide, J. I., Tsikalas, F., Breivik, A. J., Mjelde, R., Ritzmann, O., Engen, O., Wilson, J. & Eldholm, O. (2008): Structure and evolution of the continental margin off Norway and the Barents Sea. *Episodes*, 31(1): 82-91.
- Faleide, J.I., Pease, V., Curtis, M., Klitzke, P., Minakov, A., Scheck-Wenderoth, M., Kostyuchenko, S. & Zayonchek, A., (2018): Tectonic implications of the lithospheric structure across the Barents and Kara shelves. In: *Circum-Arctic Lithosphere Evolution*, Pease, V., & Coakley, B. (eds). Geological Society, London, Special Publications, 460(1): 285-314.
- Fielding, C. R. (2015): Anatomy of falling-stage deltas in the Turonian Ferron Sandstone of the western Henry Mountains Syncline, Utah: Growth faults, slope failures and mass transport complexes. *Sedimentology*, 62(1): 1– 26.
- Flood, B., Nagy, J., & Winsnes, T. S. (1971): The Triassic succession of Barentsøya, Edgeøya, and Hopen (Svalbard). *Norsk Polarinstitute Meddelelser*, 100: 1- 20
- Ford, M., Rohais, S., Williams, E. A., Bourlange, S., Jousselin, D., Backert, N., & Malartre, F. (2013): Tectono-sedimentary evolution of the western Corinth rift (Central Greece). *Basin Research*, 25(1): 3-25.
- Fossen, H., & Rotevatn, A. (2016): Fault linkage and relay structures in extensional settings—A review. *Earth-Science Reviews*, 154: 14-28.
- Gabrielsen, R. H. (2015): The Structure and Hydrocarbon Traps of Sedimentary Basins', in Bjørlykke, K. (ed.) *Petroleum Geoscience: From Sedimentary Environments to Rock Physics*, Second Edition. Springer-Verlag, 319–350.
- Gastaldo, R. A., DiMichele, W. A., & Pfefferkorn, H. W. (1996): Out of the icehouse into the greenhouse: a late Paleozoic analogue for modern global vegetational change. *Gsa today*. 6(10) 1-40.

-
- Gawthorpe, R. L., Hurst, J. M., & Sladen, C. P. (1990): Evolution of Miocene Footwall-Derived Coarse-Grained Deltas, Gulf of Suez, Egypt: Implications for Exploration (1). *AAPG Bulletin*, 74(7): 1077-1086.
- Gawthorpe, R. L., & Hurst, J. M. (1993): Transfer zones in extensional basins: their structural style and influence on drainage development and stratigraphy. *Journal of the Geological Society*, 150(6): 1137-1152.
- Gawthorpe, R. L., Fraser, A. J., & Collier, R. E. L. (1994): Sequence stratigraphy in active extensional basins: implications for the interpretation of ancient basin-fills. *Marine and petroleum geology*, 11(6): 642-658
- Gawthorpe, R. L., Sharp, I., Underhill, J. R., & Gupta, S. (1997): Linked sequence stratigraphic and structural evolution of propagating normal faults. *Geology*, 25(9): 795-798.
- Gawthorpe, R. L., & Leeder, M. R. (2000): Tectono-sedimentary evolution of active extensional basins. *Basin Research*, 12(3-4): 195-218.
- Gawthorpe, R., & Hardy, S. (2002): Extensional fault-propagation folding and base-level change as controls on growth-strata geometries. *Sedimentary Geology*, 146(1-2): 47-56.
- Gawthorpe, R. L., Leeder, M. R., Kranis, H., Skourtsos, E., Andrews, J. E., Henstra, G. A., Mack G.H., Muravich M., Turner J.A., & Stamatakis, M. (2018): Tectono-sedimentary evolution of the Plio-Pleistocene Corinth rift, Greece. *Basin Research*, 30(3): 448-479.
- Gee D.G. & Tebenkov A.M. (2004): Svalbard: a fragment of the Laurentian margin. In Gee D.G. and Pease V. (eds.), *The Neoproterozoic Timanide Orogen of Eastern Baltica*. Geological Society of London, *Memoirs* 30: 191-206.
- Gee, D. G., Bogolepova, O. K., & Lorenz, H. (2006): The Timanide, Caledonide and Uralide orogens in the Eurasian high Arctic, and relationships to the palaeo-

continents Laurentia, Baltica and Siberia. *Geological Society, London, Memoirs*, 32(1), 507-520.

- Gee, D. G., Fossen, H., Henriksen, N., & Higgins, A. K. (2008): From the early Paleozoic platforms of Baltica and Laurentia to the Caledonide Orogen of Scandinavia and Greenland. *Episodes*, 31(1): 44-51.
- Gee, D. G., Janák, M., Majka, J., Robinson, P., & van Roermund, H. (2013): Subduction along and within the Baltoscandian margin during closing of the Iapetus Ocean and Baltica-Laurentia collision. *Lithosphere*, 5(2): 169-178.
- Giba, M., Walsh, J. J., & Nicol, A. (2012): Segmentation and growth of an obliquely reactivated normal fault. *Journal of Structural Geology*, 39: 253-267.
- Gibbs, A. D. (1984): Structural evolution of extensional basin margins. *Journal of the Geological Society*, 141(4), 609-620.
- Gjelberg, J., and Steel, R., (1981): An outline of lower-middle Carboniferous sedimentation on Svalbard: effects of tectonic, climatic and sea level changes in rift basin sequences In: Kerr, J.W. (Ed.) *Geology of the North Atlantic Borderlands*. Canadian Society of Petroleum Geology, 543–561.
- Gjelberg, J., (1984): Early-Middle Carboniferous sedimentation on Svalbard: a study of ancient alluvial and coastal marine sedimentation in rift and strike-slip basins.
- Gjelberg, J., & Steel, R. J. (1995): Helvetiafjellet Formation (Barremian-Aptian), Spitsbergen: characteristics of a transgressive succession. In: R.J. Steel, V.L. Felt, E.P. Johannessen, C. Mathieu (Eds), *Sequence Stratigraphy on the Northwest European Margin Proceedings of the Norwegian Petroleum Society Conference Norwegian Petroleum Society Special Publications 5*: 571-593.

-
- Glørstad-Clark, E., Faleide, J. I., Lundschieen, B. A., & Nystuen, J. P. (2010): Triassic seismic sequence stratigraphy and paleogeography of the western Barents Sea area. *Marine and Petroleum Geology*, 27(7): 1448-1475.
- Glørstad-Clark, E., Birkeland, E. P., Nystuen, J. P., Faleide, J. I., & Midtkandal, I. (2011): Triassic platform-margin deltas in the western Barents Sea. *Marine and Petroleum Geology*, 28(7): 1294-1314.
- Groshong Jr, R. H. (2006): 3-D structural geology. Springer-Verlag Berlin Heidelberg. 1-400.
- Grundvåg, S. A., Marin, D., Kairanov, B., Śliwińska, K. K., Nøhr-Hansen, H., Jelby, M. E., Escalona, A., & Olaussen, S. (2017): The Lower Cretaceous succession of the northwestern Barents Shelf: onshore and offshore correlations. *Marine and Petroleum Geology*, 86: 834-857.
- Grundvåg, S. A., & Olaussen, S. (2017): Sedimentology of the Lower Cretaceous at Kikutodden and Keilhaufjellet, southern Spitsbergen: implications for an onshore–offshore link. *Polar Research*, 36: 1-20.
- Grundvåg, S.-A., Jelby, M. E., Śliwińska, K. K., Nøhr-Hansen, H., Aadland, T., Sandvik, S. E., Tennvassås, I., Engen, T. & Olaussen, S. (2019): Sedimentology and palynology of the Lower Cretaceous succession of central Spitsbergen: integration of subsurface and outcrop data. *Norwegian Journal of Geology*. 99(2): 1-32.
- Gudlaugsson, S. T., Faleide, J. I., Johansen, S. E., & Breivik, A. J. (1998): Late Palaeozoic structural development of the south-western Barents Sea. *Marine and Petroleum Geology*, 15(1): 73-102.
- Gupta, S., Cowie, P. A., Dawers, N. H., & Underhill, J. R. (1998): A mechanism to explain rift-basin subsidence and stratigraphic patterns through fault-array evolution. *Geology*, 26(7): 595-598.

-
- Haile, B. G., Klausen, T. G., Czarniecka, U., Xi, K., Jahren, J., & Hellevang, H. (2018): How are diagenesis and reservoir quality linked to depositional facies? A deltaic succession, Edgeøya, Svalbard. *Marine and Petroleum Geology*, 92: 519-546.
- Haremo, P., & Andresen, A. (1992): Tertiary décollement thrusting and inversion structures along Billefjorden and Lomfjorden Fault Zones, east central Spitsbergen. In *Structural and tectonic modelling and its application to petroleum geology* (pp. 481-494). Elsevier.
- Harms, T. A., & Price, R. A. (1992): The Newport fault: Eocene listric normal faulting, mylonitization, and crustal extension in northeast Washington and northwest Idaho. *Geological Society of America Bulletin*, 104(6): 745-761.
- Harland, W. B. (1969): Contribution of Spitsbergen to Understanding of Tectonic Evolution of North Atlantic Region. In: *North Atlantic: Geology and Continental Drift*, 817-851.
- Harland, W. B., & Gayer, R. A. (1972): The Arctic Caledonides and earlier oceans. *Geological Magazine*, 109(4): 289-314.
- Harland, W. B., Cutbill, J., Friend, P. F., Gobbett, D., Holliday, D., Maton, P., Parker, J., & Wallis, R., (1974): The Billefjorden Fault Zone, Spitsbergen: The long history of a major tectonic lineament, *Norsk Polarinstittutt Skrifter* 161, 1-69.
- Harland, W. B., & Kelly, S. R. A. (1997): Eastern Svalbard Platform. In: *The Geology Of Svalbard* (Ed. by Harland W.B) Geological Society, London, *Memoirs*, 17, 75-95.
- Helland-Hansen, W. (1990): Sedimentation in Paleogene Foreland Basin, Spitsbergen (1). *AAPG Bulletin*, 74(3): 260-272.
- Henriksen, E., Bjørnseth, H. M., Hals, T. K., Heide, T., Kiryukhina, T., Kløvjan, O. Larssen, G., Ryseth, A., Rønning, K., & Sollid, K. (2011): Uplift and erosion of the greater Barents Sea: impact on prospectivity and petroleum systems. In:

-
- Spencer, A.M., Embry, A.F., Gautier D.L, Stoupakova, A.V. & Sørensen, K. (eds) Arctic Petroleum Geology. Geological Society, London, Memoirs, 35: 271-281.
- Henriksen, E., Ryseth, A. E., Larssen, G. B., Heide, T., Rønning, K., Sollid, K., & Stoupakova, A. V. (2011): Tectonostratigraphy of the greater Barents Sea: implications for petroleum systems. In: Spencer, A.M., Embry, A.F., Gautier D.L, Stoupakova, A.V. & Sørensen, K. (eds) Arctic Petroleum Geology. Geological Society, London, Memoirs, 35: 163-195.
- Henstra, G. A., Gawthorpe, R. L., Helland-Hansen, W., Ravnås, R., & Rotevatn, A. (2017): Depositional systems in multiphase rifts: seismic case study from the Lofoten margin, Norway. *Basin Research*, 29(4): 447-469.
- Holliday, D., & Cutbill, J., (1972): The Ebbadalen Formation (Carboniferous), Spitsbergen. In *Proceedings of the Yorkshire Geological and Polytechnic Society*, Geological Society of London, 39: 1-32.
- Høy, T., & Lundschie, B. A. (2011): Triassic deltaic sequences in the northern Barents Sea. In Spencer, A.M., Embry, A.F., Gautier, D.L., Stoupakova, A.V. & Sørensen, K. (eds.): Arctic Petroleum Geology, Geological Society of London Memoirs 35: 249-260.
- Jackson, C. A. L., Gawthorpe, R. L., & Sharp, I. R. (2002): Growth and linkage of the East Tanka fault zone, Suez rift: structural style and synrift stratigraphic response. *Journal of the Geological Society*, 159(2): 175-187.
- Jackson, C. A. L., Gawthorpe, R. L., Carr, I. D., & Sharp, I. R. (2005): Normal faulting as a control on the stratigraphic development of shallow marine syn-rift sequences: the Nukhul and Lower Rudeis Formations, Hammam Faraun fault block, Suez Rift, Egypt. *Sedimentology*, 52(2): 313-338.

-
- Jackson, C. A. L., & Rotevatn, A. (2013): 3D seismic analysis of the structure and evolution of a salt-influenced normal fault zone: a test of competing fault growth models. *Journal of Structural Geology*, 54: 215-234.
- Jackson, C. A. L., Bell, R. E., Rotevatn, A., & Tvedt, A. B. (2017): Techniques to determine the kinematics of synsedimentary normal faults and implications for fault growth models. *Geological Society, London, Special Publications*, 439(1), 187-217.
- Jochmann, M. M., Augland, L.E., Lenz, O., Bieg, G., Haugen, T., Grundvåg, S-A., Jelby, M.E., Midtkandal, I., Dolezych M., & Hjálmarsdóttir, H. R. (2019). Sylfjellet: a new outcrop of the Paleogene Van Mijenfjorden Group in Svalbard; *Arktos*, in press
- Johannessen, E., (1980): Facies analyse av Ebbadalen formasjonen, mellom Karbon, Billefjorden traue, Spitsbergen: Unpublished Cand. Real thesis, University of Bergen. Pages
- Johannessen, E.P. & Embry, A.F. (1989): Sequence correlation: Upper Triassic to Lower Jurassic succession, Canadian and Norwegian Arctic. In: Collinson, J.D. (ed.): *Correlation in Hydrocarbon Exploration*, Norwegian Petroleum Society, Graham and Trotman, 155–170
- Johannessen, E., & Steel, R., (1992): Mid-Carboniferous extension and rift-infill sequences in the Billefjorden Trough, Svalbard. *Norwegian Journal of Geology*, 72(1): 35-48.
- Kim, Y. S., & Sanderson, D. J. (2005): The relationship between displacement and length of faults: a review. *Earth-Science Reviews*, 68(3-4): 317-334.
- Klausen, T. G., & Mørk, A. (2014): The Upper Triassic paralic deposits of the De Geerdalen Formation on Hopen: Outcrop analog to the subsurface Snadd Formation in the Barents Sea The De Geerdalen Formation on Hopen. *AAPG Bulletin*, 98(10): 1911-1941.

-
- Klausen, T. G., Ryseth, A. E., Helland-Hansen, W., Gawthorpe, R., & Laursen, I. (2015): Regional development and sequence stratigraphy of the Middle to Late Triassic Snadd formation, Norwegian Barents Sea. *Marine and Petroleum Geology*, 62: 102-122.
- Klausen, T. G., Torland, J. A., Eide, C. H., Alaei, B., Olaussen, S., & Chiarella, D. (2018): Clinoform development and topset evolution in a mud-rich delta—the Middle Triassic Kobbe Formation, Norwegian Barents Sea. *Sedimentology*, 65(4): 1132-1169.
- Klausen, T.G., Nyberg, B. & Helland-Hansen, W. (2019): The largest delta plain in Earth's history, *Geology*, 47: 470–474.
- Koehl, J. B. P., & Muñoz-Barrera, J. M. (2018): From widespread Mississippian to localized Pennsylvanian extension in central Spitsbergen, Svalbard. *Solid Earth*, 9: 1535–1558.
- Koevoets, M. J., Abay, T. B., Hammer, Ø., & Olaussen, S. (2016). High-resolution organic carbon–isotope stratigraphy of the Middle Jurassic–Lower Cretaceous Agardhfjellet Formation of central Spitsbergen, Svalbard. *Palaeogeography, Palaeoclimatology, Palaeoecology*, 449, 266-274.
- Koevoets, M. J., Hammer, Ø., Olaussen, S., Senger, K., & Smelror, M. (2018): Integrating subsurface and outcrop data of the middle Jurassic to Lower Cretaceous Agardhfjellet formation in central Spitsbergen. *Norwegian Journal of Geology*, 98(4):1-34.
- Krajewski, K. P. (2008): The Botneheia Formation (Middle Triassic) in Edgeøya and Barentsøya, Svalbard: lithostratigraphy, facies, phosphogenesis, paleoenvironment. *Polish Polar Research*, 29(4): 319-364.
- Krajewski, K. P. & Weitschat, W., (2015): Depositional history of the youngest strata of the Sassendalen Group (Bravaisberget Formation, Middle Triassic–Carnian)

in southern Spitsbergen, Svalbard. *Annales Societatis Geologorum Poloniae*, 85: 151–175.

Lamar, D. L., Reed, W. E., & Douglass, D. N. (1986): Billefjorden fault zone, Spitsbergen: Is it part of a major Late Devonian transform?. *Geological Society of America Bulletin*, 97(9): 1083-1088.

Lasabuda, A., Laberg, J. S., Knutsen, S. M., & Safronova, P. (2018): Cenozoic tectonostratigraphy and pre-glacial erosion: A mass-balance study of the northwestern Barents Sea margin, Norwegian Arctic. *Journal of Geodynamics*, 119: 149-166.

Leeder, M. R., & Gawthorpe, R. L. (1987): Sedimentary models for extensional tilt-block/half-graben basins. In: Coward, M.P., Dewey, J.F. & Hancock P.L. (eds) *Continental Extensional Tectonics*. Geological Society, London, Special Publications, 28: 139-152.

Leeder, M. R., & Jackson, J. A. (1993): The interaction between normal faulting and drainage in active extensional basins, with examples from the western United States and central Greece. *Basin Research*, 5(2): 79-102.

Leppard, C. W., & Gawthorpe, R. L. (2006): Sedimentology of rift climax deep water systems; lower rudaia formation, Hammam Faraun fault block, Suez Rift, Egypt. *Sedimentary Geology*, 191(1-2): 67-87.

Liu, Y., Chen, Q., Wang, X., Hu, K., Cao, S., Wu, L., & Gao, F. (2017): Influence of normal fault growth and linkage on the evolution of a rift basin: A case from the Gaoyou depression of the Subei Basin, eastern China. *AAPG Bulletin*, 101(2): 265-288.

Lopes, G., Mangerud, G., & Clayton, G. (2019): The palynostratigraphy of the Mississippian Birger Johnsonfjellet section, Spitsbergen, Svalbard. *Palynology*, 43(4): 631-649.

-
- Lord, G. S., Solvi, K. H., Klausen, T. G., & Mørk, A. (2014): Triassic channel bodies on Hopen, Svalbard: Their facies, stratigraphical significance and spatial distribution. *Norwegian Petroleum Directorate Bulletin*, 11: 41-59.
- Lord G.S., Mørk, M.B. E. Mørk, A. & Olausen S. (2019): Sedimentology and Petrography of the Svenskøya Formation on Hopen, Svalbard: An analogue to sandstone reservoirs in the Realgrunnen Subgroup. *Polar Research*. 38: 3523.
- Lundschieen, B. A., Høy, T., & Mørk, A. (2014): Triassic hydrocarbon potential in the Northern Barents Sea; integrating Svalbard and stratigraphic core data. *Norwegian Petroleum Directorate Bulletin*, 11(11): 3-20.
- Lønøy, A. (1995): A Mid-Carboniferous, carbonate dominated platform, central Spitsbergen: *Norsk Geologisk Tidsskrift*, 75(1): 48-63.
- Maher, H. D., & Welbon, A. I. (1992): Influence of Carboniferous structures on Tertiary tectonism at St. Jonsfjorden and Bellsund, western Svalbard *Norwegian Journal of Geology*, 72(1): 67-75.
- Maher Jr, H. D., Braathen, A., Bergh, S., Dallmann, W., & Harland, W. B. (1995). Tertiary or Cretaceous age for Spitsbergen's fold-thrust belt on the Barents Shelf. *Tectonics*, 14(6), 1321-1326
- Maher, Jr, H. D. (2001): Manifestations of the Cretaceous High Arctic large igneous province in Svalbard. *The Journal of Geology*, 109(1), 91-104.
- Maher, H., and Braathen, A., 2011, Løvehovden fault and Billefjorden rift basin segmentation and development, Spitsbergen, Norway: *Geological Magazine*, 148:154.
- Manby, G. M., Lyberis, N., Chorowicz, J., & Thiedig, F. (1994): Post-Caledonian tectonics along the Billefjorden fault zone, Svalbard, and implications for the Arctic region. *Geological Society of America Bulletin*, 106(2): 201-216.

-
- Martinsen, O. J. (1989): Styles of soft-sediment deformation on a Namurian (Carboniferous) delta slope, Western Irish Namurian Basin, Ireland. In: *Deltas: Sites and Traps for Fossil Fuels*, Whateley, M.K.G. & Pickering, K. T. (eds), Geological Society, London, Special Publications, 41(1): 167– 177.
- Marin, D., Escalona, A., Sliwinska, K., Nøhr-Hansen, H., Mordasova, A., (2016): Sequence stratigraphy and lateral variability of lower cretaceous clinofolds in the SW Barents sea. *AAPG Bull.* 101(9), 1487-1517.
- Matysik, M., Stemmerik, L., Olausson, S., & Brunstad, H. (2018): Diagenesis of spiculites and carbonates in a Permian temperate ramp succession—Tempelfjorden Group, Spitsbergen, Arctic Norway. *Sedimentology*, 65(3): 745-774.
- McCann, A. J., & Dallmann, W. K. (1996): Reactivation history of the long-lived Billefjorden Fault Zone in north central Spitsbergen, Svalbard. *Geological Magazine*, 133(1): 63-84.
- McKenzie, D. (1978): Active tectonics of the Alpine—Himalayan belt: the Aegean Sea and surrounding regions. *Geophysical Journal International*, 55(1): 217-254.
- McLeod, A. E., Dawers, N. H., & Underhill, J. R. (2000): The propagation and linkage of normal faults: insights from the Strathspey–Brent–Statfjord fault array, northern North Sea. *Basin Research*, 12(3-4): 263-284.
- Meyer, V., Nicol, A., Childs, C., Walsh, J.J., Watterson, J. (2002): Progressive localisation of strain during the evolution of a normal fault system in the Timor Sea. *Journal of Structural Geology*, 24: 1215-1231.
- Michalski, K., Lewandowski, M., & Manby, G. (2012): New palaeomagnetic, petrographic and $^{40}\text{Ar}/^{39}\text{Ar}$ data to test palaeogeographic reconstructions of Caledonide Svalbard. *Geological Magazine*, 149(4): 696-721.

-
- Midtkandal, I., Nystuen, J. P., Nagy, J., & Mørk, A. (2008): Lower Cretaceous lithostratigraphy across a regional subaerial unconformity in Spitsbergen: the Rurikfjellet and Helvetiafjellet formations. *Norwegian Journal of Geology*, 88(4): 287-304.
- Midtkandal, I., & Nystuen, J. P. (2009): Depositional architecture of a low-gradient ramp shelf in an epicontinental sea: the lower Cretaceous of Svalbard. *Basin Research*, 21(5): 655-675.
- Midtkandal, I., Faleide, J. I., Faleide, T. S., Serck, C. S., Planke, S., Corseri, R., Dimitriou, M., & Nystuen, J. P. (2019). Lower Cretaceous Barents Sea strata: epicontinental basin configuration, timing, correlation and depositional dynamics. *Geological Magazine*, 1-19.
- Minakov, A., Mjelde, R., Faleide, J. I., Flueh, E. R., Dannowski, A., & Keers, H. (2012): Mafic intrusions east of Svalbard imaged by active-source seismic tomography. *Tectonophysics*, 518: 106-118.
- Morley, C. K., Back, S., Van Rensbergen, P., Crevello, P., & Lambiase, J. J. (2003): Characteristics of repeated, detached, Miocene-Pliocene tectonic inversion events, in a large delta province on an active margin, Brunei Darussalam. Borneo. *Journal of Structural Geology*, 25(7): 1147– 1169
- Morley, C. K., and Wonganan, N. (2000): Normal fault displacement characteristics, with particular reference to synthetic transfer zones, Mae Moh mine, northern Thailand. *Basin Research*, 12(3-4): 307-327.
- Mulrooney, M. J., Rismyhr, B., Yenwongfai, H. D., Leutscher, J., Olausson, S., & Braathen, A. (2018): Impacts of small-scale faults on continental to coastal plain deposition: Evidence from the Realgrunnen Subgroup in the Goliat field, southwest Barents Sea, Norway. *Marine and Petroleum Geology*, 95: 276-302.

-
- Müller, R. D., & Spielhagen, R. F. (1990): Evolution of the Central Tertiary Basin of Spitsbergen: towards a synthesis of sediment and plate tectonic history. *Palaeogeography, Palaeoclimatology, Palaeoecology*, 80(2): 153-172.
- Müller, R., Klausen, T.G., Faleide, J.I., Olausen, S., Eide, C.H. & Suslova, A. (2019): Linking regional unconformities in the Barents Sea to compression-induced forebulge uplift at the Triassic-Jurassic transition. *Tectonophysics* 765: 35–51.
- Mørk, A., Knarud, R., & Worsley, D. (1982): Depositional and diagenetic environments of the Triassic and Lower Jurassic succession of Svalbard. In *Arctic geology and geophysics: proceedings of the Third International Symposium on Arctic Geology* (Ed. by: Embry, A.F. & Balkwill, H.R.), Calgary: Canadian Society of Petroleum Geologist, 371-398.
- Mørk, M. B. E. (1999): Compositional variations and provenance of Triassic sandstones from the Barents Shelf. *Journal of Sedimentary Research*, 69(3): 690-710.
- Mørk, A., Dallmann, W. K., Dypvik, H., Johannessen, E. P., Larssen, G. B., Nagy, J., Nøttvedt, A., Olausen, S., Pcelina, T.M & Worsley, D. (1999): Mesozoic lithostratigraphy. In *Lithostratigraphic lexicon of Svalbard. Upper Palaeozoic to Quaternary bedrock. Review and recommendations for nomenclature use* (Ed. By: Dallmann, W. K.), Tromsø, Norsk Polarinstitut, 127-214.
- Nemec, W., Steel, R. J., Gjelberg, J., Collinson, J. D., Prestholm, E., & Oxnevad, I. E. (1988): Anatomy of collapsed and re-established delta front in Lower Cretaceous of eastern Spitsbergen: Gravitational sliding and sedimentation processes. *AAPG Bulletin*, 72(4): 454– 476.
- Nicol, A., Walsh, J., Berryman, K., & Nodder, S. (2005): Growth of a normal fault by the accumulation of slip over millions of years. *Journal of Structural Geology*, 27(2): 327-342.

-
- Nicol, A., Walsh, J. J., Villamor, P., Seebeck, H., & Berryman, K. R. (2010): Normal fault interactions, paleoearthquakes and growth in an active rift. *Journal of Structural Geology*, 32(8): 1101-1113.
- Nøttvedt, A., Livbjerg, F., Midbøe, P. S. & Rasmussen, E. (1993): Hydrocarbon potential of the Central Spitsbergen Basin. In Vorren, T. O., et al. (Eds.): *Arctic Geology and Petroleum Potential*. Amsterdam, Elsevier, 333-361.
- Ocamb, R. D. (1961): Growth faults of south Louisiana. *Gulf Coast Association of Geological Societies Transactions*, 11: 139–174.
- Olaussen, S., Larssen, G. B, Helland-Hansen, W., Johannessen, E.P., Nøttvedt A., Riis, F., Rismyhr, B., Smelror, M. and Worsley, D. (2018): Mesozoic strata of the Kong Karls Land, Svalbard, Norway; a link to the northern Barents Sea basins and platforms, *Norwegian Journal of Geology*. 98: 1-69.
- Olaussen, S., Stemmerik, L., Sorento Drøhse , T., Johannessen, E. P. & Smyrak-Sikora, A. 2019: Carboniferous Permian climate changes as recorded in Svalbard. In: *Vinterkonferansen, Abstracts and Proceedings of the Geological Society of Norway*, Bergen 7-9. January, 1: 70.
- Osmundsen, P. T., Braathen, A., Rød, R. S., & Hynne, I. B. (2014): Styles of normal faulting and fault-controlled sedimentation in the Triassic deposits of Eastern Svalbard. *Norwegian Petroleum Directorate Bulletin*, 11: 61– 79.
- Paton, D. A. (2006): Influence of crustal heterogeneity on normal fault dimensions and evolution: southern South Africa extensional system. *Journal of Structural Geology*, 28(5): 868-886.
- Peacock, D. C. P., Nixon, C. W., Rotevatn, A., Sanderson, D. J., & Zuluaga, L. F. (2016): Glossary of fault and other fracture networks. *Journal of Structural Geology*, 92, 12-29.

-
- Petrov, O., Morozov, A., Shokalsky, S., Kashubin, S., Artemieva, I. M., Sobolev, N., Petrova, E., Ernstef, R.E., Sergeeva, S. & Smelror, M. (2016): Crustal structure and tectonic model of the Arctic region. *Earth-Science Reviews*, 154: 29-71.
- Pickard, N. A., Eilertsen, F., Hanken, N.-M., Johansen, T. A., Lønøy, A., Nakrem, H., Nilsson, I., Samuelsen, T., and Somerville, I., (1996): Stratigraphic framework of Upper Carboniferous (Moscovian-Kasimovian) strata in Bünsow land, central Spitsbergen: palaeogeographic implications. *Norwegian Journal of Geology*, 76(3): 169-185.
- Piepjoh K., Brinkmann L., Grewing A., Kerp H. (2000): New data on the age of the uppermost ORS and the lowermost post-ORS strata in Dickson Land (Spitsbergen) and implications for the age of the Svalbardian deformation. In P.F. Friend & B.P.J. Williams (eds.): *New perspectives on the Old Red Sandstone*. Geological Society of London Special Publications. 180: 603–609.
- Piepjoh, K., von Gosen, W., Tessensohn, F., Reinhardt, L., McClelland, W. C., Dallmann, W., Gaedicke, C., & Harrison, J. C. (2015): Tectonic map of the Ellesmerian and Eureka deformation belts on Svalbard, north Greenland, and the Queen Elizabeth Islands (Canadian Arctic). *arktos*, 1(1), 12.
- Polteau, S., Hendriks, B. W., Planke, S., Ganerød, M., Corfu, F., Faleide, J. I., Midtkandal, I., Svensen, H.S., & Myklebust, R. (2016): The Early Cretaceous Barents Sea sill complex: distribution, $^{40}\text{Ar}/^{39}\text{Ar}$ geochronology, and implications for carbon gas formation. *Palaeogeography, Palaeoclimatology, Palaeoecology*, 441: 83-95.
- Prestholm, E., & Walderhaug, O. (2000): Synsedimentary faulting in a Mesozoic deltaic sequence, Svalbard, Arctic Norway-Fault geometries, faulting mechanisms, and sealing properties. *AAPG Bulletin*, 84(4): 505– 522.

-
- Ravnås, R., & Steel, R. J. (1997): Contrasting styles of Late Jurassic syn-rift turbidite sedimentation: a comparative study of the Magnus and Oseberg areas, northern North Sea. *Marine and Petroleum Geology*, 14(4): 417-449.
- Ravnås, R., & Steel, R. J. (1998). Architecture of marine rift-basin successions: AAPG Bulletin, 82. 110-146.
- Riis, F., Lundschieen, B. A., Høy, T., Mørk, A., & Mørk, M. B. E. (2008): Evolution of the Triassic shelf in the northern Barents Sea region. *Polar Research*, 27(3): 318-338.
- Rismyhr, B., Bjærke, T., Olausson, S., Mulrooney, M. J., & Senger, K. (2019): Facies, palynostratigraphy and sequence stratigraphy of the Wilhelmøya Subgroup (Upper Triassic–Middle Jurassic) in western central Spitsbergen, Svalbard. 1-30.
- Rittersbacher, A., Buckley, S. J., Howell, J. A., Hampson, G. J. & Vallet, J. (2013): Helicopter-based laser scanning: a method for quantitative analysis of large-scale sedimentary architecture. In Martinius, A. W., Howell, J. A. & Good, T. (Eds.): *Sediment-body Geometry and Heterogeneity: Analogue Studies for Modelling the Subsurface*. London, Geological Society of London Special Publication 387: 1-18.
- Rossi, V. M., Paterson, N. W., Helland-Hansen, W., Klausen, T. G., & Eide, C. H. (2019): Mud-rich delta-scale compound clinoforms in the Triassic shelf of northern Pangea (Havert Formation, south-western Barents Sea). *Sedimentology*, 66(6), 2234-2267.
- Rotevatn, A., & Fossen, H. (2012): Soft faults with hard tips: magnitude-order displacement gradient variations controlled by strain softening versus hardening; implications for fault scaling. *Journal of the Geological Society*, 169(2): 123-126.

-
- Rotevatn, A., & Jackson, C. A. L. (2014): 3D structure and evolution of folds during normal fault dip linkage. *Journal of the Geological Society*, 171(6): 821-829.
- Rotevatn, A., Kristensen, T. B., Ksienzyk, A. K., Wemmer, K., Henstra, G. A., Midtkandal, I., Grundvåg, S-A., & Andresen, A. (2018): Structural inheritance and rapid rift-length establishment in a multiphase rift: the East Greenland rift system and its Caledonian orogenic Ancestry. *Tectonics*, 37(6): 1858-1875.
- Rotevatn, A., Jackson, C. A. L., Tvedt, A. B., Bell, R. E., & Blækkan, I. (2019): How do normal faults grow? *Journal of Structural Geology*, 125: 174-184.
- Ryseth, A. (2014): Sedimentation at the Jurassic-Triassic boundary, south-west Barents Sea. In Martinius, A.W., Ravnås, R., Howell, J.A., Steel, R.J. & Wonham, J.P. (eds.): *From Depositional Systems to Sedimentary Successions on the Norwegian Continental Margin*, International Association Sedimentology Special Publication 46:187–214.
- Rød, R. S., Hynne, I. B. & Mørk, A. (2014): Depositional environment of the Upper Triassic De Geerdalen Formation—an EW transect from Edgeøya to Central Spitsbergen, Svalbard. *Norwegian Petroleum Directorate Bulletin*, 11: 21-40.
- Röhnert, A. D. (2016): Geometry and sedimentary facies of low-angle clinoforms, Edgeøya, Svalbard (Master's thesis) 1-173.
- Schlische, R. W. (1991): Half-graben basin filling models: new constraints on continental extensional basin development. *Basin Research*, 3(3): 123-141.
- Schlische, R. W. (1995): Geometry and origin of fault-related folds in extensional settings. *AAPG bulletin*, 79(11):1661-1678.
- Schlische, R. W., Young, S. S., Ackermann, R. V., & Gupta, A. (1996): Geometry and scaling relations of a population of very small rift-related normal faults. *Geology*, 24(8): 683-686.

-
- Scotese, C. R., Bambach, R. K., Barton, C., Van der Voo, R., & Ziegler, A. M. (1979): Paleozoic base maps. *The Journal of Geology*, 87(3): 217-277.
- Senger, K., Millett, J., Planke, S., Ogata, K., Eide, C. H., Festøy, M., Galland, O., & Jerram, D. A. (2017): Effects of igneous intrusions on the petroleum system: a review. *First Break*, 35(6): 47-56.
- Senger, K., Brugmans, P., Grundvåg, S. A., Jochmann, M., Nøttvedt, A., Olausson, S., Skote, A., & Smyrak-Sikora, A. (2019): Petroleum, coal and research drilling onshore Svalbard: a historical perspective. *Norwegian Journal of Geology*, 99(3): 1-30.
- Serck, C. S., & Braathen, A. (2019): Extensional fault and fold growth: Impact on accommodation evolution and sedimentary infill. *Basin Research*, 31(5), 967-990.
- Sharp, I. R., Gawthorpe, R. L., Armstrong, B., & Underhill, J. R. (2000): Propagation history and passive rotation of mesoscale normal faults: implications for synrift stratigraphic development. *Basin Research*, 12(3-4): 285-305.
- Sharp, I. R., Gawthorpe, R. L., Underhill, J. R., & Gupta, S. (2000): Fault-propagation folding in extensional settings: Examples of structural style and synrift sedimentary response from the Suez rift, Sinai, Egypt. *Geological Society of America Bulletin*, 112(12): 1877-1899.
- Shultz, M. R., & Hubbard, S. M. (2005): Sedimentology, stratigraphic architecture, and ichnology of gravity-flow deposits partially ponded in a growth-fault-controlled slope minibasin, Tres Pasos Formation (Cretaceous), southern Chile. *Journal of Sedimentary Research*, 75(3): 440– 453.
- Sorento, T., Olausson, S., & Stemmerik, L. Controls on deposition of shallow marine carbonates and evaporates—lower Permian Gipshuken Formation, Central Spitsbergen, Arctic Norway. *Sedimentology*, 1-32.

-
- Steel, R. J., Dalland, A., Kalgraff, K., & Larsen, V. (1981): The Central Tertiary Basin of Spitsbergen: sedimentary development of a sheared- margin basin. *Can. Soc. Petroleum Geologists Mem.*, 7: 647-664.
- Steel, R. J., & Worsley, D. (1984): Svalbard's post-Caledonian strata—an atlas of sedimentational patterns and palaeogeographic evolution. In *Petroleum geology of the North European margin* (Ed by: Spencer, A. M.). Springer, Dordrecht. 109-135.
- Steel, R., Gjelberg, J., Helland-Hansen, W., Kleinspehn, K., Nøttvedt, A., & Rye-Larsen, M. (1985): The Tertiary strike-slip basins and orogenic belt of Spitsbergen. In: .T. Biddle, N. Christie-Blick (Eds.), *Strike-Slip Deformation, Basin Formation and Sedimentation*, SEPM Special Publication, Tulsa, 37: 339-359.
- Stemmerik, L., & Worsley, D. (1989): Late Palaeozoic sequence correlations, North Greenland, Svalbard and the Barents Shelf. In: *Correlation in hydrocarbon exploration*, Collinson (Ed.), Springer, Dordrecht, 99-111.
- Stemmerik, L. (2000): Late Palaeozoic evolution of the North Atlantic margin of Pangea. *Palaeogeography, Palaeoclimatology, Palaeoecology*, 161(1-2): 95-126.
- Thorsen, C.E. (1963): Age of growth faulting in southeast Louisiana. *Trans. Gulf Coast Ass. geol. Soc.*, 13: 103-110.
- Torsvik, T. H., Carlos, D., Mosar, J., Cocks, L. R. M., & Malme, T. (2002): Global reconstructions and North Atlantic paleogeography 440 Ma to recent. *BATLAS—Mid Norway plate reconstruction atlas with global and Atlantic perspectives. Geological Survey of Norway, Trondheim*, 18, 39.
- van der Zee, W., & Urai, J. L. (2005): Processes of normal fault evolution in a siliciclastic sequence: A case study from Miri, Sarawak, Malaysia. *Journal of Structural Geology*, 27(12): 2281– 2300.

-
- Verba, M.L. (2013): Kollektornye svoystva porod osadochnogo chekhla arhipelaga Shpitsbergen [Sedimentary cover reservoir of Svalbard archipelago]. *Neftegazovaya Geologiya. Teoriya I Praktika*, 8: 1–45.
- Walsh, J. J., & Watterson, J. (1988): Analysis of the relationship between displacements and dimensions of faults. *Journal of Structural geology*, 10(3): 239-247.
- Walsh, J. J., Nicol, A., & Childs, C. (2002): An alternative model for the growth of faults. *Journal of Structural Geology*, 24(11): 1669-1675.
- Walsh, J. J., Bailey, W. R., Childs, C., Nicol, A., & Bonson, C. G. (2003): Formation of segmented normal faults: a 3-D perspective. *Journal of Structural Geology*, 25(8): 1251-1262.
- Wignall, P. B., & Best, J. L. (2004): Sedimentology and kinematics of a large, retrogressive growth-fault system in Upper Carboniferous deltaic sediments, western Ireland. *Sedimentology*, 51(6): 1343-1358.
- Worsley, D., (2008): The post-Caledonian development of Svalbard and the western Barents Sea: *Polar Research*, 27(3): 298-317.

PART II

ARTICLE 3

Smyrak-Sikora, A., Osmundsen, P. T., Braathen, A., Ogata, K., Anell, I., Mulrooney, M. & Zuchuat, V. (2019): "Architecture of growth basins in a tidally-influenced, prodelta to delta-front setting: the Triassic succession of Kvalpynten, East Svalbard", Basin Research.
<https://doi.org/10.1111/bre.12410>

Architecture of growth basins in a tidally influenced, prodelta to delta-front setting: The Triassic succession of Kvalpynten, East Svalbard

Aleksandra Smyrak-Sikora^{1,2}  | Per Terje Osmundsen^{3,4} | Alvar Braathen^{1,4}  |
Kei Ogata⁵  | Ingrid Anell⁴ | Mark J. Mulrooney⁴ | Valentin Zuchuat⁴

¹Department of Arctic Geology, University Centre in Svalbard, Longyearbyen, Norway

²Department of Earth Science, University of Bergen, Bergen, Norway

³Department of Geoscience and Petroleum, Norwegian University of Science and Technology, Trondheim, Norway

⁴Department of Geosciences, University of Oslo, Oslo, Norway

⁵Faculty of Science, Geology and Geochemistry Cluster, VU Amsterdam, Amsterdam, The Netherlands

Correspondence

Aleksandra Smyrak-Sikora, Department of Arctic Geology, University Centre in Svalbard, Longyearbyen, Norway.
Email: aleksandras@unis.no

Funding information

Norges Forskningsråd, Grant/Award Number: grant 234152/E30

Abstract

World-class examples of fault-controlled growth basins with associated syn-kinematic sedimentary fill are developed in Upper Triassic prodelta to delta-front deposits exposed at Kvalpynten, SW Edgeøya in East Svalbard. They are interpreted to have interacted with north-westerly progradation of a regional delta system. The syn-kinematic successions consist of 4 to 5 coarsening-upward units spanning from offshore mudstones to subtidal heterolithic bars and compound tidal dunes, which were blanketed by regional, post-kinematic sandstone sheets deposited as laterally continuous, subaqueous tidal dune fields. The rate of growth faulting is reflected in the distribution of accommodation, which governs sedimentary architecture and stacking patterns within the coarsening-upward units. Fully compartmentalized basins (12, 200–800 m wide and c. 150 m high grabens and half grabens) are characterized by syn-kinematic sedimentary infill. These grabens and half-grabens are separated by 60–150 m high horsts composed of pro-delta to distal delta-front mudstones. Grabens host tabular tidal dunes (sandwaves), whereas half-grabens bound by listric faults (mainly south-dipping) consist of wedge-shaped, rotated strata with erosive boundaries proximal to the uplifted fault block crests. Heterolithic tidal bars (sand ridges) occur in narrow half-grabens, showing migration oblique to the faults, up the dip slope. Structureless sandstone wedges and localized subaqueous slumps that formed in response to collapse of the block crests were only documented in half-grabens. Late-kinematic deposition during the final stages of faulting occurred in partly compartmentalized basins, filled with variably thick sets of continuous sandstone belts (compound tidal dunes).

1 | INTRODUCTION

Syn-sedimentary growth faults are often associated with deltas discharging sediments into shallow seas, as recognized in: (a) foreland basins (Bhattacharya & Davies,

2001; Bouroulec et al., 2004; Braathen, Midtkandal, et al., 2018; Fielding, 2015; Shultz & Hubbard, 2005), (b) extensional basins (Martinsen, 1989; Wignall & Best, 2004), (c) epicontinental seas (Edwards, 1976; Nemeč et al., 1988; Osmundsen, Braathen, Rød, & Hynne, 2014; Prestholm

This is an open access article under the terms of the Creative Commons Attribution License, which permits use, distribution and reproduction in any medium, provided the original work is properly cited.

© 2019 The Authors. Basin Research published by International Association of Sedimentologists and European Association of Geoscientists and Engineers and John Wiley & Sons Ltd.

& Walderhaug, 2000) and (d) in forearc basins (Zecchin, Massari, Mellere, & Prosser, 2004). Large systems of growth faults are also developed along continental margins, as observed in outcrops of NW Borneo (Back, Strozyk, Kukla, & Lambiase, 2008; Burhannudinnur & Morley, 1997; Morley, Back, Rensbergen, Crevello, & Lambiase, 2003; van der Zee & Urai, 2005) and in seismic data sets (Lopez, 1990; Weber, 1987). These growth fault systems dissect offshore organic-rich mudstones overlain by reservoir sandstones and are often associated with prolific petroleum systems (Cailliet & Batiot, 2003; Weber, 1987). Recent seismic studies address large-scale 3D geometries and fault evolution (Fazlikhani, Back, Kukla, & Fossen, 2017; Hiscott, 2001; Tvedt, Rotevatn, Jackson, Fossen, & Gawthorpe, 2013), however, they miss details regarding distribution of sedimentary facies impacted by faulting.

Growth faults commonly appear listric on the seismic profiles and in outcrops, with an overall fault trend parallel to the palaeo-shelf margin or delta lobe slope (e.g. Back et al., 2008; Fielding, 2015). In a plan view they tend to show scoop or cusate shapes (e.g. Braathen, Midtkandal, et al., 2018; Wignall & Best, 2004). Growth faults often initiate and evolve due to gravitational instability of a slope and/or loading of thick sandstone succession accumulated over a mobile substrate, that is salt or shale (e.g. Garfunkel, 1984; Winker & Edwards, 1983), differential compaction (Back & Morley, 2016; Bruce, 1973; Carver, 1968; Taylor, Nicol, & Walsh, 2008), fluid escape and shale expulsion (Van Rensbergen & Morley, 2000). A collapse above rising salt diapirs (Ings & Beaumont, 2010; Tvedt, Rotevatn, & Jackson, 2016) or shale diapirs (e.g. Morley & Guerin, 1996; Ocamb, 1961) can also induce growth faulting. Growth faulting can be spontaneous or be triggered by seismic events disturbing unstable and overpressured deposits (e.g. Garfunkel, 1984; Martinsen & Bakken, 1990; Martinsen, Lien, Walker, & Collinson, 2003; Nemeč et al., 1988). The evolution of growth faults is often related to the lateral and vertical linkage of fault segments (e.g. Cartwright, Mansfield, & Trudgill, 1996; Rotevatn & Jackson, 2014; Rykkelid & Fossen, 2002; Serck & Braathen, 2019; Tvedt et al., 2013; Walsh, Bailey, Childs, Nicol, & Bonson, 2003). Field- and seismic-based studies and analogue modelling mainly show that extensional faulting tend to affect the delta top and upper delta front of the prograding deltaic system, whereas the lower delta front/prodelta can experience shortening and in some cases formation of gravity-induced deep water fold-and-thrust belts (e.g. Braathen, Midtkandal, et al., 2018; Ings & Beaumont, 2010; McClay, Dooley, & Lewis, 1998; Rouby et al., 2011; Winker & Edwards, 1983).

Syn-sedimentary architecture of fault-bounded basins in prograding delta deposits has been previously assessed through the study of exhumed Triassic strata onshore Svalbard on Edgeøya island (Figure 1a,b; e.g. Edwards, 1976;

Highlights

- The Triassic prodelta to delta-front succession in Kvalpynten (south-eastern Svalbard) is intersected by growth faults.
- Growth basins were filled with coarsening-upward units composed of prodelta mudstone, tidally-influenced, heterolithic strata and tidal dunes.
- Basin-fill reflect distinct rate and spatial distribution of creation of accommodation, which occur in: fully compartmentalized (a) half-grabens and (b) grabens, (c) late-kinematic accommodation witnessing ceasing faulting and (d) post-kinematic accommodation.
- Stacking of architectural elements within coarsening-upward growth units is controlled by the type of accommodation and sediment supply.

Osmundsen et al., 2014; Maher, Ogata, & Braathen, 2017; Ogata et al., 2018). The Kvalpynten faults are developed in a prodelta to lower delta front position within the distal part of a major deltaic system that prograded north-westwards across the Barents Shelf (Anell, Braathen, & Olausen, 2014; Anell, Faleide, & Braathen, 2016; Glørstad-Clark, Birkeland, Nystuen, Faleide, & Midtkandal, 2011; Glørstad-Clark, Faleide, Lundschieen, & Nystuen, 2010; Høy & Lundschieen, 2011; Lundschieen, Høy, & Mørk, 2014; Riis, Lundschieen, Høy, Mørk, & Mørk, 2008; Worsley, 2008). The differential compaction in combination with reactivation of deep-seated faults have been suggested as a trigger mechanism for the Kvalpynten growth faults developed in lower delta front/prodelta position (Braathen, Midtkandal, et al., 2018; Maher et al., 2017; Ogata et al., 2018). Growth fault morphology impacted the topography of the basin floor, creating footwall highs and hanging wall lows (Braathen, Midtkandal, et al., 2018; Ogata et al., 2018), that defined compartments accumulating syn-kinematic deposits.

This study analyses the sedimentary architecture encountered in the growth-faulted, tidally-influenced, deltaic deposits of Kvalpynten, on Edgeøya, East Svalbard (Figure 1a,b). It specifically targets the growth units, which consists of Upper Triassic mudstones and sandstones (Braathen, Midtkandal, et al., 2018; Edwards, 1976; Maher et al., 2017; Ogata et al., 2018; Osmundsen et al., 2014). This study focuses on fault-controlled hanging wall accommodation, where sediments were funnelled into 200- to 800-m-wide depocenters, potentially extending over hundreds to thousands of metres. In such depocenters, slopes may change repeatedly and the substrate morphology may influence the distribution of tidal energy (e.g. Rossi et al., 2017). Erosion and sedimentation variations

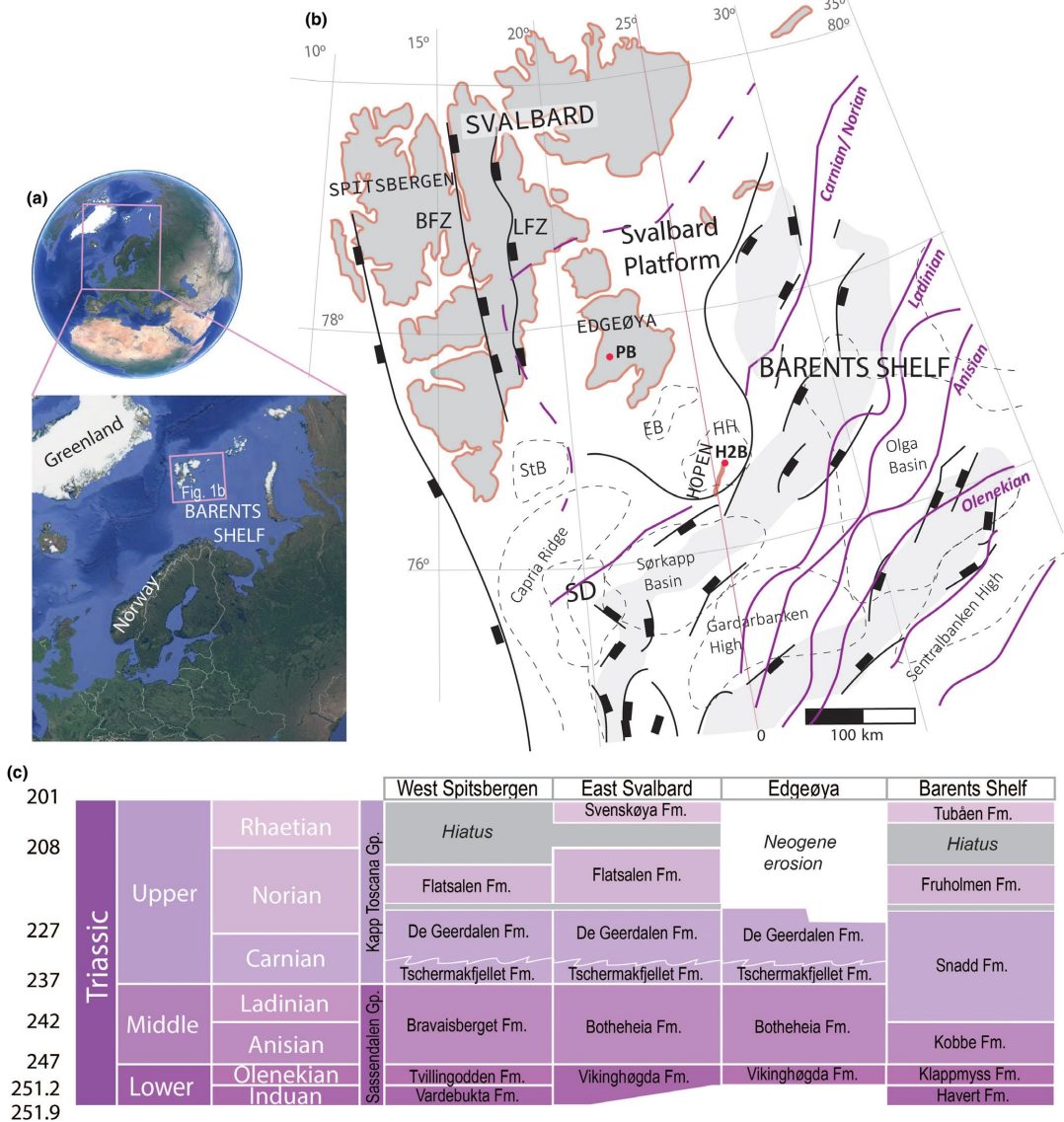


FIGURE 1 (a) Position of Svalbard on the Barents Shelf (Image sourced from <https://earth.google.com>) (b) Structural framework with upper Palaeozoic structures on the SW Barents Shelf. Palaeozoic rift basins are shaded with grey. Edgeøya island, Edgeøya Basin (EB) and Hopen High (HH) form the Svalbard Platform; Purple lines mark the position of clinoforms (deltaic platform edge in Anell et al., 2014) that prograded in the Triassic across the Barents Shelf (modified after Faleide et al., 2008 and Anell et al., 2014, 2016); Red dots show the position of Plurdalen borehole (PB) and Hopen 2 borehole (H2B); SD Sørkapp Depression, STB Storfjorden Basin; BFZ Billefjorden Fault Zone; LFZ Lomfjorden Fault Zone; (c) Triassic stratigraphy of Svalbard and Barents Shelf, grey boxes mark a hiatus; modified after Riis et al. (2008); Formations ages are from Vigran, Mangerud, Mørk, Worsley, & Hochuli, 2014; Paterson & Mangerud, 2015; Smelror, Larssen, Olausson, Rømuld, & Robert, 2018; Rismyhr et al., 2019

within an environment with high tidal currents will impact the distribution of facies belts and facies stacking patterns, reflected in distinct sedimentary architectures. The main questions that this work will address are as follows:

- What kind of facies associations are deposited in the growth basins?
- How are the rates of fault-driven accommodation creation expressed in the sedimentary architecture?

- How did the basin geometry (i.e. symmetric vs. asymmetric growth-basins) impacted stacking of architectural elements?
- What controlled on development of coarsening-upward units?

The observations and interpretations reported in this study are relevant to studies in the Barents Sea region, as the Kvalpynten strata extend offshore (Anell, Braathen, Olausen, & Osmundsen, 2013), where similar successions have been documented at sub-seismic to seismic scale (e.g. Mulrooney, Leutscher, & Braathen, 2017; Mulrooney et al., 2018; Serck, Faleide, Braathen, Kjølhamar, & Escalona, 2017). More broadly, this study provides insights into facies associations and facies architectures that can be expected in other growth-faulted deltaic successions systems around the world.

2 | GEOLOGICAL SETTING

The Svalbard archipelago represents the uplifted north-western region of the Barents Shelf (Figure 1a,b). Edgeøya is the third largest island of the archipelago. After tectonic instability in the Devonian (Braathen, Osmundsen, Maher, & Ganerød, 2018) and the subsequent Carboniferous to Middle Permian rifting (Ahlborn & Stemmerik, 2015; Braathen, Bælum, Maher, & Buckley, 2011; Johannessen & Steel, 1992; Smyrak-Sikora, Johannessen, Olausen, Sandal, & Braathen, 2019), a fairly stable Svalbard Platform was established in the Late Permian (Figure 1b). Renewed mild and localized fault activity is reflected in thickness variations in Triassic deposits preserved both on- and offshore Svalbard's eastern flank (Anell et al., 2013; 2016; Ogata et al., 2018; Osmundsen et al., 2014). Tectonic instability during the Triassic is ascribed to far-field stresses transferred from the Uralian orogeny (Anell et al., 2013). Thickness variations of the Permian and Triassic deposits recorded between well data from Edgeøya and Hopen (Plurdalen and Hopen 2 wells Figure 1; Harland & Kelly, 1997) indicate a higher subsidence towards the southeast, towards Hopen Island and further towards the Barents Shelf (Figure 1b; Anell et al., 2016; Faleide, Gudlaugsson, & Jacquart, 1984; Fielding, 2015). The subsidence rates in the Barents Sea and in Svalbard decreased near the Triassic-Jurassic boundary (Rismyhr, Bjærke, Olausen, Mulrooney, & Senger, 2019; Ryseth, 2014). A second phase of regional subsidence of the Svalbard Platform was initiated in the Middle Jurassic and led to deposition of deeper marine sediments (Dypvik, Hakansson, & Heinberg, 2002; Koevoets, Hammer, Olausen, Senger, & Smelror, 2019). Succeeding shallowing of the depositional environments is recorded by Lower Cretaceous deposits formed in response to uplift of the northern side of Svalbard (Gjelberg & Steel, 1995; Grundvåg et al., 2017; Grundvåg & Olausen, 2017; Midtkandal & Nystuen, 2009;

Midtkandal, Nystuen, Nagy, & Mørk, 2008; Olausen et al., 2018). Exhumation of Triassic sedimentary rocks on Edgeøya resulted from Late Cretaceous uplift and associated magmatism, coupled with the establishment of a fold-and-thrust belt in the west of Svalbard during the Palaeogene, and isostatic post-glacial rebound, notably during the Holocene (Anell et al., 2013; Bergh, Maher, & Braathen, 2000; Braathen, Bergh, & Maher, 1999; Dallmann, Elvevold, Majka, & Piepjohn, 2015; Dimakis, Braathen, Faleide, Elverhøi, & Gudlaugsson, 1998; Faleide et al., 2008; 2017; Henriksen et al., 2011; Steel & Worsley, 1984; Worsley, 2008).

2.1 | Triassic sedimentary system on the Barents Shelf and the eastern Svalbard Platform

During the Triassic the Barents Shelf was a boreal, epicontinental basin with water depths in the range 200–400 m (Anell et al., 2014; 2016; Høy & Lundschieen, 2011). The offshore shelfal deposits of the Lower Triassic were overlain by a mudstone-dominated deltaic successions sourced from the Uralides with minor additional sources from the Baltic shield to the south, and from Novaya Zemlya to the east (Figure 1b,c; Anell et al., 2014; 2016, 2011; Eide, Klausen, Katkov, Suslova, & Helland-Hansen, 2017; Glørstad-Clark et al., 2010; Høy & Lundschieen, 2011; Klausen, Ryseth, Helland-Hansen, Gawthorpe, & Laursen, 2015; Klausen et al., 2018; Lundschieen et al., 2014; Riis et al., 2008; Worsley, 2008). In seismic data, this system is expressed as a set of northwest-prograding clinoforms (Anell et al., 2014; 2016, 2011; Glørstad-Clark et al., 2010; Høy & Lundschieen, 2011; Riis et al., 2008). On the Barents Shelf the delta top-sets consist of tidally-influenced distributary channel systems of the Snadd Formation (Figure 1c; Klausen et al., 2018; Riis et al., 2008).

The succession exposed on Edgeøya corresponds to the distal part of the upper Middle and Upper Triassic deltaic deposits (Glørstad-Clark et al., 2010; 2011; Høy & Lundschieen, 2011; Mørk, Knarud, & Worsley, 1982) that overlap the Svalbard Platform (Figure 1b; Anell et al., 2014). The c. 80-m-thick shallow-marine, organic matter-rich mudstones of the Middle Triassic Botneheia Formation (Figure 1c; Krajewski, 2008) are capped by a 65- to 140-m-thick dark grey, mudstone-dominated, offshore to prodelta deposits of the Tschermakfjellet Formation (Figures 1c and 2). The prodelta deposits are overlain by 400-m-thick mixed sandstones and mudstones of the Carnian to Norian De Geerdalen Formation (Figures 1c and 2). This formation is characterized by shallowing-upward, tide-dominated deposits of delta-front to delta top (Flood, Nagy, & Winsnes, 1971; Haile et al., 2018; Klausen & Mørk, 2014; Lord, Johansen, Støen, & Mørk, 2017; Lord, Solvi, Klausen, & Mørk, 2014; Mørk

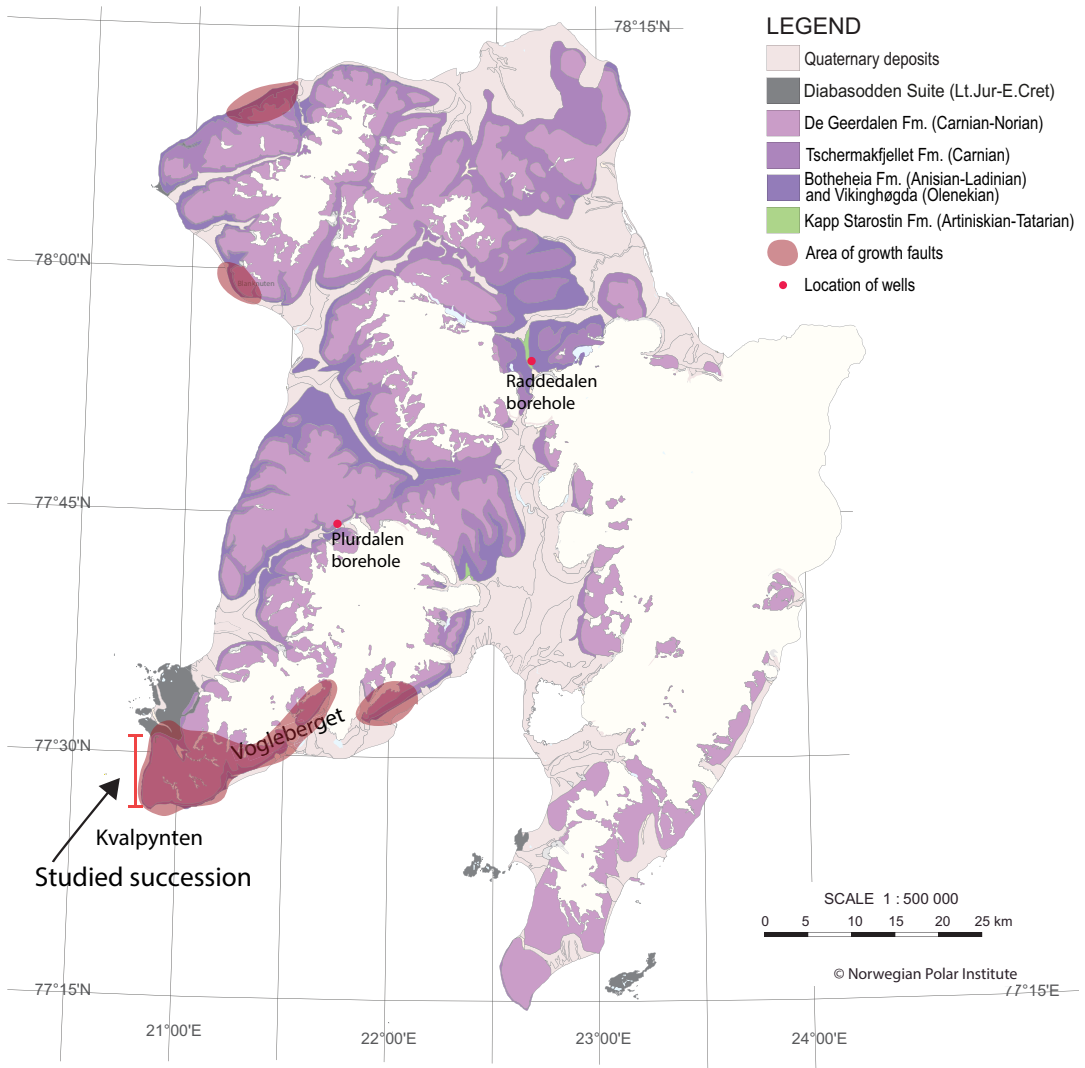


FIGURE 2 Geological map of eastern Svalbard with islands of Edgeøya and Barentsøya. The position of study area in Kvalpynten is outlined. Location of reported growth faults is marked in red

et al., 1982; Mørk, 1999; Riis et al., 2008; Rød, Hynne, & Mørk, 2014; Röhnert, 2016).

The Triassic succession on Edgeøya differs from the rest of Svalbard due to the occurrence of numerous rotated fault blocks. These structures were first identified by Edwards (1976) who interpreted them as growth faults related to the collapse of a southwards-prograding delta. Growth faults were recognized at Klinkhamaren, Øhmanfjellet and Tjufvfjordskarvet (Figure 2; Maher et al., 2017; Ogata et al., 2018; Osmundsen et al., 2014; Riis et al., 2008; Rød et al., 2014). The most spectacular outcrops of these faults are,

however, located along the north-south oriented cliffs of the Kvalpynten peninsula, as shown in Figure 3.

2.2 | The Kvalpynten succession

Growth faults occur only in the lower half of the 9 km long and c. 350–400 m high Kvalpynten cliff. Growth faults that display tens to a hundred of metres offsets are mainly observed in deposits of the Tschermakfjellet and De Geerdalen formations (Figures 2 and 3; Edwards, 1976; Ogata et al., 2018; Osmundsen et al., 2014; Rød

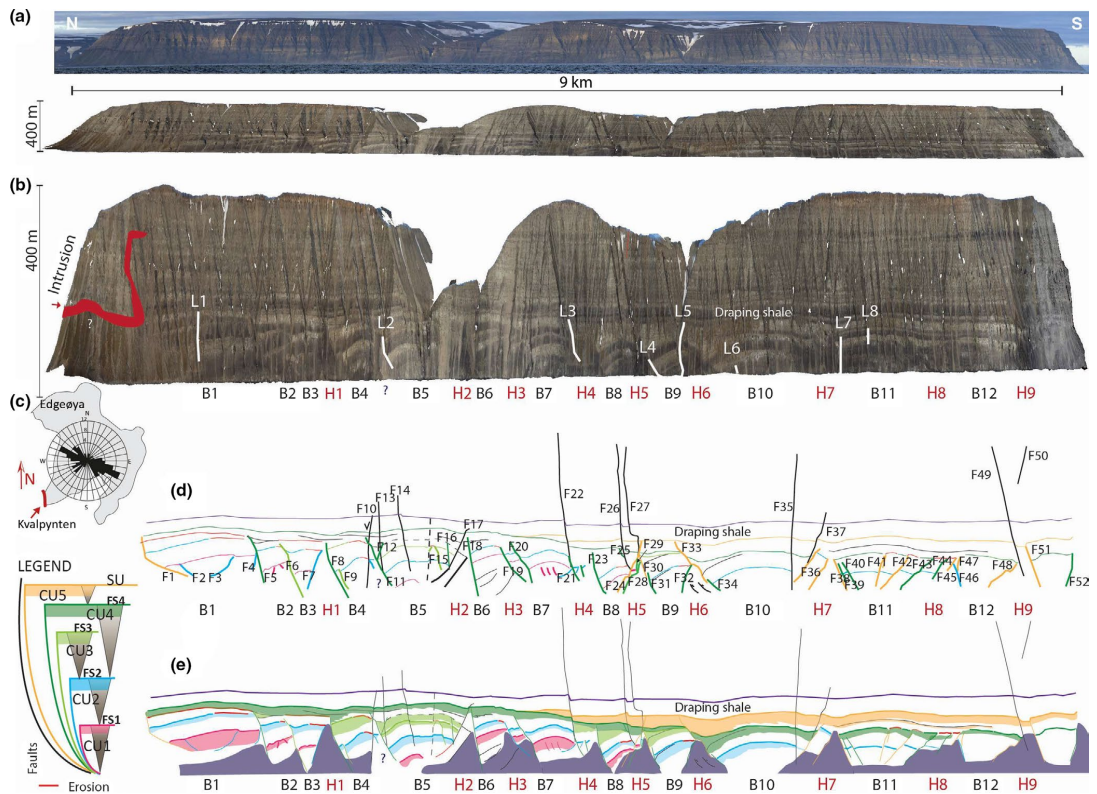


FIGURE 3 Transect of Kvalpynten with (a) photo mosaic (above) and photogrammetric outcrop model (below) of the 9-km-long and ca 400-m-high cliffs; Location in Figure 2 (b) vertically exaggerated by four photogrammetric outcrop model of Kvalpynten interpreted in LIME, presenting the position of nine horsts (H1-H9) and 12 basins (B1-B12), sedimentary logs (L1-L8) and Cretaceous intrusion (in red); (c) plot showing orientation of strike of extensional faults (d) Position of 52 extensional faults along the vertically exaggerated model; (e) Distribution of CUs 1–5 along the vertically exaggerated model with colours marking the position of upper, sandstone-dominated parts of CUs. FS: flooding surface; SAES: sub-aerially exposed surface

et al., 2014). The horsts consist of dark mudstone of the Botneheia and Tschermakfjellet formations (Figure 1c), exposing in places complex internal structures. These structures include numerous extensional faults and some minor thrust faults, the latter of which form gentle anticlinal stacks (Ogata et al., 2018). These minor structures likely represent some local shortening in the lower delta front/prodelta and challenge the mapping of the top of the Botneheia Formation.

The growth basin-fill is sandwiched between the near top of the Botneheia Formation and a flat-lying, 25- to 40-m thick, intra De Geerdalen Formation interval composed of dark mudstone, herein called the draping shale after Osmundsen et al. (2014; Figure 3a,b). The draping shale blankets the upper part of fault-related relief and serves as a marker bed (Figure 3e). It represents the boundary between two very different depositional and structural

settings. The draping shale is overlain by c. 150- to 200-m thick, paralic deposits of the De Geerdalen Formation (Edwards, 1976; Haile et al., 2018; Klausen & Mørk, 2014; Lord et al., 2014; Mørk et al., 1982; 1999; Osmundsen et al., 2014; Riis et al., 2008; Rød et al., 2014; Rönnert, 2016). Some of the larger fluvial or fluvio-marine channels seen in the upper part of the Edgeøya outcrop probably represent deposition on a delta plain.

Compilations of fault orientations recorded in Kvalpynten show that the majority of faults strike west-northwest and east-northeast; they dip southerly, and are either planar or gently to strongly listric (Figure 3c; Anell et al., 2013; Ogata et al., 2018; Osmundsen et al., 2014). Associated fault striations/corrugations show dip-slip kinematics with subordinate oblique-slip. Accordingly, the fault system has an overall down-to-the-south orientation, reflecting north to north-northeast and south to

south-southwest extension (Maher et al., 2017; Ogata et al., 2018; Osmundsen et al., 2014). Detailed analysis of the faults demonstrates a transition from hydroplastic to brittle shearing/faulting (Maher et al., 2017; Ogata et al., 2018). The Edgeøya cliff sections show that the main phase of faulting terminates below the draping shale. The latter is overlain by a post-kinematic unit, which shows occasional dm to m scale, steep, planar faulting (Ogata et al., 2018; Osmundsen et al., 2014). Pervious interpretation of the faulting advocates thin-skinned faulting, interacting with deeply rooted faults, which have been interpreted in seismic sections from the adjacent offshore areas (Anell et al., 2013). In the study area, the basal detachment for the listric faults is located near—or at the top of the Botneheia Formation (Ogata et al., 2018).

3 | DATA SETS AND METHODS

To date, published work on the steep, 9-km-long and c. 350- to 400-m-high Kvalpynten cliff succession has been based mainly on photographic analysis (Edwards, 1976; Osmundsen et al., 2014) supplemented with some field observations (Høy & Lundschie, 2011; Osmundsen et al., 2014; Riis et al., 2008; Rød et al., 2014). Eight sedimentary sections representing a total of 680 m were measured in 1:50 scale during field campaigns in 2012, 2013 and 2014 (Indicated with logs L1-L8 marked in Figure 3b; Appendices S1–S4). These sections were collected from seven of 12 identified fault-bounded basins and correspond to the only accessible localities on these extremely steep exposed cliffs. The N–S striking outcrop is oriented at 60–70 degrees to the average WNW–ESE striking faults, offering high-angle, almost perpendicular cross sections through many half-graben and graben structures. The presented data set consists of sedimentary logs, outcrop photographs and palaeo-current measurements complemented by a photogrammetric outcrop model. Standard techniques in lithofacies analysis and architectural-element analysis (Walker, 1992) were used in order to interpret various depositional settings.

Analysis of the basin geometries and associated sedimentary-structural architecture was performed using a photogrammetric outcrop model (Figure 3). The photogrammetric model covers nearly 45 km of cliff-face around southern Edgeøya; in this study, only the c. 9-km-long N–S oriented Kvalpynten section has been analysed. The photogrammetric model was created applying the Structure from Motion (SfM) method (e.g. Chandler & Buckley, 2016) with GPS-oriented images from a Canon EOS 6D, collected from boats at a fixed distance from the cliffs. The resultant high-resolution digital elevation model was draped with the detailed outcrop photographs,

which allowed examination of basin-fill geometries on scales of metres to hundreds of metres. LIME software (Buckley et al., 2019) was used for interpretation of the model. LIME allows for the measurement of distance between points, and the three-point determination of the strike and dip of surfaces. Faults were analysed in outcrops and mapped in LIME. The relative age of faulting was determined based on termination relationships with flooding surfaces traceable over large parts of the study area (FS1-4 in Figure 3d,e). In the field, sediment palaeo-transport direction throughout the succession was determined by measuring foresets in tabular and cross-stratified sandstones, asymmetric ripples, gutter casts, flutes and groove marks. Larger dunes/bars with clinoform foresets were also measured in LIME.

4 | RESULTS

In Kvalpynten, the growth faults segment the Triassic succession below the draping shale into 12, 200- to 800-m-wide half-grabens and grabens (basins B1–B12) and nine, 60- to 100-m-high horsts (H1–H9; Figure 3e). The half-graben and graben fills consist of prodelta and delta-front mudstones and sandstones of the Tschermakfjellet and lower part of the De Geerdalen formations. The lower boundary of the De Geerdalen Formation is defined as the base of first prominent sandstone unit that is located on top of the Tschermakfjellet Formation pro-delta mudstones (Mørk et al., 1999). In Kvalpynten this boundary is somewhat ambiguous and is variably expressed in different basins.

Along the north-south-trending Kvalpynten, 52 faults were mapped and analysed (Figure 3d). Detailed descriptions of the faults and corresponding analyses of the faulting evolution are provided in Maher et al. (2017) and Ogata et al. (2018) and will not be repeated here. Among the mapped faults, 31 are south-dipping and 21 are north-dipping (Figure 3d). They can be divided into three categories based on their relationships to adjacent basins:

- (i) Twenty three mainly south-dipping listric growth faults with vertical offsets exceeding 100 m that bound teen half-grabens.
- (ii) Nineteen planar, synthetic and antithetic growth faults with vertical offsets exceeding 60 m. Planar faults bound two, nearly symmetric grabens.
- (iii) Teen, post-sedimentary planar faults, with up to 3 m vertical offset, truncating the entire exposed cliff succession.

Each of the 12 basins B1–B12 is filled with 3–5, 25- to 60-m thick, coarsening-upwards units (CUs 1–5) composed

TABLE 1 Summary of the lithostratigraphic facies

Facies	Description	Grain size	Structures	Bioturbation index (BI; Taylor & Goldring, 1993) and biogenic structures	Interpretation
A	Structureless, dark- to light grey sandstone, with soft sediment deformations	Fine- to medium-grained	The individual beds are 0.2 to 1.5 m thick, and amalgamated successions measure up to 17 m. The sandstone beds have a sharp or erosive lower boundary. The soft sediment structures exhibit dish-, flame- and loading structures, convolute bedding and internal folding commonly with overturned folds.	BI = 0	Soft sediment deformations can occur by liquidization impacting layers of contrasting density, often reflecting water escape and gravitational (slump) processes (Owen, 1987). The thicker amalgamated structureless beds can be linked to very rapid deposition from suspended load (GingrasPemberton & Smith, 2014) or fluidization of sands. The amalgamated beds are adjacent to the master fault of the half graben suggesting that the soft sediment structures are induced by fault movement (Seilacher, 1991).
B	Plane parallel-stratified sandstone	Very fine to upper fine-grained	The sedimentary structures are dominated by plane parallel stratification (PPS) organized in 0.1–2 m thick beds with a commonly sharp but occasionally also gradual lower boundary. Facies B might contain symmetric- and asymmetric ripples.	BI = 0, rarely 1	PPS is a characteristic sedimentary expression of burst-and-sweep traction that flows undergoing laminar upper-flow regime conditions, although PPS can still form at lower flow intensities when the sediment concentration in the water column is high (Ashley, 1990; Cheel & Middleton, 1986; Fielding, 2006; Massari, 1996; Pickering, Stow, Watson, & Hiscott, 1986).
C	Low-angle cross-bedded, dark- to light grey sandstone	Upper-very fine- to upper-fine-grained	Sandstone displays gently dipping cross-stratification, with a sharp to occasionally erosive lower boundary and the bed thickness of 0.3–2 m. Symmetric and asymmetric ripples may be developed occasionally.	BI = 0, rarely 1	Low-angle cross-bedding represents transitional bedform between dunes and upper plane beds as flow velocity increases or as sediment concentration in the water increases (Massari, 1996; Turner, 1981). The presence of scattered oscillation ripples illustrates the impact of minor wave activity.
D	Tangential cross-bedded, dark- to light grey - sandstone	Upper very fine to fine-grained	Sandstone beds exhibit sharp to erosive basal contact. Individual cross-stratified sets measure between 0.3 to 1 m. Amalgamated beds, i.e. co-sets can reach thickness of 7.5 m. Tabular cross-bedding with tangential foresets occur. Scattered rip-up clasts, asymmetrical ripples with mud drapes and symmetrical ripples occur locally. Rare fining upward trends.	BI = 0, rarely 1, Rare plant fragments	The amalgamated cross-bedding represents non-laminar unidirectional current migration of sinuous (3D) dunes (Allen, 1982; Venditti, Church, & Bennett, 2005). Plant remains indicate a proximal position of the deposits Mud drapes suggest slack water periods probably by tidal processes
E	Asymmetric ripple cross-stratified, dark- to light grey sandstone	Very fine- to fine-grained	Sandstone is dominated by asymmetrical ripple cross-stratification with climbing ripples occurring locally.	BI = 0, rarely 1	Asymmetric ripples are the product of downstream migrating bedforms within unidirectional non-laminar flow conditions (Allen, 1982). Climbing ripples reflect a sedimentation rate exceeding the bedform progradation speed (Ashley, Southard, & BooTHROYD, 1982) resulting in a positive aggradation, which can reflect a sudden sediment input increase or a waning of the flow, or both.
F	Dark- to light grey sandstone with hummocky cross-stratification	Very fine- to upper-fine-grained	Sandstone is dominated by hummocky cross-stratification. Isolated dm-thick beds are characterized by a sharp to gradual lower boundary. Facies F sporadically display mud drapes.	BI = 0, rarely 1	Hummocky (HCS) cross-stratification is a result of combined unidirectional and wave-generated oscillatory currents. They are formed under extended wave periods and gentle oscillatory velocities and almost absent unidirectional flow (Dumas & Arnott, 2006). HCS are generally interpreted as a typical shallow water storm deposits as a result of storm-induced oscillatory current (Cheel & Leckie, 1993; Jelby, Grundvåg, Helland-Hansen, Olausen, & Stemmerik, 2017).

(Continues)

TABLE 1 (Continued)

Facies	Description	Grain size	Structures	Bioturbation index (BI; Taylor & Goldring, 1993) and biogenic structures	Interpretation
G	Dark- to light grey sandstone, with symmetric ripple cross-stratification	Very fine- to fine-grained	Sandstone is dominated by symmetric ripple cross-stratification. Isolated dm-thick beds are characterized by a sharp to gradual lower boundary. Sporadically displaying mud drapes.	BI = 0, rarely 1	Symmetric ripples are a product of the oscillatory wave movement and are generally interpreted as upper shoreface deposits (Allen, 1982; Basili, 1997).
H	Dark- to light grey, heterolithic sandstone with flaser bedding	Very fine- to fine-grained	Sandstone is dominated by symmetrical and asymmetrical ripple cross-stratification that forms individual beds or uppermost interval in upward coarsening strata from Facies K into Facies H. Scattered mud lenses, mud drapes, rip-up clasts.	BI = 0, rarely 1	Heterolithic deposits likely produced by waxing-waning tidal currents within a mixed mud-sand-rich environment (Baas, Best, & Peakall, 2016).
I	Heterolithic silt- and sandstone (dark- to light grey) with wavy bedding	Silt and very fine- to fine-grained sand	Laminated to undulated interbedded sandstone and siltstone siltstone. Facies I is commonly found as individual beds or in coarsening upward intervals from Facies K into Facies I/H. The sandstone beds are characterized by symmetric ripple cross-stratification and scattered rip-up clasts. Occasional thickening-thinning rhythmicity of the beds is observed.	BI = 0, rarely 1	Heterolithic deposits produced by a rapid flow deceleration and/or expansion within a mixed mud-sand-rich environment (Baas et al., 2016). Rhythmicity interpreted as a response to cyclic waxing-waning tidal current over the area, such as neap-spring tidal cycles (Visser, 1980).
J	Heterolithic dark grey mud- to siltstone with lenticular bedding	Silt and very fine- to fine-grained sand	Light grey sandstone lenses occur within a laminated to undulating muddy to silty dark grey matrix. The sandstone lenses are often characterized by uni- and bidirectional-asymmetrical ripple cross-stratification. Commonly developed as individual beds or fine-grained intervals within an upward coarsening succession from Facies K into Facies I/H.	BI = 0, rarely 1	Heterolithic deposits produced by a rapid flow deceleration and/or expansion within a mixed mud-sand-rich environment (Baas et al., 2016). Bidirectional-current ripples suggest a certain degree of tidal reworking.
K	Laminated (platy), dark grey to grey mudstone and siltstone	Clay and silt	Laminated to undulating mud- to siltstone with thin mm to 1–2 cm thick, planar to wavy laminae and lenses of very fine sandstone. These sediments are heavily altered at the outcrop and break-up as chips. Sparse occurrence of current ripples.	BI = 0–2	The homogenous mud- and siltstone suggest deposition from suspension within a low-energy environment, as a result of hypopycnal flows. The planar and ripple laminated sandstone laminae and lenses suggest more rapid gravity deposits probably from hyperpycnal flows (Potter, Maynard, & Depetris, 2005).

of mudstone, heterolithic and sandstones. CUs 1–5 have been mapped along the photogrammetric model (Figure 3e). In total, 12 sedimentary lithofacies can be identified (Facies A–L; Table 1; see also Appendices S5 and S6). The lithofacies are in turn grouped into four facies associations, FA1–4 (Figures 4 and 5), which have been used for depositional environment interpretation. These facies associations are as follows: FA1: Prodelta to distal delta front deposits, FA2: tidally-influenced heteroliths, FA3: tidally-reworked sandstone dunes, and FA4: mass-flow sandstone deposits. Each CU includes of 2–4 facies associations.

4.1 | Facies Associations

4.1.1 | FA1: prodelta to distal delta front deposits

Description

FA1 is composed of 2- to 20-m thick, mudstone-dominated intervals (Facies K; Table 1) with very fine to fine-grained, structureless, 1-dm to 1-m thick sandstone beds (Facies A). In the lowermost part of the studied succession (CU1), the lower boundary of FA1 is expressed as a gradual transition

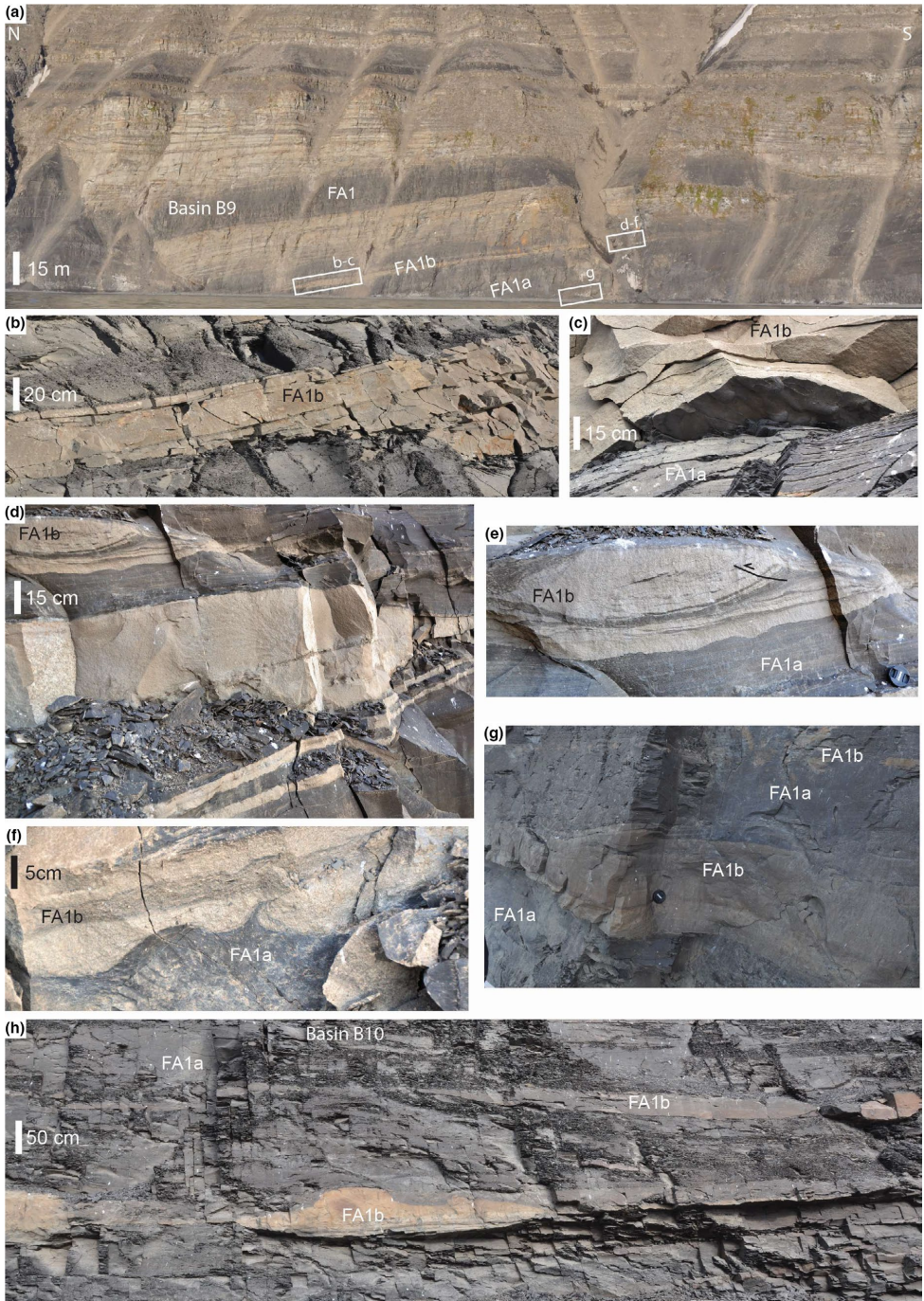


FIGURE 4 Examples of FA1. See text for the details

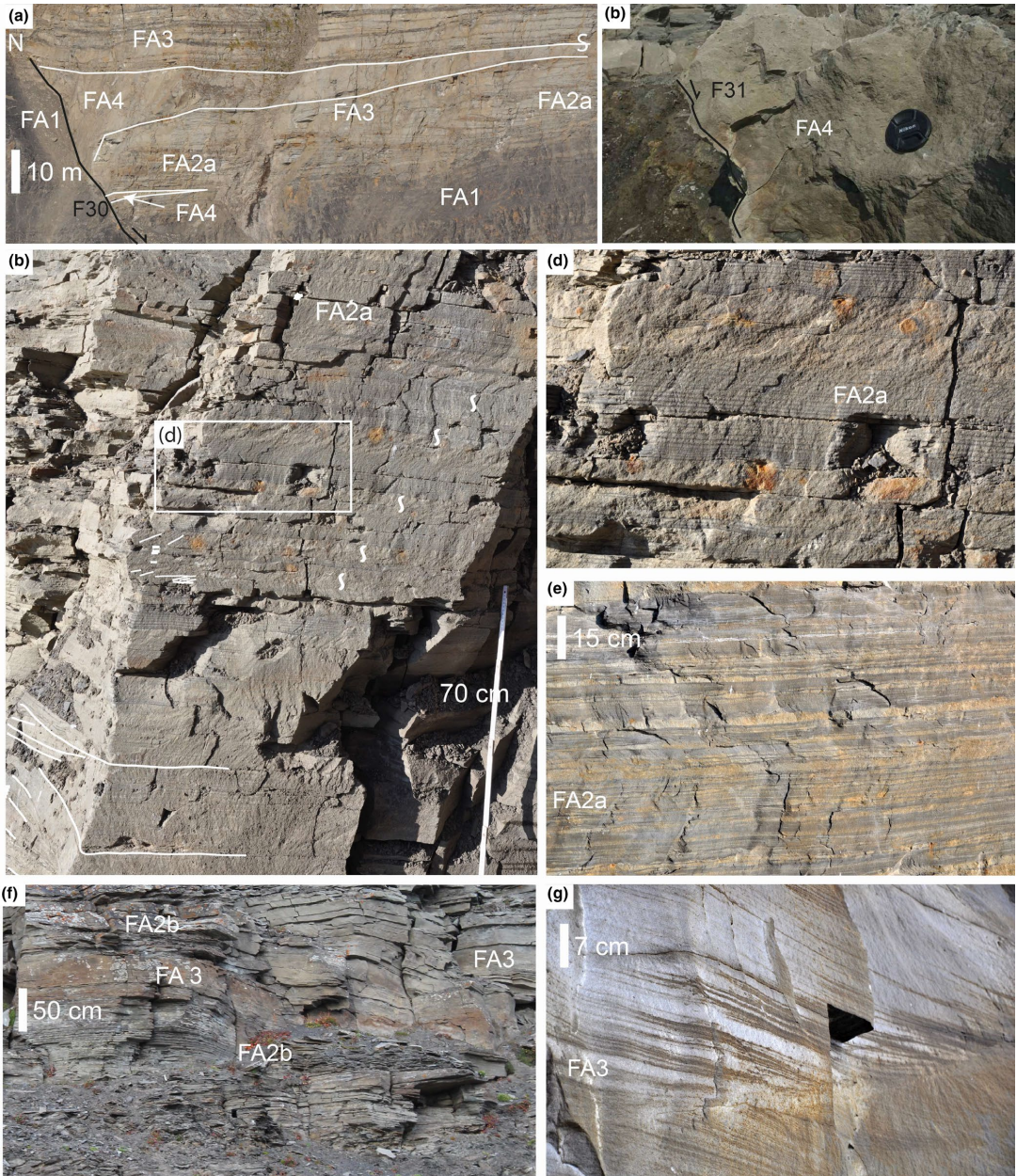


FIGURE 5 Examples of FA2, FA3 and FA4. See text for the details

from organic rich marine mudstones of the Botneheia Formation. Higher in the profile, FA1 occurs at the base of each CU and also in the lower part of the draping shale, where it has a sharp to erosive surface (Figure 4a).

FA1 is subdivided into two sub-facies associations FA1a and FA1b. FA1a (Figure 4) is composed of structureless to laminated mudstones with scattered marine shell fragments and rare to no bioturbation (Facies K). FA1b consists of

dm- to 1 m thick, very fine- to fine-grained structureless sandstone beds and lenses (Facies A, Table 1). The base of sandstone beds is sharp to erosive, with scouring and sole marks such as gutter casts, flutes and groove marks. Load structures, for example ball-and-pillow and cm-scale mud flames (Figure 4b,c) are common in the lower part of the sandstone beds, whereas faint plane-parallel lamination developed in their upper parts (Facies B). Soft-sediment deformations such as convolute lamination and mud clasts are locally abundant. Few individual FA1b's sandstone beds extend over a distance of more than 200 (Figure 4a). In addition to the sandstone beds, FA1b consists of intervals with mixed sandstones and mudstones, forming cm- to dm-thick lenses and dm- to m-thick ball-and-pillow structures with associated deformation structures, such as folds and cm-scale thrust faults (Figure 4e). FA1b also contains mudstone with planar to wavy structures and mm- to cm-thick siltstone and sandstone lamina (Facies J) as well as mm- to cm-thick and up to 10-cm-long sand lenses (Figure 4g). Rarely, very fine- to fine-grained, 1- to 2-dm-thick sandstone beds with wave ripples and hummocky cross-stratification are recognized (Facies F and G).

Interpretation

Thick mudstones with marine shell fragments assigned to FA1a represent a low-energy environment, with mud probably deposited from hypopycnal flows (e.g. Mulder, Syvitski, Migeon, Faugeres, & Savoye, 2003). The scarcity of wave-related structures and hummocky cross-stratification suggests that FA1a was deposited below the storm wave base. Structureless mudstone beds could represent completely burrowed mud. Thick sandstone beds with erosive lower boundaries and associated intense soft sediment deformation of FA1b suggest that these sediments were deposited as a result of hyperpycnal, high-density, gravity flows in a slope to basin floor setting (e.g. Mulder et al., 2003; Mutti, Tinterri, Benevelli, Biase, & Cavanna, 2003). Thin lamina and lenses of silt to very fine sandstone in the mudstone suggest deposition from distal density currents. Generally, FA1 is interpreted to represent prodelta to distal delta front deposits, in agreement with previous interpretations by Edwards (1976). Episodic deposition from density currents is represented by the sharp-based sandstone beds of FA1b intersecting the mud deposits of FA1a. The common occurrence of soft sedimentary structures suggests instability of the slope, such as gravitational collapse of the delta slope or very rapid sedimentation from a high river discharge during floods (Mutti et al., 2003). Alternatively, fault-controlled slope steepening due to fault block rotation or collapse of sediments triggered by seismic events (earthquakes) could also produce similar sedimentary structures (Nemec et al., 1988).

4.1.2 | FA2: tidal heteroliths

Description

FA2 consists of 2-dm to 3-m thick, lenticular and wavy-bedded heteroliths (Facies I and J; Table 1) alternating with light grey, fine-grained, 1- to 3-dm thick, low-angle cross-stratified sandstone beds that contain single and double mud drapes (Facies C). FA2 (Figure 5c,d) occurs either as 5- to 8-m thick, inclined heteroliths (FA2a) organized as coarsening-upward units, or as 2- to 6-m thick, tabular beds of heteroliths (FA2b) interbedded with cross-stratified sandstones of FA3 (Facies D). Occasional bioturbation is represented by scattered *Skolithos* burrows. Rhythmic alternations in thick and thin lamina inside the planar to wavy-bedded heterolithic succession occur locally (Facies I and J). Locally, dm-thick beds of sandstone with flaser bedding (Facies H), symmetrical ripples (Facies G) and/or plane-parallel lamination (Facies B) occur. The lower boundaries of the sandstone beds are either gradual or sharp, whereas their tops are commonly characterized by wave ripples. Localized intervals contain hummocky cross-stratification (Facies F). In lower parts of FA2, towards the gradual boundary with the underlying FA1, cm-scale soft-sediment deformation and loading structures are common. FA2 is capped by cross-stratified sandstones with mud drapes of FA3.

The 5- to 8-m thick, coarsening-upward heterolithic intervals of FA2a with inclined bedding consists of 3- to 5-m-high individual sets, that extend laterally over 50–75m. Their shape is tangential to planar, and they downlap on underlying layers. The occurrence of sandstone beds is accompanied by a thickness increase in the beds towards the north of the outcrop section. Heteroliths dominate towards the crest of the hanging wall fault blocks and the 'bottomset' position of the IHS. The dip angle of the IHS, when rotated back to the original depositional position by flattening on the top of CUs, ranges from 1 to 20 degrees. Foresets dip southwards, away from basin-bounding faults (Figure 5a). Therefore, the IHS appears to climb up the hanging wall dipslope in the half-grabens. Bidirectional currents towards the west and east are recorded in 2- to 3-dm thick, low-angle cross-stratified sandstone beds, as for instance seen in the CU2 of basin B9 (Figures 6 and 7d-e). These bidirectional currents were transverse to the IHS dip direction.

Tabular intervals of FA2b can be traced laterally from north to south over 300 m. Typically, FA2b forms 5- to 6-m-thick coarsening-upwards intervals (basin B1), but occasionally fining-upward 1- to 2-m-thick beds are observed (e.g. CU1, Basin B1, Appendix S1).

Interpretation

FA2 shows numerous indicators of tidal influence and modulation, such as mud drapes, flaser bedding, sandstones

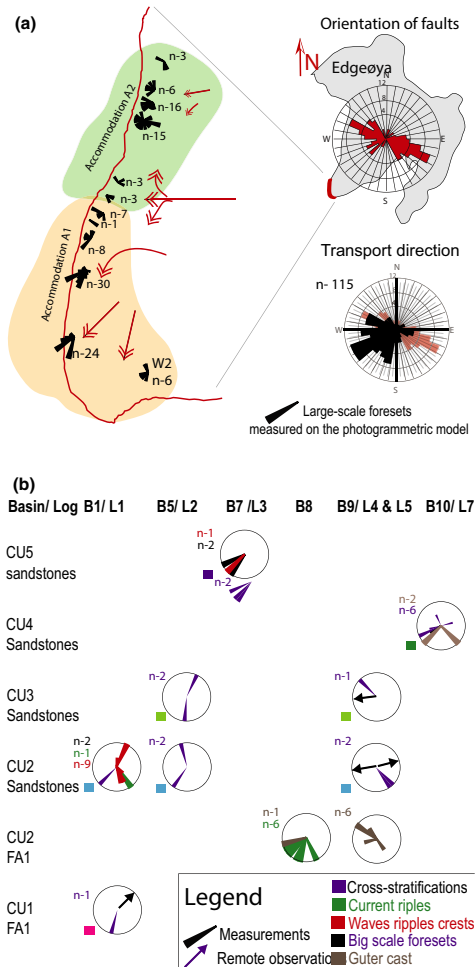


FIGURE 6 Orientation of transport indicators presented in rose diagrams, where n = number of measurements: (a) tens to hundreds of metres scale foresets within CU4 (green colour) and CU5 (orange colour) measured on the photogrammetric model; (b) compilation of field measurements of transport directions recorded within individual basins and CUs

with oppositely dipping foresets (‘herringbone cross-stratification’), as well as the development of a variety of heteroliths, and cyclical bundling of various bedforms. The m-scale, heterolithic intervals of FA2a with inclined bedding are interpreted as ‘inclined heterolithic stratification’ sensu Thomas et al. (1987). Rhythmic alternations of thick and thin lamina are interpreted as tidal bundles (Figure 5c,d; e.g. Nio & Yang, 1991). The aforementioned structures suggest a distal deposition in a tidally affected, lower delta-front environment (e.g. Longhitano, Mellere, Steel,

& Ainsworth, 2012; Willis, 2005). This interpretation is supported by the conformable position of FA2 above thick successions of deeper shelf deposits of FA1, and below the cross-stratified sandstones of FA3. Noticeably, a lack of mouth bars, erosive surfaces and typical channel geometries with infill facies suggest deposition at a distance from the delta top. Sand delivered to the basin has been further redistributed by tidal currents over the delta front and shallow shelf (e.g. Longhitano et al., 2012; Willis, 2005). The presence of sparse wave ripples, and sporadic HCS suggest periodical reworking of the sediment close to the storm wave base.

The development of FA2a and FA2b differs depending on the position and geometry within the fault-bounded basins. FA2a’s combination of IHS associated with tidal current indicators and bi-modal transport direction transverse to the dip of the master bedding, suggests that the IHS master bedding represents lateral accretion surfaces developed within a tidal bar. Their development is likely the result of west-east oriented tidal currents. Lateral accretion surfaces are commonly ascribed to lateral migration of subaqueous tidal bars (López-Blanco, Marzo, & Muñoz, 2003; Olariu, Steel, Dalrymple, & Gingras, 2012; Olariu, Olariu, Steel, Dalrymple, & Martinius, 2012). FA2a is interpreted as a free-standing tidal bar or compound tidal bars detached from the delta front/top (e.g. Longhitano et al., 2012; López-Blanco et al., 2003; Olariu, Olariu, et al., 2012).

Tabular heteroliths of FA2b that alternate with cross-stratified sandstones of FA3 are interpreted as distal equivalents of forward migrating tidal compound dunes, described in the next section (e.g. Longhitano et al., 2012; Olariu, Steel, et al., 2012; Willis, 2005).

4.1.3 | FA3: tidal dunes

Description

FA3 consists of dm- and m-scale beds of fine to medium-grained, planar and trough cross-stratified sandstone with tangential foresets (Facies D; Table 1). FA3 also contains 1- to 3-dm thick, structureless sandstone beds (Facies A) and sandstone with flaser bedding (Facies H). Trace fossils are rare in FA3. Locally, in the lower part of FA3 units, 1- to 2-dm-thick current rippled sandstones (Facies E) occur. Single and double mud drapes are widespread. Locally, dunes with oppositely dipping foresets are observed (Figure 6b). Vertically stacked beds of FA3 deposits are arranged in 10- to 15-m thick, thickening and gently coarsening-upward sandstone intervals. The base of FA3 is either sharp, or represents gradual transition from deposits of FA2, or occasionally FA1. FA2a- FA3 couples form the upper parts of CUs. Alternatively, dm- to 1- to 2-m-thick beds of FA3 alternate with FA2b in metre-scale coarsening-upwards intervals (e.g.

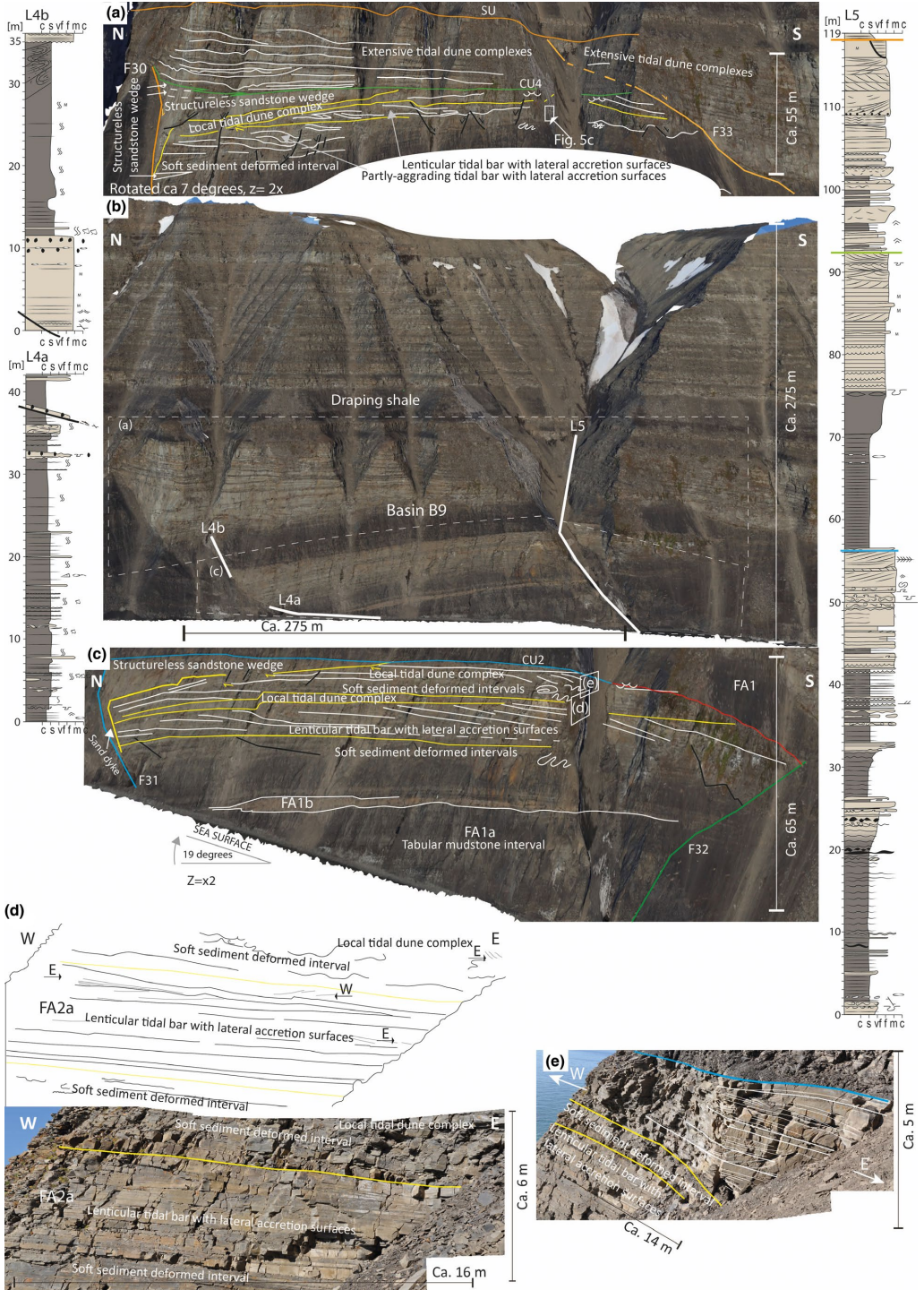


FIGURE 7 Basin B9 with marked faults, flooding surfaces and architectural elements. For the colour code of the flooding surfaces see Figure 3e. (a) Fragment of the photogrammetric model with CU3, vertically exaggerated by 2 and flattened by 7 degrees, interpreted in LIME; (b) fragments of the photogrammetric model of Basin B9 showing the position of logs L4 and L5 and outlines of figures (a) and (c); (c) Fragment of photogrammetric showing lower CU2: the model is interpreted in LIME, flattened by 19 degrees, vertically exaggerated by 2, with outlines of figures (d) and (e); (d) sketch and photograph of bidirectional transport directions within sandstone beds of lenticular tidal bars with lateral accretion surfaces in CU2. (e) A photograph of laterally restricted tidal dune complex located in the uppermost part of CU2

Basin B1). Noticeably, transport directions in FA3 vary between stratigraphic levels.

Interpretation

FA3 is dominated by tangential cross-stratified amalgamated sandstones interpreted as deposits of straight crested and sinuous dunes, developed in response to unidirectional and bidirectional currents, likely associated with tidal circulation processes (Anderton, 1976). Abundant tidal indicators and tabular beds observed in cross sections along foresets dip direction suggest deposition of forward-migrating subaqueous tidal dunes, similar to sand waves in modern subtidal environments (e.g. Olariu, Steel, et al., 2012; Willis, 2005). The structureless texture found near the faults in some beds is interpreted as the result of rapid deposition under high-energy conditions (e.g. Mutti, 1992). Lack of trace fossils indicates unfavourable conditions for burrowing organisms, potentially due to rapid sand deposition or, alternatively, to transient brackish conditions (e.g. Nemeč et al., 1988).

The high sand content and numerous tidal indicators might suggest deposition in a position more proximal and/or more tidally-influenced than FA2. However, sand waves are usually disconnected from the delta front/top sandstones, as they reflect redistribution by tidal currents across a shallow shelf (e.g. Longhitano et al., 2012; Willis, 2005). Similar to FA2, a general lack of typical delta front facies (mouth bars, distributary channels) supports this interpretation. Locally, in basin B1, alternation of FA3 with tabular tidal heteroliths of FA2b suggests interfingering of distal and proximal parts of dune fields, similar to forward-accreting tidal dune fields reported in the Ager Basin (Spain; Olariu, Steel, et al., 2012). There, they reflect tidally reworked sediments deposited in a confined, marine strait (Olariu, Steel, et al., 2012). Rossi et al. (2017) also reported similar tidal dune fields detached from a delta within the narrow, structurally controlled, tide-affected Calabria strait (Southern Italy).

4.1.4 | FA4: mass-flow sandstone deposits

Description

FA4 is characterized by structureless, fine- to medium-grained sandstone bodies (Facies A) with mud clasts (Figure 5a,b). The mud clasts occur within the structureless sandstone. FA4

forms distinct sandstone wedges that thicken towards the faults in the uppermost parts of the CUs in half-grabens. The bases of the wedges are either sharp and conformable, or gently undulating with truncation of underlying strata of FA2 and FA3 (Figure 5a e.g. CUs 2 and 3 in basin B9). The wedges range in heights of 13–17 m. At places, these wedges show stacked 1- to 5-m-thick sandstone beds that are separated by metre-wide, cm-thick mud layers. Each wedge has a flat top that corresponds to the upper boundary of CUs.

Interpretation

The metres-thick, structureless sandstone deposits with sharp to erosive base and flat tops are interpreted as high energy, subaqueous mass flow deposits (grain flows; Mutti, 1992). The fine- to medium-grained size is specific to FA 4 and could indicate discharge from a river mouth. However, the occurrence of angular mud-clasts suggests erosion and redistribution of sediments that originated near the site of deposition.

4.2 | Architectural elements

Based on the vertical and lateral distribution of facies associations and their geometries, the studied sedimentary succession can be grouped into eight distinct architectural elements (summarized in Figure 8). The stacking patterns of the various architectural elements allow a further interpretation of depositional settings beyond that of the facies associations.

4.2.1 | Tabular mudstone intervals

Tabular mudstone intervals consist of 15- to 25-m thick, symmetric successions of FA1 (Figure 8). Tabular mudstone intervals are 100- to 900-m-wide bodies that exhibit gradual upper boundaries with the deformed deposits of soft sediment deformed intervals (Figure 7). Alternatively, in the lower part of CU5, the tabular mudstone interval grades into forward migrating laterally extensive tidal dune complex that is exposed for over 4 km.

4.2.2 | Mudstone wedges

Mudstone wedges are asymmetric elements that consist of FA1. Mudstone wedges show maximum thickness of 15–25 m close to the bounding listric faults and widths of 100- to 450 m

Hierarchy of depositional elements

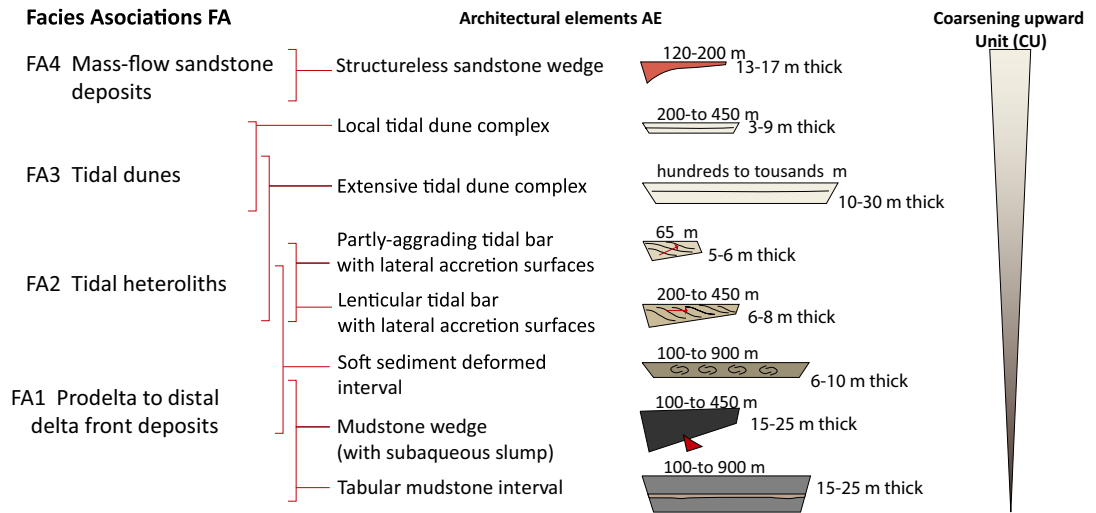


FIGURE 8 A conceptual model of architectural elements described in the text

(Figure 8). The occurrence of mudstone wedges is less common than tabular mudstone intervals. The mudstone wedges are well exposed in several locations, as part of CU4 in basins B1 and B6 (Figures 3 and 9e). Adjacent to master faults, mudstone wedges host triangular prisms of structureless, light grey to grey sediments, which are 6–10 m high and 35–50 m long (Figure 9e). These highly wedge-shaped deposits have not been logged due to the access limitation and are recognized only as a photographic-facies in pictures and in the photogrammetric model. The prisms can be linked with erosional surfaces on the adjacent footwall block (Figure 9c–e), suggesting they relate to subaqueous slumps from failure of exposed fault-scarps and footwall strata. Hence, truncation surfaces, presented in red in Figure 9e, mark the source of sediments removed from the footwall and redeposited as subaqueous mass flows. The triangular prisms are further draped by mudstones. Overall, the mudstone wedges thicknesses of 12–17 m measured on the photogrammetric model next to faults (Figure 9e) are considered to represent the maximum height of escarpments on the basin floor during periods with low sedimentation rates.

4.2.3 | Soft sediment deformed intervals

Soft sediment deformed intervals are present in all grabens and half-grabens. They consist of 4–10 m thick intervals of FA1 and FA2 with intense soft sediment deformation structures (Figure 10c–e). The degree of deformation ranges from cm-to-m scale growth faults and convoluted lamina, increasing to ball-and-pillow structures, m-scale

folds and overturned bedding, before being eventually almost completely homogenized. The intensity and diverse style of disturbance within the soft sediment deformation occurred in overpressured, partly liquefied deposits transported as slumps over dm- to m-scale distances. Development of small growth faults, however, links the soft sediment deformed intervals with activity on the basin-bounding faults. Noticeably, the location of the intervals along half-graben dip-slopes suggests a relationship between soft-sediment deformation and fault-induced tilting of the basin floor due to the formation of roll-over anticlines.

4.2.4 | Lenticular tidal bars with lateral accretion surfaces

Lenticular tidal bars with lateral accretion surfaces are observed only in half-grabens (basins B4, B5, B8 and B9), where they are expressed as 6–8 m thick intervals of FA2a. Each single lenticular tidal bar is 3–5 m high, and extends laterally over 50–75 m. The lateral accretion surfaces dip southwards, away from basin-bounding faults, indicative of a migration up the hanging wall dip-slope (Figure 8). West- and eastward oriented bidirectional currents in low-angle cross-stratified sandstone beds (CU2 in the basin B9; Figure 6) suggest tidal currents nearly parallel to the half-graben axis. In conclusion, lenticular tidal bars with lateral accretion surfaces formed elongated bodies which were confined to fault-induced accommodation and aligned with the half-graben bounding fault.

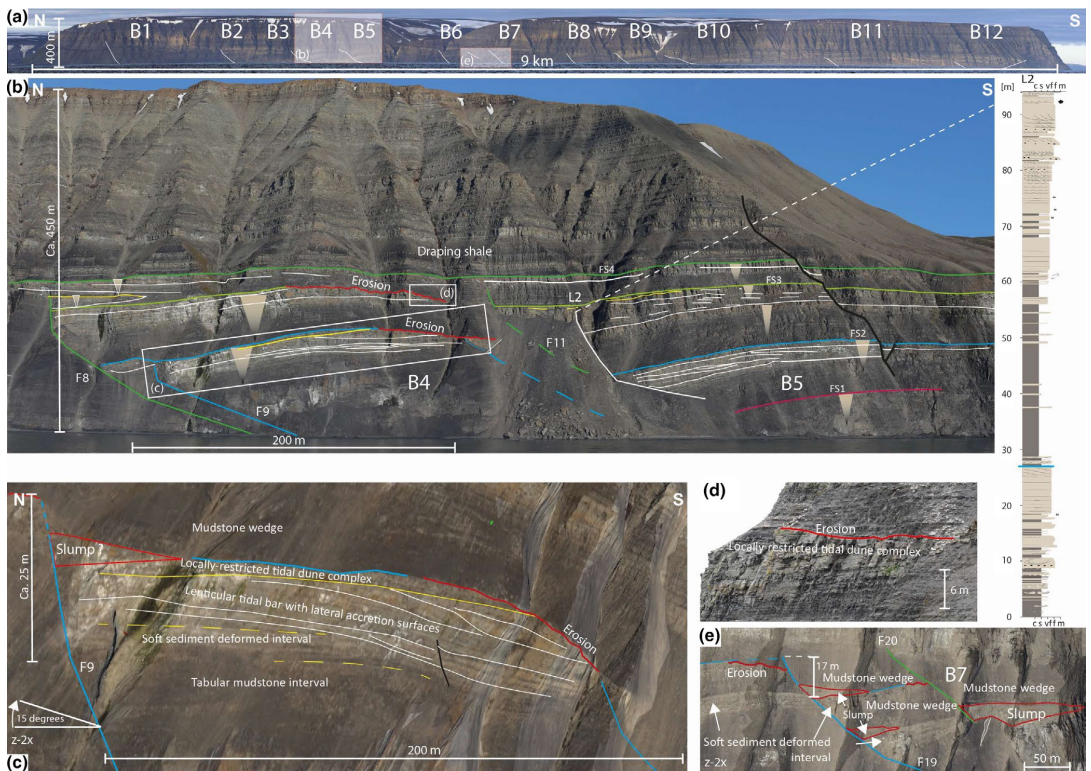


FIGURE 9 Photographs of growth basins B4 and B5 showing the distribution of architectural elements: notice the subaqueous slides and associated erosive surface marked in red. The photogrammetric model presented in figures (c) and (e) is interpreted in LIME. For the colour code of the flooding surfaces see the Figure 3e. See Appendix S7 for uninterpreted version

4.2.5 | Partly aggrading tidal bars with lateral accretion surfaces

Partly aggrading tidal bars with lateral accretion surfaces have been observed only in the CU3 in basin B9 (Figure 7a). This type of tidal bar is a variation of tidal bars with lateral accretion surfaces. It shows shorter and steeper, partly aggrading IHS that are 5 m high, with a 50 m lateral extent. Partly aggrading tidal bar formed in the half-graben adjacent to the fault.

4.2.6 | Laterally extensive tidal dune complexes

Laterally extensive tidal dune complexes usually form the upper component of CUs that are developed in grabens (basins B1 and B11) and are common in CUs 4 and 5. They consist of hundreds of metres wide, tabular and forward migrating sandstone dunes of FA3 and their distal equivalents, heteroliths of FA2b. Bidirectional palaeo-transport indicators

within the dune complexes indicate a major tidal current direction towards the southwest, with a subordinate direction towards the northeast (Figure 6). In the graben B11, the laterally extensive tidal dune complex is characterized by a sharp contact with the underlying soft sediment deformed interval. This contact is interpreted as a tidal ravinement surface (TRS), outlined in Figure 10. In B11, the tidal dune complex consists of three tabular sand-sheets that are in total 10-m thick and continue over a distance of 850 m and extend laterally over 500 m B1.

4.2.7 | Laterally restricted tidal dune complexes

Laterally restricted, tidal dune complexes are expressed as tabular, 3- to 4-m thick elements extending up to 450 m and located in a topset position, above the lenticular tidal bars with lateral accretion surfaces. Laterally restricted tidal dune complexes are distinctly thinner and narrower than the laterally extensive tidal dune complexes (Figure

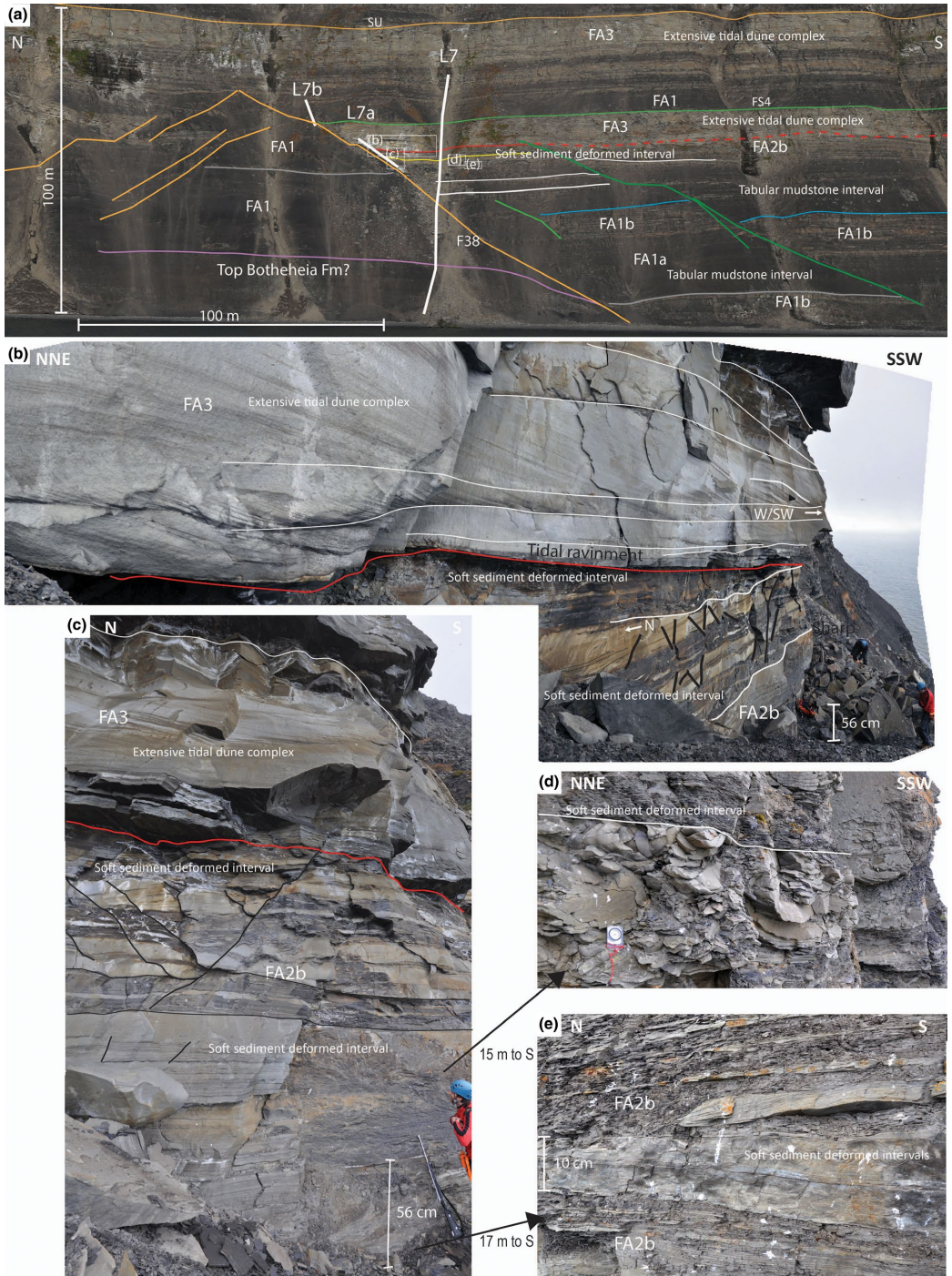


FIGURE 10 Graben B11 with marked architectural elements; notice tidal ravinement surface marked in red (b). For the colour code of the flooding surfaces see the Figure 3e. See Appendix S8 for uninterpreted version

8). Internally, laterally restricted tidal dune complexes are made up of sandstone-dominated, FA3, with beds showing m-scale foresets that dip westward (Figure 6b). Transport directions towards the west and southwest recorded by tangential cross-stratifications (e.g. CU3 in basin B9, Figures 6 and 10) conform to an interpretation of frontal migrating sinuous dunes, with currents sub-parallel to nearby faults. This mimics the sediment transport direction of the underlying tidal bars. As these migrating sinuous dunes overlay the tidal bars, these laterally restricted tidal dune complexes are interpreted as small fields of compound tidal dunes migrating over sand ridges. The transition from heteroliths-dominated tidal bars to sandy dunes reflects either an increase in tidal energy and/or sediment supply that could reflect a partly filled accommodation, as well as a change in sediment sourcing.

4.2.8 | Structureless sandstone wedges

Structureless sandstone wedges appear only in half-grabens adjacent to listric faults (e.g. top of CU3 in basin B9, Figure 7). The wedges are 13 to 17-m high and extend laterally over 120–200 m. The wedges consist of stacked sandstones of FA4. Locally, the wedges are associated with sand dikes injected downwards for 10–15 m along the bounding fault (e.g. CUs 2 and 3 in basin B9), as discussed in Maher et al. (2017) and Ogata et al. (2018). Distinct smaller structureless sandstone wedges that are dm- to 2-m thick and extending laterally over 45 m can be stacked on top of the larger sandstone wedge, as for instance demonstrated in the hanging wall of fault F30 (Figure 7a). These small wedges also appear in connection with the soft sediment deformation intervals. The asymmetrical geometry of sandstone wedges is related to syn-kinematic events. Smaller wedges may potentially represent a single increment of fault movement with throw of about dm- to 2-m scale, but the composite wedges likely reflect multiple fault-slip increments. Fault-created morphology, with associated accommodation, was filled with FA4's mass flow deposits. Some sand was likely sourced from the delta front and redistributed by mass flow along the hanging walls of the active faults. The flat tops of the wedges suggest (over-) fill of the fault-induced accommodation to the equilibrium profile followed by bypass of subsequent sediment. Alternatively, the uppermost parts of the wedges were eroded during subsequent transgressive episodes.

4.3 | Coarsening-upward units (CUs)

The first-order surfaces mapped on the photogrammetric outcrop model (Figure 3d,e) constitute the boundaries between CUs 1–5. Typically, the uppermost parts of CUs are represented by fine- to medium-grained sandstones interpreted as high-energy deposits of tidally reworked sandstone dunes

(FA3) and/or mass flows sandstones (FA4). The sandstones have a sharp to locally erosive upper boundary towards the marine mudstones (FA1) that form the lowermost part of overlying CU. These boundaries are defined as a flooding surfaces (FS; Marine flooding surface in Van Wagoner et al., 1988; see FS1-FS4 in Figure 3d,e). Some flooding surfaces can be mapped with high accuracy over an area of 10×15 km.

The CUs 1–3 are developed within half-grabens (B1–B10) and grabens (B11 and B12) and are disconnected by horsts (Figure 3e). The thickest, up to 35-m thick, sandstone package was deposited in B1. Palaeo-transport direction recorded by density currents in FA1b (gutter cast within CU2 in B9; Figure 6b) was towards the northwest, near-parallel to the fault strike. Dunes and m-scale foresets record bi-modal transport direction towards the southwest and northeast. CU4 in the northern part of Kvalpynten is partially affected by faulting, whereas, in the south, it was deposited within wide, fault-bounded basins B10–B12. The palaeo-transport directions recorded within CU4 in the northern part show a divergent pattern with one component near-parallel to the growth faults (Figure 6a,b).

CU5, observed only in the southern part of the study area (Figure 3e), forms a coarsening-upward and coarsening-northward unit that is laterally extensive (over 5 km). Very-low angle, large-scale foresets (Figure 6a) recorded progradation towards the southwest. These foresets average 500 m in length and 10 m in height.

The top of the uppermost CU5 is capped by the mudstones of FA1's draping shale. At the base of the draping shale (log L5 in Figure 7), a c. 0.5-m thick, mottled, rust coloured sandstone horizon has been recognized and interpreted as a soil profile (Appendix S4 and S6). This sandstone is interpreted as a sub-aerially exposed surface (SAES; Figure 3e) developed as a consequence of an abrupt shoreline progradation, prior to transgression and deposition of the mudstones above the entire fault array.

4.4 | Fault control on accommodation

Four types of accommodation recognized within CUs 1–5 are interpreted to represent the rate of faulting and fault geometry, as summarized in Figure 11a, and described below:

1. Symmetrical syn-kinematic accommodation developed in grabens bounded by oppositely dipping but kinematically connected planar faults with similar offset (e.g. basin B11). The accommodation was equally distributed across the graben, as evident by a tabular geometry of the sedimentary fill.
2. Asymmetrical syn-kinematic accommodation generated in half-grabens bounded by south-dipping, listric faults.

Fault geometry caused roll-over folding and enforces asymmetry in the basin, as well exposed in basins B2, B8 and B10 (Figure 3). The highest rates of accommodation creation occurred adjacent to faults and decreased up the dip slope, as reflected by an overall wedge shape of the syn-kinematic basin fill. In basins with ongoing faulting, hanging wall strata gradually rotated during progressive growth of roll-over anticlines.

3. Late-kinematic accommodation is illustrated by the deposits of CU4 (Figure 3), which form a continuous sandstone belt. This belt was perturbed by faulting which accrued c. 10-m offset. The thickness variations along the sandstone belt associated with the undulating base is due to enhanced sagging above pre-existing basins. Sagging caused renewed fault activity that triggered movement on upper fault segments, which resulted in development of small hanging wall growth wedges (Figures 9b and 11c).
4. Post-kinematic accommodation correlates with deposits of CU5, which were deposited as a belt that extends laterally over 5 km and are unaffected by syn-sedimentary faults (Figure 3). CU5 is, however, deformed by younger, post-sedimentary planar faults with dm- to 3-m-scale offsets.

For most of the half-grabens in the study area (B1, B4, B9; Figure 3) the oldest syn-kinematic strata have tabular shape. On the contrary, younger strata packages are wedge-shaped (see B4 in Figure 9c and B9 in Figure 7c). This upward and temporal change reflects initiation of basins as grabens first, bounded by planar faults, with faults moving simultaneously. Subsequently, activity became focused on the south-dipping faults, partly reactivating pre-existing structures, accompanied by the new development of listric faults. This change in fault style forced the basins to transition from grabens to half-grabens, as illustrated in Figure 11b.

4.5 | Influence of rates and distribution of accommodation on architectural elements stacking patterns

This study demonstrates that rates and distribution of accommodation creation directly controlled stacking of architectural elements within the five main coarsening upward units (Figure 11). The CUs 1–3 were deposited in fully compartmentalized basins, whereas sandstone-rich units are discontinuous across faults. Symmetrical versus asymmetrical lateral variations in the syn-kinematic accommodation

impacted the shape of the entire basin fill as well as the development and stacking of the architectural elements. In grabens (Figure 11c), the CU starts with tabular mudstone intervals, and is overlain by the relatively thin soft sediment deformed intervals and the laterally extensive tidal dune complex. The dunes form horizontal, continuous sandstone sheets with approximately constant bed thickness in the basin. Lenticular tidal bars with lateral accretion surfaces and structureless sandstone wedges are missing in grabens.

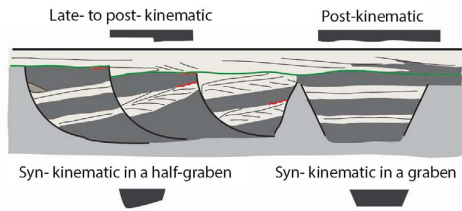
Half-graben basins (Figure 11c) with asymmetrical accommodation are 200- to 400-m wide, with exception of the 850-m-wide basin B10. Typically, coarsening-upward sections consist of a basal mudstone wedge, overlain by soft sediment deformed interval and lenticular tidal bar(s) with lateral accretion surfaces. These lenticular tidal bars are overlain by laterally restricted tidal dune complex(es), which are eventually capped by structureless sandstone wedge (Figure 11c). Some variations in stacking pattern occur, including the development of partly aggrading tidal bar with lateral accretion surfaces near the fault (e.g. CU4 in basins B9; Figure 7a). In some cases, couplets of underlying lenticular tidal bars with lateral accretion surfaces and laterally restricted tidal dune complexes are repeated, reflecting cyclic deposition that form lower-order coarsening-upward intervals within a CU unit (e.g. CU3 in basins B5; Figure 9b). 0.5- to 1-m-thick fining upward intervals can occur in the uppermost part of some CUs (CU3 in basin B9 and CU2 in B5), indicative of a waning of the energy, potentially associated with a localized increase in accommodation creation and/or system abandonment.

Late syn-kinematic accommodation is reflected in deposition of CU4. This unit varies in thickness from c. 10 m in the footwall blocks to c. 20 m in the basins. The hanging wall depocenters hosts fully developed CU4, with basal tabular mudstones and mudstone wedges overlain by south-westwards, forward-migrating laterally extensive tidal dune complex. Locally, 1- to 2-m-thick structureless sandstone wedges developed adjacent to faults. Contrastingly, in the footwall blocks, CU4 consist exclusively of laterally extensive tidal dune complex which exhibits a sharp, erosive lower boundary with the underlying CU (Figure 11c). This sharp lower boundary can be ascribed to erosion and sediment bypass in uplifted footwall position.

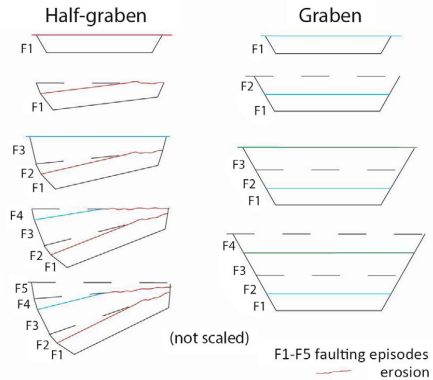
Post-kinematic accommodation is reflected by CU5 characteristics that consist of forward migrating laterally extensive tidal dune complex, which is overlain by tabular mudstone interval. In the southern part of the study area

FIGURE 11 (a) Schematic expression of four types of accommodation documented in Kvalpynten: grabens, half-grabens, late syn-kinematic accommodation and post-kinematic accommodation. (b) A conceptual evolution model of a half-graben evolving from an initial graben as the displacement along one fault starts to outpace the other (left) and a graben where both faults show similar displacement rates (right). (c) Stacking patterns of architectural elements defined in Figure 8, within different types of accommodation A1–A4

(a) Four types of accommodation space



(b) Concept model of half-graben and graben evolution



(c) Stacking patterns of architectural elements in different types of accommodation

Sedimentary architecture in late-kinematic accommodation

- Sharp based, tabular sandstone beds of laterally-extensive tidal dune complexes on the FW
- Structureless sandstone wedges on the HW

Sedimentary architecture in post-kinematic accommodation

Progradation > aggradation

- Prograding laterally-extensive tidal dune complexes

Sedimentary architecture in a half-graben

- Lenticular and partly-aggrading tidal bars with lateral accretion surfaces draped by laterally-restricted tidal dune complexes
- Structureless sandstone wedges and/or land slides
- Erosion on uplifted fault block crests

Sedimentary architecture in a graben

- Laterally-extensive tidal dune complexes form tabular, large-scale bedding

LEGEND

Architectural elements

	<i>Half-graben and late syn-kinematic</i>		<i>Half-graben</i>
	<i>Half-graben</i>		<i>Graben, half-graben, late syn-kinematic</i>
	<i>Graben, late syn-kinematic and post-kinematic</i>		<i>Half-graben and late syn-kinematic</i>
	<i>Half-graben</i>		<i>Graben, late syn-kinematic and post-kinematic</i>

(Figure 11b) CU5 is expressed as a coarsening-northward system with progradation towards the southwest (Figure 7a), as highlighted by very-low angle, large-scale foresets (500-m lateral extent, height of 10 m). This suggests that post-kinematic regional accommodation increased southwards and was filled with sand sourced from the east or northeast, accompanied by the development of (sub)tidal sandwaves migrating south-westward.

5 | DISCUSSION

5.1 | Sedimentary response to faulting events in distinct sea level sediment supply scenarios

Single-faulting events and intervening periods of quiescence are interpreted to have had a significant effect on the stacking pattern of architectural elements within CUs. This impact can be examined for different settings of relative sea level and sediment supply, as illustrated in three scenarios in Figure 12a–c. The deposition that occurred during or shortly after faulting was associated with rapid redistribution of sediments, which were likely sourced from areas proximal to the bounding faults in the footwall. Post-kinematic deposition expresses passive fill of available accommodation. (a) In a high relative sea-level/low sediment supply setting (Figure 12a), the syn-kinematic deposition led to the deposition of intervals hosting FA1b's high-energy deposits of density currents interfingering with tabular mudstone intervals and subaqueous slumps within mudstone wedges. These sandstone-rich deposits subsequently were draped by post-kinematic mudstones. (b) In an intermediate sealevel/sediment supply setting (Figure 12b), the loose sediments in the hanging wall blocks were intensely affected by soft sediment deformations. Soft sediment deformation was likely a result of basin floor tilting and shaking during slip events on listric faults. Additionally, small structureless sandstone wedges developed in half grabens (Figure 7a). Lenticular tidal bars with lateral accretion surfaces or distal laterally extensive tidal dune complexes passively filled the post-kinematic accommodation space. The position of partly aggrading tidal bars with lateral accretion surfaces adjacent to the fault likely reflects the post-kinematic deposition in a higher and more localized accommodation than tidal bars with lateral accretion surfaces. (c) In a low relative sea-level/high sediment supply setting (Figure 12c), the syn-kinematic deposition in half-grabens

led to the deposition of structureless sandstone wedges filling available accommodation. Contrastingly, in graben, syn-kinematic deposits are not obvious and, where they occur, may be linked to the development of soft sediment deformation intervals. Laterally extensive tidal dune complexes passively filled the remaining post-kinematic accommodation.

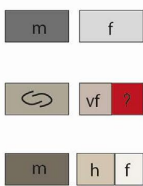
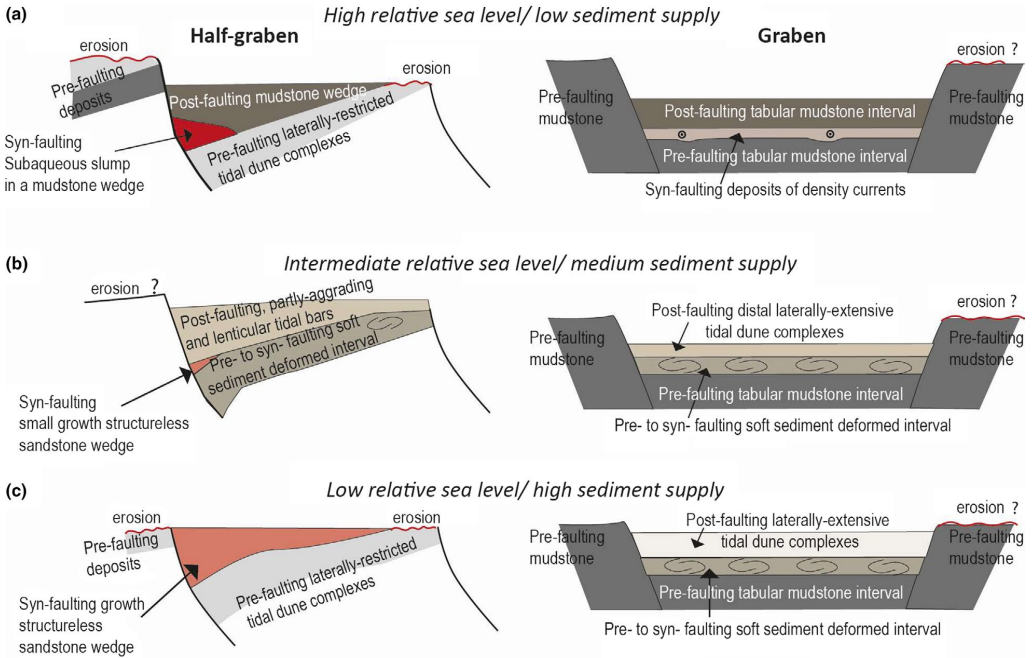
5.2 | Impact of basin floor morphology on palaeo-tidal circulation

This study discerns distinct sedimentary architectures within tidally influenced, fault-bounded grabens and half-grabens in the distal part of a prograding deltaic system. The overall sediment palaeo-current pattern suggests a southwest dominating transport direction with subordinate northwest-southeast oriented flows (Figure 6). Laterally extensive tidal dune complexes found in the post-kinematic succession (CU5) and in wide graben fills (e.g. B10), recorded sediment progradation towards the southwest (Figure 6). These broad systems may reflect regional basin circulation (Figure 12b). This transport direction is modified in late-kinematic successions by faulting as determined by scattered palaeo-transport indicators (CU4; Figure 6a). The strongest fault-control on transport direction is expressed in narrow half-grabens (e.g. B9), where lenticular tidal bars with lateral accretion surfaces and laterally restricted tidal dune complexes developed axially to slightly obliquely to the bounding faults. Palaeotidal currents circulated northwest-wards to westwards, perpendicular to the southwest subregional direction recorded in CU5 (Figure 6).

Narrow half-grabens have a funnel-shaped topography, in which tidal currents were probably amplified, especially during ebb-tides. Hydraulic conditions of tidal currents in a narrow confinement may drive development of lateral migrating surfaces, resembling bank-attached point bars (Longhitano et al., 2012). Noticeably, the half-graben dipslopes of Kvalpynten consistently dip to the north (Figure 3) and sandstone beds within lenticular tidal bars gently thicken towards the north. Contrastingly, lateral accretion built southward (away from the bounding faults), up the dipslope towards shallower water. This highlights that fault-generated basin floor morphology played a major role in half-graben hydrodynamics, mainly by amplifying basin axis-parallel tidal currents in deeper parts. This funnelling effect waned towards shallower waters higher on

FIGURE 12 (a–c) Conceptual model of the development of pre-, syn- and post-kinematic architectural elements that depend on the rate of relative sea level/sediment supply. (d) Conceptual model of growth basins and their development in prodelta/lower front of a tidally-influenced delta with heteroliths and sand redistributed by tidal bars and dunes, detached from the delta front/delta top; inspired by López-Blanco et al. (2003); blue arrows mark tidal current orientations, red arrows mark the lateral accretion of tidal bars in a half-graben, whereas a green arrow mark forward accretion of tidal dunes in a graben

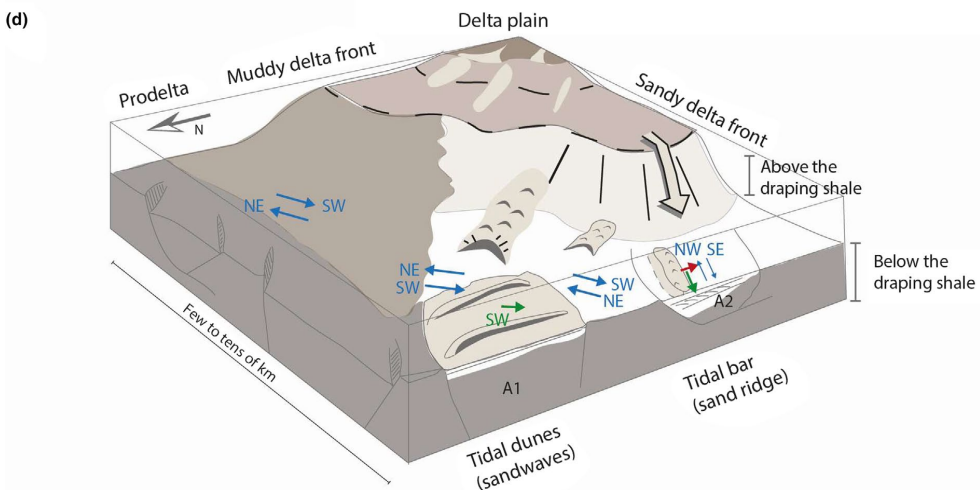
Sedimentary response to faulting event



Pre-faulting: m- mudstones (tabular mudstone intervals and mudstone wedges)
 f: fine-grained sandstones (laterally-restricted and laterally-extensive tidal dune complexes)

Syn- faulting: soft sediment deformed intervals,
 vf: very fine-grained sandstones (within tabular mudstone intervals),
 ?: very fine/fine (?) grained sandstones -subaqueous slumps
 f-m: fine to medium-grained sandstones of structureless sandstone wedges

Post-faulting: mudstones (tabular mudstone intervals and mudstone wedges),
 heterolithics (partly-aggrading and lenticular tidal bars with lateral accretion surfaces)
 and fine-grained sandstones (laterally-restricted and laterally-extensive tidal dune complexes)



the dip slope, as accommodation was filled and the relief was healed.

5.3 | Internal versus external controls on development of CU units

Cycles of CU1-5 capped by flooding surfaces bear evidence of the syn and late/post-kinematic filling of the Kvalpynten basins. CUs 1–5 are 25- to 60-m thick on average, which is 2–4 times thicker than fault-induced accommodation; therefore, CUs cannot be entirely controlled by faulting. This is also supported by deposition of CU5, that is after fault activity. The individual positions of flooding surfaces in the hanging walls of growth faults constrain the interpretation of processes that controlled their development. Besides eustatic sea level variations, different rates of delta front progradation, autogenic delta lobe switching, differential compaction and fault- or sediment-loading-induced subsidence offer complementary controls on development of CU units and flooding surfaces.

Within half-grabens, fault-introduced basin floor topography during deposition of subaqueous slumps indicates a maximum relief of 12 to 17 m (mudstone wedges in Figure 9e). This value can be considered a proxy for a fault-induced accommodation increase for one/several faulting episode(s) during times of high relative sea level/low sediment supply (Figure 12a). Similarly, during low accommodation relative to sediment supply (Figure 12c) the 13–17 m thick structureless sandstone wedges can serve as a proxy for syn-kinematic accommodation increase. This also documents that faulting occurred in both, low and high rates of sediment supply.

Edwards (1976) interpreted the southerly dipping faults in Kvalpynten to form due to loading and gravitational collapse of delta front sandstones prograding from the north. Edwards' (1976) model contradicts the recent, more regional understanding of the Upper Triassic deltaic deposits prograding towards north, north-west across the Barents shelf (Figure 1b; Anell et al., 2014, 2016; Glørstad-Clark et al., 2010, 2011; Høy & Lundschieen, 2011; Klausen et al., 2015; Lundschieen et al., 2014; Riis et al., 2008; Worsley, 2008). This study shows that growth faulting occurred in the prodelta position and corresponds to both, low and high rates of sediment supply. The growth fault system was dominated by listric faults that dip to the south and southwest, in a near-landward direction and against the prograding delta. The deepening of CU5 to the south and south-facing listric growth faults fit the model of a compaction-front arriving from a southerly direction, as advocated by Braathen, Midtkandal, et al. (Braathen, Midtkandal, et al., 2018) and Ogata et al. (2018). In this scenario, the deltaic system was prograding against and atop the roughly NE-SW oriented, palaeo-bathymetry (i.e. Svalbard platform). Ogata et al. (2018) discuss the regional differential compaction and instability along

a gently inclined, long-lived delta-facing slope as trigger mechanisms for the growth faulting. In addition, deep-rooted tectonic faults of Carboniferous age were likely reactivated by far-field tectonics related to the late Triassic Uralide orogeny to the east (Anell et al., 2013; Ogata et al., 2018).

The palaeo-bathymetry in the NW Barents Shelf caused a significant decrease in the overall available accommodation for deltaic sediments prograding against the Svalbard Platform that impacted a lack of aggradation and differential advancement rates of the clinoforms (Anell et al., 2013, 2016). In Kvalpynten, the palaeo-slope and corresponding subsidence increase towards the south can explain the southwards deepening of CU5 deposits.

Growth faults impacted palaeo-bathymetric relief of the top of the Botneheia Formation during the deposition of the Tschermakfjellet Formation (Ogata et al., 2018). The stacking patterns of CU1-4 are unique to each basin, do not show any clear progradational or retrogradational trends and therefore may be considered as aggradational. In contrast to the regional decrease in subsidence (Anell et al., 2013, 2016), the local depocentres located in the hanging walls of the growth faults allowed for the aggradation of the CU1-4 deposits.

Tidal reworking of sediments can redistribute sand across the shelf, and lead to the development of tidal bars and dunes, that are detached from the delta front/top (Longhitano et al., 2012; Olariu, Steel, et al., 2012; Olariu, Olariu, et al., 2012; Rossi et al., 2016, 2017; Rossi & Steel, 2016; Willis, 2005). In Kvalpynten, tidal bars and dunes that migrated over a distance of few to tens of km and were detached from the tidally influenced delta front/top (Figure 12d), as similarly observed in the Roda Formation (Esdolomada Member) of the Tremp-Graus Basin in Spain, where tidal (shelf) bars are detached from the delta mouth by a distance of approximately 4 km (Olariu, Olariu, et al., 2012). In Kvalpynten, the distance between the tidal bars and dunes and the delta front/top is uncertain. The position of delta top for CUs 1–4 remains unknown. 4–5 km to the east of Kvalpynten (at Vogelberget; Figure 2) in the stratigraphic level corresponding to the CU5, Röhnert (2016) interpreted a succession of heterogeneous sandstone complexes as mixed energy (tidal and wave modified) channels and mouth bars with transport directions towards southwest. This succession could represent the position of the delta front during the deposition of the uppermost CU5.

6 | CONCLUSIONS

This study documents the impact of growth faulting on the deposition of coarsening-upward units in the 400-m-high and 9-km-long cliffs of Kvalpynten, SW Edgeøya, Svalbard. The transition from prodelta mudstones to heterolithic tidal bars

and tidally reworked sandy dunes is interpreted to represent a distal part of the Upper Triassic seismic-scale deltaic system, which prograded north-westwards over the Barents Shelf. It is concluded that:

1. The stratigraphic succession fill is segmented by listric and planar growth faults into 12 isolated grabens and half-grabens situated in prodelta to delta slope.
2. The basin floor morphology was impacted by fault-scarps and progressive tilting of fault blocks that enhanced subaqueous erosion along the uplifted footwalls, triggered gravity-driven processes and introduced locally derived sediment into the grabens and half-grabens.
3. Narrow and elongated troughs in hanging walls amplified tidal energy that impacted the modality of sediment deposition.
4. Accommodation was controlled by growth faulting: fully compartmentalized syn-kinematic deposition occurred in grabens and half-grabens. In these basins, the dynamic nature of progressive fault-driven accommodation had a strong impact on the stacking patterns of sedimentary units. Architectural elements that relate directly to the rate of fault-induced accommodation were systematically stacked within the coarsening upwards units.
5. Late-kinematic deposition is expressed by continuous units, mildly influenced by compaction-driven faulting.
6. Post-kinematic accommodation has formed in response to regional subsidence and was filled by a south-westwards prograding system of mudstone passing into tidal dunes.

ACKNOWLEDGMENTS

The authors would like to acknowledge The University Centre in Svalbard for funding Smyrak-Sikora's research. Field work was supported by the Trias North Project (grant 234152/E30) financed by the Research Council of Norway and industry partners, Edison Norway, Lundin Norway, RWE Dea Norge, Statoil and Tullow Oil. We acknowledge Simon Buckley and the Virtual Outcrop Geology Group (Uni Research CIPR) for providing academic licenses for LIME. Berit Husteli and Luka Blažić are acknowledged for their contribution to the logs. Snorre Olausen, Ivar Midtkandal and Harmon Maher are thanked for their comments and discussion on the research. The associate editor in Basin Research Cari Johnson and the reviewers Stefan Back, Luigi Bruno, and anonymous reviewer are acknowledged for their constructive comments to the manuscript.

DATA AVAILABILITY STATEMENT

The data that support the findings of this study are provided in the supplementary material.

ORCID

Aleksandra Smyrak-Sikora  <https://orcid.org/0000-0001-9321-1269>

Alvar Braathen  <https://orcid.org/0000-0002-0869-249X>

Kei Ogata  <https://orcid.org/0000-0002-4978-2854>

REFERENCES

- Ahlborn, M., & Stemmerik, L. (2015). Depositional evolution of the Upper Carboniferous – Lower Permian Wordiekammen carbonate platform, Nordfjorden High, central Svalbard, Arctic Norway. *Norwegian Journal of Geology*, 95, 91–126.
- Allen, J. R. L. (1982). *Sedimentary structures, their character and physical basis* (Vol. 1). New York: Elsevier.
- Anderton, R. (1976). Tidal-shelf sedimentation: An example from the Scottish Dalradian. *Sedimentology*, 23(4), 429–458. <https://doi.org/10.1111/j.1365-3091.1976.tb00062.x>
- Anell, I. M., Braathen, A., & Olausen, S. (2014). The Triassic-Early Jurassic of the northern Barents Shelf: A regional understanding of the Longyearbyen CO₂ reservoir. *Norsk Geologisk Tidsskrift*, 94, 83–98.
- Anell, I., Braathen, A., Olausen, S., & Osmundsen, P. T. (2013). Evidence of faulting contradicts a quiescent northern Barents Shelf during the Triassic. *First Break*, 31(6), 67–76. <https://doi.org/10.3997/1365-2397.2013017>
- Anell, I. M., Faleide, J. I., & Braathen, A. (2016). Regional tectono-sedimentary development of the highs and basins of the northwestern Barents Shelf. *Norsk Geologisk Tidsskrift*, 96(1), 27–41. <https://doi.org/10.17850/njg96-1-04>
- Ashley, G. M. (1990). Classification of large-scale subaqueous bedforms: A new look at an old problem-SEPM bedforms and bedding structures. *Journal of Sedimentary Research*, 60(1), 160–172. <https://doi.org/10.2110/jsr.60.160>
- Ashley, G. M., Southard, J. B., & BoöTHROYD, J. C. (1982). Deposition of climbing-ripple beds: A flume simulation. *Sedimentology*, 29(1), 67–79. <https://doi.org/10.1111/j.1365-3091.1982.tb01709.x>
- Baas, J. H., Best, J. L., & Peakall, J. (2016). Predicting bedforms and primary current stratification in cohesive mixtures of mud and sand. *Journal of the Geological Society*, 173(1), 12–45. <https://doi.org/10.1144/jgs2015-024>
- Back, S., & Morley, C. K. (2016). Growth faults above shale–Seismic-scale outcrop analogues from the Makran foreland, SW Pakistan. *Marine and Petroleum Geology*, 70, 144–162. <https://doi.org/10.1016/j.marpetgeo.2015.11.008>
- Back, S., Strozzyk, F., Kukla, P. A., & Lambiase, J. J. (2008). Three-dimensional restoration of original sedimentary geometries in deformed basin fill, onshore Brunei Darussalam, NW Borneo. *Basin Research*, 20(1), 99–117. <https://doi.org/10.1111/j.1365-2117.2007.00343.x>
- Basilici, G. (1997). Sedimentary facies in an extensional and deep-lacustrine depositional system: The Pliocene Tiberino Basin, Central Italy. *Sedimentary Geology*, 109(1–2), 73–94. [https://doi.org/10.1016/S0037-0738\(96\)00056-5](https://doi.org/10.1016/S0037-0738(96)00056-5)
- Bergh, S. G., Maher, H. D., & Braathen, A. (2000). Tertiary divergent thrust directions from partitioned transpression, Brøggerhalvøya, Spitsbergen. *Norsk Geologisk Tidsskrift*, 80(2), 63–81.
- Bhattacharya, J. P., & Davies, R. K. (2001). Growth faults at the prodelta to delta-front transition, Cretaceous Ferron sandstone, Utah. *Marine*

- and *Petroleum Geology*, 18(5), 525–534. [https://doi.org/10.1016/S0264-8172\(01\)00015-0](https://doi.org/10.1016/S0264-8172(01)00015-0)
- Bourouellec, R., Cartwright, J. A., Johnson, H. D., Lansigu, C., Quémener, J. M., & Savanier, D. (2004). Syndepositional faulting in the Grès d'Annot Formation, SE France: High-resolution kinematic analysis and stratigraphic response to growth faulting. *Geological Society, London, Special Publications*, 221(1), 241–265. <https://doi.org/10.1144/GSL.SP.2004.221.01.13>
- Braathen, A., Bælum, K., Maher, H. J., & Buckley, S. J. (2011). Growth of extensional faults and folds during deposition of an evaporite-dominated half-graben basin; the Carboniferous Billefjorden Trough, Svalbard. *Norwegian Journal of Geology/Norsk Geologisk Forening*, 91(3), 131–161.
- Braathen, A., Bergh, S. G., & Maher, H. D. Jr (1999). Application of a critical wedge taper model to the Tertiary transpressional fold-thrust belt on Spitsbergen. *Geological Society of America Bulletin*, 111, 1468–1485.
- Braathen, A., Midtkandal, I., Mulrooney, M. J., Appleyard, T. R., Haile, B. G., & van Yperen, A. E. (2018). Growth-faults from delta collapse—structural and sedimentological investigation of the Last Chance delta, Ferron Sandstone, Utah. *Basin Research*, 30(4), 688–707. <https://doi.org/10.1111/bre.12271>
- Braathen, A., Osmundsen, P. T., Maher, H., & Ganerød, M. (2018). The Keisarhjelmen detachment records Silurian-Devonian extensional collapse in Northern Svalbard. *Terra Nova*, 30(1), 34–39. <https://doi.org/10.1111/ter.12305>
- Bruce, C. H. (1973). Pressured shale and related sediment deformation: Mechanism for development of regional contemporaneous faults. *AAPG Bulletin*, 57(5), 878–886.
- Buckley, S. J., Ringdal, K., Naumann, N., Dolva, B., Kurz, T. H., Howell, J. A., & Dewez, T. J. (2019). LIME: Software for 3-D visualization, interpretation, and communication of virtual geoscience models. *Geosphere*, 15(1), 222–235. <https://doi.org/10.1130/GES02002.1>
- Burhannuddinur, M., & Morley, C. K. (1997). Anatomy of growth fault zones in poorly lithified sandstones and shales: Implications for reservoir studies and seismic interpretation: Part 1, outcrop study. *Petroleum Geoscience*, 3(3), 211–224. <https://doi.org/10.1144/petgeo.3.3.211>
- Caillet, G., & Batiot, S. (2003). 2D modelling of hydrocarbon migration along and across growth faults: An example from Nigeria. *Petroleum Geoscience*, 9(2), 113–124. <https://doi.org/10.1144/1354-079302-499>
- Cartwright, J. A., Mansfield, C., & Trudgill, B. (1996). The growth of normal faults by segment linkage. *Geological Society, London, Special Publications*, 99(1), 163–177. <https://doi.org/10.1144/GSL.SP.1996.099.01.13>
- Carver, R. E. (1968). Differential compaction as a cause of regional contemporaneous faults. *AAPG Bulletin*, 52(3), 414–419.
- Chandler, J. H., & Buckley, S. (2016). Structure from motion (SFM) photogrammetry vs terrestrial laser scanning. In M. B. Carpenter & C. M. Keane (Eds.), *Geoscience Handbook 2016, AGI Data Sheets* (5th edn.). Section 20.1. Alexandria, USA: American Geosciences Institute.
- Cheel, R. J., & Leckie, D. A. (1993). Hummocky cross-stratification. *Sedimentology Review*, 1, 103–122.
- Cheel, R. J., & Middleton, G. V. (1986). Horizontal laminae formed under upper flow regime plane bed conditions. *The Journal of Geology*, 94(4), 489–504. <https://doi.org/10.1086/629053>
- Dallmann, W. K., Elvevold, S., Majka, J., & Piepjohn, K. (2015). Tectonics and tectonothermal events. In: *Geoscience Atlas of Svalbard* (Ed. by Dallmann, W.K.). *Norsk Polarinstitutt Rapportserie*, 148, 175–223.
- Dimakis, P., Braathen, B. I., Faleide, J. I., Elverhøi, A., & Gudlaugsson, S. T. (1998). Cenozoic erosion and the preglacial uplift of the Svalbard-Barents Sea region. *Tectonophysics*, 300(1–4), 311–327. [https://doi.org/10.1016/S0040-1951\(98\)00245-5](https://doi.org/10.1016/S0040-1951(98)00245-5)
- Dumas, S., & Arnott, R. W. C. (2006). Origin of hummocky and swaley cross-stratification—The controlling influence of unidirectional current strength and aggradation rate. *Geology*, 34(12), 1073–1076. <https://doi.org/10.1130/G22930A.1>
- Dypvik, H., Hakansson, E., & Heinberg, C. (2002). Jurassic and Cretaceous palaeogeography and stratigraphic comparisons in the North Greenland-Svalbard region. *Polar Research*, 21, 91–108. <https://doi.org/10.3402/polar.v21i1.6476>
- Edwards, M. B. (1976). Growth faults in Upper Triassic deltaic sediments. *Svalbard. AAPG Bulletin*, 60(3), 341–355.
- Eide, C. H., Klausen, T. G., Katkov, D., Suslova, A. A., & Helland-Hansen, W. (2017). Linking an Early Triassic delta to antecedent topography: Source-to-sink study of the southwestern Barents Sea margin. *Bulletin*, 130(1–2), 263–283.
- Faleide, J. I., Gudlaugsson, S. T., & Jacquart, G. (1984). Evolution of the western Barents Sea. *Marine and Petroleum Geology*, 1(2), 123–150. [https://doi.org/10.1016/0264-8172\(84\)90082-5](https://doi.org/10.1016/0264-8172(84)90082-5)
- Faleide, J. I., Pease, V., Curtis, M., Klitzke, P., Minakov, A., Sheck-Wenderoth, M., ... Zayonchek, A. (2017). Tectonic implications of the lithospheric structure across the Barents and Kara shelves. *Geological Society of London, Special Publications*, 460, 285–314. <https://doi.org/10.1144/SP460.18>
- Faleide, J. I., Tsikalas, F., Breivik, A. J., Mjelde, R., Ritzmann, O., Engen, Ø., ... Eldholm, O. (2008). Structure and evolution of the continental margin off Norway and the Barents Sea. *Episodes*, 31(1), 82–91. <https://doi.org/10.18814/epiugs/2008/v31i1/012>
- Fazlikhani, H., Back, S., Kukla, P. A., & Fossen, H. (2017). Interaction between gravity-driven listric normal fault linkage and their hanging-wall rollover development: A case study from the western Niger Delta, Nigeria. *Geological Society, London, Special Publications*, 439(1), 169–186. <https://doi.org/10.1144/SP439.20>
- Fielding, C. R. (2006). Upper flow regime sheets, lenses and scour fills: Extending the range of architectural elements for fluvial sediment bodies. *Sedimentary Geology*, 190(1–4), 227–240. <https://doi.org/10.1016/j.sedgeo.2006.05.009>
- Fielding, C. R. (2015). Anatomy of falling-stage deltas in the Turonian Ferron Sandstone of the western Henry Mountains Syncline, Utah: Growth faults, slope failures and mass transport complexes. *Sedimentology*, 62(1), 1–26. <https://doi.org/10.1111/sed.12136>
- Flood, B., Nagy, J., & Winsnes, T. S. (1971). The Triassic succession of Barentsøya, Edgeøya, and Hopen (Svalbard). *Norsk Polarinstitutt Meddelelser*, 100, 1–20.
- Garfunkel, Z. (1984). Large-scale submarine rotational slumps and growth faults in the eastern Mediterranean. *Marine Geology*, 55(3–4), 305–324. [https://doi.org/10.1016/0025-3227\(84\)90074-4](https://doi.org/10.1016/0025-3227(84)90074-4)
- Gingras, M. K., Pemberton, S. G., & Smith, M. (2014). Bioturbation: Reworking sediments for better or worse. *Oilfield Review*, 26(4), 46–58.
- Gjelberg, J., & Steel, R. J. (1995). Helvetiafjellet Formation (Barremian–Aptian), Spitsbergen: Characteristics of a transgressive succession. In R. J. Steel, V. L. Felt, E. P. Johannessen, & C. Mathieu (Eds), *Sequence stratigraphy on the Northwest European Margin* (pp. 571–593). Amsterdam: Norwegian Petroleum Society (NPF) Special Publication 5, Elsevier.

- Glørstad-Clark, E., Birkeland, E. P., Nystuen, J. P., Faleide, J. I., & Midtkandal, I. (2011). Triassic platform-margin deltas in the western Barents Sea. *Marine and Petroleum Geology*, 28(7), 1294–1314. <https://doi.org/10.1016/j.marpetgeo.2011.03.006>
- Glørstad-Clark, E., Faleide, J. I., Lundschieen, B. A., & Nystuen, J. P. (2010). Triassic seismic sequence stratigraphy and paleogeography of the western Barents Sea area. *Marine and Petroleum Geology*, 27(7), 1448–1475. <https://doi.org/10.1016/j.marpetgeo.2010.02.008>
- Grundvåg, S. A., Marin, D., Kairanov, B., Śliwińska, K. K., Nøhr-Hansen, H., Jelby, M. E., ... Olaussen, S. (2017). The Lower Cretaceous succession of the northwestern Barents Shelf: Onshore and offshore correlations. *Marine and Petroleum Geology*, 86, 834–857. <https://doi.org/10.1016/j.marpetgeo.2017.06.036>
- Grundvåg, S. A., & Olaussen, S. (2017). Sedimentology of the Lower Cretaceous at Kikutodden and Keilhaufjellet, southern Spitsbergen: Implications for an onshore–offshore link. *Polar Research*, 36, 1. <https://doi.org/10.1080/17518369.2017.1302124>
- Haile, B. G., Klausen, T. G., Czarniecka, U., Xi, K., Jahren, J., & Hellevang, H. (2018). How are diagenesis and reservoir quality linked to depositional facies? A deltaic succession, Edgeøya, Svalbard. *Marine and Petroleum Geology*, 92, 519–546. <https://doi.org/10.1016/j.marpetgeo.2017.11.019>
- Harland, W. B., & Kelly, S. R. A. (1997). Eastern svalbard platform. In W. B. Harland (Ed.), *The geology of svalbard* (Vol. 17, pp. 75–95). London: Geological Society, Memoirs. <https://doi.org/10.1144/GSL.MEM.1997.017.01.05>
- Henriksen, E., Bjørnseth, H. M., Hals, T. K., Heide, T., Kiryukhina, T., Kløvjan, O., ... Sollid, K. (2011). Uplift and erosion of the greater Barents Sea: Impact on prospectivity and petroleum systems. *Geological Society, London, Memoirs*, 35(1), 271–281.
- Hiscott, R. N. (2001). Depositional sequences controlled by high rates of sediment supply, sea-level variations, and growth faulting: The Quaternary Baram Delta of northwestern Borneo. *Marine Geology*, 175(1–4), 67–102. [https://doi.org/10.1016/S0025-3227\(01\)00118-9](https://doi.org/10.1016/S0025-3227(01)00118-9)
- Høy, T., & Lundschieen, B. A. (2011). Triassic deltaic sequences in the northern Barents Sea. *Geological Society, London, Memoirs*, 35(1), 249–260.
- Ings, S. J., & Beaumont, C. (2010). Shortening viscous pressure ridges, a solution to the enigma of initiating salt ‘withdrawal’ minibasins. *Geology*, 38(4), 339–342.
- Jelby, M. E., Grundvåg, S. A., Helland-Hansen, W., Olaussen, S., & Stemmerik, L. (2017). Basin-scale facies model of spectacular storm deposits in the High Arctic. Geological Society of Denmark Annual meeting 2017, Copenhagen, Denmark.
- Johannessen, E. P., & Steel, R. J. (1992). Mid-Carboniferous extension and rift-infill sequences in the Billefjorden Trough, Svalbard. *Norsk Geologisk Tidsskrift*, 72(1), 35–48.
- Klausen, T. G., & Mørk, A. (2014). The upper triassic paralic deposits of the De Geerdalen formation on hopen: outcrop analog to the subsurface snadd formation in the barents sea the De Geerdalen formation on hopen. *AAPG Bulletin*, 98(10), 1911–1941. <https://doi.org/10.1306/02191413064>
- Klausen, T. G., Ryseth, A. E., Helland-Hansen, W., Gawthorpe, R., & Laursen, I. (2015). Regional development and sequence stratigraphy of the Middle to Late Triassic Snadd formation, Norwegian Barents Sea. *Marine and Petroleum Geology*, 62, 102–122. <https://doi.org/10.1016/j.marpetgeo.2015.02.004>
- Klausen, T. G., Torland, J. A., Eide, C. H., Alaei, B., Olaussen, S., & Chiarella, D. (2018). Cliniform development and topset evolution in a mud-rich delta—the Middle Triassic Kobbe Formation, Norwegian Barents Sea. *Sedimentology*, 65(4), 1132–1169. <https://doi.org/10.1111/sed.12417>
- Koevoets, M. J., Hammer, O., Olaussen, S., Senger, K., & Smelror, M. (2019). Integrating subsurface and outcrop data of the Middle Jurassic to Lower Cretaceous Agardhfjellet Formation in central Spitsbergen. *Norwegian Journal of Geology*, 98, 1–34. <https://doi.org/10.17850/njg98-4-01>
- Krajewski, K. P. (2008). The Botneheia Formation (Middle Triassic) in Edgeøya and Barentsøya, Svalbard: Lithostratigraphy, facies, phosphogenesis, paleoenvironment. *Polish Polar Research*, 29(4), 319–364.
- Longhitano, S. G., Mellere, D., Steel, R. J., & Ainsworth, R. B. (2012). Tidal depositional systems in the rock record: A review and new insights. *Sedimentary Geology*, 279, 2–22. <https://doi.org/10.1016/j.sedgeo.2012.03.024>
- Lopez, J. A. (1990). Structural styles of growth faults in the US Gulf Coast Basin. *Geological Society, London, Special Publications*, 50(1), 203–219. <https://doi.org/10.1144/GSL.SP.1990.050.01.10>
- López-Blanco, M., Marzo, M., & Muñoz, J. A. (2003). Low-amplitude, synsedimentary folding of a deltaic complex: Roda Sandstone (lower Eocene), South-Pyrenean Foreland Basin. *Basin Research*, 15(1), 73–96. <https://doi.org/10.1046/j.1365-2117.2003.00193.x>
- Lord, G. S., Johansen, S. K., Støen, S. J., & Mørk, A. (2017). Facies development of the Upper Triassic succession on Barentsøya, Wilhelmøya and NE Spitsbergen, Svalbard. *Norwegian Journal of Geology*, 97(1). <https://doi.org/10.17850/njg97-1-03>
- Lord, G. S., Solvi, K. H., Klausen, T. G., & Mørk, A. (2014). Triassic channel bodies on Hopen, Svalbard: Their facies, stratigraphical significance and spatial distribution. *Norwegian Petroleum Directorate Bulletin*, 11, 41–59.
- Lundschieen, B. A., Høy, T., & Mørk, A. (2014). Triassic hydrocarbon potential in the Northern Barents Sea; integrating Svalbard and stratigraphic core data. *Norwegian Petroleum Directorate Bulletin*, 11, 3–20.
- Maher, H. D., Ogata, K., & Braathen, A. (2017). Cone-in-cone and beef mineralization associated with Triassic growth basin faulting and shallow shale diagenesis, Edgeøya, Svalbard. *Geological Magazine*, 154(2), 201–216. <https://doi.org/10.1017/S0016756815000886>
- Martinsen, O. J. (1989). Styles of soft-sediment deformation on a Namurian (Carboniferous) delta slope, Western Irish Namurian Basin, Ireland. *Geological Society, London, Special Publications*, 41(1), 167–177. <https://doi.org/10.1144/GSL.SP.1989.041.01.13>
- Martinsen, O. J., & Bakken, B. (1990). Extensional and compressional zones in slumps and slides in the Namurian of County Clare, Ireland. *Journal of the Geological Society*, 147(1), 153–164. <https://doi.org/10.1144/gsjgs.147.1.0153>
- Martinsen, O. J., Lien, T., Walker, R. G., & Collinson, J. D. (2003). Facies and sequential organisation of a mudstone-dominated slope and basin floor succession: The Gull Island Formation, Shannon Basin, Western Ireland. *Marine and Petroleum Geology*, 20(6–8), 789–807. <https://doi.org/10.1016/j.marpetgeo.2002.10.001>
- Massari, F. (1996). Upper-flow-regime stratification types on steep-face, coarse-grained, Gilbert-type progradational wedges (Pleistocene, southern Italy). *Journal of Sedimentary Research*, 66(2), 364–375.
- McClay, K. R., Dooley, T., & Lewis, G. (1998). Analog modeling of progradational delta systems. *Geology*, 26(9), 771–774. [https://doi.org/10.1130/0091-7613\(1998\)026<0771:AMOPDS>2.3.CO;2](https://doi.org/10.1130/0091-7613(1998)026<0771:AMOPDS>2.3.CO;2)

- Midtkandal, I., & Nystuen, J. P. (2009). Depositional architecture of low-gradient ramp shelf in an epicontinental sea: The lower Cretaceous of Svalbard. *Basin Research*, 21(5), 655–675. <https://doi.org/10.1111/j.1365-2117.2009.00399.x>
- Midtkandal, I., Nystuen, J. P., Nagy, J., & Mørk, A. (2008). Lower Cretaceous lithostratigraphy across a regional subaerial unconformity in Spitsbergen: The Rurikfjellet and Helvetiafjellet formations. *Norwegian Journal of Geology*, 88(4), 287–304.
- Mørk, A., Dallmann, W. K., Dypvik, H., Johannessen, E. P., Larssen, G. B., Nagy, J., Nøttvedt, A. ... Worsley, D. (1999). Mesozoic lithostratigraphy. In *Lithostratigraphic lexicon of Svalbard. Upper Palaeozoic to Quaternary bedrock. Review and recommendations for nomenclature use* (Ed. By: Dallmann, W. K.). *Tromsø, Norsk Polarinstittut*, 127–214.
- Mørk, A., Knarud, R., & Worsley, D. (1982). Depositional and diagenetic environments of the Triassic and Lower Jurassic succession of Svalbard. In A. F. Embry, & H. R. Balkwill (Eds.), *Arctic geology and geophysics: proceedings of the Third International Symposium on Arctic Geology Memoir* 8, (371–398) Calgary: Canadian Society of Petroleum Geologist.
- Mørk, M. B. E. (1999). Compositional variations and provenance of Triassic sandstones from the Barents Shelf. *Journal of Sedimentary Research*, 69(3), 690–710. <https://doi.org/10.2110/jsr.69.690>
- Morley, C. K., Back, S., Van Rensbergen, P., Crevello, P., & Lambiasi, J. J. (2003). Characteristics of repeated, detached, Miocene-Pliocene tectonic inversion events, in a large delta province on an active margin, Brunei Darussalam. *Borneo. Journal of Structural Geology*, 25(7), 1147–1169. [https://doi.org/10.1016/S0191-8141\(02\)00130-X](https://doi.org/10.1016/S0191-8141(02)00130-X)
- Morley, C. K., & Guerin, G. (1996). Comparison of gravity-driven deformation styles and behavior associated with mobile shales and salt. *Tectonics*, 15(6), 1154–1170. <https://doi.org/10.1029/96TC01416>
- Mulder, T., Syvitski, J. P., Migeon, S., Faugeres, J. C., & Savoye, B. (2003). Marine hyperpycnal flows: Initiation, behavior and related deposits. A Review. *Marine and Petroleum Geology*, 20(6–8), 861–882. <https://doi.org/10.1016/j.marpetgeo.2003.01.003>
- Mulrooney, M. J., Leutscher, J., & Braathen, A. (2017). A 3D structural analysis of the Goliat field, Barents Sea, Norway. *Marine and Petroleum Geology*, 86, 192–212. <https://doi.org/10.1016/j.marpetgeo.2017.05.038>
- Mulrooney, M. J., Rismyhr, B., Yenwongfai, H. D., Leutscher, J., Olaussen, S., & Braathen, A. (2018). Impacts of small-scale faults on continental to coastal plain deposition: Evidence from the Realgrunnen Subgroup in the Goliat field, southwest Barents Sea, Norway. *Marine and Petroleum Geology*, 95, 276–302. <https://doi.org/10.1016/j.marpetgeo.2018.04.023>
- Mutti, E. (1992). Turbidite sandstones. *AGIP, Istituto di geologia, Università di Parma, San Donato Milanese*, 275 pp.
- Mutti, E., Tinterri, R., Benevelli, G., di Biase, D., & Cavanna, G. (2003). Deltaic, mixed and turbidite sedimentation of ancient foreland basins. *Marine and Petroleum Geology*, 20(6–8), 733–755. <https://doi.org/10.1016/j.marpetgeo.2003.09.001>
- Nemec, W., Steel, R. J., Gjelberg, J., Collinson, J. D., Prestholm, E., & Oxnevad, I. E. (1988). Anatomy of collapsed and re-established delta front in Lower Cretaceous of eastern Spitsbergen: Gravitational sliding and sedimentation processes. *AAPG Bulletin*, 72(4), 454–476.
- Nio, S. D., & Yang, C. S. (1991). Diagnostic attributes of clastic tidal deposits: A review. In *Clastic Tidal Sedimentology* (Ed. by D. G. Smith et al.). *CSPG Special Publications, Clastic Tidal Sedimentology, Memoir* 16. Mem can Soc Pet Geol, 16, 3–27.
- Ocam, R. D. (1961). Growth faults of south Louisiana. *Transactions of the Gulf Coast Association of Geological Societies*, 139–174.
- Ogata, K., Mulrooney, M. J., Braathen, A., Maher, H., Osmundsen, P. T., Anell, I., ... Balsamo, F. (2018). Architecture, deformation style and petrophysical properties of growth fault systems: The Late Triassic deltaic succession of southern Edgeøya (East Svalbard). *Basin Research*, 30(5), 1042–1073. <https://doi.org/10.1111/bre.12296>
- Olariu, C., Steel, R. J., Dalrymple, R. W., & Gingras, M. K. (2012). Tidal dunes versus tidal bars: The sedimentological and architectural characteristics of compound dunes in a tidal seaway, the lower Baronia Sandstone (Lower Eocene), Ager Basin, Spain. *Sedimentary Geology*, 279, 134–155. <https://doi.org/10.1016/j.sedgeo.2012.07.018>
- Olariu, M. I., Olariu, C., Steel, R. J., Dalrymple, R. W., & Martinus, A. W. (2012). Anatomy of a laterally migrating tidal bar in front of a delta system: Esdolomada Member, Roda Formation, Tremp-Graus Basin, Spain. *Sedimentology*, 59(2), 356–378. <https://doi.org/10.1111/j.1365-3091.2011.01253.x>
- Olaussen, S., Larssen, G. B., Helland-Hansen, W., Johannessen, E. P., Nøttvedt, A., Riis, F., ... Worsley, D. (2018). Mesozoic strata of the Kong Karls Land archipelago, Arctic Norway: a link to the northern Barents Sea basins. *Norwegian Journal of Geology*, 98, 1–69.
- Osmundsen, P. T., Braathen, A., Rød, R. S., & Hynne, I. B. (2014). Styles of normal faulting and fault-controlled sedimentation in the Triassic deposits of Eastern Svalbard. *Norwegian Petroleum Directorate Bulletin*, 11, 61–79.
- Owen, G. (1987). Deformation processes in unconsolidated sands. *Geological Society, London, Special Publications*, 29(1), 11–24. <https://doi.org/10.1144/GSL.SP.1987.029.01.02>
- Paterson, N. W., & Mangerud, G. (2015). Late Triassic (Carnian-Rhaetian) palynology of Hopen, Svalbard. *Review of Palaeobotany and Palynology*, 220, 98–119. <https://doi.org/10.1016/j.revpa.2015.05.001>
- Pickering, K., Stow, D., Watson, M., & Hiscott, R. (1986). Deep-water facies, processes and models: A review and classification scheme for modern and ancient sediments. *Earth-Science Reviews*, 23(2), 75–174. [https://doi.org/10.1016/0012-8252\(86\)90001-2](https://doi.org/10.1016/0012-8252(86)90001-2)
- Potter, P. E., Maynard, J. B., & Depetris, P. J. (2005). Mud and mudstones: Introduction and overview. *Springer Science & Business Media*, 1–296.
- Prestholm, E., & Walderhaug, O. (2000). Synsedimentary faulting in a Mesozoic deltaic sequence, Svalbard, Arctic Norway—Fault geometries, faulting mechanisms, and sealing properties. *AAPG Bulletin*, 84(4), 505–522.
- Riis, F., Lundschieen, B. A., Høy, T., Mørk, A., & Mørk, M. B. E. (2008). Evolution of the Triassic shelf in the northern Barents Sea region. *Polar Research*, 27(3), 318–338. <https://doi.org/10.1111/j.1751-8369.2008.00086.x>
- Rismyhr, B., Bjærke, T., Olaussen, S., Mulrooney, M. J., & Senger, K. (2019). Facies, palynostratigraphy and sequence stratigraphy of the Wilhelmøya Subgroup (Upper Triassic–Middle Jurassic) in western central Spitsbergen, Svalbard. *Norsk Geologisk Tidsskrift*, 99(4), 35–36. <https://doi.org/10.17850/njg001>
- Rød, R. S., Hynne, I. B., & Mørk, A. (2014). Depositional environment of the Upper Triassic De Geerdalen Formation—an EW transect from Edgeøya to Central Spitsbergen, Svalbard. *Norwegian Petroleum Directorate Bulletin*, 11, 21–40.
- Röhnert, A. D. (2016). Geometry and sedimentary facies of low-angle clinoforms, Edgeøya, Svalbard. (Master's Thesis, duo.uio.no).

- Rossi, V. M., Kim, W., Leva López, J., Edmonds, D., Geleynse, N., Olariu, C., ... Passalacqua, P. (2016). Impact of tidal currents on delta-channel deepening, stratigraphic architecture, and sediment bypass beyond the shoreline. *Geology*, *44*(11), 927–930. <https://doi.org/10.1130/G38334.1>
- Rossi, V. M., Longhitano, S. G., Mellere, D., Dalrymple, R. W., Steel, R. J., Chiarella, D., & Olariu, C. (2017). Interplay of tidal and fluvial processes in an early Pleistocene, delta-fed, strait margin (Calabria, Southern Italy). *Marine and Petroleum Geology*, *87*, 14–30. <https://doi.org/10.1016/j.marpetgeo.2017.02.021>
- Rossi, V. M., & Steel, R. J. (2016). The role of tidal, wave and river currents in the evolution of mixed-energy deltas: Example from the Lajas Formation (Argentina). *Sedimentology*, *63*(4), 824–864. <https://doi.org/10.1111/sed.12240>
- Rotevatn, A., & Jackson, C. A. L. (2014). 3D structure and evolution of folds during normal fault dip linkage. *Journal of the Geological Society*, *171*(6), 821–829. <https://doi.org/10.1144/jgs2014-045>
- Rouby, D., Nalpas, T., Jermannaud, P., Robin, C., Guillocheau, F., & Raillard, S. (2011). Gravity driven deformation controlled by the migration of the delta front: The Plio-Pleistocene of the Eastern Niger Delta. *Tectonophysics*, *513*(1–4), 54–67. <https://doi.org/10.1016/j.tecto.2011.09.026>
- Rykkelid, E., & Fossen, H. (2002). Layer rotation around vertical fault overlap zones: Observations from seismic data, field examples, and physical experiments. *Marine and Petroleum Geology*, *19*(2), 181–192. [https://doi.org/10.1016/S0264-8172\(02\)00007-7](https://doi.org/10.1016/S0264-8172(02)00007-7)
- Ryseth, A. (2014). Sedimentation at the Jurassic-Triassic boundary, south-west Barents Sea. In A. W. Martinus, R. Ravnås, J. A. Howell, R. J. Steel, & J. P. Wonham (Eds.), *From Depositional Systems to Sedimentary Successions on the Norwegian Continental Margin* (187–214). Egham, UK: International Association of Sedimentologists Special Publication.
- Seilacher, A. (1991). Events and their signatures—an overview. *Cycles and Events in Stratigraphy*, 222–226.
- Serck, C. S., & Braathen, A. (2019). Extensional fault and fold growth: Impact on accommodation evolution and sedimentary infill. *Basin Research*, *31*(5), 967–990. <https://doi.org/10.1111/bre.12353>
- Serck, C. S., Faleide, J. I., Braathen, A., Kjøllhamar, B., & Escalona, A. (2017). Jurassic to early cretaceous basin configuration (s) in the Fingerdjupet Subbasin, SW Barents Sea. *Marine and Petroleum Geology*, *86*, 874–891. <https://doi.org/10.1016/j.marpetgeo.2017.06.044>
- Shultz, M. R., & Hubbard, S. M. (2005). Sedimentology, stratigraphic architecture, and ichnology of gravity-flow deposits partially ponded in a growth-fault-controlled slope minibasin, Tres Pasos Formation (Cretaceous), southern Chile. *Journal of Sedimentary Research*, *75*(3), 440–453. <https://doi.org/10.2110/jsr.2005.034>
- Smelror, M., Larssen, G. B., Olausen, S., Rømuld, A., & Robert, W. (2018). Late Triassic to Early Cretaceous palynostratigraphy of Kong Karls Land, Svalbard. *Arctic Norway. Norwegian Journal of Geology*, *98*, 1–31. <https://doi.org/10.17850/njg004>
- Smyrak-Sikora, A., Johannessen, E. P., Olausen, S., Sandal, G., & Braathen, A. (2019). Sedimentary architecture during Carboniferous rift initiation—the arid Billefjorden Trough, Svalbard. *Journal of the Geological Society*, *176*(2), 225–252. <https://doi.org/10.1144/jgs2018-100>
- Steel, R. J., & Worsley, D. (1984). Svalbard's post-Caledonian strata—an atlas of sedimentational patterns and palaeogeographic evolution. In A. M. Spencer (Ed.), *Petroleum geology of the North European margin* (pp. 109–135). Dordrecht: Springer.
- Taylor, A. M., & Goldring, R. (1993). Description and analysis of bioturbation and ichnofabric. *Journal of the Geological Society*, *150*(1), 141–148.
- Taylor, S. K., Nicol, A., & Walsh, J. J. (2008). Displacement loss on growth faults due to sediment compaction. *Journal of Structural Geology*, *30*(3), 394–405. <https://doi.org/10.1016/j.jsg.2007.11.006>
- Thomas, R. G., Smith, D. G., Wood, J. M., Visser, J., Calverley-Range, E. A., & Koster, E. H. (1987). Inclined heterolithic stratification—terminology, description, interpretation and significance. *Sedimentary Geology*, *53*(1–2), 123–179. [https://doi.org/10.1016/S0037-0738\(87\)80006-4](https://doi.org/10.1016/S0037-0738(87)80006-4)
- Turner, B. R. (1981). Possible origin of low angle cross-strata and horizontal lamination in Beaufort group sandstones of the Southern Karoo Basins. *South African Journal of Geology*, *84*(3), 193–197.
- Tvedt, A. B., Rotevatn, A., & Jackson, C. A. (2016). Supra-salt normal fault growth during the rise and fall of a diapir: Perspectives from 3D seismic reflection data, Norwegian North Sea. *Journal of Structural Geology*, *91*, 1–26. <https://doi.org/10.1016/j.jsg.2016.08.001>
- Tvedt, A. B., Rotevatn, A., Jackson, C. A. L., Fossen, H., & Gawthorpe, R. L. (2013). Growth of normal faults in multilayer sequences: A 3D seismic case study from the Egersund Basin, Norwegian North Sea. *Journal of Structural Geology*, *55*, 1–20. <https://doi.org/10.1016/j.jsg.2013.08.002>
- van der Zee, W., & Urai, J. L. (2005). Processes of normal fault evolution in a siliciclastic sequence: A case study from Miri, Sarawak, Malaysia. *Journal of Structural Geology*, *27*(12), 2281–2300. <https://doi.org/10.1016/j.jsg.2005.07.006>
- Van Rensbergen, P., & Morley, C. K. (2000). 3D seismic study of a shale expulsion syncline at the base of the Champion delta, offshore Brunei and its implications for the early structural evolution of large delta systems. *Marine and Petroleum Geology*, *17*(8), 861–872. [https://doi.org/10.1016/S0264-8172\(00\)00026-X](https://doi.org/10.1016/S0264-8172(00)00026-X)
- Van Wagoner, J. C., Posamentier, H. W., Mitchum, R. M., Vail, P. R., Sarg, J. F., Loutit, T. S., & Hardenbol, J. (1988). An overview of the fundamentals of sequence stratigraphy and key definitions. In: *Sea-Level Changes—an Integrated Approach* (Ed by: Wilgus, C.K., Posamentier, H., Ross, C. A. & Kendall, C. G. St. C). *Society of Economic Paleontologists and Mineralogists Special Publication*, *42*, 39–45.
- Venditti, J. G., Church, M., & Bennett, S. J. (2005). On the transition between 2D and 3D dunes. *Sedimentology*, *52*(6), 1343–1359. <https://doi.org/10.1111/j.1365-3091.2005.00748.x>
- Vigran, J. O., Mangerud, G., Mørk, A., Worsley, D., & Hochuli, P. (2014). Palynology and geology of the Triassic succession of Svalbard and the Barents Sea. *Geological Survey of Norway Special Publication*, *14*, 1–270.
- Visser, M. J. (1980). Neap-spring cycles reflected in Holocene subtidal large-scale bedform deposits: A preliminary note. *Geology*, *8*(11), 543–546. [https://doi.org/10.1130/0091-7613\(1980\)8<543:NCRIH S>2.0.CO;2](https://doi.org/10.1130/0091-7613(1980)8<543:NCRIH S>2.0.CO;2)
- Walker, R. G. (1992). Facies, facies models and modern stratigraphic concepts. In R. G. Walker & N. P. James (Eds.), *Facies models: Response to sea-level change* (pp. 1–14). Newfoundland, Canada: Geological Association of Canada.
- Walsh, J. J., Bailey, W. R., Childs, C., Nicol, A., & Bonson, C. G. (2003). Formation of segmented normal faults: A 3-D perspective. *Journal*

- of *Structural Geology*, 25(8), 1251–1262. [https://doi.org/10.1016/S0191-8141\(02\)00161-X](https://doi.org/10.1016/S0191-8141(02)00161-X)
- Weber, K. J. (1987). Hydrocarbon distribution patterns in Nigerian growth fault structures controlled by structural style and stratigraphy. *Journal of Petroleum Science and Engineering*, 1(2), 91–104. [https://doi.org/10.1016/0920-4105\(87\)90001-5](https://doi.org/10.1016/0920-4105(87)90001-5)
- Wignall, P. B., & Best, J. L. (2004). Sedimentology and kinematics of a large, retrogressive growth-fault system in Upper Carboniferous deltaic sediments, western Ireland. *Sedimentology*, 51(6), 1343–1358. <https://doi.org/10.1111/j.1365-3091.2004.00673.x>
- Willis, B. J. (2005). Deposits of tide-influenced river deltas. In: *River Deltas- Concepts, Models, and Examples* SEPM Special Publication No.83 pp. 87–129.
- Winker, C. D., & Edwards, M. B. (1983). Unstable progradational clastic shelf margins. *Special Publications of SEPM*, Vol. 33 pp.139–157.
- Worsley, D. (2008). The post-Caledonian development of Svalbard and the western Barents Sea. *Polar Research*, 27(3), 298–317. <https://doi.org/10.1111/j.1751-8369.2008.00085.x>
- Zecchin, M., Massari, F., Mellere, D., & Prosser, G. (2004). Anatomy and evolution of a Mediterranean-type fault bounded basin: The Lower Pliocene of the northern Crotona Basin (Southern Italy). *Basin Research*, 16(1), 117–143. <https://doi.org/10.1111/j.1365-2117.2004.00225.x>

SUPPORTING INFORMATION



Additional supporting information may be found online in the Supporting Information section at the end of the article.

How to cite this article: Smyrak-Sikora A, Osmundsen PT, Braathen A, et al. Architecture of growth basins in a tidally influenced, prodelta to delta-front setting: The Triassic succession of Kvalpynten, East Svalbard. *Basin Res.* 2019;00:1–30. <https://doi.org/10.1111/bre.12410>

ARTICLE 4

Ogata, K., Mulrooney, M. J., Braathen, A., Maher, H., Osmundsen, P. T., Anell, I., **Smyrak-Sikora, A.** & Balsamo, F. (2018): "Architecture, deformation style and petrophysical properties of growth fault systems: the Late Triassic deltaic succession of southern Edgeøya (East Svalbard) ", *Basin Research*, 30(5), 1042-1073.
<https://doi.org/10.1111/bre.12296>

Architecture, deformation style and petrophysical properties of growth fault systems: the Late Triassic deltaic succession of southern Edgeøya (East Svalbard)

Kei Ogata¹  | Mark J. Mulrooney^{2,3} | Alvar Braathen³  | Harmon Maher⁴ | Per Terje Osmundsen⁵ | Ingrid Anell³ | Aleksandra Anna Smyrak-Sikora^{2,6} | Fabrizio Balsamo⁷

¹Faculty of Science, Geology and Geochemistry Cluster, VU Amsterdam, Amsterdam, the Netherlands

²Department of Arctic Geology, University Centre in Svalbard, Svalbard, Norway

³Department of Geosciences, University of Oslo, Oslo, Norway

⁴Department of Geography and Geology, University of Nebraska at Omaha, Omaha, NE, USA

⁵Geological Survey of Norway, Trondheim, Norway

⁶Department of Earth Science, University of Bergen, Bergen, Norway

⁷NEXT - Natural and Experimental Tectonics Research Group, Department of Chemistry, Life Sciences and Environmental Sustainability, University of Parma, Parma, Italy

Correspondence

Kei Ogata, Faculty of Science, Geology and Geochemistry Cluster, VU Amsterdam, Amsterdam, the Netherlands.
Email: k.ogata@vu.nl

Funding information

Petromaks Trias North Project, Grant/Award Number: 234152/E30; Research Council of Norway; Edison Norway; Lundin Norway; RWE Dea Norge; Statoil and Tullow Oil

Abstract

The Late Triassic outcrops on southern Edgeøya, East Svalbard, allow a multiscale study of syn-sedimentary listric growth faults located in the prodelta region of a regional prograding system. At least three hierarchical orders of growth faults have been recognized, each showing different deformation mechanisms, styles and stratigraphic locations of the associated detachment interval. The faults, characterized by mutually influencing deformation envelopes over space-time, generally show SW- to SE-dipping directions, indicating a counter-regional trend with respect to the inferred W-NW directed progradation of the associated delta system. The down-dip movement is accommodated by polyphase deformation, with the different fault architectural elements recording a time-dependent transition from fluidal-hydroplastic to ductile-brittle deformation, which is also conceptually scale-dependent, from the smaller- (3rd order) to the larger-scale (1st order) end-member faults respectively. A shift from distributed strain to strain localization towards the fault cores is observed at the meso to micro-scale (<1 mm), and in the variation in petrophysical parameters of the litho-structural facies across and along the fault envelope, with bulk porosity, density, pore size and microcrack intensity varying accordingly to deformation and reworking intensity of inherited structural fabrics. The second- and third-order listric fault nucleation points appear to be located above blind fault tip-related monoclines involving cemented organic shales. Close to planar, through-going, first-order faults cut across this boundary, eventually connecting with other favourable lower-hierarchy fault to create seismic-scale fault zones similar to those imaged in the nearby offshore areas. The inferred large-scale driving mechanisms for the first-order faults are related to the combined effect of tectonic reactivation of deeper Palaeozoic structures in a far field stress regime due to the Uralide orogeny, and differential compaction associated with increased sand sedimentary input in a fine-grained, water-saturated, low-accommodation, prodeltaic depositional environment. In synergy to this large-scale picture, small-scale causative factors favouring second- and third-order faulting seem to be related to mechanical-rheological instabilities related to localized shallow diagenesis and liquidization fronts.

This is an open access article under the terms of the Creative Commons Attribution License, which permits use, distribution and reproduction in any medium, provided the original work is properly cited.

© 2018 The Authors. Basin Research © 2018 John Wiley & Sons Ltd, European Association of Geoscientists & Engineers and International Association of Sedimentologists

KEYWORDS

detachment, fault zone architecture, listric growth faulting, strain partitioning, structural diagenesis, syn-sedimentary tectonics

1 | INTRODUCTION

Extensional, listric growth faults are commonly observed in deltaic settings, where sand-rich sedimentary sequences prograde out over prodelta shales causing overpressure and density disequilibria. Such faults have been identified at various scales in the ancient (e.g. Bhattacharya & Davies, 2001; Calot et al., 2009; Edwards, 1976; Nemeč et al., 1988; Rider, 1978; Wignall & Best, 2004) and the modern sedimentary record (e.g. Cohen & McClay, 1996; Damuth, 1994; Imber et al., 2003; Maestro, Barnolas, Somoza, Lowrie, & Lawton, 2002; Yeager et al., 2012). Syn-sedimentary faults can occur over widespread areas from the upper delta slope to the delta top, and inland, up to the distal alluvial plain, usually showing strike directions roughly parallel to the coastline and delta lobe contours (Back, Jing, Thang, & Morley, 2005; Pochat, Castellort, vanden Driessche, Besnard, & Gumiaux, 2004). Such systems are commonly associated with compressional zones basin-ward, commonly located at the delta toe (i.e. base of the delta slope), with the development of mid- to deep-water “fold-and-thrust belts,” defined as toe-thrust zones (see e.g. Mandl & Crans, 1981). This general arrangement is not always observed, and in several cases the growth faults domains are bounded by counter-regional, landward dipping, large-scale listric faults (Pochat et al., 2004; Rouby, Raillard, Guillocheau, Bouroullec, & Nalpas, 2002; Sapin, Ringenbach, Rives, & Pubellier, 2012), a pattern also replicated in analogue models (McClay, Dooley, & Lewis, 1998; McClay & Ellis, 1987). Such situations have been related to local to regional differential compaction and sedimentary loading between the finer, water-saturated outer prodelta and the inner, coarser delta front-top zones (Back & Morley, 2016; Braathen et al., 2017).

The practical importance of these structures to hydrocarbon exploration and production, hydrogeological exploitation and geohazard assessment (e.g. mitigation of coastal instability and land loss prediction) is well known (e.g. Armstrong, Mohrig, Hess, George, & Straub, 2014; Gagliano, 2005). Their large-scale, structural and stratigraphic characteristics have been largely revealed by remote-sensing, acoustic and seismic imaging, mainly because of the impact of changing fault dips, and marked impedance of the related fault rock types on the seismic signal (Back & Morley, 2016; King, Backé, Morley, Hillis, & Tingay, 2010; Panpichityota, Morley, & Ghosh, 2018). Field-based studies, specifically aimed to provide insights on the micro to mesoscale (i.e. from less

Highlights

- The Triassic growth fault systems of southern Edgeøya comprise three orders of faults, from deep-rooted planar faults to shallow listric faults;
- Polyphase deformation from soft-sediment to brittle deformation from first-order to third-order faults
- Variation in the growth fault architectural elements and intrinsic petrophysical properties across and along the fault zones;
- Counter-regional (landward), progressive faulting in prodelta region due to combine far-field stress and differential compaction;

than 1 mm to the size of the outcrop) syn-sedimentary deformation mechanisms of growth faulting at shallow crustal conditions (< than 1 km burial), are underrepresented in the current literature, partially due to the relative scarcity of favourable exposures. A few exceptions are available (Bhattacharya & Davies, 2001; Bouroullec et al., 2004; Braathen et al., 2017; Onderdonk & Midtkandal, 2010; Zecchin, Masari, Mellere, & Prosser, 2003), and usually describe neo-tectonic faulting in poorly consolidated lithologies (Bense & Person, 2006; Heynekamp, Goodwin, Mozley, & Haneberg, 1999; Loveless, Bense, & Turner, 2011; Mozley & Goodwin, 1995; Rawling & Goodwin, 2003, 2006). This outcrop-based study presents the results of a combined structural-stratigraphic and petrophysical analysis the superbly exposed, Late Triassic growth fault system cropping out in the southern part of Edgeøya, Svalbard (Arctic Norway). The main objective of this study was to provide a high-resolution, multiscale characterization of these growth fault architectures and structural elements, in order to understand: (1) the primary deformation mechanisms and their control on petrophysical properties, (2) their associated spatial-temporal variations and structural diagenesis and (3) identify local (i.e. autogenic) and regional (i.e. allogenic) factors that influenced fault nucleation and growth.

2 | GEOLOGIC OUTLINE

Edgeøya is the second largest island of the Svalbard archipelago and is located in its eastern part (Figure 1a,b). The

Svalbard archipelago is the emergent, uplifted, northwestern margin of the Barents Shelf, with a geological record that includes: (1) the Caledonian Orogeny (and older events; Braathen et al., 1999), (2) Devonian crustal-scale extension and later contraction, (3) Carboniferous rifting, (4) a relatively stable, long-term subsiding platform sedimentation from Permian to Cretaceous with Late Triassic compression and regional uplift (Klausen, Müller, Slama, & Helland-Hansen, 2016), (5) intrusive, mafic Late Cretaceous magmatism of the High Arctic Large Igneous Province (HALIP, see Maher, 2001; Senger, Tveranger, Ogata, Braathen, & Planke, 2014) and (vi) development of a Cenozoic transform margin (e.g. Harland, 1997). The emergence of the Svalbard archipelago above sea level is the combined product of: (1) Early Cretaceous magmatism and the associated uplift and unroofing in the northwestern Barents Shelf, (2) development of the WSFTB, (3) uplift and unroofing in the western areas during the Oligocene and eventually (4) rapid, glacial isostatic-rebound during the Quaternary, which caused unroofing and consequent decompaction of the sedimentary succession (Corfu, Andersen, & Gasser, 2014; Minakov, Faleide, Glebovsky, & Mjelde, 2012; Nejbirt, Krajewski, Dubinska, & Pecskay, 2011; Senger et al., 2014). On a larger scale, this part of the Barents Shelf is thought to represent a broad foreland setting bound by two opposite orogenic fronts, the Ordovician-Devonian Caledonides roughly to the W and the Carboniferous-Permian Uralides approximately to the E/SE (along with its Middle-Late Triassic/Jurassic indentations/protrusions represented by Novaya Zemlya), which caused curvilinear trends of the stress trajectories and a complex interaction of the foreland deformation patterns (Lyberis & Manby, 1999; Marello, J. Ebbing, & Gemigon, 2013; Scott, Howard, Guo, Schekoldin, & Pease, 2011).

Edgeøya comprises of a conformable Middle-Late Triassic succession, which contain the uppermost and lowermost parts of the Sassendalen and Kapp Toscana Groups respectively (Figure 1c,d; Dallmann et al., 1999). The lithologies within the lower part of the cliff sections belong to the Ladinian Blanknuten Member of the Botneheia Formation (Sassendalen Grp.), with tens of metres-thick, organic-rich shales, both massive and laminated and characterized by scattered phosphate nodules, abundant macrofossils (mainly brachiopods) and occasionally marine reptile bones (e.g. Hurum, Roberts, Nakrem, Stenløkk, & Mørk, 2014). These laterally extensive shales are an important regional source

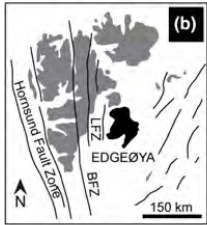
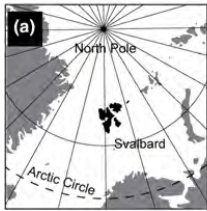
rock (Senger et al., 2014) and represents a period of prolonged anoxic condition across the Barents Shelf during the Middle Triassic (e.g. Krajewski, 2013). The succession continues with the Early Carnian Tschermakfjellet Formation of the Kapp Toscana Group, which, together with the overlying and partly heteropic Middle Carnian De Geerdalen Formation, is inferred to represent the first major clastic (sand-rich) input in this part of the subsiding Barents Shelf (see Figure 1c,d). These formations partly correspond to the offshore Kobbe and Snadd equivalents (e.g. Anell, Faleide, & Braathen, 2016; Mørk et al., 1999; Nøttvedt et al., 1992; Vigran, Mangerud, Mørk, Worsley, & Hochuli, 2014), and are outstandingly exposed in the steep cliffs of southern Edgeøya (Figure 1c,e-g).

In summary, the broader depositional picture that emerges from these sedimentary successions is that of a large-scale delta system, built out over the northwestern coastal margin of an extended alluvial plain sourced from the Uralide orogen, and prograding into an anoxic, shallow and gentle relief shelf characterized by Middle Triassic platform deposits (e.g. Anell, Braathen, & Olausen, 2014; Anell et al., 2016; Fleming et al., 2016; Haile et al., 2018; Klausen & Mørk, 2014; Klausen, Ryseth, Helland-Hansen, Gawthorpe, & Laursen, 2015; Mørk et al., 1999; Rød, Hynne, & Mørk, 2014). The maximum burial depth inferred for this succession has been calculated of several kilometres (Haile et al., 2018).

3 | STUDY AREAS AND METHODS

Growth faults are the product of syn-sedimentary activity and record progressive thin-skinned extension with associated localized sedimentation over variable time spans. They usually exhibit scale-invariant, listric geometries, with relatively steep fault planes close to the surface that progressively flatten with depth and sole-out into weak lithological intervals known as detachment zones or *décollements* (e.g. Bally, Bernoulli, Davis, & Montadert, 1981). Due to their geometry (see Figure 2a), listric faults are able to accommodate more horizontal extension by simple-shear than their planar counterparts, showing, for the same amount of displacement, larger horizontal displacements (i.e. heaves) and comparably smaller vertical displacements (i.e. throws; see e.g. Lohr, Krawczyk, Oncken, & Tanner, 2008).

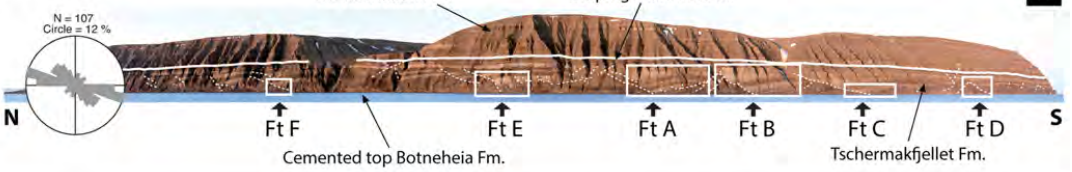
FIGURE 1 Outline of the study area. (a) Geographic location of the Svalbard archipelago. (b) Simplified map of Svalbard with labelling of the major tectonic lineaments and location of Edgeøya (in black). (c) Schematic geological map of Edgeøya (redrawn from Osmundsen et al., 2014) with location of the study areas and representation of the main topographic lineaments (inset rose diagram). (d) Chronostratigraphic diagram showing the timing of syn-sedimentary faulting in the region and the main groups and formations cropping out on Edgeøya. (e-g) Overview of the study sites (e. Kvalpynten, f. Øhmanfjellet and g. Negerpynten) with labelling of the investigated faults, the cumulative listric and planar growth strike trends (inset rose diagrams)



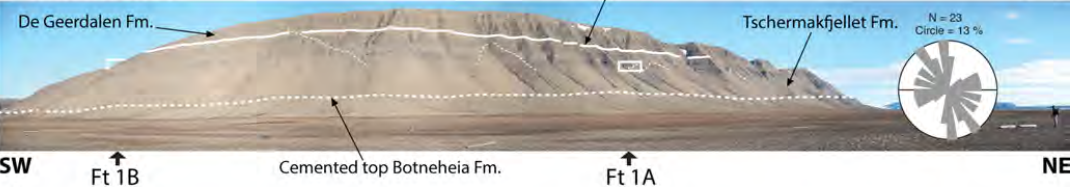
AGE	Grp.	Formation			
LATE	Norian	Eroded	Sandstone-dominated		
				Carnian	De Geerdalen Formation
MIDDLE	Ladinian	Botneheia Formation	Shale-dominated		
				Anisian	Vikinghøgda Formation
EARLY	Olenekian	below s.l.			
				Induan	



Kvalpynten



Øhmanfjellet



Negerpynten



FIGURE 2 (a) conceptual representation of the investigated growth fault systems with indication of collected large-scale structural parameters (i.e. spacing, displacement, throw and heave) and the type of used markers (i.e. cut-off angle contacts, pregrowth and growth-wedges). (b) Interquartile box-plots of cumulative listric and planar growth faults' spacings (median values labelled). (c) Throw-heave-displacement plots for each investigated fault. (d) throw/heave ratio for each investigated fault. (e) Rectified slice of the photogrammetric 3D outcrop model of Kvalpynten with interpretation (f-g; normal and 69° vertically exaggerated line-drawings respectively) of the growth fault blocks and relative sedimentary wedges (in the inset, a simplified representation of the geometrical relationships among the three levels of fault hierarchies)

The study areas are located in the southern part of Edgeøya, where the laterally continuous, up to 500 m-high cliffs of Kvalpynten, Øhmanfjellet and Negerpynten (see locations in Figure 1c) provide detailed insights into the character of the Tschermakfjellet Formation growth fault systems and the over- and underlying De Geerdalen and Botneheia formations (see Figure 1e–g). These three sites represent an NNW-SSE transect stretching about 50 km in length across Tjuvfjorden bay, which provide a large-scale, three-dimensional perception of the stratigraphic interval containing the investigated growth-fault array.

Field data collection has been backed up by a photogrammetric 3D virtual outcrop model collected through ground-based (i.e. boat-mounted for a continuous shooting), georeferenced photo acquisition with combined high-resolution DSLR camera and differential GPS. The model has been interpreted analysed in LIME (<http://virtualoutcrop.com/lime>) to quantify large-scale (e.g. hundreds of metres) fault attributes, adapting the workflow described in Rittersbacher, Howell, and Buckley (2014): 1) horizontal spacing, 2) throw, 3) heave and 4) displacement (see Figure 2a). The principal offset marker used for these measurements, both in the field (where possible) and on the geomodel, is the cut-off line of lithologic contacts. Especially useful is the one between the fine-grained, early growth successions and the sandstone-dominated late-growth parts in the footwall sections (close to the fault tips), and relative counterparts in the hangingwall (see below), due to the clear colour contrast and lateral continuity on the large scale. Fine-tuning of these measurements has been performed by checking also the consistency of the geometrical relationships in the internal stratification of the sedimentary growth wedge and ground-truthing the information in the field. It is important to note that, due to the highly curvilinear attitude of the fault planes jeopardizing the consistency of the 3D measurements, the fault spacing has been taken as the horizontal 2D distance between two consecutive inflection points of the fault plane (i.e. where the listric fault plane sole out in the related detachment) marked by clear “shale cusps” instead of the actual perpendicular distance between two consecutive faults planes (see Figure 2a).

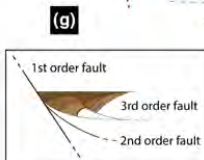
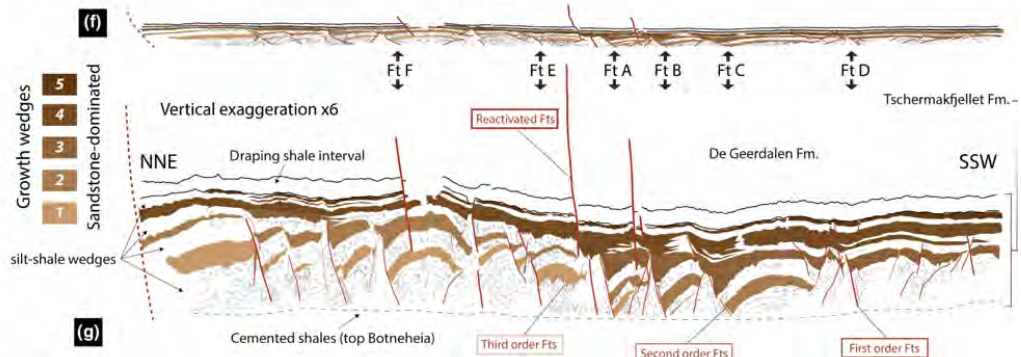
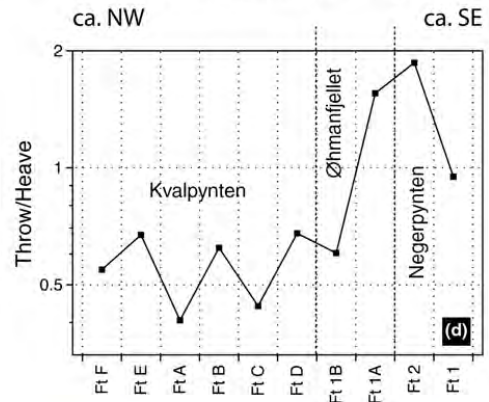
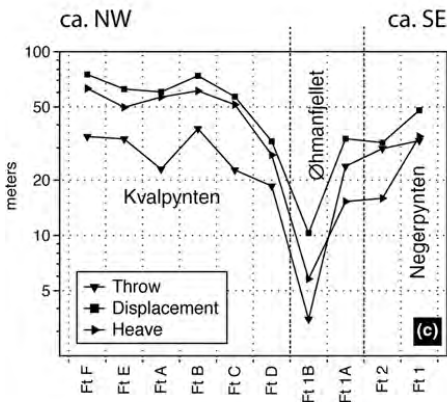
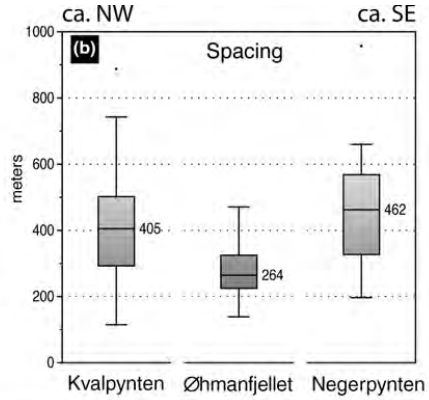
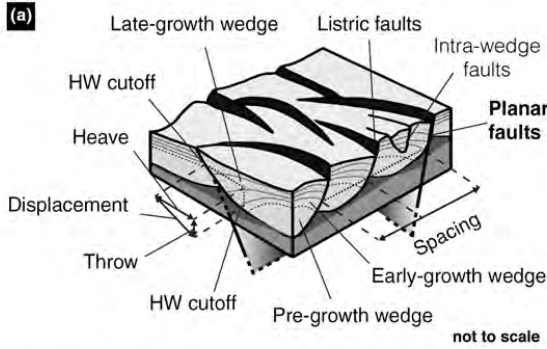
Approximately 35, 1:20 scale structural-stratigraphic logs were obtained in the coastal exposures of Kvalpynten, Øhmanfjellet and Negerpynten (see Figure 1e–g), to collect quantitative data on discrete fault elements and the overall

structural architecture (i.e. apparent rock cohesion, lithology, sedimentary and tectonic structures and kinematic indicators, thickness/size of the fault elements) of eight listric and two planar growth faults at the outcrop scale (Figure 3a–c). For the mesoscale (centimetres to tens of metres) structural data acquisition, we follow the Fault Facies concept introduced by Braathen et al. (2009), in which the fault envelope consists of a varying number of discrete fault facies originating from the host rock and (re) organized spatially according to strain distribution and displacement gradients. Fault facies are thus related to size, geometry, internal structure, petrophysical properties and spatial distribution of fault structures, and can be hierarchically organized in architectural elements, hereafter defined by fault facies associations (FFA) and individual fault facies (IFF). These litho-structural units and their relationships define the basic elements of a conceptual fault zone or envelope (e.g. Caine, Evans, & Forster, 1996; Braathen et al., 2009), populated by a fault core, damage and mixing zones, in turn comprising lenses, smears and membranes of gouge, breccia) and shatter zones (e.g. Braathen, Osmundsen, & Gabrielsen, 2004).

As shown in Figure 3, for growth faults from A to E (Kvalpynten), and 1A (Øhmanfjellet), at least three correlated logs were recorded in the “proximal” (lower-displacement), “intermediate” and “distal” (higher-displacement) positions. For the remaining faults (i.e. fault 1B in Øhmanfjellet, and 1 and 2 in Negerpynten), due to the limited outcrop accessibility, structural stations (i.e. punctual and distributed measurements on a defined, laterally discontinuous area encompassing the favourable fault exposure) have been adopted instead.

Along with the structural-stratigraphic logging, systematic oriented sampling of the different fault facies and elements (from the pristine hanging wall and footwall country rock to the fault core) was conducted. Petrophysical and microstructural analyses have been performed on 42 samples to quantify porosity, pore size and density variations across fault zones, and to identify the microfabric, lithological changes and related deformation mechanisms.

A PoreMaster 33 porosimeter (Quantchrome Instruments) was used to measure porosity and pore size distribution by mercury-intrusion on unoriented samples, ca. 1 cm³ in size. Before measurement, samples were dried at 40°C for 24 hr, and then ~1.5–2 g of material was analysed. The parameters



Growth sequence 1

Growth sequence 2

used for measurements are as follows: sample cell is 1.0 × 3.0 cm, pressure range is 0.5–33000 psi, pore size range is 0.0064 to 950 μm, contact angle of mercury is 140 degrees, and surface tension of mercury is 0.48 N/m (480 dyn/cm). The volume of mercury penetrating into porous samples can be measured as a function of the applied hydraulic pressure. The obtained intrusion and extrusion curves were interpreted into pore size distributions in terms of the Washburn equation (Washburn, 1921), in which the applied hydraulic pressure P is related to the cross-sectional radius R of pore-throats accessible by the pressured mercury, together with two material-related, thermodynamic parameters: surface tension of mercury γ and its contact angle θ with the sample material involved (León Y León, 1998). Density measurements were performed with a Helium Pycnometer Ultrac 1200e Quantachrome.

Optical microscopy observations in direct and polarized transmitted light were performed on oriented thin sections with a digital camera-equipped Zeiss AxioPlan 2 microscope. The same samples were then processed for SEM analyses with a vacuum evaporator JEOL JEE-4X, and backscatter electron images were produced using a Scanning Electron Microscope JEOL 6400, operating under high vacuum conditions (10–4 Pa) and equipped with Energy Dispersive X-Ray Microanalysis System (EDS) Oxford-INCA, and Si(Li) window-less detector.

4 | RESULTS

4.1 | Growth fault basin architectures and infills: baseline observations

A first regional interpretation of aerial photographs and digital elevation models of Edgeøya allowed the identification of two main regional structural trends (i.e. main topographic lineaments) striking NW-SE and NE-SW, which strongly influenced the overall geomorphology (e.g. linear valleys, fjords, hill-bridges and other linear features; see rose diagram in Figure 1c). These orientations are slightly to strongly oblique to the mean WNW-ESE (and subordinate NNW-SSE) strike of the investigated growth faults (see rose diagrams in Figure 1e–g).

Based on the outcrop-scale geometry and lateral-vertical continuity (e.g. hanging wall rollover occurrence, relationship with the lower detachment and upper draping units), a first rough distinction between listric and planar growth faults is recognized (as described in Osmundsen, Braathen, Rød, & Hynne, 2014). Listric faults concentrate in SW Edgeøya around Kvalpynten (Figure 1c) and planar faults dominate around the SE (i.e. Negerpynten; see Figure 1). The listric faults are characterized by 1) a generalized ductile-plastic style of deformation (i.e. “soft”), 2) clearly exposed scoop-shaped, concave-upwards geometries at the

outcrop scale and 3) well-developed rollover anticlines, while planar faults generally lack such features. The incremental displacement achieved on planar faults appear to sometimes rotate the synthetic listric faults arrays located in their hanging wall blocks, suggesting a deep-rooted listric origin for at least some of them. The spatial variation in the fault strikes for the different localities (see rose diagrams in Figure 1e–g), can be attributed to the partly curvilinear attitude of some of the single listric growth fault strands and/or how exposures intersect the faults.

The combined structural parameters obtained for both planar and listric faults in the Tschermakfjellet interval (see Figure 2a) show a similar range of spacing across the investigated areas, with comparable median values for Kvalpynten and Negerpynten, and lower numbers in the Øhmanfjellet fault array (see Figure 2b). The same pattern appears in terms of relative values of throw, heave and displacement, with absolute lower values for Øhmanfjellet area. Notably, a switch in the throw and heave values seems to mark a transition from more listric-like to more planar-like faults from the NW towards the SE (see Figure 2c). This tendency is also testified and strengthened if these values are normalized, as shown by the trend of throw/heave ratios (see Figure 2d).

A detailed 3D outcrop model interpretation of the faults and fault blocks of the Kvalpynten area (Figure 2e–g) allowed the recognition of at least two major growth fault sequences comprising four to five fill cycles (i.e. coarsening upward from shale to sandstone parasequences) with well-developed sandstone-dominated, late-growth wedges in the upper part (see Figure 2e–g). On the basis of the geo-model and *in situ* observations, three orders of faults appear to occur, hereby classified from first to third order. Their ranking based on the following criteria: 1) the associated sole out detachment, 2) the lateral-vertical continuity, 3) the reciprocal position and 4) outcrop-scale extension (Table 1). The first-order faults extend below sea level and therefore the associated detachment is not exposed, appearing truly planar and through-going. The second-order faults zones share a basal detachment interval located atop the well-cemented uppermost Botneheia Formation and show clear listric geometries. The third-order listric faults are usually synthetic to the second-order ones and located in their hanging wall blocks, with their detachment level located near the base of the sandstone-dominated, coarsening upward parasequences (i.e. late-growth wedges) of the Tschermakfjellet. In particular, for the more symmetric grabens, a significantly larger amount of third-order faults antithetic to the first-order one occur with respect to the less symmetric ones (see Figure 2g). All the three types of faults were top-bounded by a sealing, laterally continuous shale interval that cap and drapes the growth faulting interval (see Figure 2f). Few later faults in the De Geerdalen

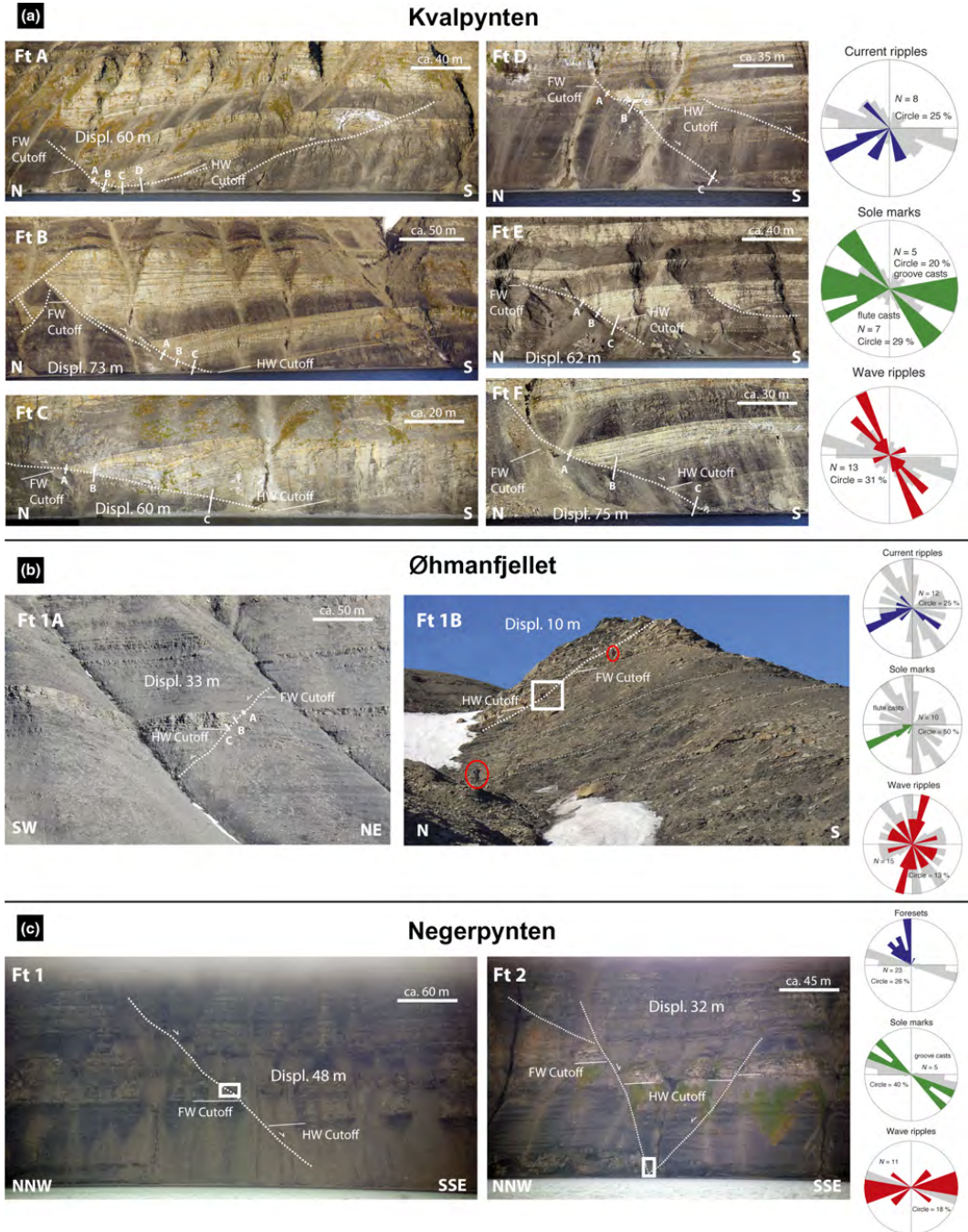


FIGURE 3 Overview of the analysed faults, with locations of the collected fault logs and structural stations, for each study area: (a) Kvalpynten, (b) Øhmanfjellet (persons for scale in Ft b), and (c) Negerpynten. For each study area, rose diagrams summarizing the local palaeocurrent data (current ripples/foresets, groove and flute marks, and wave ripple crests) are shown along with the cumulative listric and planar growth fault strike (see Figure 1e–g) in the background (in grey)

TABLE 1 Diagnostic criteria used for fault classification

Fault	Detachment	Lateral-vertical continuity	Reciprocal position	Fault length/height
1st order	Not exposed (below s.l.)	Planar	-	Through-going
2nd order	Top Botneheia Fm.	Listric	HW of 1st order	10-100s metres
3rd order	Within Tschermakfjellet Fm.	Listric	HW of 2nd order	1-10s of metres

cut downward through the draping shale and appear to exploit the favourably oriented first- and second-order fault segments to reach and sometimes cut across the top Botneheia detachment, with complex interlinking relationships across the growth faulting interval (see Figure 2g).

The sandstone-dominated, growth fault wedges developed in the hangingwall of first- to second-order faults comprise thickening- and coarsening-upward successions, represented from the base upwards, of (1) laminated mudstones-siltstones with thin-bedded fine-grained sandstones interpreted as prodelta deposits, which become progressively punctuated by (2) graded beds with planar and ripple laminations, sometimes characterized by erosive bases, sharp tops, hummocky-type cross stratification and “pinch-and-swell” trends, and, towards the top, (3) heterolithic interbedded sand/siltstones with wavy-, lenticular- and flaser- bedding, passing upward into cross-bedded (planar and through-), very fine- to fine-grained sandstones arranged in metres- to tens of metres thick and tens to hundreds of metres-wide sedimentary wedges. In this stratigraphic framework, the laminated mudstones-siltstones that characterize the lower part of the hangingwall represent the early growth stages passing into upper syn-growth sandstone-rich intervals, as also testified by the lateral stratigraphic wedging marked by rapid thickness changes and, in places, bounded by progressive (laterally fanning and converging) unconformities.

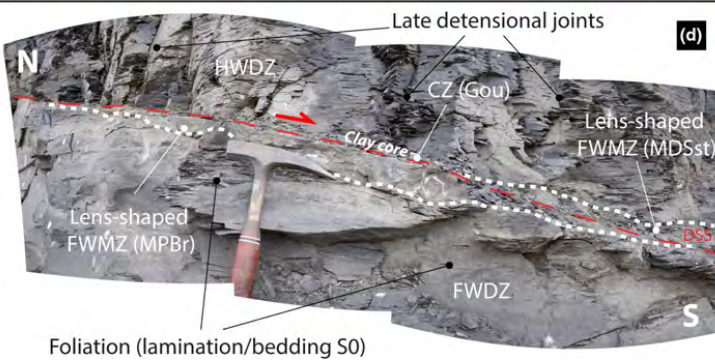
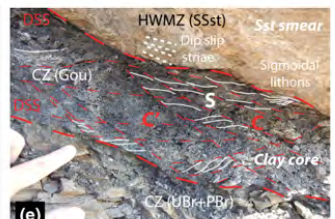
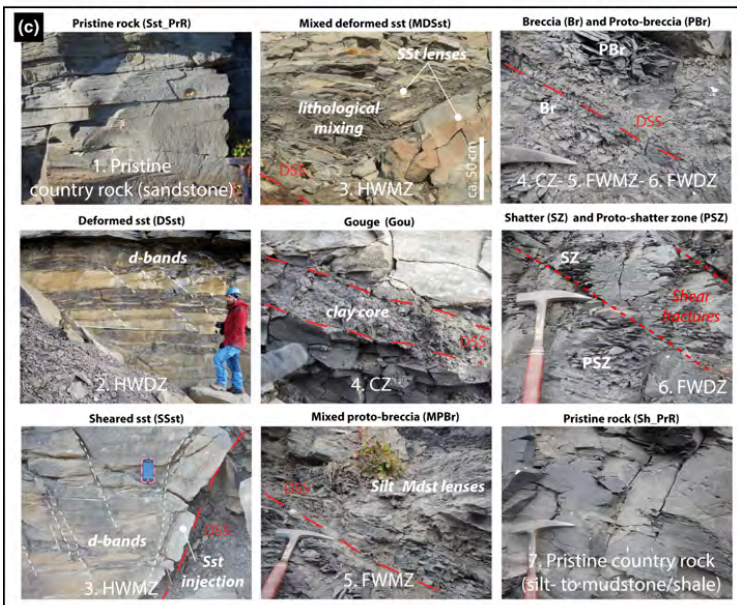
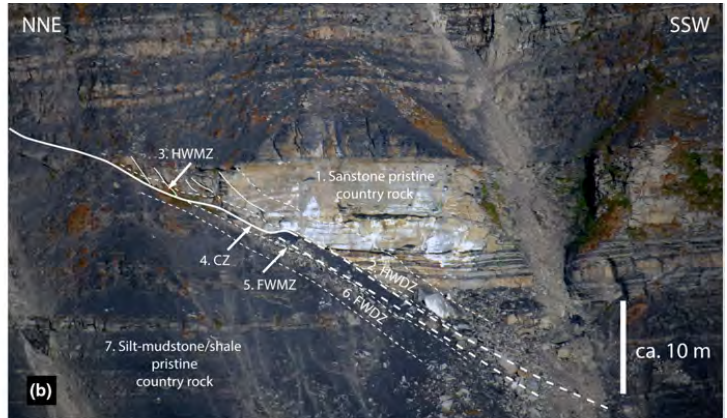
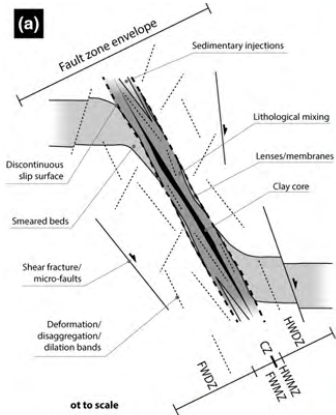
The footwall sections are entirely represented by pre-growth, laminated mudstones-siltstones, with thin overlying early growth sequences, in places showing stratigraphic wedging. In these FW sections, bedding rotations are sometimes observed as well within folded and intensely deformed intervals, not always clearly distinguishable due to the low

lithological contrast. These pre-growth FW sediments are sometimes characterized by bedding-parallel and unconformable surfaces with high erosional outcrop relief (i.e. standing out from the exposure). They show characteristics similar to the well-cemented top Botneheia Formation), and usually mark the lower contact onto which thin (up to few metres-thick), highly erosive FW sandstones wedges that rapidly pinch out laterally, away from the fault (see Figure 2e–g and Figure 3). Due to these characteristics, these surfaces are used as FW cut-off markers (see Figure 2a).

At Kvalpynten, the transition between the Tschermakfjellet and De Geerdalen formations is defined by a conformable, laterally extensive interval of draping dark shales, which mark the upper boundary of the growth fault system, with only few later, reactivated fault zones cutting across and displacing this interval and the overburden. On the other hand, at Negerpynten most of the dominant, planar faults cut up high into the De Geerdalen Formation (see Figure 2e–g). This latter Formation locally consists of fine- to medium-grained sandstone and heterolithic bed-sets, characterized by an upward increase in organic content (i.e. plant fragments) and (marine to continental) bioturbation, and by the occurrence of condensed and red-bed intervals towards the top. Channelized bodies comprising amalgamated sandstone bed-sets with through-cross laminations punctuate the overall succession.

Complementary palaeo-current measurements collected along with stratigraphic-structural logging of fault blocks show significant variations among the reference areas, with primary sedimentary flows recorded by sole marks (e.g. groove and flute casts) suggesting NW to SW directions, secondary flows recorded by traction-plus-fallout structures (e.g. cm- to m-sized forests and asymmetric ripples) with

FIGURE 4 Fault architectural elements (AE) defined by fault facies associations (FFA), and single fault facies (SFF) in the framework of a conceptual fault envelope. (a) Conceptual representation of the investigated fault profile with indication of the main structural features and AEs and SFFs. Inspired, modified and updated from Loveless et al. (2011). (b) Overview of the upper part Fault d with labelling of the main AEs (see text). (c) Examples of the identified FFAs, with indication of their associated SFFs (bold italic white labels in pictures) and associated AEs (see text and Table 1 for details). (d) Detail of the lower part of Fault D (close to the main detachment) showing shale-shale juxtaposition. Note the occurrence of detached lenses of FWMZ and HWMZ. (e–h) Brittle-ductile structures, kinematic indicators, and CZ features from Fault b (e), Fault c (f), Fault f (g) and Fault d (h). Note in E the occurrence of preserved (inherited) ductile (e.g. SCC'-type structures) bounded, reworked and crosscut by brittle structures (e.g. microduplex, striated lithons, discontinuous shear surfaces) in the fault gouge. A feature observed in all the examples is the systematic occurrence of high degree of oxidation, due to localized increase content of Fe-sulphides (pyrite) in the soft sediment sheared part of the inner HWDZ, HWMZ and CZ. The same oxidation pattern is observed in fault gouges, both in sand-shale and shale-shale juxtapositions (see F and G, and H respectively). Person, hammer, GPS or gloved/bare finger for scale



similar orientations but wider spread, and tidal-wave interference structures (e.g. symmetric ripples) providing directions approximately perpendicular to the former (from ca. E-W in Negerpynten, to NNE-SSW and NNW-SSE in Tjuvfjorden and Kvalpynten respectively; see rose diagrams in Figure 3a–b).

4.2 | Growth fault zones, elements and litho-structural facies

Fault zone architecture has been herein described according to the classic definition proposed in the literature for mesoscale brittle faults: a deformed volume of rock that accommodates movement between two blocks, commonly comprising an inner fault core which accommodate most of the displacement (and include the principal slip surface) surrounded by a footwall-hanging wall damage zones (see e.g. Braathen et al., 2009; Caine et al., 1996; Sibson, 1977). Complementary studies extended this model to fault envelopes in poorly lithified sediments, introducing the mixed (or mixing) zone as a third architectural element that separate fault core from damage zone. The mixed zone consists of variably deformed, entrained and attenuated beds forming continuous smears along the fault trace, resulting in a largely homogenized zone with lithological mixing down to the grain scale (see e.g. Balsamo, Bezerra, Vieira, & Storti, 2013; Bense & Person, 2006; Braathen et al., 2013; Heynekamp et al., 1999; Loveless et al., 2011; Mozley & Goodwin, 1995; Rawling & Goodwin, 2003, 2006).

According to this general framework, we subdivide the investigated fault envelopes into fault architectural elements (AE; Figure 4a,b): 1) hanging wall damage zone (HWDZ), 2) hanging wall mixing zone (HWMZ), 3) fault core zone (CZ), 4) footwall mixing zone (FWMZ) and 5) footwall damage zone (FWDZ). These AEs are in turn made up by specific litho-structural, fault facies associations (FFA), distinguished on the basis of the dominant lithologies and single fault facies (SFF), as shown in Figure 4c–h and listed in Table 2. Their relative abundance and mutual relationships differ between the third- and first-order faults, which can be considered as purely listric (soft) and planar (hard) end-members respectively.

In the listric faults' hanging wall, the pristine, relatively undeformed, sandstone country rock (Sst_PrR; Figure 4c), is progressively plastically deformed, from lower strain conditions in the HWDZ (DSst; Figure 4c), to higher strain conditions involving localized mesoscale lithological mixing in the HWMZ (MDsst; Figure 4c), and eventually becoming more intensively deformed close to the contact with the CZ (SSst; Figure 4c). Such elements are characterized by the combined occurrence of disaggregation (dilation/compaction), deformation and phyllosilicate bands (e.g. Fossen, 2010), hydroplastic intrafolial folds and

boudinage-related products, testifying to an increasing intensity of deformation towards the fault core (see below). In the planar fault zones, the HWMZ is usually missing, sometimes appearing as remnants within the HWDZ and/or incorporated as lenses into the CZ.

Disregarding later overprinting by brittle deformation structures (e.g. tensional and shear fractures, cliff-side joints), which usually rework inherited discontinuities (e.g. deformation disaggregation and phyllosilicate bands), the CZ of listric faults comprise one or more discontinuous principal slip planes with crude pseudostriations. These slip surfaces bound membranes of plastically mixed sand and/or clay, and an assemblage of elongated elements (e.g. detached smears, membranes, lenses, etc.) with their long axes trending roughly parallel to the fault trace. These latter elements are enclosed in, or associated with, gouge levels (Gou; Figure 4c). In contrast, in planar faults, one or more striated principal slip surfaces are commonly observed to bound relatively continuous gouge and breccia membranes.

The footwall sections of listric faults start with a lithologically mixed protobreccia (MPBr; Figure 4c) at a transition defining or within the FWMZ, with a relatively constant lenticular trend and thus locally missing due to lateral pinch-outs. In the inner FWDZ, the progressive deformation in a dominantly semibrittle regime leads to significant loss in cohesion, resulting in a protobreccia (PrB; Figure 4c) that eventually grades into noncohesive breccia zones (Br; Figure 4c) in close proximity and within the CZ. The outer FWDZ is made up by slightly to pervasively fractured mud rocks, termed, respectively, as proto-shattered zones (PSZ) to shattered zones (SZ). These zones, characterized by inwards decreased spacing of structural discontinuities and fractures (Figure 4c), progressively involve the undeformed background lithology (i.e. pristine country rock) of laminated to massive silty shales (Sh_PrR; Figure 4c). As for the hangingwall (HW), in planar faults the FWDZ is wider (up to tens of metres) and characterized by pervasive fracturing of the preexisting fabric, whereas the FWMZ (and sometimes the HWMZ) is usually preserved as lenses and membranes of plastically deformed footwall (FW) lithologies, juxtaposed to and within the CZ (Figure 4d–h). These litho-structural elements are cut and bounded by discontinuous slip surfaces, tensile and shear fractures and disaggregation-deformation and phyllosilicate bands (e.g. Fossen, Schulz, Shipton, & Mair, 2007; Torabi, Fossen, & Braathen, 2013), as well as hydroplastic structures (e.g. Maher, Ogata, & Braathen, 2017).

Sedimentary injection-type structures occur mainly within the inner HWMZ (Figure 5a,b) and are commonly preserved along antithetic and synthetic, subsidiary normal faults internal to the growth fault block. Smearing of sand-rich sediments along the fault traces occurs in many cases

TABLE 2 Description and interpretation of the single fault facies (SFF) as illustrated in Figure 4c

Single fault facies (SFF)	Description	Lithologies	Structures	Interpretation
Undeformed sandstone (Sst_PrR)	Pristine, relatively undeformed, sandstone	Fine to medium sandstones with interbedded siltstones-mudstones	Grading, sedimentary structures preserved	Country rock "protolith"
Deformed sandstone (DSst)	Massive to crudely banded sandstone with arrays of structural discontinuities	Fine to medium sandstones with interbedded siltstones-mudstones	Massive, unsorted texture with deformation and disaggregation bands; isolated framboidal pyrite nodules; hydroplastic intrafolial folds; boudinage-related products	Plastically deformed country rock at low strain conditions
Sheared sandstone (SSst)	Massive sandstone	Fine to medium sandstones with interbedded siltstones-mudstones	Massive, unsorted texture with pervasive shear-related structures; continuous pyrite cementation	Plastically deformed country rock at high strain conditions
Mixed deformed sandstone (MDSst)	Massive to brecciated sandstone -mudstone assemblage	Fine to medium sandstones with interbedded siltstones-mudstones and mudstones	Massive, unsorted and finer grained texture with pervasive shear-related structures; lithological mixing; continuous pyrite cementation; hydroplastic intrafolial folds; boudinage-related products	Plastically deformed and mixed sandstone-mudstone elements
Gouge (Gou)	Fine grained, unconsolidated material with scattered angular country rock microclasts	Fine to very fine, uncemented, swelling siltstones-mudstones	Usually massive with sometimes scaly fabric, SCC'-structures, microduplexes, striated sigmoidal lithons	Brittle crushing and comminution of plastically deformed and mixed mudstone elements
Mixed breccia (MBr)	Fine grained, consolidated material with angular country rock fragments	Fine to very fine cemented siltstones-mudstones mixed with sandstone levels	Relatively constant lenticular trend; caly fabric, SCC'-structures, microduplexes, striated sigmoidal lithons	Plastic mixing of brittle mudstones and ductile silt-sandstones
Breccia (Br)	Noncohesive assemblage of angular silt-mudstone elements	Fine to very fine cemented siltstones-mudstones	Breccia texture, sometimes with localized scaly fabric, SCC'-structures, microduplexes, striated sigmoidal lithons	Pervasive fracturing of plastically deformed, indurated mudstone elements
Protobreccia (PBr)	Poorly cohesive assemblage of fracture-bounded silt-mudstone elements	Fine to very fine cemented siltstones-mudstones	Very closely spaced nonsystematic pervasive fracturing (tensional and shearing)	Progressive deformation in a dominantly ductile-brittle regime
Shatter zone (SZ)	Cohesive and pervasively fractured silt-mudstone	Fine to very fine cemented siltstones-mudstones	Closely spaced nonsystematic pervasive fracturing (tensional and shearing)	Progressive deformation in a dominantly semibrittle regime
Protoshatter zone (PSZ)	Cohesive and relatively fractured silt-mudstone	Fine to very fine cemented siltstones-mudstones	Spaced nonsystematic pervasive fracturing (tensional and shearing)	Progressive deformation in a dominantly brittle regime
Undeformed shale (Sh_PrR)	Pristine, relatively undeformed, silt-mudstone (shale)	Fine to very fine cemented siltstones-mudstones	Sedimentary structures and fossils preserved	Country rock "protolith"

(Figure 5c), together with hydroplastic drag folding of the wall rock beds, sometimes with rotation and complete detachment of the fold hinges (Figure 5d,e). Other

associated structures recording plastic-ductile stages of deformation, are symmetric and asymmetric pinch-and-swell structures and boudinage, mostly preserved within

FIGURE 5 Soft-sediment deformation, liquification and hydroplastic features. (a) Example of sandy sedimentary injections along fault zone (Fault b). In this case the up- and down-going clastic wedges merge in the middle of the picture (see b). Circled person for scale. (b) Detail of B showing the sedimentary injections interacting. Note the increasing abundance of “clay chips” ripped up from the shale HW interbeds in the down-going injection, and the increasing oxidation towards the CZ in the up-going one. The locations of two sampling points are also shown (see DR 2). Camera lens cap for scale (ca. 7 cm in diameter). (c) Soft-sediment (hydroplastic) striations-lineations at HWMZ-CZ boundary (Fault 1a) with relative stereoplot (dotted circle is the main fault trace, solid circles are the shear surfaces, dots represent azimuth and plunge of striations-lineations). Field notebook for scale (ca. 20 cm long). (d) Hydroplastic folding in the inner part of FWMZ (Fault d). Gloved finger for scale. (e) Soft-sediment, detached and rotated sigma-shaped, sandstone lens in the third-order detachment zones. Note the high degree of incipient lithologic mixing. Circled camera lens cap for scale (ca. 7 cm in diameter). (f) Array of normal, soft-sediment microfaults (deformation-disaggregation bands) in HWDZ (Fault d). Camera lens cap for scale (ca. 7 cm in diameter). (g) Thin section from F showing one of these deformation-disaggregation bands (mm-displacement). (h) Detail of g under optical microscope. Note the dragging of laminae and the repacking/rearrangement and preferential alignment of grains without breakage. (i) Hydroplastic, reverse microfault zone in the third-order detachment zones. (j) Thin section from I showing a deformation-disaggregation bands (mm-displacement) comprising the reverse microfault zone. (k) Detail of j under optical microscope showing the preferential alignment of grains and platy minerals along a narrow shear zone. No syn-deformation cracking nor recrystallization are observed

the sandstone-dominated HWMZ. At the microscale (see below for a detailed discussion), the most representative structures are conjugate disaggregation-deformation bands characterized by mixed shear dilation-compaction in the sandstone-dominated HW (Figure 5f–h), and disaggregation-phyllonite bands and hydroplastic, intrafolial microfolds within the finer grained FWMZ (Figure 5i–k). Later, pervasive shear and tensile fracturing appears to be formed by reworking/reactivation of these primary (early postdepositional) structural features, which are preserved, for instance within structurally bounded lithons in CZs (see Figure 4e).

Notably, cone-in-cone (CIC) and beef (BF) carbonate veins arranged in lens-shaped aggregates ornament growth fault footwalls and detachment zones, and especially the low-angle shear zones at the top Botneheia (Figure 6a), as described in Maher et al. (2017). These features, arranged parallel to bedding and fault surfaces, are cm-thick, asymmetric, antitaxial tensile vein assemblages that enucleate from planar structural discontinuities (e.g. microcracks, disaggregation-phyllonite bands, fossil shell debris), permeating the silty-shaly country rock (Figure 6b–d). In the investigated sites, the CIC/BF assemblages are progressively deformed according to their position within the fault envelope, eventually recognizable in the CZ as isoclinally folded and fragmented lenses (Figure 6e–g). CIC lenses are also observed to be passively folded within ductile shear zones in the shaly FW, at fault tips and within the associated detachment zones, and within low-angle shear zones, as depicted in Figure 6a and 6h (see section 4.4 for further discussion).

Simple shear-related structures (e.g. SC-type structures), small-scale (cm- to dm-sized) duplexes and conjugate Riedel shears are widespread in the CZs. They indicate a shear sense compatible with the normal movement, consistent with striations characterizing the anastomosing and discontinuous slip surfaces (see Figure 4e–h). In this framework, the SC-type structures are ascribed to a plastic style of

deformation transitioning towards a more brittle style along with duplexing and Riedel shear development. These latter structures appear developed at the expense of structural discontinuities formed in the earlier phases of ductile/plastic deformation, such as SC-type structures and conjugate arrays of deformation disaggregation bands, which a mechanical anisotropy prone to brittle reactivation.

Of particular note is the systematic occurrence of oxidation banding in the inner HWMZ and HWDZ (i.e. SSst) and oxidized gouge in CZ (see Figure 4e–h). These oxidation patterns derive from alteration of Fe-sulphide (i.e., pyrite), locally concentrated in the form of dispersed, discrete framboidal nodules and/or intergranular cement intervals. They trend parallel to the discontinuous shear surfaces characterizing subsidiary and principal fault zones.

The overall increasing deformation pattern from the outer to the inner FW is highlighted by an overall decrease in cohesion of the silty-shale lithologies, clearly recognizable from the erosional profile and semiquantitatively represented in form of fault logs (e.g. shown in Figure 7a; complete database in DR1). The lateral-vertical geometric relationships and spatial arrangement of the AEs, subdivided for each FFA, are summarized in Figure 7b. At mesoscale (i.e. cm- to tens of m-sized), with the exception of the mixing zones, fault architectural element thickness increases with increasing displacement, consistent with their widening with time. The HW architectural elements usually follow this general trend, apart from exceptions within the HWMZ and FWMZ, such as downward wedging sand dykes, and lens-shaped, pinch-and-swell arrangements of the plastically formed material (i.e. faults B and 1A respectively; see Figure 7b).

The two pure planar faults 1 and 2, characterized by sand-shale and shale-shale juxtaposition relationships, respectively, are taken as representative of the end-member brittle faults (1st order) for comparison (Figure 8). In both cases, the overall fault envelope is that of a classical normal fault, with well-developed core and damage zones

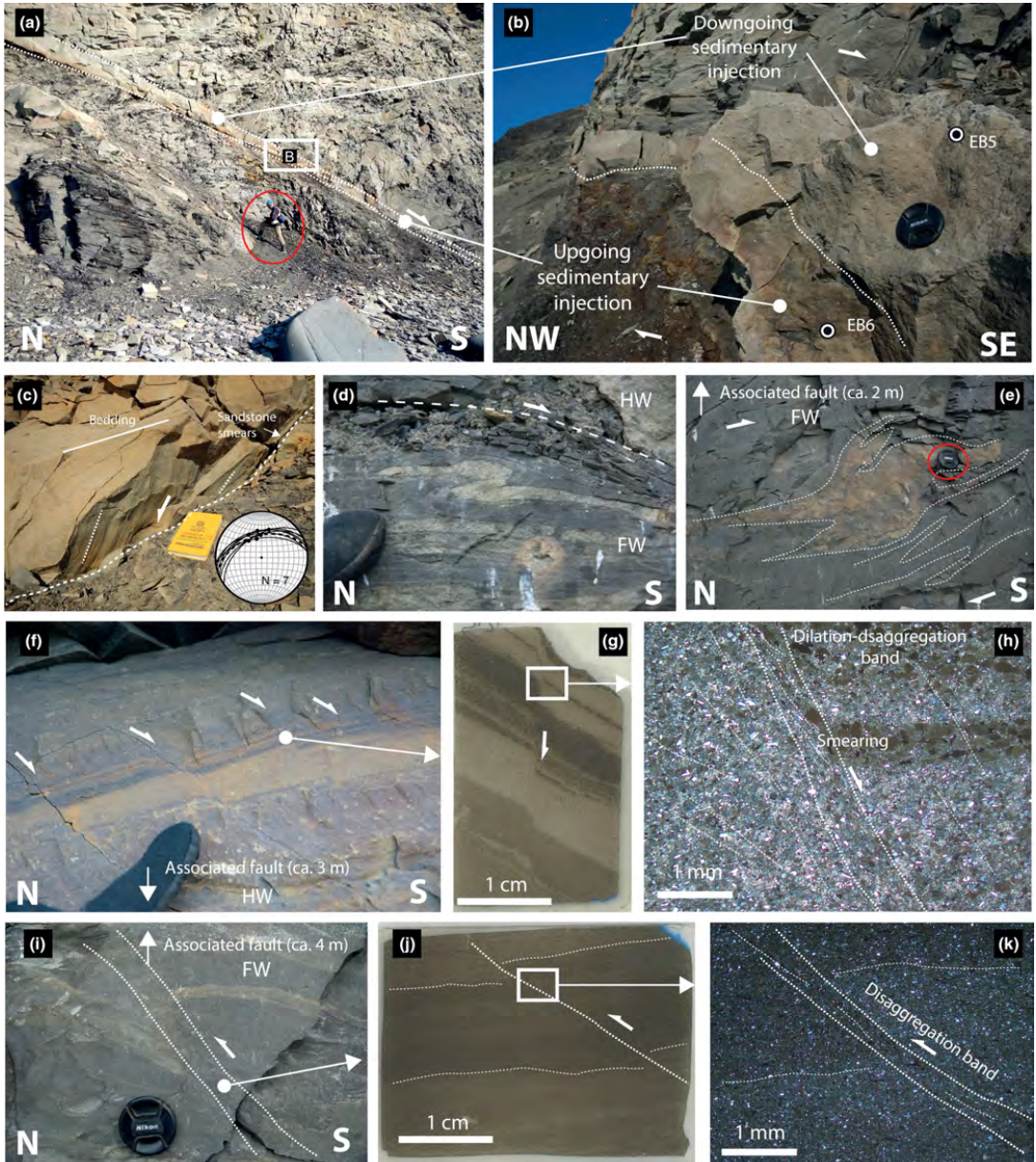


(Figure 8a,d), and without evidence of mixed zones. In these cases, the dominance of brittle deformation structures is evidenced by the occurrence of continuous slip surfaces with striations, bounding isolating sigmoidal lithons (Figure 8c), shale gouge membranes and CZ (Figure 8e). These are in turn characterized by microduplex and a general anastomosing patterns of shear surfaces, resembling in

places a spaced scaly fabric (Figure 8e,f), which likely rework previous structures inherited from previous deformation phases (e.g. SC-type structures). Notably, detached FWMZ and HWMZ lenses, CIC veins and remnants of sedimentary injections-type structures are in places preserved in the HW and FW (see Figure 8b), and as lenses within the CZ.

FIGURE 6 Location and appearance of CIC/BF aggregates. (a) Overview of a shear zone belonging to the second-order detachment, showing HW and FW drag folds and internal occurrences of lenses and detached CIC/BF aggregates (white arrows). Person for scale. (b) Appearance of one of these CIC/BF aggregates (location in a). Camera lens cap for scale (ca. 7 cm in diameter). (c) Thin section from b showing a CIC vein. (d) Detail of c under optical microscope showing the V-shaped, fibrous growth of calcite nests from a common point, and surrounded by entrapped fine-grained sediments (for a detailed description of these mineral growths see Maher et al., 2017). (e) Lower part of Fault a, a few metres above the associated second-order detachment, showing staked and folded sandstone lenses, represented by detached and disarticulated sedimentary injections, in the FWMZ, and in situ metre-sized CIC/BF aggregate lenses in the FWDZ, subparallel to the fault trace. (f) Lower part of Fault f, few metres above the associated second-order detachment, showing a detached lens of FWDZ with CIC/BF veins. Hammer for scale. (g) Detail of F showing drag folding of both laminae and CIC veins. Finger tip for scale. (h) Detail of a shear zone in a second-order detachment showing detached CIC/BF aggregates sheared into rootless, isoclinal folds and sigma-shaped lenses

4.3 | Microstructures and petrophysical attributes

The different architectural elements show changes in microfabric evolution, intensity and linear frequency of (micro) structures, with distinct litho-structural control on bulk pore size, in both vertical (i.e. across fault) and lateral (i.e. along fault) direction. The loose packing of the CZ and FWDZ litho-structural facies, and the high alteration prevented reliable sampling for microstructural observations on these fault elements.

At the millimetre-scale, the original primary (sedimentary) texture of the litho-structural facies are overprinted by systematic microfabric, made up by conjugate systems of disaggregation-deformation bands arranged at high- and low-angles with the fault trace, and resembling Riedel-type, P-R-R' shear systems (Figure 9a–d).

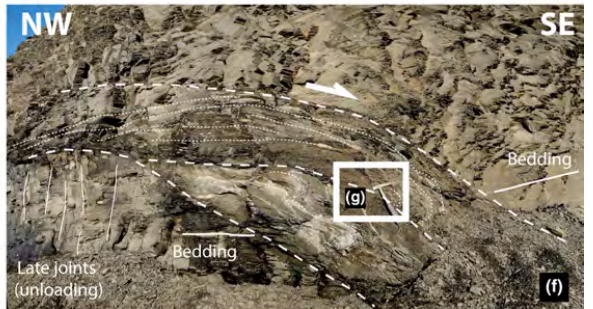
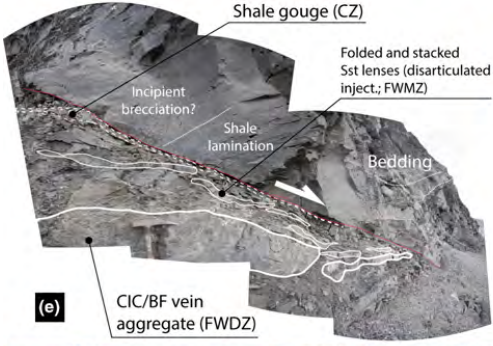
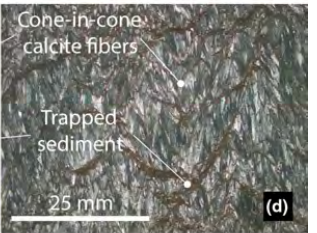
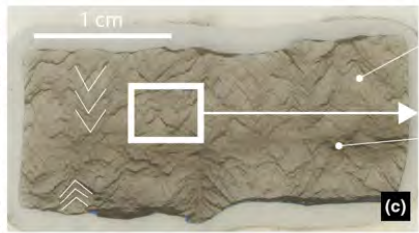
The samples coming from HWMZ and FWMZ show a high degree of ductile deformation with asymmetric hydroplastic microfolding, with the same shear sense and direction as the mesoscale folds observed in the HWDZ and HWDZ, along with pervasive lithologic mixing at the grain size scale and pervasive development of low-angled disaggregation-deformation bands.

Another systematic feature observed in these samples is the bimodal pore size distributions (see below), with positively skewed 1st and negatively skewed second mode values, highlighting the bulk contributions of two main classes of pores/openings separated by a threshold at approximately 5 μm (Figure 9e; complete database in DR 2).

The cementation trends observed in backscatter electron SEM-EDS images confirm the mesoscale observations on a systematic Fe-sulphide (i.e. pyrite) cement, which become progressively more important towards subsidiary synthetic HW faults (sometimes marking the transition from the HWDZ to the HWMZ), and in general towards the CZ. Pyrite mineralization varies from sparse nodules in the HWDZ and HWMZ, to a completely pyrite-cemented, fault trace-parallel halo in a mm- to dm-wide area immediately adjacent to the discontinuous slip surfaces (Figure 9f). Apart from localized grain cracking and flacking (i.e.

mechanical abrasion of grain boundaries) within stress bridges inside the microlithons, no pervasive cataclasis is observed (Figure 9g–h). Instead, local particle rotations, lithologic/grain size mixing, plastic deformation of clay minerals and cement/matrix-supported zones, suggest creation of interparticle space and plastic deformation of the ductile features during the deformation (Figure 9i–k). The sedimentary injections-type structures that sometimes comprise the HWMZ are characterized by a massive, structureless appearance, consistent with complete obliteration of the original texture, and usually bear subangular and subrounded microclasts of the finer-grained HW and FW wall-rock (see Figure 5b). These early fabric features are locally, incrementally reworked/reactivated as microcracks, and subordinately as microshears towards the CZ, suggesting a progressively more brittle regime with time. This brittle overprint is particularly evident in the Negerpynten planar faults (Figure 9l).

The observed microfabric variations across the fault architectures coincide with changes in porosity, pore size and density, consistent with a litho-structural control on diagenesis (Figure 10). The porosity pattern shows a decreasing trend from the HWDZ to the FWDZ, in line with the obvious lithological transition from the sandstone-dominated HW to the shale-dominated FW, with punctuated increase in the inner HWMZ due to localized dilation of granular material (Figure 10a). The marked density increase in the innermost fault envelope reflects the localized Fe-sulphide mineralization (Figure 10b). Due to the systematic bimodality of the results (see above), the median pore size show highly variable values across the fault zone, with large data scatter (Figure 10c). Interestingly, this dispersion narrows when the two single, minor and major modes are considered separately (Figure 10d,e), defining two main trends. The first mode values mimic the cumulative trend, suggesting a diffused primary (matrix) control on pore size distribution, with Gaussian-type end-members and pore size <5–10 μm , and one order of magnitude difference from pristine HW sandstone FW silt-mudstones (see Figure 10d). The second mode values on the other hand show an increase towards the fault core, regardless of the lithologies, with spiky/heterogeneous end-



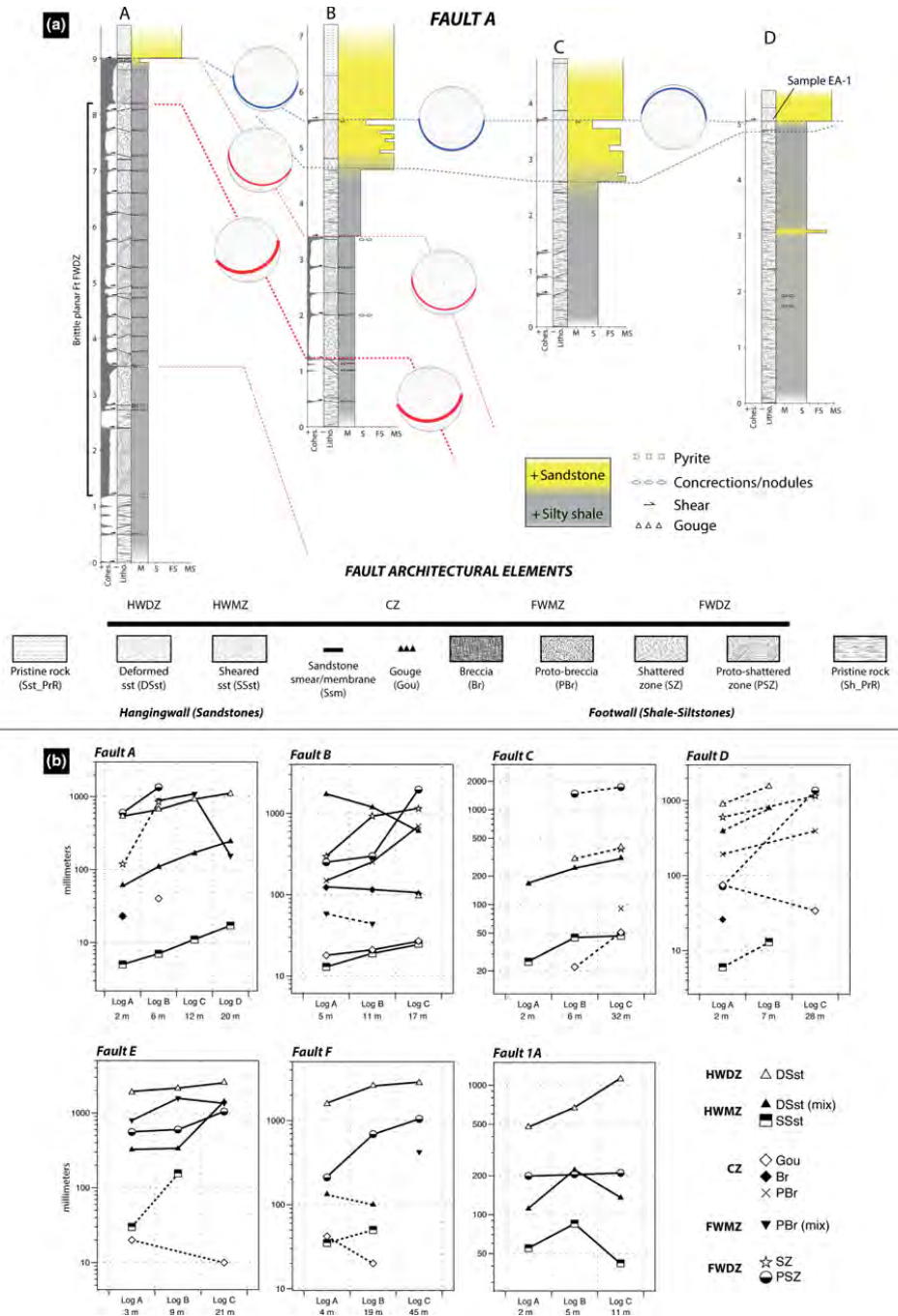


FIGURE 7 Litho-structural fault logs: (a) Example of a correlated fault logs constructed for Fault a (the complete correlation panel for all investigated faults is provided in DR 1). (b) Logarithmic FFs thickness versus relative displacement (fault logs positions) diagrams for the investigated faults. Note the general increasing trends along with relative increasing displacement, apart from FWMZ and HWDZ, and some CZ elements

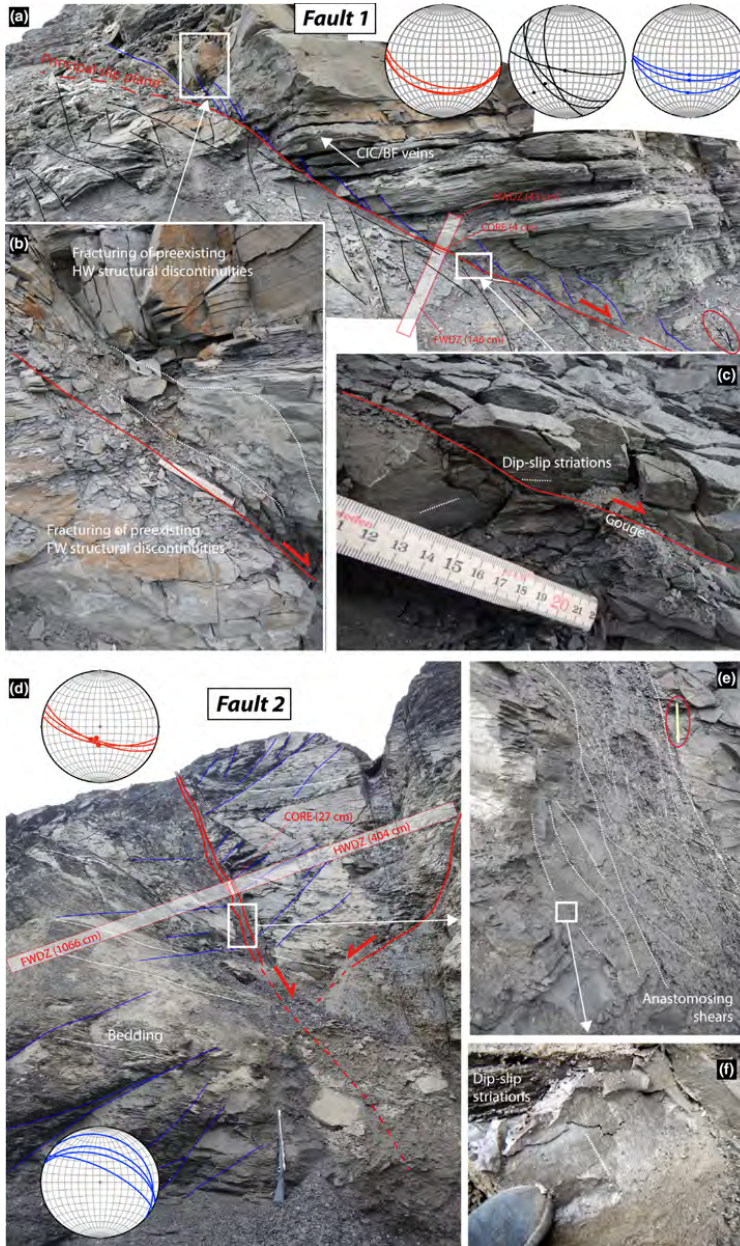


FIGURE 8 Planar (first order) faults investigated at Negerpynten. (a) Overview of Fault 1 with line-drawing and stereoplots of principal slip planes (red) and hangingwall (blue) and footwall (black) shears (dots are striations directions). Rifle for scale (ca. 150 cm). (b) Sheared, liquidized sandstone lens aligned to the hanging wall shears, which likely represent a remnant of HWMZ preserved in the hanging wall from the previous hydroplastic fault phases. Folded metre stick for scale (ca. 22 cm). (c) Detail of the narrow (1 cm) fault gouge interval of the CZ bounded by striated surfaces. Rifle for scale (ca. 150 cm). (d) Overview of Fault 2 with line-drawing and stereoplots of principal slip planes (red) and shears (blue) and labelling of the bedding (dots are striation directions). Rifle for scale (ca. 150 cm). (e) Detail of d showing the CZ and the inner parts of HWDZ and FWDZ. Note the sigmoidal appearance of the innermost FWDZ created by anastomosing shear surfaces and defining an attached footwall lens. Pencil for scale (ca. 10 cm). (f) Detail of the striations on the bounding surfaces of the attached footwall lens depicted in E. Gloved finger tip for scale

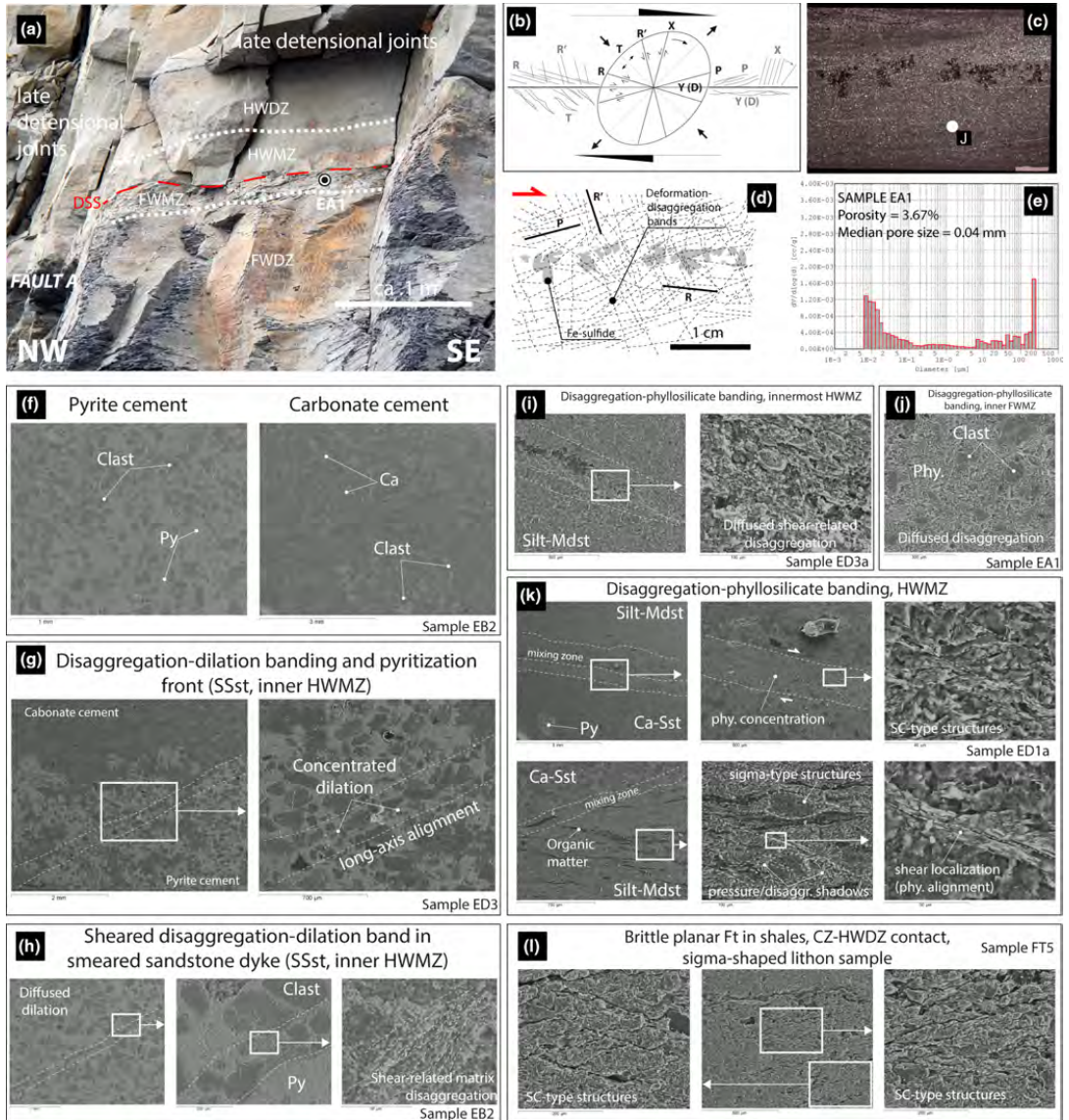


FIGURE 9 Examples of the results obtained from the microstructural and petrophysical analyses (a–e), and BSE SEMEDS images (f–l). (a) Overview of the gently dipping part of Fault A with labelling of the main AEs and location of the sample EA1 (the complete database is provided in DR 2). (b) conceptual representation of simple shear-related, Riedel-type structures. (c–e) Thin section and related microstructural interpretation, and pore size diagram (see cumulative plots in DR 2). (f) Fe-sulphide (pyrite) versus carbonate (calcite/dolomite) cement in the HWDZ and HWMZ. (g) Deformation-disaggregation (dilation) bands and iron-oxide mineralization front in SSst of the HWMZ. (h) Grain alignment and SC-type microstructures in deformation-disaggregation band in sheared sandstone intrusion involved in the HWMZ. (i) Deformation-disaggregation band cored with sheared phyllisilicates in the innermost HWMZ. (j) Deformation-disaggregation phyllisilicates band in the inner FWMZ. (k) Close-up examples of deformation-disaggregation phyllisilicates in the HWMZ. (l) SC-type, anastomosing structures and microduplex in the sheared shales of the CZ-HWDZ contact zone of brittle planar faults

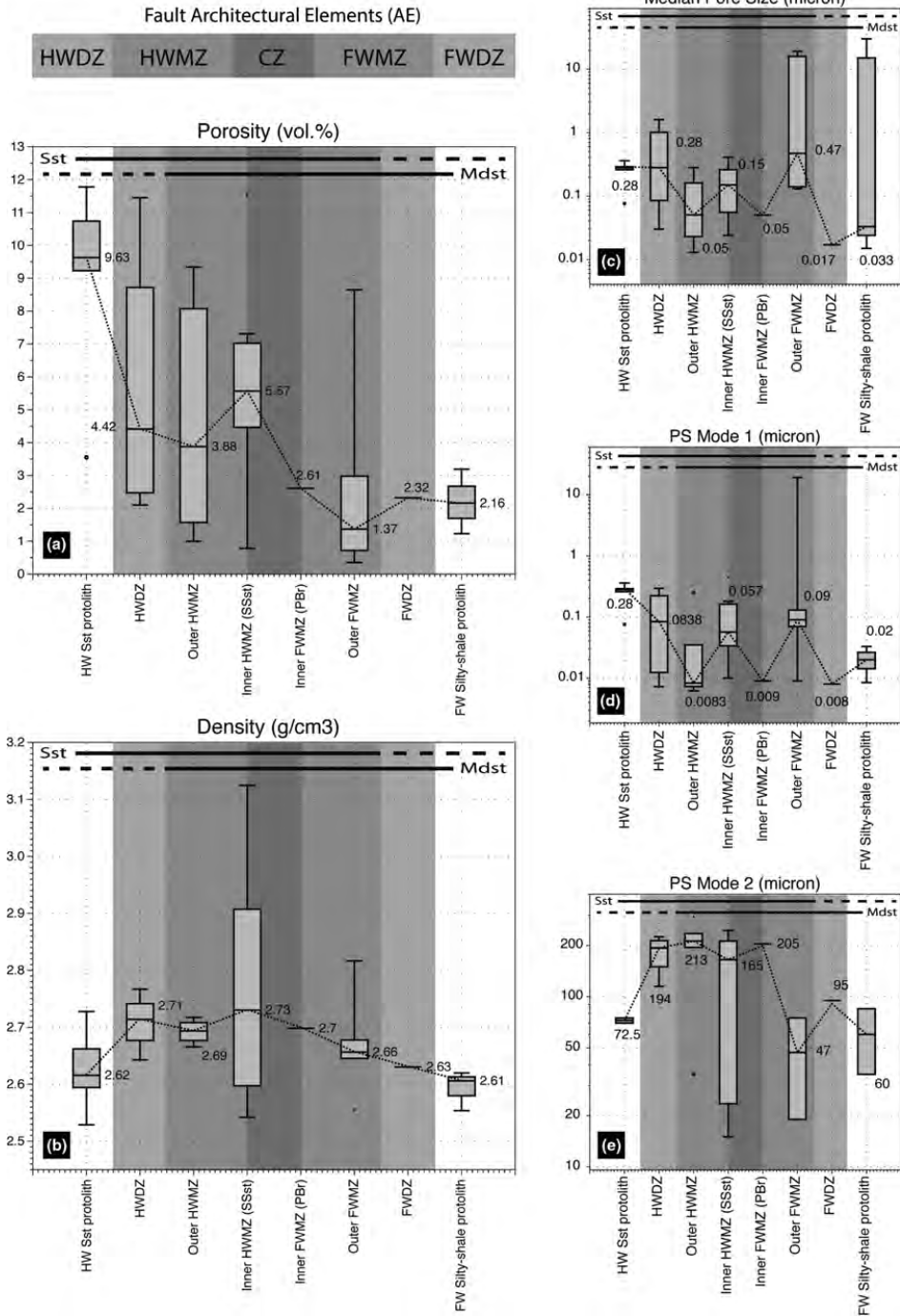


FIGURE 10 Summary of petrophysical parameters across the fault envelope. (a) Porosity. (b) Density. (c) Median pore-size. (d) First modal pore-size. (e) Second modal pore-size. Relative sandstone-mudstone content indicated for end-member comparison

FIGURE 11 Examples of plastic, shear-flow structures and soft sediment deformation intervals in the third-order detachments (a–g) and local, mesoscale extensional and compressional features at top Botneheia Fm., where second-order faults sole out (H–N). (a) Slump-type folds. Hammer for scale. (b) Detached sand pillows. Gloved fingertip for scale. (c) Sand load casts and pillows in liquidized interval. (d) Detail of the sandy load casts and attached pillows. Camera lens cap for scale (ca. 7 cm in diameter). (e) Soling out interval in the lower part of Fault b. Note the fault-parallel sand injection in the left-hand side that became progressively shalier downward (towards the right). (f) Detail of E showing the “mud-sand breccia” appearance of the lower tip of the of the up-going sand injection shown in Fig. Camera lens cap for scale (ca. 7 cm in diameter). (g) Detail of the soling out interval showing a completely mixed, liquidized mud-sand interval. Camera lens cap for scale (ca. 7 cm in diameter). (h) Detail of the soft sediment sandy elements embedded in silty-muddy matrix. (i) Detail of asymmetrical hydroplastic fold from the same interval. Circled backpack for scale (ca. 70 cm). (j) Fault tip mono line developed in the cemented Botneheia Fm., which enucleates a listric growth fault in the overlying Tschermakfjellet Fm. (k) Soling out lower part of Fault d. Note the hanging wall syncline-anticline, enhanced by bed dragging. (l) Thrust zone in the cemented Botneheia Fm., showing a drag fold with a top-to-the-right shear sense. Person for scale. (m) Thrust stack developed in the cemented Botneheia Fm. between Fault b and Fault c. Circled Zodiac for scale (ca. 2 m). (n) Duplex structure in the thrust zone shown in d developed at expenses of a fine sandstone bed. Circled pencil for scale (ca. 10 cm). (o) Folded interval of the second-order detachments involving silty-shale lithologies and CIC/BF layered aggregates. Person for scale (ca. 7 cm in diameter). (p) Folded CIC/BF layered aggregate with layered veins of blocky calcite cutting the hinge zone. Camera lens cap for scale (ca. 7 cm in diameter)

members testifying openings $>5\text{--}10\ \mu\text{m}$, consistent with a secondary, superimposed (structural) control (see Figure 10e). Complex relationships arise in the HWMZ and FWMZ due to lithological mixing (e.g. in Figure 9e).

4.4 | Detachment interval(s)

The third- and second-order fault detachment intervals are, respectively, contained within the lower, fine-grained Tschermakfjellet Formation (Figure 11a–g) and the transitional zone atop the Botneheia Formation (Figure 11h–n). Both display hydroplastic shear-flow structures and ductile/plastic soft sediment deformation intervals, within distal delta front depositional environments in the first case, and organic-rich offshore basinal shales in the second. The most common structures are slump-type, noncylindrical folds and loading structures (e.g. load casts and ball-and-pillows), observed to progressively evolve from attached to detached with proximity to the core of the shear zones (Figure 11a–d). In these shear zones, cm- to metres-thick, hydroplastically deformed sandstone-dominated elements appear folded, sheared and rotated, with the development of pseudopressure shadows, tails and inclusion trails, revealing a shear sense compatible with the displacement of nearby fault tips and traces (Figure 11e–g).

Local, mesoscale compressional and extensional features are observed in the lowermost organic shale interval, directly overlying a well-cemented, phosphate-rich interval that marks the transition with the Botneheia Formation (second-order faults detachment interval). In the inner part of Tjuvfjorden bay, about 2 km NE to the Øhmanfjellet study site, the top of the Botneheia Formation is folded into monoclinical geometries draped by silty shales, that seem to localize the nucleation points of the overlying growth faults (Figure 11h,i).

Outcrop-scale thrust splays, discrete thrust and low-angle normal faults with associated drag folds and duplex

structures are also locally observed (Figure 11j–l). Other low-angle, cm- to metres-thick shear zones with normal and reverse movements contain isoclinally folded CIC lenses (Figure 11m,n), similar to those observed in the FW and CZ of the dipping part of the second-order growth faults and their associated detachment (see e.g. Figure 6).

5 | DISCUSSION

5.1 | Growth fault architectures and deformation mechanisms

The lateral-vertical geometric relationships of the architectural elements (AE; fault core zones CZ, mixed zones MZ and damage zones DZ), suggest a general widening of the soft-sediment deformation products along with increasing displacement, which transition downward into detachment zones represented by relatively thick intervals of remoulded and mixed lithologies (see Figures 7b and 11a–g). Such original relationships are maintained in the third-order growth faults, which are preserved and passively deformed and rotated within the first- and second-order growth fault blocks. On the other hand, the 2nd and especially the first-order faults are characterized by a significant brittle overprinting with strain localization towards in the inner fault zones. Based on the trend and location of the few faults cutting through the De Geerdalen Formation (i.e. post-Triassic; see Figure 2g), we suggest that some of the favourably oriented segments of the first-order faults (and associated second-order ones) eventually interlinked into seismic-scale fault zones crosscutting the entire stratigraphy. Relatively low displacements on these reactivated faults can be explained by the “attenuation” operated by the growth fault interval of the Tschermackfjellet Formation (see Figure 2g). In this framework, this interval acts as structurally anisotropic buffer zone of mechanical decoupling between well-bedded, under- and over-lying

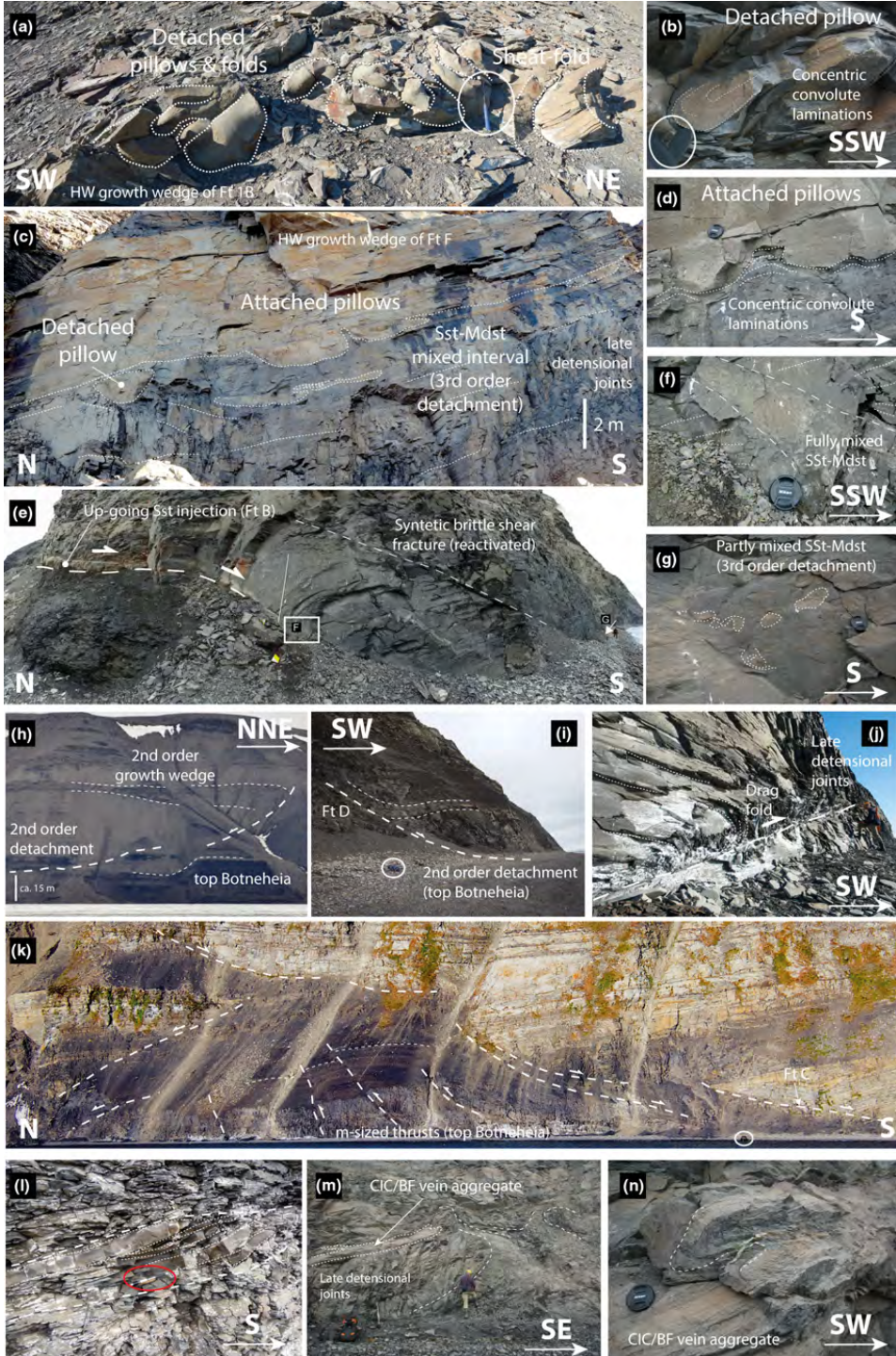


FIGURE 12 (a) Evolutionary cartoon illustrating the stepwise, conceptual progressive deformation from ductile to brittle deformation regime along with burial/lithification inferred for the investigated faults, with emphasis on the sandstone-shale and shale-shale juxtaposition parts. (b) Summary figure depicting fault hierarchy (based on the type of detachment) and mutual relationships, with indication of the possible formation setting. (c) Synoptic logs showing the petrophysical variations observed across the fault envelope. (d) Conceptual profile showing the local growth sections' distribution and local differential compaction sedimentary loading inferred to enucleates the different types of faults. (e) Reconstruction of the possible palaeogeographic setting, sedimentary and structural processes, with indication of the regional differential sedimentary loading-compaction

sequences, with subhorizontal accommodation of the deformation (e.g. rotation of second-order fault blocks).

This progressive reworking of soft-sediment structural discontinuities indicates shallow multistage growth faulting, achieved through micro to mesoscale polyphased deformation controlled by rheological-mechanical changes during progressive burial, shallow diagenesis and lithification. This suggests a syn-tectonic, plastic/ductile (*sensu* Rutter, 1986) to brittle regime transition, from distributed strain (hydroplastic phase) to strain localization (brittle phase) end-members (Figure 12a).

In particular, this polyphase evolution is recorded by the superposition and mutual overprinting of different deformation mechanisms. In the sandier HW, these vary from 1) an early stage of independent particulate flow aided by localized liquidization (i.e. liquefaction + fluidization; Allen, 1982) phenomena of granular material due to excess pore pressure, testifying to the unconsolidated and water-saturated state of the lithologies, 2) an intermediate stage of localized particulate flow aided by limited grain breakage and 3) a later stage of fracturing along structural and diagenetic discontinuities such as deformation band swarms and oxidation/reduction fronts. In the silt/shale-dominated FW, the deformation evolves from 1) an early stage of (hydro)plastic deformation, 2) an intermediate stage where the state of stress is between the elastic limit of the material and its breaking strength, and thus exhibiting both elastic and plastic properties (e.g. elasto-plastic deformation; lithological mixing), to 3) a later stage of diffused fracturing in low porosity rocks (e.g. shattered and brecciated shales; see Figure 12a). On the basis of the main driving mechanism and the inferred state of material during deformation (see e.g. Balsamo et al., 2013), the extrapolated detachment depth ranges from a few metres to ca. 30–40 m for the third-order faults, and down to 100–200 m for the second-order ones. The different conceptual phases depicted in Figure 12a represent the “frozen-in” status for any given fault and position along the fault itself. In this picture, these single evolutionary steps and/or locations along the fault envelope are recorded by different fault facies associations (FFAs), being also characterized by different preservation potential depending on the fault hierarchy (see Figure 12a).

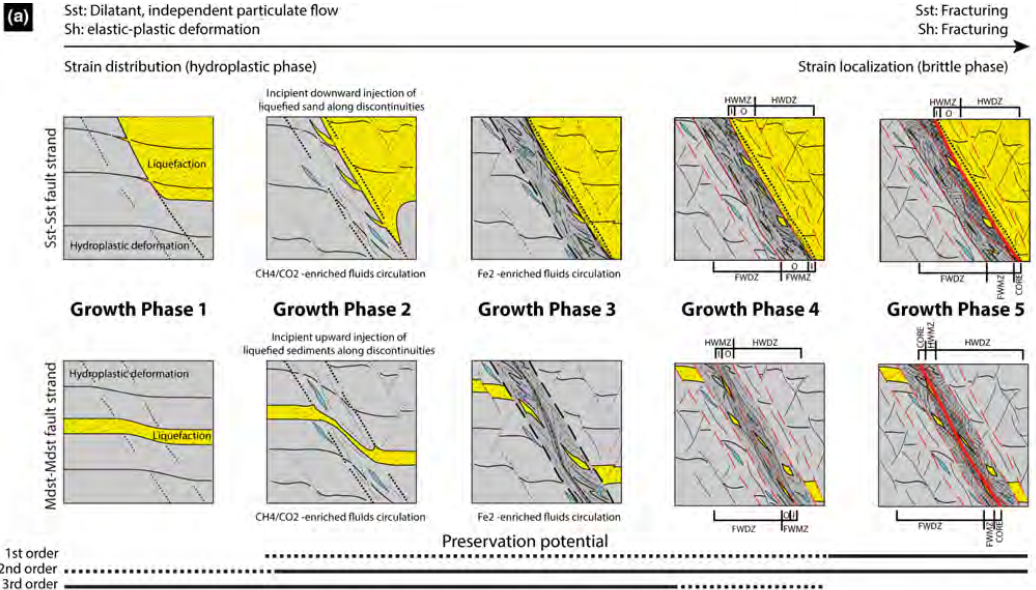
In some cases, entrainment of FWMZ and HWMZ lenses of second-order faults into the CZ of first-order

support the subsequent reactivation of some of the favourably oriented segments of listric faults into planar faults, eventually linking to the later faults crosscutting the De Geerdalen Formation (see above).

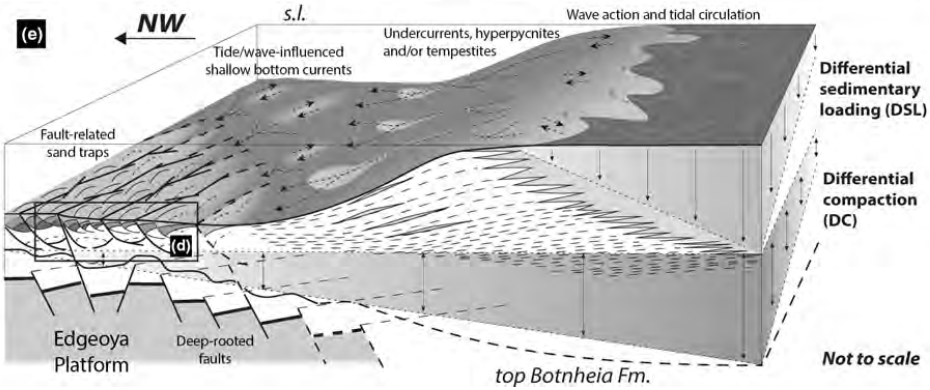
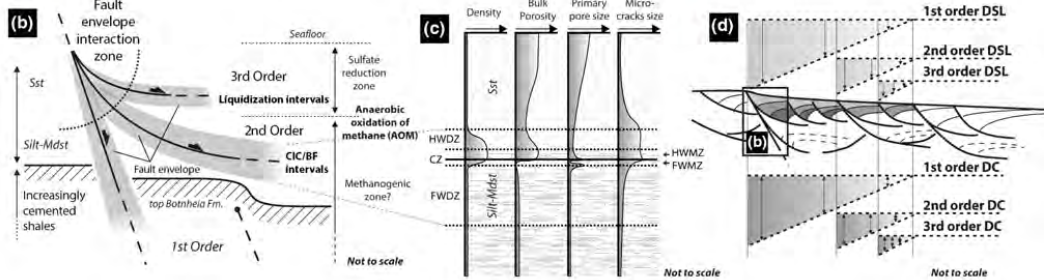
5.2 | Petrophysical evolution and structural diagenesis

The variation in deformation intensity across the growth fault zones and along their displacement direction is mirrored by microstructural-petrophysical changes. Microfabric-related structural anisotropy controls porosity-permeability and promoted localized microfracturing as suggested by the systematic bimodal pore size distributions. Greater data variability in porosity recorded in the HWMZ and FWMZ are due to enhanced pyrite mineralization and high degree of lithological mixing. In particular, evidence of a microscale “dual poro-perm” system is derived from the systematic bimodality in the pore size diagrams (see Figure 9e and DR 2). This pattern has been interpreted as the result of microcracking along the structural discontinuities (e.g. deformation-disaggregation/compaction bands) making up the microfabric network (i.e. petrophysical framework-related permeability anisotropy; Cavailhes et al., 2013). On the basis of the SEM data and as suggested by Bolton, Maltman, and Fisher (2000), this bimodal grain size distribution is inferred to be in line with the estimated grain size (positively skewed first mode recording primary depositional grain packing affected by normal compaction) and measured microcrack dimensions (negatively skewed second mode recording secondary microfracture network favoured by structural heterogeneity and directional anisotropy). In this framework, the two lithological and structural inputs appear to be separated into primary (sedimentary) and secondary (fracturing) contributions, changing vertically (and laterally) along the fault zone (see Figure 10b–c). In this framework, the bulk contribution to fluid storage and motion during deformation is provided by the progressive superposition of a secondary porosity due to microcracking along structural discontinuities onto a primary matrix porosity, which is in turn modified by increasing dilation, grain packing rearrangement, cementation and limited grain cracking.

Simple shear- and dilation-related textures are observed in association with matrix/cement-supported fabric and



- Dilation/disaggregation bands
- Deformation/disaggregation bands
- sand
- silty mud
- Distributed shear zone
- Localized shear zone
- CIC lenses
- Fractures
- Folded CIC lenses
- Sst lenses, membranes and smears
- Folded Sst lenses, membranes and smears
- breccia
- Ft core gouge
- Mdst lenses, membranes and smears
- Folded Mdst lenses, membranes and smears
- Ductile slip surface
- Brittle slip surface
- Principal slip surface



localized, dispersed grain packing, especially within Fe-sulphide cemented zones. A microstructural control on the calcite and pyrite cement distribution is also apparent, with a systematic occurrence of Fe-sulphide impregnated haloes in the sheared and smeared sandstone elements within or in the close proximity of the CZ and surrounding discrete shear surfaces in the HW (see Figure 9). Such dilation conditions favoured early circulation of formation fluids enriched in Fe₂ in the sandier HW of the shallower faults (3rd order) leading to the localized pyrite cementation. At deeper stratigraphic levels, mineralizing (CH₄-enriched?) fluids circulation in the second-order fault zones is suggested by the occurrence of CIC/BF vein aggregates, arranged as elongated fault-parallel lenses, progressively folded towards the CZ. The presence of these localized calcite mineralizations in the FW of some third-order faults and within the detachment of the second-order faults, along with their change in shape and size (from isolated cm-sized veins to m-sized, lenticular composite vein aggregates respectively), testify to early fluid flow communication along the fault zones, and a structural control on their distribution.

This structural-diagenetic framework may suggest the combined contribution of fluid seepage forces (up to overpressure?) and flow, associated with pore pressure gradients due to differential compaction-dewatering in poorly consolidated sediments at shallow burial conditions (<300 m depth), and leading to the shear strength reduction of the second- and third-order faults, as hypothesized by Maher et al. (2017). This possible scenario is in line with a very shallow environment (few metres to tens of metres below the seafloor), between the methanogenic and the sulphate reduction zone (Anaerobic oxidation of methane or Sulphate Methane Transition; e.g. Mitterer, 2010), marking the boundary between a lower zone where anaerobic bacterial oxidation of CH₄ enhances calcite precipitation and CIC/BF development, from an upper zone where sulphate reduction favours pyrite mineralization (Figure 11b), as described by Meng, Hooker, and Cartwright (2017). The hydrocarbon decomposition-aided, microbialitic origin of some sedimentary CIC structures in the same lithologies of eastern Svalbard studied by Tugarova and Fedyavsky (2014) is in line with the present observations. These diagenetic boundaries are susceptible to variations in the basin-scale, boundary environmental conditions (e.g. pressure-temperature variations at the seafloor), and likely represent preconditioning factors in the development of density-gravity instabilities that eventually can contribute to extensional listric faulting (see Figure 11b, c). Similar diagenetic features have been recognized elsewhere in the Triassic record of eastern Svalbard unrelated to growth faulting but attributed to near-surface biological processes (Tugarova & Fedyavsky, 2014). Analyses on C-O

stable isotopic signatures to shed light on these issues are currently ongoing.

5.3 | Growth wedges stratigraphy and depositional setting

Three main types of growth wedges are recognized: 1) combined, silt/mud- and sand-dominated (pre to late-growth) wedges, related to first-order faulting, 2) sandstone-dominated (late-growth) wedges related to second-order faulting (see below) and 3) intragrowth wedges (syn-growth) related to third-order faulting. The stacking patterns of the sandstone-dominated wedges, and the geometrical (i.e. erosion-deposition) relationships between the major half-graben growth fault sequences reveal that the general infilling trends, and consequent syn-sedimentary faulting, proceeded from N to S, in an overall “progressive,” in-sequence fashion (see relationships between growth wedges 1-3 and 4-5 marking the transition between major growth sequences 1 and 2 in Figure 2g). The switch from late-growth (sandstone-dominated) wedges 1 to 2 seems to be achieved through the downward movement of the southern block during the deposition of the growth wedges 3 (see Figure 2g). This is in line with the stacking patterns observed for the different facies associations comprising the late-growth wedge, sandstone-dominated sequences (Osmundsen et al., 2014). Notably, at the scales covered by our observations it is also possible to recognize that the initial phases of listric faulting (up to growth wedge 2) produced approximately symmetric graben-type sags bounded by both S to SSW and N to NNE dipping faults and characterized by dominant fine-grained sedimentary infill (see Figure 2g). The asymmetric half-grabens developed in the later stages (from growth wedge 2 and up), along with increasing sand-rich sedimentary input and enhanced activity on the S to SSW-dipping faults (see Figure 2g). This, combined with the increasing dominance of first-order faults to the SE proceeding from Kvalpynten to Negerpynten (see Figure 2c,d) seems to confirm the control of the latter on the development of the second-order ones to the NW of the study area. Notably, this seems in contrast with the original interpretation of a retrogressive delta-front slope collapse of a S-SW directed delta system, as postulated by Edwards (1976).

The silt/shale-dominated parts of growth wedges (i.e. pre and early growth), along with the continuous draping shale interval atop the growth faulted interval, share the common features of prodelta deposits, with punctuated evidence of sandstone lobes, especially towards the top of the sequences. In this framework, the four time-equivalent stratigraphic surfaces representing the upper boundaries of the late-growth wedges 1 to 3 (see Figure 2e–g) are interpreted as transgressive surfaces with a seafloor-exposure

(e.g. hard-ground) surfaces developed on top of late-growth wedge 4 according to Smyrak-Sikora et al. (2017). The internal stratigraphy of the syn-growth sandstones shows combined characteristics of wave-tidal deposits (e.g. subaqueous tidal bars and dunes). The same succession is observed at the base of the De Geerdalen Formation which overlies the draping shale interval and is interpreted to record a progressive transition from tide/wave-dominated delta front to delta top environments (see Haile et al., 2018; Osmundsen et al., 2014).

According to this scenario, “delta front lobe(s)” deposited by the remobilization of classic delta front and mouth bar sands by floods (e.g. hyperpycnal flows) and/or storms (e.g. surge return flows) would be reworked by tidally and/or downwelling-influenced, along-shore, shallow bottom-currents to be reoriented as sand bars parallel to the strike of active (1st order) faults and infilling their related superficial bathymetric depressions (see e.g. Pochat & van den Driessche, 2007). The degree of reorientation would depend on the amount of fault-generated physiography of the seafloor and amount of generated relief, which can be quantified by the maximum thickness of the sedimentary growth wedge infills (e.g. metres for the third-order wedges and tens of metres for second-order ones).

Beside the structural-stratigraphic relationships preserved in the HW sandstone wedges, evidence of palaeo-bathymetric complexity is also suggested by the unconformities observed in the FW silt-mudstone succession, interpreted as mixed nondeposition and/or erosion surfaces. Moreover, their localized cementation, strikingly similar to the one characterizing the top of Botneheia Formation, testifies *in situ*, early (phosphate-related) diagenesis and prolonged seafloor exposition (see Krajewski, 2011, 2013).

Additionally, while significantly disperse, the mean strike direction of the growth faults along the virtual NNW-SSE transect crossing the investigated sites in southern Edgeøya seems aligned with the local palaeo-current orientations, supporting the early fault-related control on sediment distribution (see Figure 2). Fault strikes seem to follow the wave ripple crest trends, which, in turn, are inferred to express an articulated and locally strongly curving palaeo-coastline. Haile et al. (2018) also argues for such a palaeo-coastline geometry.

This type of depositional setting would have favoured differential compaction-driven subsidence between the prodelta and the relatively more proximal zones, leading to the creation of landward-dipping listric growth faulting at the delta toe (Back & Morley, 2016; Braathen et al., 2017). In this framework first order and larger-scale (seismic) faults with spacing in the order of kilometres would provide a counter-regional, monoclinial slope dipping towards the delta system. This gentle (ca. 1-3 degrees) slope would be affected by a relatively uneven physiography, with local

seafloor relief created by synthetic (and antithetic) second- and third-order fault systems. The resultant half-graben depozones would have been able to trap deltaic sands redistributed by mass wasting and along-coast (wave- and tidally influenced) offshore currents, enhanced by the localized structural confinement of the depositional setting. The increase in localized sedimentary loading and the consequent retreat of the compaction front would have progressively activated growth fault sequences in a landward direction, as documented in this work. Localized differential compaction and sedimentary loading, and consequent disequilibria are inferred to influence growth faults activity also at lower scales, within the second- and third-order sandstone wedges (Figure 12d). In this framework, the monoclines atop the Botneheia Formation are likely related to the development of a trishear zone of deformation above deep-rooted fault tips, roughly striking in the same direction as the first- and second-order growth faults, and testify to the creation of syn-sedimentary relief and consequently uneven seafloor topography during the deposition of the lower Tschermafjellet Formation. In other words, these can be considered as earlier first-order faults that simply did not reactivate later on.

5.4 | Growth fault distributions and possible causal mechanisms

According to the literature and supported by presented data, the investigated growth fault systems develops in the prodelta region of a large Triassic delta systems. This progrades across relatively shallow, epeiric (epicontinental) shelfal basins developed in the extended foreland, located between the older Caledonides to the W-SW and the palaeo-Uralides in formation (see e.g. Anell et al., 2016; Klausen et al., 2016). The predeltaic succession is characterized by the deposition in limited water circulation and high-organic supply, as testified by the widespread anoxic conditions periodically recorded on the seafloor (see e.g. Krajewski, 2013). In such a geodynamic situation, combined far-field stress trajectories curve and intersect at different angles and different distances from orogenic front, leading to complex regional deformation and associated network of structural patterns with dominance of high- to low-angle (re)activation of longitudinal, cross and conjugate systems (e.g. Hancock & Bevan, 1987). In this case, the result is a fault-basin oblique inversion of inherited structural architectures (i.e. Carboniferous basins) achieved during the increasing tectonic activity in the E due to the Uralide orogeny in Late Triassic (Klausen et al., 2016). Renewed compression and formation of the West Spitsbergen Fold-and-Thrust Belt (Steel et al., 1985; Braathen, Bergh, & Maher, 1997) during the Cenozoic reactivates the tectonic lineaments arranged into a N-S structural domain

(e.g. Billefjorden in Svalbard, Loppa High in NW Barents shelf) and a NE-SW structural domain (E Svalbard, SW Barents shelf), as shown for instance in Faleide et al. (2008). The interpretation proposed by Anell, Braathen, Olausen, and Osmundsen (2013), Anell et al. (2016) and Klausen, Ryseth, Helland-Hansen, Gawthorpe, and Laursen (2014), Klausen et al. (2015), is that of a major delta system sourced from the palaeo-Uralides, prograding with a general complex pattern towards the N-NW. This delta system advances above the SE flank of a fault-bounded, elongated and roughly E-W to NE-SW oriented, palaeobathymetric high (i.e. Edgeøya platform), with a significant decreasing in the overall accommodation for sediments. This reduction results in lack of aggradation and causes differential advancement rates of the clinoforms, with local delta lobe indentation. Such differential progradation produced local to regional differential compaction at different stratigraphic levels, with the development of frontal (and subordinately lateral) gradients in subsidence. In this scenario, gravitational discharge of a regional, few-degrees slope dipping towards the land is responsible for the creation of an articulated physiography featured by local half-graben depocentres, developed at different scales (Figure 12e).

Due to the systematic areal persistency and parallelism with the regional tectonic lineaments recognized in the area (e.g. Franz-Victoria Basin, Edgeøya Platform), the first-order growth faults likely relate to the surficial expression of major, long-lived and deep-rooted fault systems, inherited from the Palaeozoic (e.g. Marelló et al., 2013) and/or lately reactivated. In this framework, the relationships between 1st and second-order growth faults, and the later seismic-scale fault zones (i.e. cutting across the upper draping shale interval and/or across the top Botneheia; see above), can be generally described in term of “soft linkage” (i.e., mechanical decoupling of detachment intervals), with eventual, local evolution towards “hard linkage” (Gabrielsen, Sokoutis, Willingshofer, & Faleide, 2016), where through-going, first-order (and larger) planar fault zones are observed to cluster and cut across the top of the Botneheia Formation (see Figure 12b,e). Due to the listric arrangement of the second-order growth fault array, the (re)exploitation of their favourably oriented branches by later faulting does not result in appreciable vertical offsets, but rather, part of the related deformation is accommodated by cumulative slip displacement in the gently inclined and horizontal segments (see Figure 2g). Accordingly, the growth-faulted interval of the Tschemakfjellet Formation would have act as a “buffer zone” for the vertical, downward propagation of the posttectonic faults.

The development of second- and third-order faults in these first-order growth fault blocks seems related to mechanical-rheological instabilities at distinct stratigraphic

intervals, within mechanically weak, bedding-parallel stratigraphic zones prone to be reactivated as detachments, located within the top Botneheia Formation and the pro-delta deposits of the lower Tschemakfjellet Formation respectively (diagenetic front and a liquidization level; see above and Figure 12b). In the depicted local to regional palaeo-geographic context, the trigger for the syn-sedimentary movement could be due to tectonic activity on the first-order (and larger) faults, acting as preferential avenues that allow fluid movement and associated diagenesis. This is in turn possibly favoured by localized sedimentation and differential compaction, and changes in the hydrogeological regime (climatically or tectonically controlled, or a combination thereof). In particular, tips of the second-order faults are often associated to local accumulations of sand-rich gravity flow lobes with HCS, suggesting a causal relationship with autocyclic sedimentary processes (e.g. hyperpycnites and/or tempestites; see Figure 12e).

In summary, the processes inferred to control this auto-to allo-cyclic interplay of differential sedimentary loading, faults' activity and creation of sedimentary accommodation, include: (1) shallow substrate remobilization (e.g. from seismic shocks and/or abrupt shifts of diagenetic fronts), (2) increasing grain size and sedimentation rates of clastic input (e.g. distributary channel avulsion, severe climatic events, enhanced continental weathering), (3) redistribution of grain size populations (e.g. segregation of sand- and mud-rich depozones by focused, tidally/storm-induced, along-shore, shallow bottom currents). On the basis of the available data we cannot pick up one major causal mechanism out of the spectrum of the possible proposed ones and dedicated studies are envisioned for a better constrain.

6 | CONCLUSIONS

The Triassic growth fault systems of southern Edgeøya (East Svalbard, Arctic Norway) comprise three orders of faults, with the second- and third-order representing listric faults that control the internal growth parasequences, and intra-(syn) growth wedges respectively. Planar, first-order faults influence the accommodation in both growth stages. The first-order faults and their interlinkage possibly represent the uppermost expression of larger, seismic-scale faults that have been imaged offshore.

The progressive micro to mesoscale brittle reworking of structural discontinuities related to soft-sediment deformation suggests polyphase deformation during progressive lithification and compaction, and records a transition from hydroplastic, distributed strain, to brittle strain localization. This progresses along with the combined evolution of the different orders of faulting and related sedimentary growth wedge cycles, and, ideally, records a gradual shift of the

locus of deformation from the third-order to the first-order fault zone end-members. In HW sandstones, deformation mechanisms vary from liquidization processes and independent particulate flow at low confining pressure causes shear-dilation, to diffused disaggregation and compaction banding with localized incipient cataclasis, eventually leads to localized shear and extensional fracturing. In the FW silty-shales, deformation mechanisms vary from hydroplastic deformation and disaggregation-phyllonite tabular shear zones, to diffuse brittle-ductile shearing and later localized shear failure and extensional fracturing. This evolving rheological-mechanical behaviour is due to changes in material properties during burial and shallow diagenesis.

The petrophysical properties of the litho-structural facies comprising the growth fault architectural elements show marked variation trends across and along the fault zone. The microscale, fabric-related structural anisotropy generated during the early deformation phases appears to control the bulk pore size distribution, promoting the development of bimodal porosity systems. Accordingly, the background primary (sedimentary) matrix pore network is overprinted by a secondary (tectonic) pore network composed of microcracks located along the preexisting microfabric discontinuities. The cementation patterns of pervasive Fe-sulphide impregnation halos in the inner parts of fault zones reflect enhanced dilation-related fluid circulation in the early intermediate phases of growth faulting. These results may have important practical implications, for instance in terms of fault-seal analysis (e.g. vertical-lateral connectivity of sandstone wedges and fault blocks, structural-stratigraphy of half-graben reservoirs) and geophysical visualization of (sub)seismic fault zones (e.g. higher densities due to Fe-sulphide impregnation and consequent higher impedance of cores and inner damage zones), routinely performed in hydrocarbon exploration and production.

This growth fault system is inferred to develop in the prodelta region of a large Triassic delta system, prograding northwestward against and atop a regional palaeo-bathymetric high that was approximately oriented NE-SW. These faults are inferred to be responsible for the creation of palaeo-bathymetric relief atop the Botneheia Formation during the deposition of the Tschermakfjellet Fm, which favoured localized depozones (i.e. half-grabens) and consequent differential compaction, and thus preconditioning the formation of the lower order faults. The spatial arrangement, geometric relationships and infilling history of these half-grabens, and the internal sedimentary growth wedges also testify to an overall landward (i.e. counter-regional) growth faulting style with respect to the N-NW-directed progradation direction inferred for the associated delta systems. In such a setting, deep-rooted tectonic faults (Carboniferous) that bound the topographic high were likely

reactivated by far-field tectonics related to the late Triassic Uralide orogeny to the E. This acted in synergy with regional differential compaction that created a landward-moving subsidence front sustaining a gently inclined, long-lived delta-facing slope. This slope instability in turn triggered shallow gravitational deformation and local depocentres, creating structurally controlled sand-mud accumulations, which also record detailed, climatically controlled variations of deltaic sediment supply redistribution and relative sea-level variations.

ACKNOWLEDGEMENTS

This study is part of the Petromaks Trias North Project (grant 234152/E30); we extend gratitude to the projects financial supporters, the Research Council of Norway and industry partners, Edison Norway, Lundin Norway, RWE Dea Norge, Statoil and Tullow Oil. Our many discussions with Snorre Olaussen, Kim Senger, Elisabeth Miller, Elisabeth Olsen, Luka Blažić, Beyene Haile, Tore Grane Klausen and Helge Hellevang during the field campaigns enriched the work. Moreover, we would like to deeply thank the Editor Atle Rotevatn and the referees Jack Williams, Thibault Cavailhes and Tore Grane Klausen for their accurate and constructive reviews.

ORCID

Kei Ogata  <http://orcid.org/0000-0002-4978-2854>

Alvar Braathen  <http://orcid.org/0000-0002-0869-249X>

REFERENCES

- Allen, J. R. L. (1982). *Sedimentary structures: Their character and physical basis*, Vol. 657. Amsterdam, the Netherlands: Elsevier.
- Anell, I., Braathen, A., & Olaussen, S. (2014). Regional constraints of the Sørkapp Basin: A Carboniferous relic or a Cretaceous depression? *Marine and Petroleum Geology*, 54, 123–138. <https://doi.org/10.1016/j.marpetgeo.2014.02.023>
- Anell, I., Braathen, A., Olaussen, S., & Osmundsen, P. T. (2013). Evidence of faulting contradicts a quiescent northern Barents Shelf during the Triassic. *First Break*, 31(6), 67–76.
- Anell, I., Faleide, J. I., & Braathen, A. (2016). Regional tectono-sedimentary development of the highs and basins of the northwestern Barents Shelf. *Norwegian Journal of Geology*, 96, 27–41.
- Armstrong, C., Mohrig, D., Hess, T., George, T., & Straub, K. M. (2014). Influence of growth faults on coastal fluvial systems: Examples from the late Miocene to Recent Mississippi River Delta. *Sedimentary Geology*, 301, 120–132. <https://doi.org/10.1016/j.sedgeo.2013.06.010>
- Back, S., Jing, T. H., Thang, T. X., & Morley, C. K. (2005). Stratigraphic development of synkinematic deposits in a large growth-fault system, onshore Brunei Darussalam. *Journal of the Geological Society London*, 162, 243–258. <https://doi.org/10.1144/0016-764903-006>

- Back, S., & Morley, C. (2016). Growth faults above shale – Seismic-scale outcrop analogues from the Makran foreland, SW Pakistan. *Marine and Petroleum Geology*, 70, 144–162. <https://doi.org/10.1016/j.marpetgeo.2015.11.008>
- Bally, A. W., Bernoulli, D., Davis, G. A., & Montadert, L. (1981). Listric normal faults. *Oceanologica Acta*, 4, 87–101.
- Balsamo, F., Bezerra, F. H., Vieira, M., & Storti, F. (2013). Structural control on the formation of iron oxide concretions and Liesegang bands in faulted, poorly lithified Cenozoic sandstones of the Paraíba basin, Brazil. *Geological Society of America Bulletin*, 125, 913–931. <https://doi.org/10.1130/B30686.1>
- Bense, V. F., & Person, M. A. (2006). Faults as conduit-barrier systems to fluid flow in siliciclastic sedimentary aquifers. *Water Resources Research*, 42, W05421.
- Bhattacharya, J. P., & Davies, R. K. (2001). Growth faults at the pro-delta to delta-front transition, Cretaceous Ferron sandstone, Utah. *Marine and Petroleum Geology*, 18, 525–534. [https://doi.org/10.1016/S0264-8172\(01\)00015-0](https://doi.org/10.1016/S0264-8172(01)00015-0)
- Bolton, A. J., Maltman, A. J., & Fisher, Q. (2000). Anisotropic permeability and bimodal pore-size distributions of fine-grained marine sediments. *Marine and Petroleum Geology*, 17, 657–672. [https://doi.org/10.1016/S0264-8172\(00\)00019-2](https://doi.org/10.1016/S0264-8172(00)00019-2)
- Bourouillec, R., Cartwright, J. A., Johnson, H. D., Lansigu, C., Quémer, J.-M., & Savanier, D. (2004). Syndepositional faulting in the Grès d'Annot Formation, SE France: High-resolution kinematic analysis and stratigraphic response to growth faulting. *Geological Society, London, Special Publications*, 221, 241–265. <https://doi.org/10.1144/gsl.sp.2004.221.01.13>
- Braathen, A., Bergh, S. G., & Maher, H. D. (1997). Thrust kinematics in the central part of the Tertiary transpressional fold-thrust belt in Spitsbergen. *NGU Bulletin*, 433, 32–33.
- Braathen, A., Maher, H. D., Haabet, T. E., Kristensen, S. E., Tørudbakken, B. O., & Worsley, D. (1999). Caledonian thrusting on Bjornoya: Implications for Palaeozoic and Mesozoic tectonism of the western Barents Shelf. *Norsk Geologisk Tidsskrift*, 79(1), 57–68. <https://doi.org/10.1080/002919699433915>
- Braathen, A., Midtkandal, I., Mulrooney, M. J., Appleyard, T. R., Haile, B. G., & Yperen, A. E. (2017). Growth-faults from delta collapse – structural and sedimentological investigation of the Last Chance delta, Ferron Sandstone, Utah. *Basin Research*, 1–20. <https://doi.org/10.1111/bre.12271>
- Braathen, A., Osmundsen, P. T., & Gabrielsen, R. H. (2004). Dynamic development of fault rocks in a crustal-scale detachment: An example from western Norway. *Tectonics*, 23, 1–27.
- Braathen, A., Osmundsen, P. T., Hauso, H., Semshaug, S., Fredman, N., & Buckley, S. J. (2013). Fault-induced deformation in a poorly consolidated, siliciclastic growth basin: A study from the Devonian in Norway. *Tectonophysics*, 586, 112–129. <https://doi.org/10.1016/j.tecto.2012.11.008>
- Braathen, A., Tveranger, J., Fossen, H., Skar, T., Cardozo, N., Semshaug, S. L., ... Sverdrup, E. (2009). Fault facies as concept and its applications to sandstone reservoirs. *American Association for Petroleum Geologists Bulletin*, 93, 891–917. <https://doi.org/10.1306/03230908116>
- Caine, J. S., Evans, J. P., & Forster, C. B. (1996). Fault zone architecture and permeability structure. *Geology*, 24(11), 1025–1028. [https://doi.org/10.1130/0091-7613\(1996\)024<1025:FZAAPS>2.3.CO;2](https://doi.org/10.1130/0091-7613(1996)024<1025:FZAAPS>2.3.CO;2)
- Callot, P., Odonne, F., Debroas, E.-J., Maillard, A., Dhont, D., Basile, C., & Hoareau, G. (2009). Three-dimensional architecture of submarine slide surfaces and associated soft-sediment deformation in the Lutetian Sobrarbe deltaic complex (Ainsa, Spanish Pyrenees). *Sedimentology*, 56, 1226–1249. <https://doi.org/10.1111/j.1365-3091.2008.01030.x>
- Cavaliher, T., Sizun, J.-P., Labaume, P., Chauvet, A., Buatier, M., Soliva, R., ... Gout, C. (2013). Influence of fault rock foliation on fault zone permeability: The case of deeply buried arkosic sandstones (Grès d'Annot, southeastern France). *AAPG Bulletin*, 97/9, 1521–1543. <https://doi.org/10.1306/03071312127>
- Cohen, H. A., & McClay, K. R. (1996). Sedimentation and shale tectonics of the northwestern Niger Delta front. *Marine and Petroleum Geology*, 13, 313–328. [https://doi.org/10.1016/0264-8172\(95\)00067-4](https://doi.org/10.1016/0264-8172(95)00067-4)
- Corfu, F., Andersen, T. B., & Gasser, D. (2014). The Scandinavian Caledonides: Main features, conceptual advances, and critical questions. In: F. Corfu, T. B. Andersen & D. Gasser (Eds.), *New perspectives on the caledonides of Scandinavia and related areas* (pp. 9–43). London: Geological Society, Special Publications, 390.
- Dallmann, W. K., Dypvik, H., Gjelberg, J. G., Harland, W. B., Johannessen, E. P., Keilen, H. B., ... Worsley, D. (1999). *Lithostratigraphic Lexicon of Svalbard: Review and recommendations for nomenclature use*, 318 pp. Tromsø, Norway: Norsk Polarinstittutt.
- Damuth, J. E. (1994). Neogene gravity tectonics and depositional processes on the deep Niger Delta continental margin. *Marine and Petroleum Geology*, 11, 320–346. [https://doi.org/10.1016/0264-8172\(94\)90053-1](https://doi.org/10.1016/0264-8172(94)90053-1)
- Edwards, M. B. (1976). Growth faults in upper Triassic deltaic sediments, Svalbard. *AAPG Bulletin*, 60, 341–355.
- Faleide, J. I., Tsikalas, F., Breivik, A. J., Mjelde, R., Ritzmann, O., Engen, O., ... Eldholm, O. (2008). Structure and evolution of the continental margin off Norway and the Barents Sea. *Episodes*, 31, 82–91.
- Fleming, E. J., Flowerdew, M. J., Smyth, H. R., Scott, R. A., Morton, A. C., Omma, J. E., ... Whitehouse, M. J. (2016). Provenance of Triassic sandstones on the southwest Barents Shelf and the implication for sediment dispersal patterns in northwest Pangaea. *Marine and Petroleum Geology*, 78, 516–535. <https://doi.org/10.1016/j.marpetgeo.2016.10.005>
- Fossen, H. (2010). Deformation bands formed during soft-sediment deformation: Observations from SE Utah. *Marine and Petroleum Geology*, 27, 215–222. <https://doi.org/10.1016/j.marpetgeo.2009.06.005>
- Fossen, H., Schulz, R. A., Shipton, Z. K., & Mair, K. (2007). Deformation Bands in Sandstone – a Review. *The Geological Society of London*, 164, 755–769. <https://doi.org/10.1144/0016-76492006-036>
- Gabrielsen, R. H., Sokoutis, D., Willingshofer, D., & Faleide, J. I. (2016). Fault linkage across weak layers during extension: An experimental approach with reference to the Hoop Fault Complex of the SW Barents Sea. *Petroleum Geoscience*, 22, 123–135. <https://doi.org/10.1144/petgeo2015-029>
- Gagliano, M. S. (2005). Effects of geological faults on levee failures in South Louisiana. In: Testimony of Sherwood Gagliano. Ph.D. U.S. Senate Committee on Environment and Public Works, Senator James M. Inhofe, Chairman, Washington, D.C., pp. 1–28.
- Haile, B. G., Klausen, T. G., Czarniecka, U., Xi, K., Jahren, J., & Hellevang, H. (2018). How are diagenesis and reservoir quality linked to depositional facies? A deltaic succession, Edgeøya, Svalbard. *Marine and Petroleum Geology*, 92, 519–546. <https://doi.org/10.1016/j.marpetgeo.2017.11.019>

- Hancock, P. L., & Bevan, T. G. (1987). Brittle modes of foreland extension. In P. Coward, J. F. Dewey & P. L. Hancock (Eds.), *Continental extensional tectonics* (pp. 127–137). London: Geological Society, Special Publications, 28. <https://doi.org/10.1144/GSL.SP.1987.028.01.10>
- Harland, W. B. (1997). Proto-basement in Svalbard. *Polar Research*, 16, 123–147. <https://doi.org/10.3402/polar.v16i2.6631>
- Heynekamp, M. R., Goodwin, L. B., Mozley, P. S., & Haneberg, W. C. (1999). Controls on fault-zone architecture in poorly lithified sediments, Rio Grande Rift, New Mexico: Implications for fault-zone permeability and fluid flow. In W. C. Haneberg, P. S. Mozley, J. Casey Moore & L. B. Goodwin (Eds.), *Faults and subsurface fluid flow in the shallow crust*, Vol. 113 (pp. 27–51). Washington, DC: AGU Geophysical Monograph. American Geophysical Union. <https://doi.org/10.1029/GM113>
- Hurum, J. H., Roberts, A. J., Nakrem, H. A., Stenlökk, J. A., & Mørk, A. (2014). The first recovered ichthyosaur from the Middle Triassic of Edgeøya, Svalbard. *Norwegian Petroleum Directorate Bulletin*, 11, 97–110.
- Imber, J., Childs, C., Nell, P. A. R., Walsh, J. J., Hodgetts, D., & Flint, S. (2003). Hanging wall fault kinematics and footwall collapse in listric growth fault systems. *Journal of Structural Geology*, 25(2), 197–208. [https://doi.org/10.1016/S0191-8141\(02\)00034-2](https://doi.org/10.1016/S0191-8141(02)00034-2)
- King, R. C., Backé, G., Morley, C. K., Hillis, R. R., & Tingay, M. R. P. (2010). Balancing deformation in NW Borneo: Quantifying plate-scale vs. gravitational tectonics in a delta and deepwater fold-thrust belt system. *Marine and Petroleum Geology*, 27(1), 238–246. <https://doi.org/10.1016/j.marpetgeo.2009.07.008>
- Klausen, T., & Mørk, A. (2014). The upper Triassic paralic deposits of the De Geerdalen formation on hopen: Outcrop analog to the subsurface snadd formation in the Barents Sea. *AAPG Bulletin*, 98, 1911–1941. <https://doi.org/10.1306/02191413064>
- Klausen, T. G., Müller, R., Slama, J., & Helland-Hansen, W. (2016). Evidence for Late Triassic provenance areas and Early Jurassic sediment supply turnover in the Barents Sea Basin of northern Pangea. *Lithosphere*, 9(1), 14–28.
- Klausen, T. G., Ryseth, A. E., Helland-Hansen, W., Gawthorpe, R., & Laursen, I. (2014). Spatial and temporal changes in geometries of fluvial channel bodies from the Triassic Snadd Formation of offshore Norway. *Journal of Sedimentary Research*, 84, 567–585. <https://doi.org/10.2110/jsr.2014.47>
- Klausen, T. G., Ryseth, A. E., Helland-Hansen, W., Gawthorpe, R., & Laursen, I. (2015). Regional development and sequence stratigraphy of the middle to late Triassic snadd formation, Norwegian Barents Sea. *Marine and Petroleum Geology*, 62, 102–122. <https://doi.org/10.1016/j.marpetgeo.2015.02.004>
- Krajewski, K. P. (2011). Phosphatic microbialites in the Triassic phosphogenic facies of Svalbard. In V. C. Tewari & J. Seckbach (Eds.), *Stromatolites: Interaction of microbes with sediments. Cellular origin, life in extreme habitats and astrobiology*, vol. 18 (pp. 187–222). Springer. https://doi.org/10.1007/978-94-007-0397-1_9
- Krajewski, K. P. (2013). Organic matter–apatite–pyrite relationships in the Botneheia Formation (Middle Triassic) of eastern Svalbard: Relevance to the formation of petroleum source rocks in the NW Barents Sea shelf. *Marine and Petroleum Geology*, 45, 69–105. <https://doi.org/10.1016/j.marpetgeo.2013.04.016>
- León Y León, C. A. (1998). New perspectives in mercury porosimetry. *Advances in Colloid and Interface Science*, 76–77, 341–372. [https://doi.org/10.1016/S0001-8686\(98\)00052-9](https://doi.org/10.1016/S0001-8686(98)00052-9)
- Lohr, T., Krawczyk, C., Oncken, O., & Tanner, D. (2008). Evolution of a fault surface from 3D attribute analysis and displacement measurements. *Journal of Structural Geology*, 30(6), 690–700. <https://doi.org/10.1016/j.jsg.2008.02.009>
- Loveless, S., Bense, V., & Turner, J. (2011). Fault deformation processes and permeability architecture within recent rift sediments, central Greece. *Journal of Structural Geology*, 33, 1554–1568.
- Lyberis, N., & Manby, G. (1999). Continental collision and lateral escape deformation in the lower and upper crust: An example from Caledonide Svalbard. *Tectonics*, 18(1), 40–63. <https://doi.org/10.1029/1998TC900013>
- Maestro, A., Barnolas, A., Somoza, L., Lowrie, A., & Lawton, T. (2002). Geometry and structure associated to gas-charged sediments and recent growth faults in the Ebro Delta (Spain). *Marine Geology*, 186, 351–368. [https://doi.org/10.1016/S0025-3227\(02\)00212-8](https://doi.org/10.1016/S0025-3227(02)00212-8)
- Maher, H. D. (2001). Manifestations of the cretaceous high arctic large igneous province in Svalbard. *The Journal of Geology*, 109(1), 91–104. <https://doi.org/10.1086/317960>
- Maher, H. D., Ogata, K., & Braathen, A. (2017). Cone-in-cone and beef mineralization associated with Triassic growth basin faulting and shallow shale diagenesis, Edgeøya, Svalbard. *Geological Magazine*, 154(2), 201–216. <https://doi.org/10.1017/S0016756815000886>
- Mandl, G., & Crans, W. (1981). Gravitational Gliding in Deltas. In K. R. McClay & N. J. Price (Eds.), *Thrust and nappe tectonics* (pp. 41–54). London: Geological Society, Special Publications, 9.
- Marello, L., J. Ebbing, J., & Gernigon, L. (2013). Basement inhomogeneities and crustal setting in the Barents Sea from a combined 3D gravity and magnetic model. *Geophysical Journal International*, 193(2), 557–584. <https://doi.org/10.1093/gjg/ggt018>
- McClay, K. R., Dooley, T., & Lewis, G. (1998). Analog modelling of progradational delta systems. *Geology*, 26(9), 771–774. [https://doi.org/10.1130/0091-7613\(1998\)026<771:AMOPDS>2.3.CO;2](https://doi.org/10.1130/0091-7613(1998)026<771:AMOPDS>2.3.CO;2)
- McClay, K. R., & Ellis, K. R. (1987). Geometries of extensional fault systems developed in model experiments. *Geology*, 15, 341–344. [https://doi.org/10.1130/0091-7613\(1987\)15<341:GOEFSD>2.0.CO;2](https://doi.org/10.1130/0091-7613(1987)15<341:GOEFSD>2.0.CO;2)
- Meng, Q., Hooker, J., & Cartwright, J. (2017). Early overpressuring in organic-rich shales during burial: Evidence from fibrous calcite veins in the Lower Jurassic Shales-with-Beef Member in the Wessex Basin, UK. *Journal of the Geological Society*, 174, 869–882. <https://doi.org/10.1144/jgs.2016.146>
- Minakov, A., Faleide, J. I., Glebovsky, V. Y., & Mjelde, R. (2012). Structure and evolution of the northern Barents-Kara Sea continental margin from integrated analysis of potential fields, bathymetry and sparse seismic data. *Geophysical Journal International*, 188, 79–102. <https://doi.org/10.1111/j.1365-246X.2011.05258.x>
- Mitterer, R. M. (2010). Methanogenesis and sulfate reduction in marine sediments: A new model. *Earth and Planetary Science Letters*, 295, 358–366. <https://doi.org/10.1016/j.epsl.2010.04.009>
- Mørk, A., Dallman, W. K., Dypvik, H., Johannessen, E. P., Larssen, G. B., Nagy, J., ... Worsley, D. (1999). Mesozoic lithostratigraphy. In W. K. Dallman (Ed.), *Lithostratigraphic lexicon of Svalbard. Upper Palaeozoic to Quaternary bedrock. Review and recommendations for nomenclature use* (pp. 127–214). Tromsø, Norway: Norsk Polarinstittut.
- Mozley, P. S., & Goodwin, L. B. (1995). Patterns of cementation along a Cenozoic normal fault: A record of paleoflow orientations.

- Geology*, 23, 539–542. [https://doi.org/10.1130/0091-7613\(1995\)023<0539:POCAAC>2.3.CO;2](https://doi.org/10.1130/0091-7613(1995)023<0539:POCAAC>2.3.CO;2)
- Nejbert, K., Krajewski, K. P., Dubinska, E., & Pecskey, Z. (2011). Dolerites of Svalbard, north-west Barents Sea Shelf: Age, tectonic setting and significance for geotectonic interpretation of the High-Arctic Large Igneous Province. *Polar Research*, 30(7306), 1–24.
- Nemec, W., Steel, R. J., Gjelberg, J., Collinson, J. D., Prestholm, E., Øxnevad, I. E., & Worsley, D. (1988). Exhumed rotational slides and scar infill features in a Cretaceous delta front, eastern Spitsbergen. *Polar Research*, 6, 105–112. <https://doi.org/10.3402/polar.v6i1.6850>
- Nøttvedt, A., Cecchi, M., Gjelberg, J. C., Kristensen, S. E., Lønøy, A., Rasmussen, A., ... van Veen, P. M. (1992). Svalbard-Barents Sea correlation: A short review. In T. Vorren, E. Bergsager, Ø. A. Dahl-Stammes, E. Holter, E. Johansen, B. Lie & T. B. Lund (Eds.), *Arctic geology and petroleum potential* (pp. 15–17). Amsterdam, the Netherlands: Elsevier, Norwegian Petroleum Society, Special Publication 2.
- Onderdonk, N., & Midtkandal, I. (2010). Mechanisms of collapse of the Cretaceous Helvetiafjellet Formation at Kvalvagen, Eastern Spitsbergen. *Marine and Petroleum Geology*, 27, 2118–2140. <https://doi.org/10.1016/j.marpetgeo.2010.09.004>
- Osmundsen, P. T., Braathen, A., Rød, R. S., & Hynne, I. B. (2014). Styles of normal faulting and fault-controlled sedimentation in the Triassic deposits of Eastern Svalbard. *Norwegian Petroleum Directorate Bulletin*, 11, 61–69.
- Panpichityota, N., Morley, C. K., & Ghosh, J. (2018). Link between growth faulting and initiation of a mass transport deposit in the northern Taranaki Basin, New Zealand. *Basin Research*, 30(2), 237–248. <https://doi.org/10.1111/bre.12251>
- Pochat, S., Castellort, S., vanden Driessche, J., Besnard, K., & Gumioux, C. (2004). A simple method of determining sand / shale ratios from seismic analysis of growth faults: An example from Upper Oligocene to Lower Miocene Niger Delta deposits. *American Association of Petroleum Geologists Bulletin*, 88, 1357–1367. <https://doi.org/10.1306/04290403117>
- Pochat, S., & van den Driessche, J. (2007). Impact of syndimentary metre-scale normal fault scarps on sediment gravity flow dynamics: An example from the Grès d'Annot Formation, SE France. *Sedimentary Geology*, 202, 796–820. <https://doi.org/10.1016/j.sedgeo.2007.09.005>
- Rawling, G., & Goodwin, L. (2003). Cataclasis and particulate flow in faulted, poorly lithified sediments. *Journal of Structural Geology*, 25, 317–331. [https://doi.org/10.1016/S0191-8141\(02\)00041-X](https://doi.org/10.1016/S0191-8141(02)00041-X)
- Rawling, G., & Goodwin, L. (2006). Structural record of the mechanical evolution of mixed zones in faulted poorly lithified sediments, Rio Grande rift, New Mexico, USA. *Journal of Structural Geology*, 28, 1623–1639. <https://doi.org/10.1016/j.jsg.2006.06.008>
- Rider, M. H. (1978). Growth faults in Carboniferous of Western Ireland. *AAPG Bulletin*, 62, 2191–2213.
- Rittersbacher, A., Howell, J., & Buckley, S. J. (2014). Analysis of fluvial architecture in the Blackhawk formation, Wasatch plateau, Utah, U.S.A., using large 3D photo-realistic models. *Journal of Sedimentary Research*, 84, 72–87. <https://doi.org/10.2110/jsr.2014.12>
- Rød, R. S., Hynne, I. B., & Mørk, A. (2014). Depositional environment of the Upper Triassic De Geerdalen Formation—an EW Transect from Edgeøya to Central Spitsbergen, Svalbard. *Norwegian Petroleum Directorate Bulletin*, 11, 21–40. Stavanger 2014, ISSN Online 1894-7670, ISBN 978-82-7257-117-6.
- Rouby, D., Raillard, S., Guillocheau, F., Bouroulec, R., & Nalpas, T. (2002). Kinematics of a growth fault/raft system on the West African margin using 3-D restoration. *Journal of Structural Geology*, 24(4), 783–796. [https://doi.org/10.1016/S0191-8141\(01\)00108-0](https://doi.org/10.1016/S0191-8141(01)00108-0)
- Rutter, E. (1986). On the nomenclature of mode of failure transitions in rocks. *Tectonophysics*, 122, 381–387. [https://doi.org/10.1016/0040-1951\(86\)90153-8](https://doi.org/10.1016/0040-1951(86)90153-8)
- Sapin, F., Ringenbach, J.-C., Rives, T., & Pubellier, M. (2012). Counter-regional normal faults in shale-dominated deltas: Origin, mechanism and evolution. *Marine and Petroleum Geology*, 37, 121–128. <https://doi.org/10.1016/j.marpetgeo.2012.05.001>
- Scott, R. A., Howard, J. P., Guo, L., Schekoldin, R., & Pease, V. (2011). Offset and curvature of the Novaya Zemlya fold-and-thrust belt, Arctic Russia. *Geological Society, London, Petroleum Geology Conference Series*, 7, 645–657. <https://doi.org/10.1144/0070645>
- Senger, K., Tveranger, J., Ogata, K., Braathen, A., & Planke, S. (2014). Late Mesozoic magmatism in Svalbard: A review. *Earth Science Reviews*, 139, 123–144. <https://doi.org/10.1016/j.earscirev.2014.09.002>
- Sibson, R. H. (1977). Fault rocks and fault mechanisms. *Journal of the Geological Society*, 133(3), 191–213. <https://doi.org/10.1144/gsjgs.133.3.0191>
- Smyrak-Sikora, A., Osmundsen, P. T., Braathen, A., Ogata, K., Anell, I., Husteli, B., ... Olaussen, S. (2017). Sedimentary architecture of siliciclastic, syntectonic graben and half-graben fill in Kvalpynnten, Edgeøya, Svalbard. Norsk Geologisk Vinterkonferanse. January 2017.
- Steel, R., Gjelberg, J., Nøttvedt, A., Helland-Hansen, W., Kleinspehn, K. L., & Rye Larsen, M. (1985). The Tertiary strike slip basins and orogenic belt of Spitsbergen. In K. T. Biddle & N. Christie-Blick (Eds.), *Strike-slip deformation, basin formation, and sedimentation* (pp. 339–359). Society of Economic Paleontologists and Mineralogists, Special Publication 37.
- Torabi, A., Fossen, H., & Braathen, A. (2013). Insight into petrophysical properties of deformed sandstone reservoirs. *American Association of Petroleum Geologists Bulletin*, 97, 619–637. <https://doi.org/10.1306/10031212040>
- Tugarova, M. A., & Fedyaevsky, A. G. (2014). Calcareous microbialites in the Upper Triassic succession of Eastern Svalbard. *Norwegian Petroleum Directorate Bulletin*, 11, 137–152.
- Vigran, O. S., Mangerud, G., Mørk, A., Worsley, D., & Hochuli, P. A. (2014). Palynology and geology of the Triassic succession of Svalbard and the Barents Sea. *Geological Survey of Norway Special Publications*, 14, 270.
- Washburn, E. W. (1921). Note on a method of determining the distribution of pore sizes in a porous material. *Proceedings of the National Academy of Sciences of the United States of America*, 7, 115–116. <https://doi.org/10.1073/pnas.7.4.115>
- Wignall, P. B., & Best, J. L. (2004). Sedimentology and kinematics of a large, retrogressive growth-fault system in Upper Carboniferous deltaic sediments, western Ireland. *Sedimentology*, 51, 1343–1358. <https://doi.org/10.1111/j.1365-3091.2004.00673.x>
- Yeager, K. M., Brunner, C. A., Kulp, M. A., Fischer, D., Feagin, R. A., Schindler, K. J., ... Bera, G. (2012). Significance of active growth faulting on marsh accretion processes in the lower Pearl River, Louisiana. *Geomorphology*, 153, 127–143. <https://doi.org/10.1016/j.geomorph.2012.02.018>

Zecchin, M., Massari, F., Mellere, D., & Prosser, G. (2003). Architectural styles of prograding wedges in a tectonically active setting, Crotona Basin, Southern Italy. *Journal of the Geological Society, London*, 160, 863–880. <https://doi.org/10.1144/0016-764902-099>

How to cite this article: Ogata K, Mulrooney MJ, Braathen A, et al. Architecture, deformation style and petrophysical properties of growth fault systems: the Late Triassic deltaic succession of southern Edgeøya (East Svalbard). *Basin Res.* 2018;30:1042–1073. <https://doi.org/10.1111/bre.12296>

APPENDICES

Appendix A

Haile, B. G., Czarniecka, U., Xi, K., **Smyrak-Sikora, A.**, Jahren, J., Braathen, A., & Hellevang, H. (2018): "*Hydrothermally induced diagenesis: Evidence from shallow marine-deltaic sediments, Wilhelmøya, Svalbard*", *Geoscience Frontiers*, 10.2, 629-649.

Abstract: Sedimentary basins containing igneous intrusions within sedimentary reservoir units represent an important risk in petroleum exploration. The Upper Triassic to Lower Jurassic sediments at Wilhelmøya (Svalbard) contains reservoir heterogeneity as a result of sill emplacement and represent a unique case study to better understand the effect of magmatic intrusions on the general burial diagenesis of siliciclastic sediments. Sills develop contact metamorphic aureoles by conduction as presented in many earlier studies. However, there is significant impact of localized hydrothermal circulation systems affecting reservoir sediments at considerable distance from the sill intrusions. Dolerite sill intrusions in the studied area are of limited vertical extent (~12 m thick), but created localized hydrothermal convection cells affecting sediments at considerable distance (more than five times the thickness of the sill) from the intrusions. We present evidence that the sedimentary sequence can be divided into two units: (1) the bulk poorly lithified sediment with a maximum burial temperature much lower than 60–70 °C, and (2) thinner intervals outside the contact zone that have experienced hydrothermal temperatures (around 140 °C). The main diagenetic alteration associated with normal burial

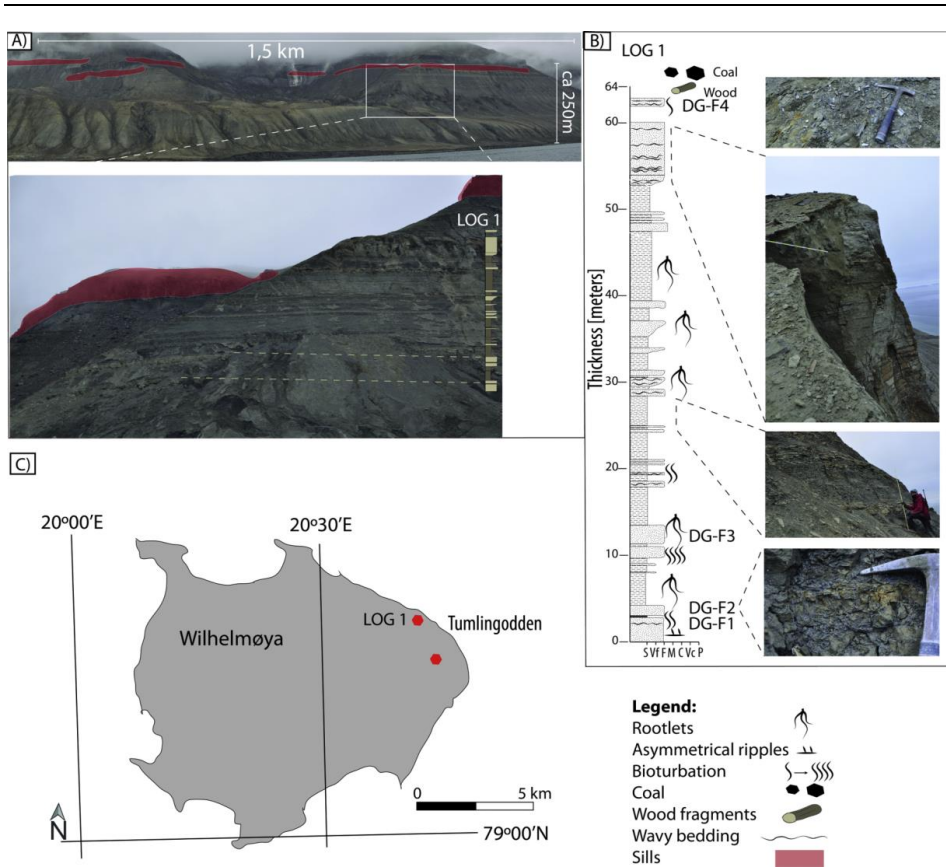


Figure 2 from 13. Sample locations and distribution of Early Cretaceous mafic sill intrusion. (A) An overview field picture showing the spatial distribution of the sill intrusion (top part) in the sedimentary strata and closer view of the lowermost sediment section where logging and sampling was done. View is westward. The sill intrusions are sub-parallel to layering. (B) Showing conventional sediment log of the lowermost succession (De Geerdalen Formation) below the sill intrusion. (C) Schematic map of Wilhelmøya showing sampling and sediment logging localities. S = silt, Vf = very fine sand, F = fine sand, M = medium sand, C = coarse sand, Vc = very coarse sand, and P = pebbles.

diagenesis is minor mechanical plastic deformation of ductile grains such as mica. Mineral grain contacts show no evidence of pressure dissolution and the vitrinite reflectance suggests a maximum temperature of ~ 40 °C. Contrary to this, part of the sediment, preferentially along calcite cemented flow baffles, show evidence of hydrothermal alteration. These hydrothermally altered sediment sections are characterized by recrystallized carbonate cemented intervals. Further, the hydrothermal solutions have resulted in localized sericitization (illitization) of feldspars, albitization of both K-feldspar and plagioclase and the formation of fibrous illite nucleated on kaolinite. These observations suggest hydrothermal alteration at $T > 120\text{--}140$ °C at distances considerably further away than expected from sill heat dissipation by conduction only, which commonly affect sediments about twice the thickness of the sill intrusion. We propose that carbonate-cemented sections acted as flow baffles already during the hydrothermal fluid mobility and controlled the migration pathways of the buoyant hot fluids. Significant hydrothermally induced diagenetic alterations affecting the porosity and hence reservoir quality was not noted in the noncarbonate-cemented reservoir intervals.

Appendix B

Senger, K., Brugmans, P., Grundvåg S.A., Jochmann, M., Nøttvedt, A., Olaussen, S., Skotte, A. & **Smyrak-Sikora, A. (2019):** “*Petroleum, coal and research drilling onshore Svalbard: a historical perspective*”, Norwegian Journal of Geology, 99(3).

Abstract: The beginning of the Norwegian oil industry is often attributed to the first exploration drilling in the North Sea in 1966, the first discovery in 1967 and the discovery of the supergiant Ekofisk field in 1969. However, petroleum exploration already started onshore Svalbard in 1960 with three mapping groups from Caltex and exploration efforts by the Dutch company Bataaffse (Shell) and the Norwegian private company Norsk Polar Navigasjon AS (NPN). NPN was the first company to spud a well at Kvadehuken near Ny-Ålesund in 1961. This drilling marked the start of an exciting period of petroleum exploration in Svalbard, with eighteen exploration wells drilled in the period from 1961 to 1994. The deepest well so far, Caltex’s Ishøgda-I near Van Mijenfjorden, reached 3304 m in 1966. NPN was involved in nine of the eighteen wells. The remaining wells were drilled by American (Caltex/Amoseas), Belgian (Fina), French (Total), Soviet/Russian (Trust Arktikugol), Swedish (Polargas Prospektering) and Norwegian companies Norsk Hydro and Store Norske Spitsbergen Kulkompani. None of the wells resulted in commercial discoveries, though several wells encountered gas in measureable quantities. Only the two wells drilled in the early 1990s were drilled on structures defined using a sparse 2D seismic grid, while the other wells were drilled based on geological mapping at the surface. Furthermore, more recent research and coal exploration boreholes have confirmed moveable hydrocarbons in close proximity to the Longyearbyen and Pyramiden settlements. In this contribution, we present a historical and brief geological overview of the petroleum exploration wells onshore Svalbard. We

illustrate that the eighteen petroleum exploration wells have together penetrated over 29 km of stratigraphy, with the Late Palaeozoic–Mesozoic successions particularly well covered. Coal exploration and research boreholes primarily focus on the Mesozoic–Cenozoic successions. As such, the boreholes represent an important window to decipher the stratigraphic evolution of both Svalbard and the greater Barents Shelf

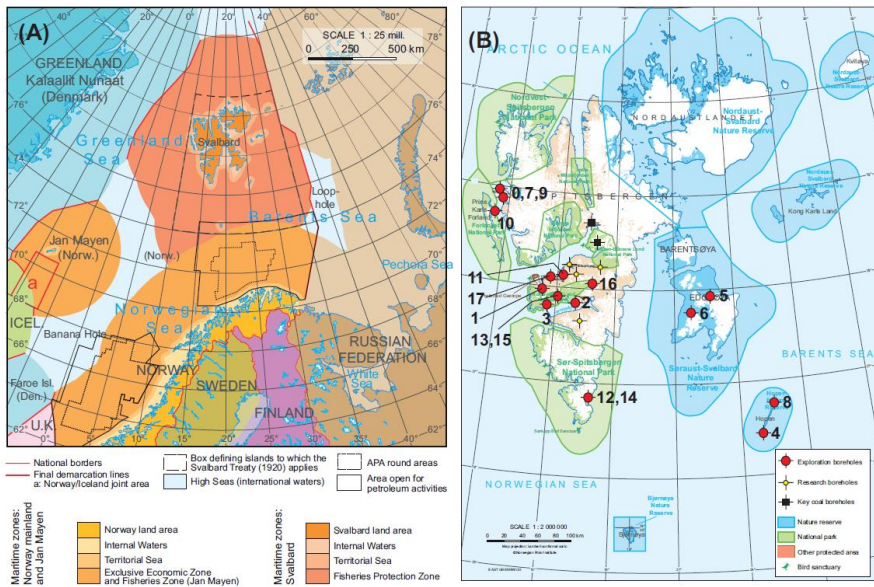


Figure 1 from 13. Geographical setting of Svalbard in the North Atlantic. (A) Norwegian territories and maritime zones in the Arctic. APA– Awards in predefined areas, an annual licence round in mature parts of the Norwegian continental shelf. (B) Location of key boreholes on a map of Svalbard highlighting the protected areas. The numbers represent the chronological drilling order and provide more information on the boreholes in Table 1. Both maps modified from Dallmann et al. (2015).

Appendix C

Maher, H., Senger, K., Braathen, A., Mulrooney, M.J., Smyrak-Sikora, A., Osmundsen, P.T & Ogata, K. (Submitted to *Tectonics*): “*Mesozoic-Cenozoic regional stress field evolution in Svalbard*”

Abstract: Cooling fractures in diabase sills associated with the Cretaceous High Arctic Large Igneous Province and syn-sedimentary Triassic faults help constrain a model for Svalbard’s (NE Barents shelf area) Mesozoic stress field evolution. Fracture data from Edgeøya and adjacent islands in SE Svalbard, from S Spitsbergen, and from the literature, was used to model preferred orientations and temporal relationships. Orthogonal, roughly E-W and N-S, joints and veins in sills from SE Svalbard are interpreted as cooling fractures influenced by the ambient stress field. Aligned preferred orientations within the Triassic host strata are associated with a regional Cretaceous jointing episode driven by sill emplacement and/or erosional unloading. A dominant set indicates the regional maximum horizontal (and likely σ_1) stress was \approx E-W. Spitsbergen’s joint data has more complex patterns associated with proximity to the Cenozoic West Spitsbergen Fold-and-Thrust Belt. However, E-W and N-S orientations occur and are typically an earlier set. Syn-sedimentary Triassic normal faults in the Edgeøya and Hopen areas align with a NW-SE maximum horizontal stress, indicating a Triassic to Cretaceous counterclockwise stress field shift. The maximum horizontal stress subsequently shifted further counterclockwise during Cenozoic dextral transpression, between Svalbard and Greenland. Joint strikes consistent with both decoupled and coupled transpression occur. Changes in the regional maximum horizontal stress and deformation regime may reflect the changing position of which margin was crucial in influencing Svalbard’s plate interior stress field, starting with Triassic Uralian activity to the E, then Cretaceous Amerasian basin development to the NW, culminating with dextral transpression and transtension to the SW.

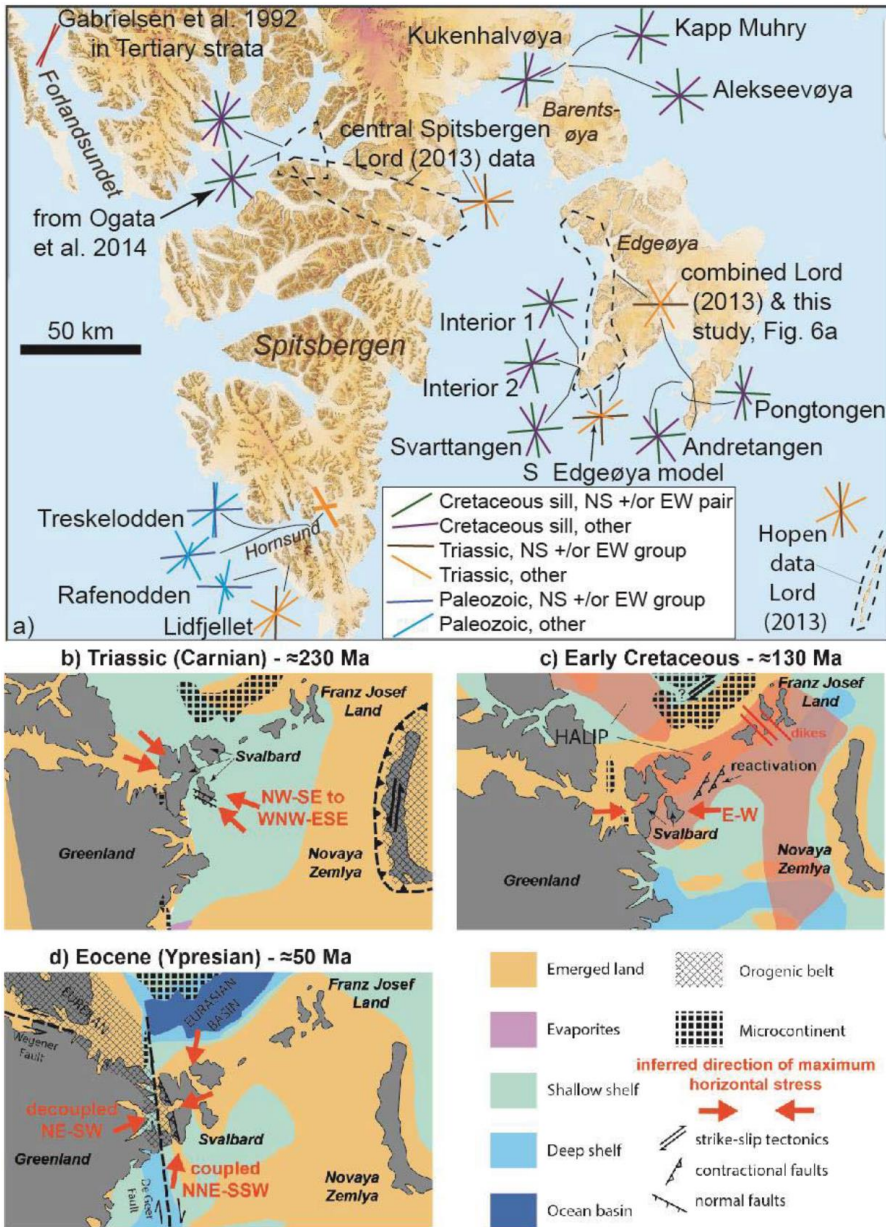


Figure 13 from 13: a) Summary plot of preferred orientation of joints. Dashed lines areas covered in previous studies. b-d) Summary model for stress field evolution in the Svalbard area based on diagram from Torsvik and Cocks (2016).

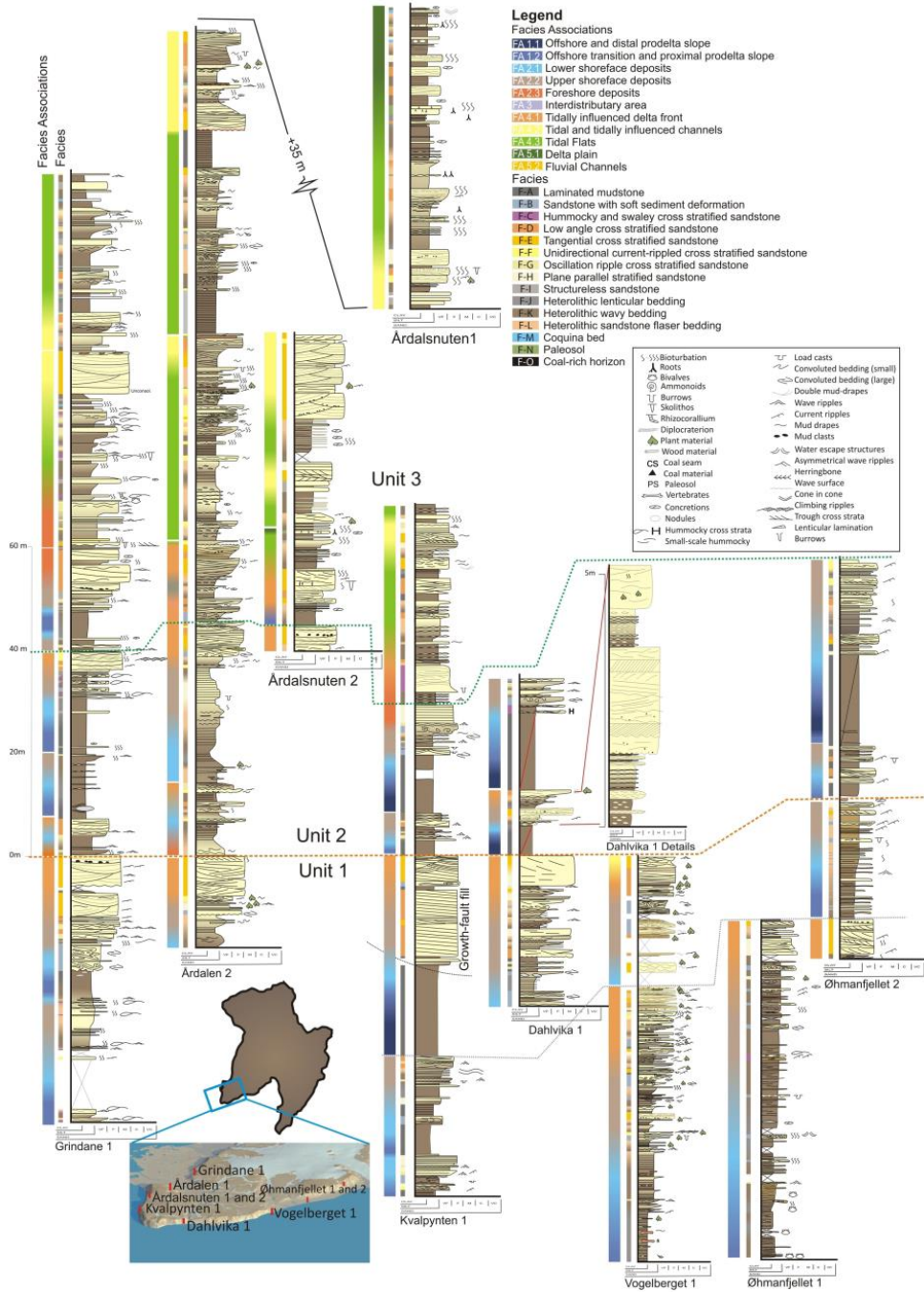
Appendix D

Anell, I., Zuchuat, V., Röhnert, A. D., **Smyrak-Sikora, A.**, Buckley, S., Lord, G., Ogata, K., Osmundsen, P. T., Olaussen, S., Maher, H., Midtkandal, I., Braathen, A. (Submitted to Basin Research) "Increased tide influence on the sedimentary architecture and sand distribution of a prograding Triassic coastline across a structural high, SW Edgeøya, Svalbard".

Abstract: The study describes the depositional development, sedimentary geometries and sand distribution in the Triassic succession on SW Edgeøya, based on study of sedimentary logs and photogrammetric analysis. The succession formed part of large prograding clinoform system. Across the shallower Svalbard Platform (and Edgeøya) the slope-angle of the clinoforms lowered, advance and deposition was more rapid and the shallower setting amplified the tidal signal. The stronger tidal energy redistributed sediment, generating increasingly sandy sub-aqueous delta-front deposits, as seen in a series of large heterolithic 2D dunes. Progressive infill limited accommodation atop the 2D dune fields and changed the depositional style towards smaller reworked and thus cleaner 3D dunes. Rapid deposition of significant amounts of sand and possibly a tectonic trigger, led to growth-faulting in the delta front. Subsequently, an up to 20 m thick shale deposit, which is likely a seismic reflector and regional seal, dictates a large transgression. The subaqueous sandsheets are overlain by convex 200-600 m long, 6-12 meter high bars with outcropping flanks oriented SW-NE migrating laterally N/NE. These sand-rich features are likely NW elongated tide-reworked mouth-bars, and are confined to a single interval which reflects the transition into the tidal flat and tidal channel environment. The strong tidal regime in the system kept the coarser sediment confined up-river leading to development of a heterolithic nearshore tidally dominated channel system, and sandier fluvial channels up-river. The tidal channels are wide, deep and highly meandering. Channel fill is dominated

by 15-20 m high inclined heterolithic point bars which form extensive kilometer long belts. The fluviially dominated channels which govern deposits on the delta plain are much narrower (150-350 m) and slightly less deep (9-19 m) than the tidal channels, straighter, generally symmetric and filled with cleaner sands.

Next page, Figure 4 from 12: Logs from Kvalpynten (Wesern study Area) with color-bars displaying the facies and facies association to the left of the logs.



Appendix E

Other published articles:

Szymański, W., Siwek, J., Skiba, M., Wojtuń, B., Samecka-Cymerman, A., Pech, P. & **Smyrak-Sikora, A.** (2019): *Properties and mineralogy of topsoil in the town of Longyearbyen (Spitsbergen, Norway)*. Polar Record, 1-13.

Submitted manuscripts:

Senger, K., Betlem, P., Buckley, S.J., Coakley, B., Eide, C.H., Flaig, P.P., Forien, M., Galland, O., Gonzaga, L. Jr, Jensen, M., Lecomte, I., Mair, K., Malm, R. H., Mulrooney, M., Naumann, N., Nordmo, I., Nolde, N., Ogata, K., Schaaf, N.W., **Smyrak-Sikora, A.** *Circum-Arctic Geology for Everyone: using virtual outcrops to make the high Arctic more accessible through the Svalbox database* (Journal of Geoscience Education).

Appendix F

List of conference and workshop presentations:

Smyrak-Sikora A., Braathen A., Olausen S., 2013: Onshore-offshore examples of Upper Carboniferous and Triassic growth faults; Svalbard and NW Barents Shelf. Vinterkonferansen, 2013, Norsk Geologisk Forening. 8.-10 January 2013, Oslo. (POSTER PRESENTATION)

Smyrak-Sikora, A. and Sandal, G. 2013: Fault affected facies distribution within an early synrift Billefjorden Trough, Svalbard. 3P Arctic The Polar Petroleum Potential 15 - 18 October 2013, Stavanger. (POSTER PRESENTATION)

Smyrak-Sikora, A., Olausen, S., Sandal, G., Braathen, A. 2015: Fluvial response to faulting during an early stage of rift basin evolution; Arctic Conference Days 2014, 2-6 June 2014, Tromsø. (ORAL PRESENTATION)

Smyrak-Sikora, A., Olausen, S., Sandal, G., Stemmerik, L., Johannessen, E.P., 2015: Rift basin infill - interplay of sedimentary and tectonic processes with eustatic sea level variation - Billefjorden Trough, Svalbard. Vinterkonferansen 2015, Norsk Geologisk Forening, 12-14 January 2015, Stavanger. (ORAL PRESENTATION)

Smyrak-Sikora, A., Osmundsen, P.T., Braathen, A., Ogata, K., Anell, I., Husteli, B., Olausen, S., 2015: Depositional setting and internal architecture of syn-tectonic, siliciclastic half-graben fill, Edgeøya, Svalbard. Vinterkonferansen 2015, Norsk Geologisk Forening, 12-14 January 2015, Stavanger. (POSTER PRESENTATION)

Smyrak-Sikora, A., Osmundsen, P.T., Braathen, A., Mulrooney, M. & Olausen, S. 2016: Three-dimensional model of facies distribution within a Triassic half-graben, SW Edgeøya, Svalbard. In: Buckley, S. J., Naumann, N., Kurz, T. H. & Eide, C. H. (ed.), 2nd Virtual Geoscience Conference, Proceedings Volume. Uni Research AS. ISBN 978-82-8361-004-8. Artikkel. s 194 – 195. (POSTER PRESENTATION)

Smyrak-Sikora, A., Braathen, A., Johannessen, E.P., Kristensen, J.B., Olaussen, S., Sandal, G. & Stemmerik, L., 2017: Upper Carboniferous synrift basin fill of the Billefjorden Through - an analogue to the offshore counterparts in the Barents Sea. NGF Abstracts and Proceedings, no. 1, p 78 (ORAL PRESENTATION)

Smyrak-Sikora, A., Osmundsen, P.T., Braathen, A., Ogata, K., Anell, I., Husteli, B., Mulrooney, M.J. & Olaussen, S. 2017: Sedimentary architecture of siliciclastic, syntectonic graben and halfgraben fill in Kvalpynten, Edgeøya, Svalbard. NGF Abstracts and Proceedings, no. 1, p 79 (POSTER PRESENTATION)

Smyrak-Sikora, A., Johannessen, E.P., Olaussen, S., Braathen, A., 2017: Fault-growth impacting early-rift fluvial deposits – Carboniferous Billefjorden Trough, Svalbard. In International Meeting of Sedimentology 2017 – Toulouse, 10-12 October 2017 p. 837 (POSTER PRESENTATION)

Smyrak-Sikora, A., Kristensen, J.B., Braathen, A., Olaussen, S., Stemmerik, L., 2017: Tectonic and eustatic controls on deposition in evaporite- carbonate dominated rift basin fill, Billefjorden Trough, Norway. In International Meeting of Sedimentology 2017 – Toulouse, 10-12 October 2017 p. 838 (ORAL PRESENTATION)

Smyrak-Sikora, A. 2017: Sedimentary architecture of halfgrabens and grabens fill; Kvalpynten, SW Edgeøya. Talking Trias 2017 (ORAL PRESENTATION).

Appendix G

List of other abstracts:

Osmundsen, P.T., Braathen, A., Maher, H., Smyrak-Sikora, A., Ogata, K. 2, Husteli, B., Anell, I., Olaussen, S., Rød, R. S., Hynne, I., & Mørk, A. 2012: Architecture of syndepositional faults and half-graben in the Triassic succession at Kvalpynten, Edgeøya, East Svalbard. ONSHORE-OFFSHORE RELATIONSHIPS ON THE NORTH ATLANTIC MARGIN, Trondheim.

Ogata K., Anell I., Braathen A., Osmundsen P.T., Smyrak-Sikora A., Husteli B., Olaussen S. & Maher H. 2014: Syndepositional faulting in the Late Triassic succession of Kvalpynten, Edgeøya, East Svalbard. The Future of the Italian Geosciences. September 10-12, Milan, Italy.

Anell, I., Braathen, A., Midtkandal, I., Smyrak- Sikora, A., Husteli, B., Ogata, K., Osmundsen, P.T., 2015: Tracking the Triassic platform-edge: Inferences on clinoform geometries upon reaching the Edgeøya platform. Vinterkonferansen, Norsk Geologisk Forening, 12-14 January, Stavanger.

Braathen, A., Mulrooney, M. J., Ogata, K., Anell, I. M., Smyrak-Sikora, A., Lecomte, I., Osmundsen, P.T. & Maher, H. 2015: Trias North: Late Triassic shallow faulting in Edgeøya, Svalbard; structural style, deformation mechanisms and seismic expression. Vinterkonferansen, Norsk Geologisk Forening, 12-14 January, Stavanger.

Braathen, A., Anell, I., Smyrak- Sikora, A., Mulrooney, M., Haile, B.G., Ogata, K., Osmundsen, P.T., Maher, H., Buckley, S., Hellevang, H., Olaussen, S., 2015: Tectonic influence on platform infill patterns in the mid-late Triassic, Southern Edgeøya, Svalbard. Boreal Triassic II conference, Longyearbyen 28 Aug.-2 Sept.

Buckley, S. J., Dolva, B., Mulrooney, M., Smyrak-Sikora, A., Lecomte, I. 2015: 3D photogrammetric modelling of Kvalpynten: background and overview of LIME functionality. Datasharing workshop 2015.

Maher, H., Braathen, A., Mulrooney, M., Ogata, K., Osmundsen, P. T., & Smyrak-Sikora, A., 2015: South Edgeøya shale detachment geometry and mechanics. Datasharing workshop 2015.

Osmundsen, P. T., Smyrak-Sikora, A., Braathen, A., Olaussen, S., Ogata, K. & Anell, I. M. 2015: Growth basins at Edgeøya: sedimentary architecture and facies relationships. Datasharing workshop 2015.

Osmundsen, P. T., Smyrak-Sikora, A., Braathen, A., Olaussen, S., Ogata, K. & Anell, I. M. 2015: Sedimentary architecture and facies distribution in Late Triassic, reservoir-scale half-graben, De Geerdalen Formation, East Svalbard. *Boreal Triassic II*.

Maher, H. Senger, K., Ogata, K., Braathen, A., Mulrooney, M., Smyrak-Sikora, A., & Osmundsen, P. T. 2016: Mesozoic Regional Stress Field Evolution in Svalbard. *Geological Society of America Abstracts with Programs*. Vol. 48, No. 7; doi: 10.1130/abs/2016AM-281384

Ogata, K., Mulrooney, M., Braathen, A., Maher, H. Smyrak-Sikora, A., Anell, I. Osmundsen, P. T. Olaussen, S., CavoZZi, C., Balsamo, F., Nestola, Y., & Storti, F. 2016: Field-based characterisation and analogue modelling of the South Edgeøya growth faults systems. *Trias North annual workshop 2016*.

Senger, K., Mulrooney, M., Smyrak-Sikora, A., Olaussen, S., Jensen, M., Braathen, A. & Buckley, S. 2016: Making the Arctic accessible: The use of digital outcrops in research and education at 78°N, In: Buckley, S. J., Naumann, N., Kurz, T. H. & Eide, C. H. (ed.), 2nd Virtual Geoscience Conference, Proceedings Volume. Uni Research AS. ISBN 978-82-8361-004-8. Artikkel. s 188 – 189.

Anell, I. M, Braathen, A., Røhnert, D., Ogata, K., Osmundsen, P. T., Smyrak-Sikora, A., Lord, G. S., Buckley, S. J., Maher, H., Olaussen, S. 2017: Findings of five field foragings. Sandbody distribution, clinofom geometries and depositional environments of Edgeøya, Svalbard. *Talking Trias 2017*.

Braathen, A., Mulrooney, M. J., Haile, B. G., Appleyard, T. R., Van Yperen, A. E., Smyrak-Sikora, A., Anell, I. M., Ogata, K., Midtkandal, I., Osmundsen, P. T., Maher, H., Olaussen, S. 2017: "Delta collapse" – Edgeøya delta system compared to the Ferron delta (Utah). Talking Trias 2017.

Ogata, K., Mulrooney, M. J., Braathen, A., Maher, H., Smyrak-Sikora, A., Anell, I. M., Osmundsen, P. T., Olaussen, S., CavoZZi, C., Balsamo, F., Nestola, Y., Storti, F. 2017: Architecture, deformation style and petrophysical properties of a Late Triassic growth fault system in southern Edgeøya, East Svalbard. Talking Trias 2017.

Smyrak-Sikora, A., Kristensen, J. B., Braathen, A., Johannessen, E. P., Olaussen, S., Sandal, G., & Stemmerik, L. 2017: Sedimentary response to halfgraben dip slope faults evolution-Billefjorden Trough, Svalbard. In EGU General Assembly Conference Abstracts Vol. 19, p. 1371.

Senger, K., Farnsworth, W. R., Christiansen, H. H., Gilbert, G. L., Hancock, H. J., Hodson, A. J., Håkansson, L., Jensen, M., Jochmann, M. M., Mulrooney, M., Noormets, R., Olaussen, S., Prokop, A., Smyrak-Sikora, A., Retelle, M. & Rubensdotter, L. 2018: Field-based geology education in the high Arctic: How digital tools can support active learning. Nordic Geological Winter Meeting, Copenhagen

Olaussen, S., Grundvåg, S-A., Senger, K., Birchall, T., Smyrak-Sikora, A., Understanding Barents Sea Play Concepts Based on 18 wildcats, and some R&D wells, in Svalbard. Geonova NCS Exploration Strategy, 14-15 November.

Olaussen, S., Stemmerik, L., Sorento Drøhse, T., Johannessen, E. P. & Smyrak-Sikora, A. 2019: Carboniferous Permian climate changes as recorded in Svalbard. In: Vinterkonferansen, Abstracts and Proceedings of the Geological Society of Norway, Bergen 7-9. 01, 1: 70.

Senger, K., Brugmans, P., Grundvåg, S. A., Jochmann, M., Nøttvedt, A., Olaussen, S. & Smyrak-Sikora, A. 2019: Petroleum Exploration Onshore Svalbard: A Historical Perspective on the Start of the Norwegian Oil Adventure. AAPG Annual Convention and Exhibition.

Appendix H

Teaching contributions:

Teaching was conducted at UNIS, within the Arctic Geology (AG) and the Arctic Technology (AT) departments.

2013:

AG-209 Tectonic and Sedimentary history of Svalbard (15 ECTS)

- Teaching during the fieldwork (11 days in the field), practical exercises, responsible for assessing the field reports and term projects

AG-336/836 Rift Basin Reservoirs: From outcrop to model (10 ECTS)

- Teaching in the field

2014:

AG-209 Tectonic and Sedimentary history of Svalbard (15 ECTS)

- Teaching during the fieldwork (11 days in the field), practical exercises, responsible for assessing the field reports and term projects

AG-322 Fold and Thrust Belts and Foreland Basin Systems (10 ECTS)

- Teaching during the fieldwork (6 days in the field), practical exercises, assessing presentations

AG-334 Arctic Basins and Petroleum Provinces (10 ECTS)

- Teaching during the fieldwork (2 days in the field)

2015:

AG-209 The Tectonic and Sedimentary history of Svalbard (15 ECTS)

Position as a course coordinator:

- Administrative duties, design the final exam and assessment process, supervising and assessing the term projects and field reports
- Teaching duties: lectures 8 hours and exercises 6 hours

2016:

AG-322/822 Fold and Thrust Belts and Foreland Basin Systems (10 ECTS)

- Field excursion to Billefjorden (see the video in the course description)

AG-336/836 Rift Basin Reservoirs: From outcrop to model (10 ECTS)

- Lecture on the Billefjorden Trough (2 hours)
- Fieldwork in Pyramiden (4 days)

2017:**AG-209 Tectonic and Sedimentary history of Svalbard (15 ECTS)**

- Lecture on the Billefjorden Trough

AG-349/849 Geological Constraints on CO₂ Storage (5 ECTS)

- Lectures on Introduction to Geology of Svalbard and the Billefjorden Trough (5 hours)

AT 333/833 Arctic Petroleum: Challenges for Society, Technology, and Environment (10 ECTS)

- Lectures on Introduction to Geology and Introduction to Geology of Svalbard (2 hours)

AG-336/836 Rift Basin Reservoirs: From outcrop to model, 10 ECTS, MSc/PhD level

- Lecture on the Billefjorden Trough (2 hours)
- Attending the fieldwork in Pyramiden (8 days)

2018:**AG-209/AG-222 Bachelor package (30 ECTS)**

- 50% position as teaching assistant, supervision of term projects, lecturing and leading of the Pyramiden fieldwork

AG- 349/849 Geological Constraints on CO₂ Storage (5 ECTS)

- Lectures and exercises on Introduction to Geology of Svalbard and the Billefjorden Trough

AG-334/834 Polar Petroleum Provinces (10 ECTS)

- Lectures and exercises on Introduction to Geology of the Billefjorden Trough

Arctic Petroleum Field School in Pyramiden (UNIS/ founded by Petroleum Research School of Norway, NFIP)

- 6 days of field excursion/fieldwork

2019:**AG-336/836 Rift Basin Reservoirs: From outcrop to model (10 ECTS)**

- Lectures on the Billefjorden Trough (6 hours)



Graphic design: Communication Division, UiB / Print: Skjipes Kommunikasjon AS



uib.no

ISBN: 9788230865002 (print)
9788230853016 (PDF)